Author/s:
Wykes, Alexander David

Title:
Novel molecular tools for cellular- and subcellular-targeting of neuronal transgene expression

Date:
2021

Persistent Link:
https://hdl.handle.net/11343/281905

Novel molecular tools for cellular- and subcellular-targeting of neuronal transgene expression

Alexander David Wykes, B.Sc. (Hons)

ORCID: 0000-0001-8264-7585

Submitted in total fulfilment of the requirements of the degree of

Doctor of Philosophy

Florey Department of Neuroscience and Mental Health

Faculty of Medicine, Dentistry and Health Sciences

The University of Melbourne

Parkville, Victoria, Australia

May 2021

Abstract

Among the questions addressed by modern neuroscience is how distinct cellular structures within the nervous system give rise to particular behaviours and cognitive functions. Our ability to address such questions has been greatly enhanced with the emergence of 'transgenic' technologies, which allow the introduction of foreign or engineered genes into biological systems of interest, such as neural circuits. This capacity to introduce and express transgenes in neurons has led to the development of a diverse catalogue of genetically encoded markers, sensors, and actuators, which provide powerful insights into the structure and function of the nervous system. In addition to their intrinsic utility, mechanisms exist by which expression of these transgenic tools can be selectively directed to cell-types and subcellular structures of interest. Studies described in this thesis sought to establish new molecular tools and approaches for localised transgene expression in neural structures of scientific and therapeutic importance.

Transgene delivery to neural circuits of interest was mediated here in rats using viral vectors, particularly adeno-associated viral (AAV) vectors, from which targeted transduction of neurons expressing the highly conserved neuropeptide, relaxin-3, was achieved using a novel cell-type specific promoter. Relaxin-3 is most abundantly expressed by a subpopulation of neurons in the pontine *nucleus incertus* (NI) and has been identified as an important modulator of arousal and other interrelated cognitive functions and behaviours, making the relaxin-3 system a promising therapeutic target. To better understand this circuitry using transgenic approaches, I sought to identify a promoter sequence capable of regulating cell-type specific transgene expression in relaxin-3 neurons. In parallel to a relaxin-3 promoter sequence (1,736 bp), I also characterised transgene expression under an 880 bp tropomyosin receptor kinase A (TrkA) promoter, as TrkA is exclusively co-expressed with relaxin-3 in rat NI neurons. Eight weeks following stereotaxic injection of an AAV vector, expressing mCherry under the TrkA promoter, to rat NI, widespread non-specific transduction was observed. However, rats receiving injections of an equivalent AAV vector, where transgene expression was regulated by the relaxin-3 promoter, displayed almost exclusive mCherry production in relaxin-3-expressing neurons, demonstrating targeted, cell-type specific transgene delivery.

Localisation of transgene expression at the subcellular level is also an important consideration. The need for rapid and efficient electrochemical communication between neurons has led these

cells to evolve highly complex morphologies, with subcellular compartments each having distinct structural, biochemical, and functional properties. These differences can impact transgene function, as seen with the chloride-conducting opsin, *Gt*ACR2, where differing subcellular ion gradients cause *Gt*ACR2 to have hyper- and depolarising effects in either the somatodendritic or axonal membrane, respectively. To resolve these paradoxical effects, whilst simultaneously providing a mechanism for the functional dissection of closely interconnected circuitry, I developed fusion constructs between *Gt*ACR2 and trafficking motifs derived from either neurexin 1α (*Gt*ACR2^{nrxn}) or the potassium channel, Kv2.1 (*Gt*ACR2$^{Kv2.1}$), which endogenously localise to the axonal or somatic membrane, respectively. The preBötzinger complex (preBötC), a key driver of inspiration and respiratory rhythm, with close but poorly understood functional connections to neighbouring cardiovascular nuclei in the medulla, was selected as an ideal system for characterisation of these *Gt*ACR2 constructs. AAV vectors expressing *Gt*ACR2$^{Kv2.1}$, *Gt*ACR2^{nrxn}, or a control *Gt*ACR2-EYFP construct, under constitutively active promoters, were injected into the rat preBötC. Fusion of *Gt*ACR2 with the Kv2.1 motif was associated with enriched neuronal expression of this construct, but did not eliminate axonal expression, while subcellular localisation of *Gt*ACR2^{nrxn} could not be determined histologically. However, a selective dissociation of respiratory and cardiac responses to optical manipulation, both of which were seen in rats expressing *Gt*ACR2-EYFP, was observed in rats expressing *Gt*ACR2$^{Kv2.1}$ or *Gt*ACR2^{nrxn}, respectively, supporting their differential trafficking *in vivo*.

To further clarify these results and optimise the utility of *Gt*ACR2 fusion constructs in future experiments, a capacity for cell-type specific expression was required. I therefore developed an additional AAV vector for recombinase-dependent *Gt*ACR2$^{Kv2.1}$ expression in neurons. In characterising expression from this construct, I first validated a novel approach for cell-type specific transduction of an amygdaloid efferent population (CeA) projecting to the nucleus of the solitary tract (NST) in rats (referred to as CeA→NST neurons), using locally injected AAV vectors in the amygdala and a retrogradely transported, Cre-recombinase expressing canine adenovirus (CAV) vector delivered into the rostral NST. The CeA→NST pathway was chosen as a model system, given its empirically supported but poorly understood role in modulating autonomic function in response to emotional stimuli, which would benefit from cell-type specific transgenic investigations, and its long-range axonal projections, which provide a further opportunity to assess *Gt*ACR2$^{Kv2.1}$ trafficking *in vivo*. While cell-type specific *Gt*ACR2$^{Kv2.1}$ expression in CeA→NST circuitry was achieved, some axonal expression of *Gt*ACR2$^{Kv2.1}$ was again present in these neurons.

Overall, studies described in this thesis provide valuable contributions to the available toolset for targeted neuronal transgene expression. Changes in *Gt*ACR2 trafficking observed, following fusion with the Kv2.1 motif, are supported by independent publications which appeared in the literature concurrently with my studies, where a somatic enrichment, and significant, but not complete, reduction in axonal expression, was demonstrated for analogous *Gt*ACR2-Kv2.1 fusion constructs. As such, although effects arising from residual axonal expression must be considered and minimised, *Gt*ACR2$^{Kv2.1}$ provides an improved and potent optogenetic construct for neuronal inhibition. Further studies may also establish *Gt*ACR2^{nrxn} as a robust tool for manipulation of the axonal membrane. These, as well as a variety of other established and emerging transgenic actuators, sensors, and markers, can be selectively expressed in relaxin-3 NI or CeA→NST circuitry, among other precisely defined networks, using the strategies and resources developed here. In doing so, powerful insights into a range of neural systems of both scientific and therapeutic importance can be gained through future research.

Declaration

This is to certify that:

i. the thesis comprises only my original work towards the Ph.D., except where indicated in the Preface,

ii. due acknowledgement has been made in the text to all other material used,

iii. the thesis is less than 100,000 words in length, exclusive of tables, figures, references, and appendices.

Signed,

Alexander D. Wykes Date: 16/05/2021

Preface

All works presented in this thesis, other than where specified here, or in reference to published literature or reagent and equipment suppliers in the main text, are claimed as original contributions by the author.

Input and guidance towards the design and execution of the experiments described herein was provided by my Ph.D. supervisors, Prof. Andrew Gundlach, Prof. Andrew Allen, Prof. Ross Bathgate, and Dr Sherie Ma. Additional guidance was provided by the Chair of my Supervisory Committee, Prof. Christopher Reid. Valuable input on experimental design and analysis was also received from my colleagues in the laboratory, particularly Dr Mariana Del Rosso De Melo and Mitchell Wong in relation to experiments described in Chapters 3 and 4, respectively.

The initial polymerase chain reaction (PCR) isolation of the rat relaxin-3 promoter sequence from genomic DNA, as described in Chapter 2, was performed by Sharon Layfield. The stereotaxic delivery of colchicine in rats, and subsequent immunohistochemical determination of tropomyosin receptor kinase A (TrkA) and relaxin-3 co-expression in *nucleus incertus* neurons described in Chapter 2, was performed by Dr Sherie Ma.

Primary cultures of mouse hippocampal neurons described in Chapter 3 were generated by Dr Sarah Gordon and Holly Melland. Stereotaxic viral vector injections, post-operative care, *in vivo* optogenetic experiments and physiological recordings, transcardial perfusion, and immunohistochemistry procedures described in Chapter 3 were performed by Dr Mariana Del Rosso De Melo, who also contributed to the acquisition of epifluorescence images used to map the spread of *in vivo* neuronal transduction in Chapter 3.

Editorial input on Chapter drafts compiled to produce this thesis was provided by Prof. Andrew Gundlach, Prof. Andrew Allen, Prof. Ross Bathgate, and Dr Sherie Ma.

The contents of this thesis, other than that presented in Chapter 2, have not yet been published or submitted for publication. Aspects of these unpublished original works will be incorporated into planned future publications.

Chapter 2 is adapted from an author-accepted manuscript of a published article (Wykes et al. (2020) *IBRO Reports* 8, 1-10, https://doi.org/10.1016/j.ibror.2019.11.006), with minor editing for formatting consistency with other Chapters in this thesis. Specific changes made to the author-accepted manuscript for inclusion as a Chapter here were:

- assignment of a numerical designation to each Section and Subsection,
- incorporation of Supplementary Figures and Tables in the Chapter text,
- alterations to the numerical designation given for each Figure,
- "Experimental procedures" section title changed to "Methods", and
- removal of reference to the city in which resource suppliers are located (country/state alone provided).

Funding towards a Ph.D. Scholarship that supported my candidature was contributed by Dementia Australia (formerly Alzheimer's Australia Dementia Research Foundation) and a generous, private donor to The Florey Institute. Funding support from grants, awarded by the National Health and Medical Research Council of Australia to Prof. Andrew Gundlach, Prof. Andrew Allen, and Prof. Ross Bathgate, also supported aspects of the research presented herein.

Acknowledgements

The completion of this thesis, and the methodological and scientific advances it describes, would not have been possible without the incredibly generous support I have received from my supervisors, Prof. Andrew Gundlach, Prof. Andrew Allen, Prof. Ross Bathgate, and Dr Sherie Ma. The guidance, encouragement, and mentorship you provide for your students and staff is something I truly admire and hope to emulate in my own career.

Following my Honours studies, the opportunity for me to return to The Florey Institute as a Ph.D. candidate was made possible by funding towards a scholarship, which I would not have secured without the support of Prof. Gundlach. Andrew, being a member of your laboratory and working alongside our local and international colleagues and collaborators has been a terrific experience. Thank you for your guidance and support throughout my candidature, especially your scientific advice in planning experiments and your keen attention to detail in preparing manuscripts and posters to communicate their outcomes.

The supervision of Dr Ma was also essential to my research with the Gundlach laboratory, and our publication of the exciting data which it produced. The training and assistance in rat stereotaxic surgery, post-operative care, transcardial perfusion, histological techniques, and confocal imaging provided by Dr Ma was particularly important. I am glad to have had the chance to work with you Sherie, your patience and sense of humour in the laboratory made learning these techniques and performing experiments enjoyable. Your continued support during my candidature was also very much appreciated.

Throughout my Honours and Ph.D. projects, I have also benefited from the supervision of Prof. Bathgate, whose guidance was especially important in developing the molecular tools at the core of my experiments. Ross, working with your group, as well as on the collaborative projects you established during my candidature, has been an exciting and incredibly valuable opportunity for me. Thank you for your help with my many questions, both in getting projects off the ground and interpreting data from them, as well as your insightful and constructive feedback on my work, and dedicated support during my time with the laboratory.

As the focus of my Ph.D. project evolved, I had the opportunity to work under Prof. Allen's supervision and to contribute to the exciting research undertaken by his laboratory. Andrew,

although arising from difficult circumstances, I am very glad to have had the chance to be a member of your laboratory. It has been a great opportunity and I have learnt a lot from you and our colleagues. I am very grateful for your thoughtful advice, both scientific and professional, as well as your encouragement and guidance, initially as a member of my Supervisory Committee, and especially so later as my supervisor.

Additional guidance was provided by Prof. Christopher Reid as the Chair of my Supervisory Committee. Chris, thank you for overseeing my project in this capacity. Your interest, advice, and guidance towards my research and candidature, as well as your availability for academic and career support beyond this, are all very much appreciated.

While comprehensive acknowledgments of the colleagues I have worked with and learnt from during my candidature are impractical, both in terms of their length and, perhaps more to the point, my lack of confidence in being able to recall everyone that ought to be mentioned, I would like to express my gratitude to those individuals whose contributions have been particularly impactful.

In addition to the direct contributions to this thesis outlined in the above Preface, I would also like to thank the following people for their provision of technical training and support; Sharon Layfield, who provided training in cell culture, molecular biology, and viral vector production techniques; Tania Ferraro, who provided training in the use and detection of proteins; Jaspreet Bassi, who provided training in stereotaxic surgery and histological procedures; Angela Connelly, who provided training in histological procedures; Dr Mariana Del Rosso De Melo, who provided training in the use of Spike2 software and data analysis; Dr Sarah Gordon and Holly Melland, who provided training in transfection of primary neuronal cultures and immunocytochemical techniques; and Dr Carolina Chavez, who provided training in confocal microscopy. My additional thanks to Angela, Jaspreet, Sharon, and Tania, for their dedicated efforts in managing and maintaining laboratories at The Florey Institute and The University of Melbourne, providing a safe and productive environment in which we could work.

I would also like to thank the many other members and collaborators, both past and present, of the Peptide Neurobiology Laboratory, Neuropeptide Receptor Group, and Central Cardiovascular Regulation Laboratory, who did so much to enrich my experience both in and outside the laboratory during my candidature.

My Ph.D. candidature, and the works resulting from it, were made possible by a range of support services provided by The University of Melbourne and The Florey Institute. Core Animal Services at both The Florey Institute and The University of Melbourne were essential to experiments involving the use and maintenance of animals. Confocal images were acquired using resources established and maintained by the Florey Advanced Microscopy and Immunochemistry Service (FAMIS). My additional thanks to members of the Students of the Florey Institute (SOFI) student committees who have contributed to my personal and professional growth over the years, particularly my fellow members of the 2018 committee.

Finally, throughout my studies I have received a tremendous amount of love and support from my family and friends. I would especially like to thank my parents, David and Luanne, their partners, Margie and Raymond, and my sister and fellow scientist, Louise. Having you there for me, during both exciting and difficult times in my candidature, means more to me than I can express. I am incredibly grateful to have shared this journey with you and look forward to seeing what lies ahead.

Awards and publications

Awards

2018 | Australian Neuroscience Society (ANS) Student Travel Award

2018 | EMBL Australia Postgraduate Symposium Travel Grant

2018 | Miller Postgraduate Travel Award

2016 | Alzheimer's Australia Dementia Research Foundation (AADRF) Ph.D. Scholarship

Original articles and communication arising during my candidature:

Peer-reviewed articles

Wykes A.D., Ma S., Bathgate R.A.D., and Gundlach A.L. (2020) Targeted viral vector transduction of relaxin-3 neurons in the rat nucleus incertus using a novel cell-type specific promoter. *IBRO Reports*, 8, 1-10, https://doi.org/10.1016/j.ibror.2019.11.006.

Haidar M., Tin K., Zhang C., Nategh M., Covita J., Wykes A.D., Rogers J., and Gundlach A.L. (2019) Septal GABA and glutamate neurons express RXFP3 mRNA and depletion of septal RXFP3 impaired spatial search strategy and long-term reference memory in adult mice. *Frontiers in Neuroanatomy*, 13, https://doi.org/10.3389/fnana.2019.00030.

Conference posters

Wykes A.D., Melo M.R., Ma S., Gordon S.L., Gundlach A.L., Allen A.M., Bathgate R.A.D. (2019) Novel molecular tools for targeted cellular and subcellular neuronal transgene expression: Applications in deciphering brainstem neuromodulatory circuits, *Gordon Research Seminar and Conference on Neuromodulatory Mechanisms Underlying Flexible Brain Functions and Behaviour*, Les Diablerets, Switzerland.

Wykes A.D., Ma S., Bathgate R.A.D., Gundlach A.L. (2018) Targeted viral vector transduction of relaxin-3 neurons in the rat nucleus incertus using a novel cell-type specific promoter, *38th Annual Scientific Meeting of the Australasian Neuroscience Society*, Brisbane, Australia.

Wykes A.D., Ma S., Bathgate R.A.D., Gundlach A.L. (2018) Targeted viral vector transduction of relaxin-3 neurons in the rat nucleus incertus using a novel cell-type specific promoter, *5th Annual EMBL Australia Postgraduate Symposium*, Brisbane, Australia.

Table of contents

List of figures

List of tables

Glossary of terms and abbreviations

AAV	adeno-associated virus
AAVHSC	class of adeno-associated viral vectors derived from hematopoietic stem cell
AAVR	AAV receptor (required for cellular transduction by AAV vectors)
AAV293	HEK293-derived cell line expressing the adenovirus E1 gene, used for AAV vector production
AAV-PHP	class of adeno-associated viral vectors generated using the CREATE platform for systemic delivery
aca	anterior commissure, anterior part
ACR	anion-conducting channelrhodopsin
AIS	axon initial segment
Alexa Fluor	family of fluorescent dyes (conjugated to secondary antibodies)
AnkG	ankyrin G
AP	anterior-posterior axis (in reference to stereotaxic coordinates) or area postrema (in reference to neuroanatomy)
Arch	archaeorhodopsin (light-gated proton pump)
ASLV	avian sarcoma and leukosis virus
Ast	allatostatin peptide
AstR	allatostatin peptide receptor
ATP	adenosine triphosphate
att	proprietary recombination sequences used in Gateway cloning system (includes paired attB/P and attL/R sites)
BAC	bacterial artificial chromosome
***Bam*HI**	restriction endonuclease derived from *Bacillus amyloliquefaciens*
BLA	basolateral nucleus of the amygdala
BLAST	basic local alignment search tool
BLAT	BLAST-like alignment tool
BNST	bed nucleus of the stria terminalis
BötC	Bötzinger complex
BMP	basomedial amygdaloid nucleus, posterior part
bp	base pair (within a nucleic acid molecule)
bpm	beats per minute
BSA	bovine serum albumin
Ca^{2+}	calcium cation

CAG	cytomegalovirus/chicken β-actin synthetic promoter
CaM	calmodulin
cAMP	cyclic adenosine monophosphate
CAN	central autonomic network
CAR	coxsackievirus and adenovirus receptor (required for cellular transduction by CAV2 vectors)
Cas9	CRISPR associated protein 9
CAV2	canine adenovirus type 2
cc	corpus callosum
CC	central canal
CCR	cation-conducting channelrhodopsin
CeA	central amygdaloid nucleus
CeC	central amygdaloid nucleus, capsular part
CeL	central amygdaloid nucleus, lateral division
CeM	central amygdaloid nucleus, medial division
ChAT	choline acetyltransferase
ChETA	channelrhodopsin-2-derived opsin with faster kinetics
chr	chromosome
ChR2	channelrhodopsin 2 (algal cation-conducting opsin)
ChRmine	cation-conducting channelrhodopsin with red-shifted light sensitivity
Cl^-	chloride anion
CNO	clozapine-N-oxide (ligand used to activate DREADDs)
CNS	central nervous system
cpGFP	circularly permutated green fluorescent protein
Cre	'caused recombination' recombinase (recombines *LoxP* sites)
CREATE	Cre recombination-based AAV targeted evolution
CreGFP	Cre recombinase fused to a green fluorescent protein tag
CRF_1	corticotropin-releasing factor receptor 1
CRISPR	clusters of regularly interspaced short palindromic repeats
cVRG	caudal ventral respiratory group
Cy	family of synthetic cyanine dyes (conjugated to secondary antibodies)
C57BL/6J	C57 black 6 strain of inbred mice, substrain 6J
d	day (unit of time)
DAG	diacylglycerol
DB	diagonal band

DCA	cytomegalovirus/chicken β-actin synthetic promoter (see also CAG)
dEMG	diaphragm electromyography
DIO	double-floxed inverse orientation (configuration that facilitates permanent gene reorientation by Cre-recombination of flanking *Lox* sites; synonymous with FLEX)
DIV	days *in vitro* (referring to primary cell cultures)
DJ	chimeric AAV-2, -8, and -9 vector capsid serotype
Dlg1	discs large homolog 1
DNA	deoxyribonucleic acid
DREADD	designer receptor exclusively activated by a designer drug
***Ds*Red**	*Discosoma striata*-derived red fluorescent protein
DTg	dorsal tegmental nucleus
DV	dorsoventral axis (in reference to stereotaxic coordinates)
D_2	dopamine receptor 2
E	embryonic days of age (specified by accompanying number)
EAC	sublenticular extended amygdala, central part
eArch3.0	modified Arch opsin with enhanced expression in mammalian cells
ECFP	enhanced cyan fluorescent protein
ECG	electrocardiogram
***Eco*RI**	*Escherichia coli* strain RY13 restriction endonuclease I
Ef1α	elongation factor 1α (promoter)
EGFP	enhanced green fluorescent protein
e*Np*HR3.0	modified *Np*HR opsin with enhanced expression in mammalian cells
EnvA	ASLV envelope glycoprotein (used to generate psuedotyped rabies vectors)
ERK	extracellular signal-regulated kinase
EYFP	enhanced yellow fluorescent protein
FLEX	flip excision (configuration that facilitates permanent gene reorientation by Cre-recombination of flanking *Lox* sites; synonymous with DIO)
Flp	flippase recombinase (recombines *frt* sites)
fmol	femtomole (measurement for the amount of a substance; 10^{-15} of a mole)
FRET	Förster resonance energy transfer
frt	flippase recognition target (targeted by Flp recombinase)
g	gram (unit of mass)
G	gauge (measurement of the inner diameter of a needle)
GABA	γ-aminobutyric acid

$GABA_A$	γ-aminobutyric acid receptor type A
GAL4p65	chimeric transactivator constituted by fusion of a GAL4-binding domain with the NF-κBp65 transcriptional activation domain
gc	genomic copies (reported per unit of volume to indicate viral vector titre)
GCaMP	a type of fluorescent calcium indictor based on fusion of a circularly permutated fluorescent protein fused with calmodulin and the calmodulin-binding M13 peptide
GEVI	genetically encoded voltage indicator
GECI	genetically encoded calcium indicator
GFP	green fluorescent protein
GIRK	G protein-coupled inwardly-rectifying potassium channel
GluCl	glutamate-gated chloride channel
GlyR	glycine receptor
GMO	genetically modified organism
GPCR	G-protein coupled receptor
Gr	gracile nucleus
gRNA	guide ribonucleic acid (confers target specificity for CRISPR/Cas9 gene editing)
***Gt*ACR**	*Guillardia theta*-derived anion channelrhodopsin
G*t*ACR1	*Guillardia theta*-derived anion channelrhodopsin, type 1
G*t*ACR2	*Guillardia theta*-derived anion channelrhodopsin, type 2
***Gt*ACR2$^{Kv2.1}$**	opsin fusion construct involving *Gt*ACR2 linked to the Kv2.1 trafficking motif by a muGFP fluorescent tag
***Gt*ACR2^{nrxn}**	opsin fusion construct involving *Gt*ACR2 linked to the Nrxn1α trafficking motif by a series of two HA tags
GTPase	type of enzyme that hydrolyses guanosine triphosphate (GTP) to guanosine diphosphate (GDP)
h	hour (unit of time)
H^+	hydrogen cation/proton
HA	haemagglutinin tag
hCAR	human coxsackievirus and adenovirus receptor
HDB	nucleus of the horizontal limb of the diagonal band
HEK293FT	human embryonic kidney cell line 293, expressing the SV40 large T antigen
***Hin*dIII**	restriction endonuclease isolated from *Haemophilus influenzae*
HK4-144-10	hybridoma cell line producing a monoclonal antibody against relaxin-3
hM3Dq	human muscarinic M3 receptor-derived DREADD, G_q protein-coupled
hM3Ds	human muscarinic M3 receptor-derived DREADD, G_s protein-coupled

hM4Di	human muscarinic M4 receptor-derived DREADD, $G_{i/o}$ protein-coupled
hM4D^{nrxn}	chemogenetic fusion construct involving the hM4Di DREADD linked to the Nrxn1α trafficking motif by a series of two HA tags
HR	heart rate
HRV	heart rate variability
HSV	herpes simplex virus
hSyn	human synapsin 1 promoter
Hz	hertz (unit of frequency)
ic	internal capsule
ICC	immunocytochemistry
IHC	immunohistochemistry
i.m.	intramuscular (injection route)
INSRR	insulin receptor-related protein (gene)
INTRSECT	intronic recombinase sites enabling combinatorial targeting
i.p.	intraperitoneal (injection route)
iP (rats)	alcohol-preferring rats
IP_3	inositol triphosphate
IP_3R	inositol triphosphate receptor
IR	immunoreactivity
IRES	internal ribosomal entry site (facilitates bicistronic transgene expression)
IRt	intermediate reticular nucleus
IS	inferior salivatory nucleus
ITR	inverted terminal repeat sequence
i.v.	intravenous (injection route)
IVM	ivermectin (used as a chemogenetic ligand to activate GluCl/GlyR receptors)
K^+	potassium cation
KA2	kainate receptor subunit 2
kb	kilobase (one thousand base pairs of a nucleic acid molecule)
KCC2	potassium chloride cotransporter 2
kg	kilogram (unit of mass)
kHz	kilohertz (unit of frequency)
KIF1A	kinesin family member 1A
KORDi	κ-opioid-derived DREADD, $G_{i/o}$ protein-coupled
Kv2.1	potassium voltage-gated channel 2.1 (or related trafficking motif)

L-ITR	AAV inverted terminal repeat sequence, left
Ld	lambdoid septal zone
LGIC	ligand-gated ion channel
Lox	locus of crossing (x) over (targeted by Cre recombinase)
LoxP	locus of crossing (x) over, P1 variant (targeted by Cre recombinase)
Lox2722	locus of crossing (x) over, 2722 variant (targeted by Cre recombinase)
LSM	laser scanning microscope
LV	lateral ventricle
M	molar (unit of concentration)
MAP2	microtubule associated protein 2
mCherry	monomeric red fluorescent protein derived from *Ds*Red
MdD	medullary reticular nucleus, dorsal part
MDL	mediodorsal thalamic nucleus, lateral part
MDM	mediodorsal thalamic nucleus, medial part
MeAD	medial amygdala, anterodorsal part
mfb	medial forebrain bundle
mg	milligram (unit of mass)
mGFP	membrane-bound green fluorescent protein
min	minute (unit of time)
ml	millilitre (unit of volume)
ML	mediolateral axis (in reference to stereotaxic coordinates)
mlf	medial longitudinal fasciculus
mm	millimetre (unit of length)
mM	millimolar (unit of concentration)
mmHg	millimetre of mercury (unit of pressure)
mPFC	medial prefrontal cortex
mRFP1	monomeric red fluorescent protein 1
mRNA	messenger ribonucleic acid
mRuby	monomeric red fluorescent protein derived from *Entacmaea quadricolor*
ms	millisecond (unit of time)
MS	medial septum
MSG	monosodium glutamate
muGFP	monomeric ultra-stable green fluorescent protein
mV	millivolt (unit of electrical potential difference)

mW	milliwatt (unit of power)
M13	calmodulin-binding peptide derived from the myosin light-chain kinase
n	number (used to indicate number of subjects in a group)
Na^+	sodium cation
NaCl	sodium chloride
NAmb	nucleus ambiguus
NKCC1	sodium potassium chloride cotransporter 1
ng	nanogram (unit of mass)
NGF	nerve growth factor
***Nhe*I**	*Neisseria mucosa heidelbergensis*-derived restriction endonuclease
NHS	normal horse serum
NH_4Cl	ammonium chloride
NI	*nucleus incertus*
NIc	NI *pars compacta*
NId	NI *pars dissipata*
NIH	United States National Institutes of Health
nl	nanolitre (unit of volume)
nm	nanometre (unit of length)
***Np*HR**	*Natronomonas*-derived halorhodopsin (light-gated chloride pump)
nrxn	trafficking motif derived from neurexin 1α
Nrxn1α	neurexin 1α
ns	not (statistically) significant
NST	nucleus of the solitary tract
NTRK1	Neurotrophic receptor kinase 1 (gene) (synonymous with TrkA)
NVI	neurovisceral integration (model)
OX_2	orexin receptor 2
P	postnatal days of age (specified by accompanying number)
P	P value (measure of statistical significance)
pAAV	DNA plasmid containing a recombinant AAV genome
pAAV-RC	plasmid containing AAV *Rep* and *Cap* genes, used for AAV vector production
***Pac*I**	*Pseudomonas alcaligenes*-derived restriction endonuclease
PAG	periaqueductal grey
pAM	DNA plasmid containing a recombinant AAV genome
PBN	parabrachial nucleus

PBS	phosphate-buffered saline
PCR	polymerase chain reaction
PCRt	parvicellular reticular nucleus
pDONR	DNA plasmid containing a Gateway cloning cassette flanked by attP sites (used to generate pENTR plasmids by recombination with an attB-flanked PCR product)
pDPI/pDPII	helper plasmids containing AAV *Rep* and *Cap* genes, used for vector production
PDZ	structural domain first identified in PSD95, Dlg1, and zo-1 proteins
pENTR	DNA plasmid containing a Gateway cloning cassette flanked by either attL sites, or a combination of attL and attR sites (used to generate a final construct by recombination with other pENTR plasmid/s and a destination vector, such as pAM-Gateway)
pFUGW	plasmid containing a lentiviral vector genome
PFA	paraformaldehyde
pH	potential of hydrogen (scale measuring acidity/basicity an aqueous solution)
pHelper	plasmid containing adenovirus E2A, E4, and VA, genes, used for AAV vector production
PIP_2	phosphatidylinositol 4,5-bisphosphate
PKA	protein kinase A
PKC	protein kinase C
PLC	phospholipase C
PLCo	posterolateral cortical amygdaloid nucleus
PN	phrenic nerve
polyA	polyadenylation sequence
preBötC	preBötzinger complex
PRV	pseudorabies virus
PSAM	pharmacologically selective actuator module (receptors activated by PSEMs)
PSEM	pharmacologically selective effector molecule (ligands used to activate PSAMs)
PSD95	post synaptic density protein 95
PSol	parasolitary nucleus
pTYF	plasmid containing a lentiviral vector genome
pUC57	plasmid vector commonly used for cloning in *E. coli*, from a series originating at the University of California (UC)
P2A	porcine teschovirus-1 2A self-cleaving peptide (used for bicistronic transgene expression)

P2X	family of purinergic receptors
R-ITR	AAV inverted terminal repeat sequence, right
RASSL	receptor activated solely by a synthetic ligand
RFP	red fluorescent protein
Rln3	relaxin-3 (promoter)
RLN3	relaxin-3 (gene/peptide)
RNA	ribonucleic acid
RSA	respiratory sinus arrhythmia
RVLM	rostral ventrolateral medulla
rVRG	rostral ventral respiratory group
RXFP3	relaxin-family peptide receptor 3
s	second (unit of time)
SALB	salvinorin B (ligand used to activate KORDs)
SEM	standard error of the mean
SN	substantia nigra
SNA	sympathetic nerve activity
SNAP	soluble *N*-ethylmaleimide-sensitive factor (NSF) attachment protein
SNARE	SNAP receptor protein (involved in vesicle fusion with target membrane)
SNR	signal-to-noise ratio
sol	solitary tract
SolC	nucleus of the solitary tract, commissural part
SolCe	nucleus of the solitary tract, central part
SolDL	nucleus of the solitary tract, dorsolateral part
SolDM	nucleus of the solitary tract, dorsomedial part
SolG	nucleus of the solitary tract, gelatinous part
SolI	nucleus of the solitary tract, interstitial part
SolIM	nucleus of the solitary tract, intermediate part
SolL	nucleus of the solitary tract, lateral part
SolM	nucleus of the solitary tract, medial part
SolRL	nucleus of the solitary tract, rostrolateral part
SolV	nucleus of the solitary tract, ventral part
SolVL	nucleus of the solitary tract, ventrolateral part
SP	substance P
***Spe*I**	restriction endonuclease isolated from *Sphaerotilus species*

SST	somatostatin
sst_{2A}	somatostatin receptor subtype 2A
st	stria terminalis
STV	synaptic protein transport vesicle
SubP	subpostrema area
SV40	simian virus 40
Syp-mRuby	fusion construct between a synaptophysin and mRuby
tdTomato	type of red fluorescent protein which forms tandem dimers
TH	tyrosine hydroxylase
TH waves	Traube-Hering waves (oscillations in blood pressure caused by respiratory modulation of sympathetic activity)
TPH2	tryptophan hydroxylase 2 (promoter)
TrkA	tropomyosin receptor kinase A
TRP	transient receptor potential family of heat-sensitive cation channels
TRPV	TRP channels belonging to the vanilloid subfamily
TVA	receptor for avian leukosis viruses (allows uptake of EnvA-psuedotyped rabies vectors)
T2A	*Thosea asigna* virus 2A self-cleaving peptide (used for bicistronic transgene expression)
UCSU	University of California, Santa Cruz
US/USA	United States/United States of America
v	volume
V	volt (unit of electrical potential difference)
vaf/VAF	ventral amygdalofugal (pathway)
VDB	nucleus of the vertical limb of the diagonal band
vGAT	vesicular GABA transporter
VGCC	voltage-gated calcium channel
VIIn	facial motor nucleus
VLM	ventrolateral medulla
VN	vagus nerve
VRC	ventral respiratory column
w	weight
WHBP	working heart-brainstem preparation
wk	week (unit of time)
WPRE	woodchuck hepatitis virus post-transcriptional regulatory element
W3SL	condensed WPRE and SV40 polyadenylation signal

zo-1	zonula occludens-1 protein
10N	dorsal motor nucleus of vagus
12N	hypoglossal nucleus
2A	self-cleaving peptide, used for bicistronic transgene expression
293FT	cell line used for AAV vector production (see also HEK293FT)
4V	fourth ventricle
5-HT$_{1A}$	5-hydroxytryptamine (serotonin) receptor 1A
5-HT$_{1B}$	5-hydroxytryptamine (serotonin) receptor 1B
5-HT$_{3}$	5-hydroxytryptamine (serotonin) receptor 3
5N	trigeminal nucleus
λ*dvgal*	a synthetic DNA construct containing phage λ replication genes and the *gal* operon
µg	microgram (unit of mass)
µl	microlitre (unit of volume)
µm	micrometre (unit of length)
˚C	degrees Celsius (scale of temperature)

Chapter 1

General introduction

1.1 Foundations of neuroscience

Endeavours to understand human experience and interactions with the natural world stretch back to our earliest recorded histories. Greek philosophers of antiquity, including Alcmaeon and Plato, were among the first to attribute thought, sensation, and behaviour to the nervous system (Crivellato et al. 2007). Despite experimental support from Hellenistic scholars, most notably the Egyptian anatomists Herophilus and Erasistratus (Wills 1999; Acar et al. 2005) and the Roman physician Galen (Gross 1998), progress in understanding the nervous system largely stagnated until the sixteenth century Scientific Revolution. Section 1.1 presents a summary of the key ideas and techniques developed over the following centuries which would contribute to the development of modern neuroscience, with a focus towards methods that are now complemented or, in some instances, essentially supplanted by transgenic technologies.

1.1.1 Origins of localisation theory

A key aspect of neuroscience is the attribution of specific functions to defined neural structures. Much of today's research focuses on functional specialisation at the level of neuronal populations and networks, defined by features such as gene expression, firing properties, and connectivity. However, functional localisation at the cellular level is a quite recent development in neuroscience, being partly enabled by earlier localisation theories stemming from the first detailed anatomical and functional studies of the brain.

The works of Herophilus and Galen led to the earliest version of localisation theory, taking the form of the 'cell doctrine'. Under the cell doctrine, mystical or spiritual forces thought to mediate cognition and behaviour were assigned to different ventricles within the brain (Tascioglu et al. 2005). At the time of the Scientific Revolution, various forms of cell doctrine had been influential for over a millennium, stimulating further exploration of 'ventricular localisation' by many scientists and philosophers during this period. Among these scholars was Leonardo da Vinci, whose fascination with the cell doctrine led to the first accurate drawings of the ventricular system using a cast set from molten wax (Figure 1.1A), which da Vinci formed through injections into the ox brain (Pevsner 2002).

The sixteenth-century also saw long-held taboos against human dissection begin to soften, allowing the first detailed studies of human neuroanatomy since those of Herophilus and

Erasistratus some eighteen centuries earlier (Wills 1999). Indeed, the main basis of anatomical education until this period came from the writings of Galen, who studied a variety of species but never humans (Wickens 2014). Based on his extensive experience in human dissection, Andreas Vesalius published his *De humani corporis fabrica* in 1543. This tome provided detailed illustrations of the human nervous system (see e.g. Figure 1.1B), while also showing numerous instances in which Galen's long-accepted anatomy was in error (Gomes et al. 2015; Afshar et al. 2019). The widely believed cell doctrine was also questioned by Vesalius, who saw no special differences between the ventricles of humans and other mammals. However, Vesalius did not speculate as to an alternative source for behavioural and cognitive functions, simply lamenting the limited capacity for anatomical insights to shed light on this question (Finger 1994).

As the Scientific Revolution progressed into the seventeenth century, continued progress was made away from the cell doctrine and entrenched ideas of spiritual forces being required to animate behaviour. The first materialistic view of the nervous system can be attributed to René Descartes. Descartes asserted that living beings were part of the natural world, dependent on physical and chemical processes, and thus amenable to scientific investigation. He saw physiology as a mechanical process and described animals as 'automatons' (Ablondi 1998), although he maintained a 'dualistic' distinction between such bodily mechanics and the human mind (Baker et al. 1996). Descartes also used reflex processes, such as withdrawal from painful stimuli, to illustrate how behaviour could be explained without reference to mystical forces (Fearing 1929). A significant advance in neuroanatomy was provided by Descartes' contemporary, Thomas Willis, whose *Cerebri anatome* became an authoritative text for two centuries following its 1664 publication (Figure 1.1C). Indeed, many terms in use today, including anterior commissure, corpus striatum, inferior olives, stria terminalis, and vagus nerve, can be traced back to Willis (Arraez-Aybar et al. 2015). Based on its structure and vascularisation, Willis also dismissed the cell doctrine in favour of assigning mental functions to the brain's grey matter, seeing the ventricles as mere empty spaces for waste collection (Wickens 2014).

Although the works of Vesalius and Willis moved conceptions of behavioural and cognitive function from the ventricles to the grey matter, the idea that specific modalities were associated with localised brain regions was not seriously considered until the nineteenth century. The first widely accepted example of functional localisation was provided by an 1812 publication from Julien Jean César Legallois. By removing the cerebrum, cerebellum, and progressively more caudal slices from the brainstem in rabbits, Legallois identified a region of the medulla which if

cut would cause respiration to immediately cease (Pitts 1946). By 1851, Jean Pierre Flourens had used localised lesions to refine the critical respiratory zone to an area he believed no larger than a pinhead (Figure 1.2A) (Barbara et al. 2012). Despite his technical prowess, Fluorens did not observe specific effects from localised lesions elsewhere in the brain, leading him to believe that most vital functions, movement, and higher cognition arose from diffuse activity across the medulla, cerebellum, and cerebrum, respectively – a view which he vociferously defended against the increasingly popularised concept of phrenology (Pearce 2009). Initially developed by Franz Joseph Gall during the late eighteenth century, phrenology posited that specific traits and abilities corresponded to dedicated regions of the cerebral cortex, whose 'development', or lack thereof, shaped the overlying skull (Temkin 1947). While the idea that skull features reflected behavioural or psychological traits was met with scepticism by the scientific establishment, and essentially disproven by the 1830s, phrenologist were correct in their conception of the cortex as being divided into functionally distinct regions (Greenblatt 1995; Zola-Morgan 1995).

Despite lingering hostility towards phrenology, the 'localisationist' view of brain function would soon come to be supported by clinical evidence, as well as cortical stimulation experiments following the discovery that nervous tissue was electrically excitable (see below, Section 1.1.2). The case study of 'Tan', who lost his capacity for articulate speech following a stroke affecting the left frontal cortex (Figure 1.2B), provided a turning point in the localisation debate when described by Paul Broca in 1861 (Broca 2011). Broca quickly accumulated additional cases of aphasic patients with damage to the left frontal lobe (Lazar et al. 2011), and by 1874 Carl Wernicke had identified a second type of aphasia, characterised by a lack of language comprehension and fluent but unintelligible speech, associated with left temporal lobe lesions (Kirshner et al. 1989). Around the same time, the case of Phineas Gage was reported by John Harlow. A railway foreman involved in an accidental explosion, which launched a metre-long tamping iron through his left check and out the top of his head, Gage appeared largely unaffected following the incident, other than a marked loss of behavioural inhibition attributed to anterior frontal lobe damage (Figure 1.2C) (Macmillan 1992; Harlow 1993). Numerous other cases of focal injury, alongside the application of lesion studies in laboratory animals, have since shed light on how specific anatomical structures within the nervous system contribute to complex behaviours and cognition.

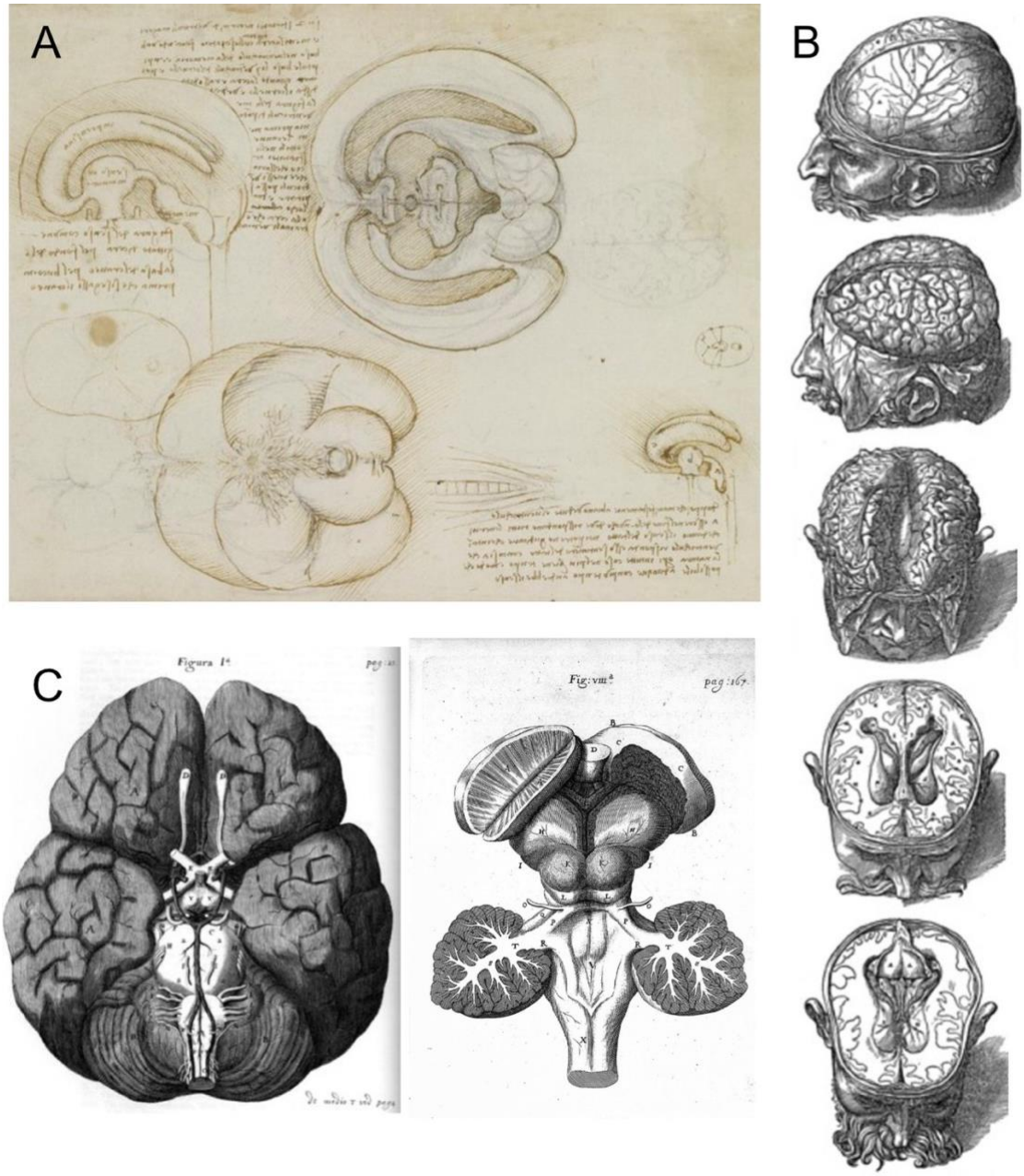

Figure 1.1. *Refer to next page for figure legend.*

Figure 1.1. *Progress in neuroanatomy during the Scientific Revolution*. The Scientific Revolution (1543-1687) saw the first substantial progress in neuroanatomy since Galen's contributions during the second century. Motivated by his interest in the 'cell doctrine', Leonardo Da Vinci created the first accurate sketches of the brain's ventricular system by injecting molten wax into the brain of an ox. His record of this experiment is shown in **(A)**, with a coronal (upper centre) and ventral (lower centre) view of the brain accompanied by three-dimensional representations of the ventricles (upper left and lower right) (image source: The Royal Collection Trust, https://www.rct.uk/collection/919127/the-brain). **(B)** A set of images from Andreas Vesalius' *De humani corporis fabria* (1543) depicting the human brain, based his observations from post-mortem human dissection (adapted from Lanska et al. (2013)). This publication also corrected many mistakes in the anatomy of Galen, which was extrapolated from animal, rather than human, dissections. Further detail was provided by Thomas Willis' *Cerebri Anatome* (1664), which became the authoritative text on neuroanatomy for two centuries following its publication. Example illustrations provided in **(C)** show a ventral view of the brain, with cranial nerves and the eponymous 'circle of Willis' depicted (left), and a dorsal view of the brainstem showing the basal ganglia (right) (adapted from Rengachary et al. (2008) and Parent (2012)).

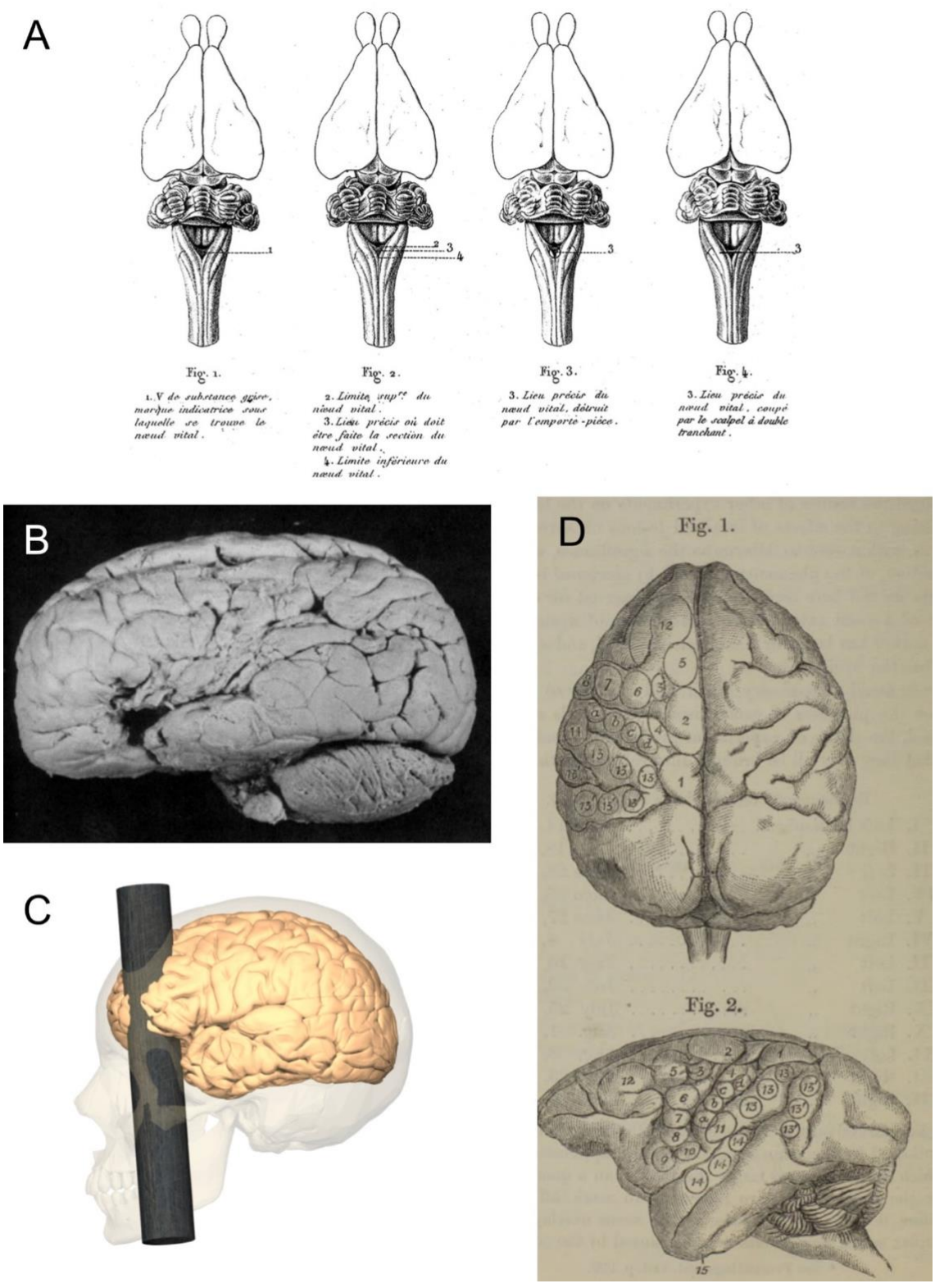

Figure 1.2. *Refer to next page for figure legend*.

Figure 1.2. *Early evidence for localised brain function*. The emergence of methods for targeted lesions in laboratory animals, reports on patients with focal brain damage, and techniques to electrically stimulate the cerebral cortex provided early evidence that cognition and behaviour are produced by specific brain regions. The first widely accepted example was the respiratory centre, or '*noeud vital*', which Jean Pierre Flourens mapped in the rabbit medulla using a series of localised lesions, shown in **(A)** (as illustrated by Alfred Vulpian in 1858; image adapted from Wijdicks (2019)). The highly publicised cases of 'Tan', who suffered from aphasia associated with damage to 'Broca's area' in the left frontal lobe, and Phineas Gage, who exhibited marked behavioural disinhibition after injury to a more anterior region of the left frontal lobe, added further weight to the concept of functional localisation. Tan's preserved brain is depicted in **(B)** (adapted from Baars et al. (2010)), and a digital reconstruction of the Gage's injury in **(C)** (adapted from (Ratiu et al. 2004)), showing the affected regions. Alongside loss of function following localised damage, electrical stimulation of different brain regions also revealed specific functional associations. Among the first to conduct such experiments was David Ferrier, whose depictions of functionally distinct cortical regions in monkeys is provided in **(D)** (adapted from Ferrier (1875)).

1.1.2 Animal electricity

Lesion studies, which provide us with an understanding of different nuclei within the nervous system through the subsequent loss of related functions, would be complemented from the late nineteenth century onwards by electrical stimulation techniques, allowing these same regions to be stimulated and drive specific changes in behaviour and cognition.

The ability of electric currents to pass through the human body, and to elicit physiological responses such as tachycardia, glandular secretions, and muscle contractions, has been known since at least the 1740s, when 'electrical healers' began promoting electricity as a treatment for a variety of ailments (Bertucci 2016). Through his experiments using a neuromuscular preparation, in which frog legs were dissected with the associated spinal nerves intact, Luigi Galvani discovered that nervous tissue was especially sensitive to the effects of electricity. For example, Galvani observed that applying electric currents to the exposed nerve caused much more forceful contractions than stimulating the muscle directly (Wickens 2014). This work culminated his 1791 *De viribus electricitatis in motu musculari commentaries* and led Galvani to believe that a form of intrinsic 'animal electricity' resided within nerves. To identify the nerves, rather than his metallic instruments, as a source of electricity, Galvani went on to show that touching a cut nerve to either the muscle of the same leg, or the surface of the nerve from a separate leg, also caused contraction (Piccolino 1998). This concept of animal electricity was extended to the brain from 1798 by Giovanni Aldini, who, by applying electric currents to the brain, was able to 'reanimate' recently deceased animals and human cadavers (Parent 2004).

By the late nineteenth century, the relatively crude approach of Aldini, which was as much public spectacle as it was scientific experiment, was refined to the point where electrical stimulation was being used to map cortical regions which controlled movements as fine as the twitch of an individual eyelid or digit. In 1870, Eduard Hitzig and Gustav Fritsch reported their finding that motor activity was controlled by the medial-posterior part of the frontal cortex in dogs (Fritsch et al. 2009). Hitzig and Fritsch made this discovery by applying mild electric currents to cortical regions which caused muscular responses in the contralateral forepaw, hindpaw, face, or neck, and by observing a corresponding loss of motor, but not sensory, function following ablation of the forepaw region in two animals. These findings were greatly expanded by David Ferrier, who found that Hitzig and Fritsch's motor area existed in a wide variety of vertebrates. Ferrier extended his studies to monkeys in 1874, discovering nineteen different cortical areas

responsible for an array of specialised movements (Figure 1.2D) (Ferrier 1874; Wickens 2014). That same year, Robert Bartholow described the first evidence of cortical excitability, including motor activity, in a conscious human, although at the time his report was widely criticised on ethical grounds (Cambiaghi et al. 2014). However, electrical stimulation, in the form of the 'Montreal Procedure' pioneered by Wilder Penfield, has become an important method for mapping cortical function in conscious patients prior to surgery (Ladino et al. 2018). Penfield first reported on this method in 1937 (Penfield et al. 1937), providing a fascinating window into cortical localisation and function in humans.

Alongside the establishment of electrical stimulation as a means of functionally defining brain regions, the nineteenth century also saw technological advances which allowed electric currents to be measured in biological tissue. Instrumental to this development was the invention of the astatic galvanometer by Leopoldo Nobili in 1825 (Possenti et al. 2017), which he would use to measure the flow of electric current between two saline-filled beakers, one containing a skinned frog's leg, and the other the associated spinal cord, with both being connected by the intact sciatic nerve – thus providing the first measurement of electricity passing through a nerve (Wickens 2014). This 'frog-current' was further confirmed in muscle by Carlo Matteucci, who measured an electric current passing from one wire of a galvanometer, laid on the surface of a dissected muscle, to another, inserted deep inside the muscle (Moruzzi 1996). In a series of experiments building from these results, Emil du Bois-Reymond found in 1843 that applying an electric shock to the exposed sciatic nerve caused a wave of 'relative negativity' to travel along its surface, and that this 'action current' (now known as an 'action potential') made the muscle contract (Wickens 2014). In 1850, Hermann von Helmholtz measured the speed of conduction along the sciatic nerve at around 27 meters per second (Piccolino 2002).

While these vertebrate studies allowed many properties of the action potential to be discovered, the miniscule size of individual neurons and their axons presented an obstacle to understanding the underlying biochemical mechanisms. Julius Bernstein proposed in 1902 that an unequal distribution of ions across a selectively permeable cell membrane could explain how action potentials propagate (De Palma et al. 2011). However, this hypothesis could not be tested until several decades later, when the discovery of the squid giant axon provided a means of measuring and manipulating electrical current and ionic environments inside and outside the cell (Young 1936; Keynes 2005). Studies utilising the squid axon, in combination with the invention of the 'voltage clamp' technique in 1948, allowed Alan Hodgkin and Andrew Huxley to

detail the movement of ions, particularly sodium and potassium, across the membrane during an actional potential (Huxley 2002). Their results, and subsequent modelling, led Hodgkin and Huxley to believe that the permeability of the membrane to each ionic species must be mediated by specialised channels. The existence of these channels, and their voltage- and ligand-gated nature, was demonstrated in the 1970s through the 'patch-clamp' method. This method enables the activity of single channels to be recorded by bringing a micropipette containing an electrode into contact with the cell membrane (Neher et al. 1992). Furthermore, the patch-clamp method removes the need to penetrate cells with electrodes, meaning that electrophysiological recordings can be made from cells of virtually any type and size, including neurons in the brain.

1.1.3 Establishing the neuron doctrine

While technological developments, particularly the invention of the galvanometer during the nineteenth century, allowed the electrical properties of nervous tissue to be directly measured for the first time, parallel advances in optics and microscopy would reveal that the nervous system is composed of many discrete units; namely, neurons.

The earliest documented compound microscope was invented by Dutch lens maker Hans Janssen in 1590, providing up to 9-fold magnification (Ball 1996). Continued refinements led to microscopes with around 50-fold magnification by the mid-seventeenth century, such as that used by Robert Hooke while making observations which would form his *Micrographia*, published in 1665. This book was the first to illustrate the microscopic world, and primarily focused on biological materials, including a sliver of cork which Hooke noted contained many small holes resemblant of tiny rooms or 'cells' (Wickens 2014). Among the first microscopic observations of nervous tissue were those of Antoni van Leeuwenhoek, using instruments he had developed that provided as much as 250-fold magnification (Gest 2004). Leeuwenhoek's reports on the cow optic nerve and turkey cortex, which were included in a series of letters to the Royal Society during the 1670s and 1680s, described the presence of many oily 'globules'. The lack of detail in these early reports reflects an absence of tissue fixation and staining techniques, as well as the small size and intricate structure of neurons and their processes, which would have been difficult to visualise even with Leeuwenhoek's powerful microscopes. Indeed, while biologists had adapted Hooke's terminology to describe the basic building blocks necessary for plant and animal life by 1839, the cellular nature of nervous tissue would remain an issue of contention throughout the nineteenth century (Mazzarello 1999).

Following Leeuwenhoek's observations, further progress towards understanding the microscopic structure of the nervous system would not be made until the 1830s, following a number of technical advances. These included the development of improved achromatic lenses, which substantially reduced optical artefacts (Hughes 1955), the microtome, enabling tissue to be cut at precise, thin intervals (Ideker et al. 2009), and methods for fixing and staining tissue (Jones 2001; Titford 2005). With these tools at their disposal, Jan Evangelista Purkinje and his student, Gabriel Valentin, focused their studies on the brain. In 1836, Valentine published his observation that the nervous system was comprised not only of the nucleated globules previously reported (Figure 1.3A), which we would recognise today as cell bodies or somas, but also a kind of fibre, which he believed existed separately from the cell bodies (Shepherd 2015). Purkinje himself would show in 1837 that different brain regions, including most famously the cerebellum, contained distinct cell types (Cavero et al. 2017). By 1838, Robert Remak had observed the growth of fibres (axons) from cell bodies of the embryonic spinal cord, indicating they must be connected as a coherent structure - findings confirmed by Albert von Kölliker in 1849 (Wickens 2014). However, the cellular nature of nervous tissue was still disputed, due to suggestions that the need for rapid communication necessitated a continuous 'reticular' network of anastomosed fibres.

Despite the first isolated neurons being depicted by Otto Deiters in around 1860 (Figure 1.3B) (Deiters et al. 2013), a definitive refutation of reticular theory would require visualisation of individual neurons, and the full extent of their projections, in intact tissue. While established staining techniques, such as the use of carmine introduced by Joseph von Gerlach in 1858, allowed some cellular structures such as the nucleus to be visualised, they did little to differentiate individual neurons (Heinrichs 2009). This issue was serendipitously resolved by Camillo Golgi in 1873, who, after spilling a silver nitrate solution on tissue hardened using potassium dichromate, found black, sparsely labelled neurons clearly contrasted against a pale-yellow background (Wickens 2014). Golgi applied this technique to study the cellular composition of the cerebellum, neocortex, olfactory bulb, hippocampus, and spinal cord during the 1870s and 1880s (Bentivoglio et al. 2019), revealing for the first time the heterogeneous morphologies of neurons in these regions (Figures 1.3C-E). Based on his observations, Golgi concluded that dendrites ended freely and did not anastomose, updating previous theories to suggest that axons alone fuse to form a reticular network (DeFelipe 2015). However, evidence against reticular theories was building. Auguste Forel, for example, showed in 1887 that

Wallerian degeneration of cranial nerves could be traced to highly localised brainstem regions, clearly contradicting the notion of a continuous reticular network (Parent 2003). Based on his observations of axonal growth in embryonic material, Wilhelm His had also firmly rejected reticulum theory in 1886 (Lopez-Munoz et al. 2006).

It would be Santiago Ramón y Cajal whose application and refinement of Golgi's silver staining method most decisively showed neurons as autonomous units, consistent with the cellular nature of other biological tissues. Shortly after learning about Golgi's method in 1887, Ramón y Cajal set about improving the reliability of the technique using double and triple impregnation steps (Sotelo 2003). This modification also robustly labelled fine axonal processes, allowing them to be traced much further. Using his improved staining method, Ramón y Cajal produced detailed illustrations of neuronal circuitry (see e.g. Figure 1.3F) in regions including the cerebellum, cerebral cortex, olfactory bulb, spinal cord, and retina (Shepherd 2015), while also mapping neuronal development in chick embryos (de Castro et al. 2007). During his observations, Ramón y Cajal found no evidence to support Golgi's reticular hypothesis of axonal fusing, instead noting that many axons ended freely and in close proximity to dendrites. This finding led to the formulation of Ramón y Cajal's 'law of dynamic polarisation' in 1889 (Figure 1.3G), which states that nerve impulses are transmitted unidirectionally from axon to dendrite, accumulating in the soma before being relayed in turn along the recipient neuron's axon (Sotelo 2003). In an 1891 review series, Wilhelm von Waldeyer formalised Ramón y Cajal's conception of nerve cells as the fundamental unit of the nervous system under the 'neuron doctrine' (Jones 1994), which became widely accepted by the early twentieth century. Charles Sherrington would coin the term 'synapse' to describe the hypothesised junction between neurons in 1897 (Molnar et al. 2010), although at the time scientists could only speculate as to how information might pass between neurons.

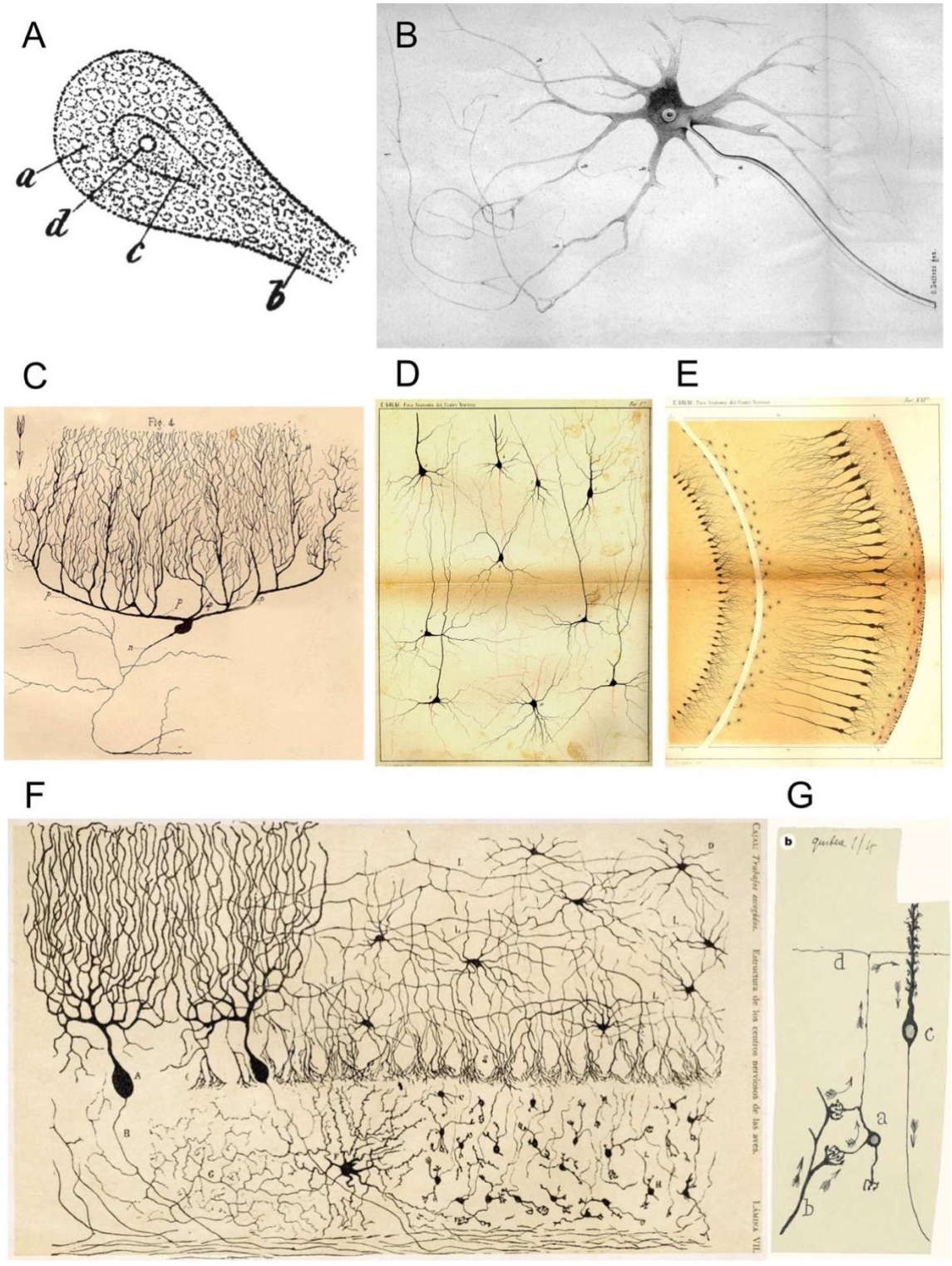

Figure 1.3. *Refer to next page for figure legend*.

Figure 1.3. *Discovery of the neuron, from globules to circuits*. Although the observation of microscopic 'globules' in nervous tissue was first described over a century before, our earliest depictions of these structures come from Gabriel Valentin's 1836 illustrations **(A)** (adapted from Wickens (2014)), which included notation of the cell body (a), a tail-like process (b), the central region of the cell (c), and the nucleus (d). Valentin also recognised the existence of fibres in nervous tissue, which would later be identified as neuronal process and hypothesised to form a continuous 'reticular network'. The first individual neurons to be microscopically examined were isolated and illustrated by Otto Dieters in around 1860 **(B)** (adapted from Deiters et al. (2013)), who found no evidence of a fused system of reticular fibres. The *in situ* morphology of individual neurons was first shown by Camilo Golgi, using the silver staining method he discovered in 1873. This allowed Golgi to describe numerous cell-types across different regions, including the cerebellum **(C)**, cortex **(D)**, and hippocampus **(E)** (adapted from (Bentivoglio et al. 2019). Further advances in silver staining were made by Santiago Ramón y Cajal, enabling him to illustrate the first detailed maps of neural circuitry, characterised by freely ending (rather than anastomosed) fibres (see e.g. **(F)**, depicting different cerebellar cell-types and their interconnections (adapted from Sotelo (2003))). Ramón y Cajal's observations also led him to propose the law of 'dynamic polarisation' **(G)** (adapted from Llinas (2003)), stating that information flows unidirectionally within neurons, from dendrites to axon.

1.1.4 The war of the soups and the sparks

At the turn of the twentieth century, many of the pillars upon which our modern understanding of the nervous system rest were in place; specific behavioural and cognitive modalities had been traced to localised regions in the brain, nervous tissue was known to be electrically active and excitable, and the neuron had been established as the fundamental cellular unit of the nervous system. However, the mechanism by which neurons communicate across the synapse remained unclear. The debate over this issue, which mainly centred on the so-called 'war of the soups and the sparks' during the 1930s and 1940s, pitted pharmacologists advocating for a chemical mechanism against neurophysiologists who favoured electrical transmission (Valenstein 2007).

During the nineteenth century a variety of new compounds, many of which were plant extracts collected from the Americas, Africa, and Asia, were being assayed for biological activity. A convenient test method was to expose visceral organ and skeletal muscle preparations to these substances while assessing effects from stimulating the associated nerves. Using this approach in the 1840s, Claude Bernard found that curare, a poison gifted to him on arrow heads from South America, caused muscle paralysis by acting specifically at the neuromuscular junction (Wickens 2014). Similarly, during the late nineteenth and early twentieth century, John Langley studied a variety of drugs by 'painting' them onto nerves with fine brushes or thread. Among these were muscarine and its antagonist atropine, which he found were active at the terminals of parasympathetic cardiac vagal fibres, and adrenaline, which broadly mimicked the effects of sympathetic nerve stimulation (Valenstein 2007). Langley's observations led him to hypothesise the existence of a 'receptive substance' present in the effector cells (e.g. myocytes), which was activated upon combining with a drug or by delivery of a nerve impulse. Formalised in a 1905 publication, this idea was an important step toward the modern concept of receptor-ligand binding (Maehle 2004). By 1914, Henry Dale had identified noradrenaline and acetylcholine as far more potent sympatho- and parasympathomimetic substances than adrenaline and muscarine, respectively (Todman 2008). However, at the time neither noradrenaline nor acetylcholine were known to be produced naturally in the body.

A series of experiments which would come to prove acetylcholine is secreted from the vagus nerve commenced with a 1921 publication from Otto Loewi (Loewi 1945). Loewi's pioneering experiment used an established frog heart preparation, where the beating heart is bathed in a saline solution with the vagal-sympathetic trunk attached. Following vagal stimulation, which

induced bradycardia, Loewi transferred the solution from this first 'donor' heart to that bathing a second, denervated 'recipient' heart, which then also slowed its beating (Zimmer 2006). Likewise, if the sympathetic nerve was stimulated on the donor heart, transfer of the bathing solution was associated with tachycardia in the recipient heart (Sasse 2018). In Loewi's view, this showed that nerve stimulation did not act on the heart directly, but rather caused the release of specific 'chemical substances' (Loewi 1945). While the veracity of this initial report was questioned, subsequent replication and modifications, including addition of the cholinesterase inhibitor, physostigmine, to the bathing solutions, soon led to general acceptance of neurohumoral transmission to the heart (Valenstein 2007). The likely release of acetylcholine from the vagus nerve was further bolstered by Dale's identification of this substance as a natural product of the body in 1929, based on its isolation from ox and horse spleen (Dale et al. 1929). Despite this, the heart was seen as an exception, with chemical secretions thought too slow to mediate transmission at other peripheral synapses, let alone those in the brain (Eccles 1976).

Further studies at the height of the soups vs. sparks debate would demonstrate that neurotransmitters are released by all peripheral nerves, and also provide strong evidence against electrical transmission. During the 1930's, Dale's laboratory adopted a method for detecting acetylcholine whereby a leech muscle is exposed to blood drawn from veins surrounding the nerve under investigation - in the presence of even very dilute acetylcholine, the leech muscle would contract (Valenstein 2007). In this way, acetylcholine was shown to be released from all parasympathetic terminals, spinal nerves innervating skeletal muscle, and also at sympathetic ganglia, with this latter example being the first evidence for chemical transmission between neurons (Dale 1937). Clarification of postganglionic sympathetic transmission would follow in the 1940s, with Ulf von Euler first isolating noradrenaline from the bovine spleen, showing that it was naturally produced, and then providing evidence for its synaptic release (Sawin 1999). However, neurophysiologists continued to resist the idea of chemical transmission, particularly between neurons. A key issue, which John Eccles would address in 1951, was how electrical transmission could cause neural inhibition. Among the first intracellular recordings from neurons, using a method newly developed by Eccles' laboratory, it was found that inhibitory inputs to spinal motor neurons caused inhibitory post-synaptic potentials (IPSPs) (Eccles 1965). Crucially, this effect was directly opposed to the model of electrical transmission originally favoured by Eccles and instead supported chemical transmission (Wickens 2014), signalling a decisive turning point in the debate.

Over the following decades, evidence for chemical synaptic transmission as the dominant mode of signalling in the brain would steadily accumulate. During the 1950s and 1960s, histochemical staining techniques revealed the first evidence of brain neurons expressing cholinesterase, implying the presence of acetylcholine, and monoamines, including noradrenaline, dopamine, and serotonin (Koelle 1950; Hillarp et al. 1966). Combined with tracing methods, such as Wallerian degeneration of axons from lesion sites (Koeppen 2004) and later the use of antero- and retrograde axonal transport of molecules such as horseradish peroxidase (Lavail et al. 1973), such labelling allowed brain circuitry formed by these neurochemically defined populations to start being mapped. This period also saw refinement of intracerebroventricular and related infusion protocols by Wilhelm Feldberg, who used this approach to study the effects of drugs in various brain regions (Feldberg et al. 1959; 1965). While their discovery was largely serendipitous, the first psychotropic pharmaceuticals were also identified around this time. These substances had major therapeutic benefits for conditions such as depression and schizophrenia and began to shift perspectives on neuropsychiatric disorders towards being a product of 'chemical imbalances' in the brain. Furthermore, the potential to understand, manage, and even cure such conditions provided a clear impetus towards researching how localised brain circuitry modulates cognition and behaviour.

1.2 The development of transgenic neuroscience

A hallmark of twentieth century neuroscience was the identification of chemical substances as neurotransmitters, being released by defined populations of neurons to mediate functional responses in the nervous system and other effector organs. Mechanistic explanations of how neurotransmitters, and all other cellular products, are manufactured would also be discovered during this period, through the developing fields of molecular biology and genetics. Technological developments from these disciplines, introduced here in Section 1.2, have allowed neuroscientist to genetically engineer the nervous system, providing unprecedented insights into its composition and function at circuit, cellular, and subcellular resolution.

1.2.1 Recombinant DNA technology

The identification of DNA as the molecular mediator of heredity was key to the development of techniques that would enable genetic engineering. Theories of particulate inheritance can be traced back to the 1860s, when Charles Darwin hypothesised that 'gemmules' were passed from one generation to the next, and Gregor Mendel described his now famous hybridisation experiments, which implied the existence of discrete hereditary particles (Hartl et al. 1992; Benson 2001). By the early twentieth century, these hereditary particles, or 'genes', had been associated with chromosomes contained in the cell's nucleus (Keros et al. 2010). However, uncertainty remained as to whether genes were carried in DNA, with many scientists instead favouring the more structurally complex protein molecules also found in chromosomes. In 1928, Frederick Griffith reported the first example of bacterial transformation, a type of horizontal gene transfer whereby bacteria acquire new characteristics; the 'transforming' material responsible for this phenomenon was identified in 1944 by Oswald Avery and colleagues as DNA (Cobb 2014). Similarly, in 1952 Alfred Hershey and Martha Chase demonstrated that it was bacteriophage DNA, and not protein, which entered and 'reprogrammed' bacteria to produce viral particles (Hershey et al. 1952). The following year, in a crucial step towards deciphering the genetic code, James Watson and Francis Crick published their landmark paper on the double helix structure of DNA (Watson et al. 1953), building from the crystallographic data of Rosalind Franklin and Maurice Wilkins (Zallen 2003).

With DNA established as the repository of genetic information, the stage was set for scientists to explore the structure and function of individual genes. During the 1960s, progress in

understanding prokaryotic genes was possible in part through a quirk of bacteriophage replication, which causes random segments of the host bacterium's DNA to occasionally be packaged into infectious viral particles (Zinder 1992; Salmond et al. 2015). Using this technique, the function of genes could be assessed by transferring them between different bacterial strains (see e.g. Luria et al. (1960)). While a similar phenomenon had been documented in some viruses which infect mammalian cells, such as simian virus 40 (SV40), this approach was impractical in eukaryotes, partly due to their much larger genomes (Berg et al. 2010). To resolve this issue, Paul Berg explored whether a selected, rather than random, DNA fragment could be integrated into the SV40 genome *in vitro*, with the intention of eventually introducing this foreign DNA into mammalian cells. Combining SV40 DNA with a construct called λ*dvgal*, which contained phage λ replication genes and the *gal* operon, would allow the hypothetical fusion product to be selected for and propagated in *Escherichia coli* (Berg et al. 2010). A key development facilitating this experiment was the discovery of bacterial enzymes, called restriction endonucleases, which defend against viral infection by cleaving DNA at specific recognition sites. Berg and his student Janet Mertz found that *Eco*RI, a restriction endonuclease isolated by Herbert Boyer in 1971 (Boyer 2009), cut the SV40 and λ*dvgal* plasmids only once, leaving cohesive or 'sticky' overhangs which annealed to one another and allowed the two sequences to be ligated (Mertz et al. 1972).

Despite Berg being convinced by colleagues not to continue with his experiment (Berg et al. 2010), based on concerns about the potential hazards of introducing SV40, an oncogenic virus, into bacteria which natively colonise the human gut, Boyer and Stanley Cohen would soon confirm that recombinant DNA could be propagated and expressed in *E. coli*. Around the time of Berg and Mertz's experiments with *Eco*RI, Cohen's laboratory had devised a method for transforming calcium chloride-treated *E. coli* with plasmid DNA (Cohen et al. 1972). This method not only introduced antibiotic resistance genes, but also provided a means of cloning plasmids, which were autonomously replicated and passed to the transformed *E. coli*'s progeny. In 1973, Boyer and Cohen collaborated on a project in which separate kanamycin and tetracycline-resistant plasmids were cut with *Eco*RI and ligated, with the resultant construct transformed into *E. coli*. Growth of the transformed bacteria in the presence of both antibiotics, and subsequent molecular analyses, proved that recombinant DNA had for the first time been successfully cloned and expressed (Cohen et al. 1973). The first instance of gene transfer between species was reported in 1974 by Cohen and Annie Chang, who transformed *E. coli* with a recombinant plasmid containing a *Staphylococcus aureus* gene for penicillin resistance (Chang et al. 1974). Soon after, eukaryotic DNA, specifically that encoding ribosomal RNA from the

African clawed frog (*Xenopus laevis*), was also cloned and expressed in *E. coli* (Morrow et al. 1974), with the profound implication that this approach could be applied to DNA from essentially any source (Cohen 2013).

The years following these pioneering experiments have seen the toolbox for producing recombinant DNA molecules and genetically modified organisms (GMOs) greatly expand, being applied in such diverse fields as agriculture and medicine, while also sparking debate over the potential risks of this powerful new technology (Cederbaum et al. 1984; Berg et al. 1995; Devos et al. 2008; Fagerstrom et al. 2012). In addressing uncertainty around risks posed by the experiments planned in Berg's laboratory in 1971, as well as those carried out by Boyer, Cohen, and colleagues in the subsequent years, guidelines on the safe handling and containment of GMOs were agreed to by researchers in 1973 (Berg et al. 1974; 1975). These recommendations, along with a self-imposed moratorium on certain types of experiments, were replaced in 1976 with the publication of the *Guidelines for Research Involving Recombinant DNA* by the United States (US) National Institutes of Health (NIH). Guidelines on the use of recombinant DNA and genetic engineering continue to be issued by the NIH and equivalent regulatory bodies globally, with adherence to these policies likely responsible for the absence of any documented public health or environmental hazards associated with this technology to date, despite its widespread use. In 1982, recombinant human insulin, marketed as 'Humulin', became the first recombinantly expressed therapeutic approved by the US Food and Drug Administration, with over 90 other recombinantly produced therapeutics having been approved since (Kinch 2015). The use of GMOs in research has also allowed fundamental questions of biology to be addressed in innovative ways, with this approach now common practice in neuroscience.

1.2.2 Transgene delivery to the nervous system

A natural extension from introducing foreign genes to bacteria was applying this concept to eukaryotes. As the safety of laboratory work involving GMOs became apparent, Berg resumed his experiments and by 1980 had succeeded in expressing a variety of exogenous genes in cultured mammalian cells (Mulligan et al. 1980). Berg was also the first to develop recombinant viruses for this purpose, adapting SV40 as a vector to deliver foreign genes into target cells (Goff et al. 1976). This approach has proven to be among the most effective methods for transgene delivery in eukaryotic cells, although early SV40 and retroviral constructs suffered from transient expression and cytotoxicity, in part due to their retention of native viral genes and manner of

integration into the host cell's genome (Elder et al. 1981; Xu et al. 1989). Replication-deficient adenoviral constructs, which emerged in the early 1990's, were the first vectors to efficiently transduce post-mitotic cells *in vivo*, including neurons (Akli et al. 1993; Crystal 2014). However, early adenoviral vectors also exhibited transient expression, largely due to immune activation by adenovirus capsid proteins and expression of viral genes (Wold et al. 2013). This issue was soon resolved with the development of recombinant adeno-associated viral (AAV) (Kaplitt et al. 1994) and lentiviral (Naldini et al. 1996) vectors containing transgenic sequences alone, without any native viral genes (Figure 1.4A), rendering them both replication-deficient and much less immunogenic (Blomer et al. 1997). As such, both AAV and lentiviral vectors can provide long-term neuronal transgene expression *in vivo* and have become two of the most widely adopted vectors in modern neuroscience.

Depending on their method of administration and entry into neurons, certain viral vectors can undergo retro- or anterograde spread within neural circuits. This typically involves exposure of a neuron's distal projections to the vector, either directly in injectate or via transsynaptic 'jumping' from another neuron, which is then internalised and trafficked to the soma, where its transgene cargo can be expressed (Figure 1.4B). As the nervous system is not the primary target of naturally acquired adenoviral (Wold et al. 2013), AAV (Wang et al. 2019a), or lentiviral (Haase 1986) infection, vectors derived from these viruses are most effective in transducing neural soma at site of injection, and tend not to undergo active transport in neurons. Exceptions to this include vectors with artificially engineered capsids or envelopes (Tervo et al. 2016; Kobayashi et al. 2017), as well as some naturally occurring AAV serotypes (Rothermel et al. 2013; Zingg et al. 2017), which can exhibit antero- or retrograde transport. Canine adenovirus type 2 (CAV2) has also been developed as an efficient vector for retrograde transduction of neurons (Del Rio et al. 2019). In contrast, many vectors used for transsynaptic gene delivery are derived from viruses that specifically target the nervous system, either to actively replicate or establish latent infections. These include herpes simplex virus (HSV), pseudorabies virus (PRV), and rabies viral vectors. Due to their cytotoxicity, such vectors are limited to short-term applications, particularly replication-competent vectors which spread across multiple synapses (Saleeba et al. 2019). Replication-deficient rabies (Wickersham et al. 2007a) and HSV (Zeng et al. 2017) vectors have also been developed that are compatible with monosynaptic retro- or anterograde spread, respectively, from a population of 'seed' neurons, in which genes required for vector production are supplied *in trans*.

Simultaneous with the development of recombinant viral vectors, the first transgenic lines of mice were also being created. With the development of genetics as a distinct discipline at the turn of the twentieth century, inbred mouse strains were acquired from 'fanciers' for standardisation and use in research (Rader 2004). Although the aesthetic traits artificially selected for in these strains provided immediate utility in studying heredity, there remained a need for methods to study gene regulation and cell differentiation *in vivo*. In searching for tools to address these questions, multiple independent laboratories introduced recombinant DNA constructs containing foreign genes into the pronucleus of fertilised mouse eggs *in vitro* during the late 1970s and early 1980s (Myelnikov 2019). Transfer of microinjected eggs to the oviduct of pseudopregnant females led to the development of mice in which most, if not all, cells appeared to contain and be capable of expressing the introduced genes (Gordon et al. 1980; Wagner et al. 1981a), which also underwent germline transmission (Costantini et al. 1981; Wagner et al. 1981b). Chromosomal integration of this recombinant DNA allowed for its stable propagation, however the site at which integration occurred was random. By 1988, techniques were established for the efficient introduction of DNA constructs to specific chromosomal loci through homologous recombination in mouse embryonic stem cells (Mansour et al. 1988), which could be used to generate germline chimeras and eventually homozygous mutants. These targeted mutations allowed endogenous genes to be 'knocked-out', and edited or foreign DNA to be 'knocked-in', typically causing a loss or gain of function, respectively (Capecchi 2005). Embryonic stem cell approaches have recently been superseded by CRISPR/Cas9-based gene editing, which is faster, simpler, and much more easily applied across different species (Singh et al. 2015).

In addition to providing effective local or global genetic modifications, the combinatorial use of viral vectors and transgenic animals greatly expands the utility of these assets. Such approaches are often facilitated through the use of microbial recombinases, such as the phage-derived Cre-*Lox* system (Sauer et al. 1988), or the analogous Flp-*frt* system from yeast (O'Gorman et al. 1991). In the presence of Cre or Flp recombinase, sequences flanked by the corresponding recognition sites (i.e. *Lox* or *frt*) can be inverted in, or excised from, a DNA molecule, providing a mechanism for conditional gene expression or deletion (Figure 1.4C,D). For example, expression of a 'floxed' (*Lox*-flanked) gene carried by a transgenic animal can be altered by transduction with a Cre-expressing viral vector (see e.g. Stec et al. (2002)). While the nature of these manipulations ultimately depends on the desired experimental outcomes, the ever-increasing variety of recombinant viral vectors and transgenic animals available provides great

flexibility in introducing transgene expression to the nervous system. These resources are also of fundamental importance to cell-type specific expression of transgenes in neural populations of interest, as explored below in Section 1.3.3.

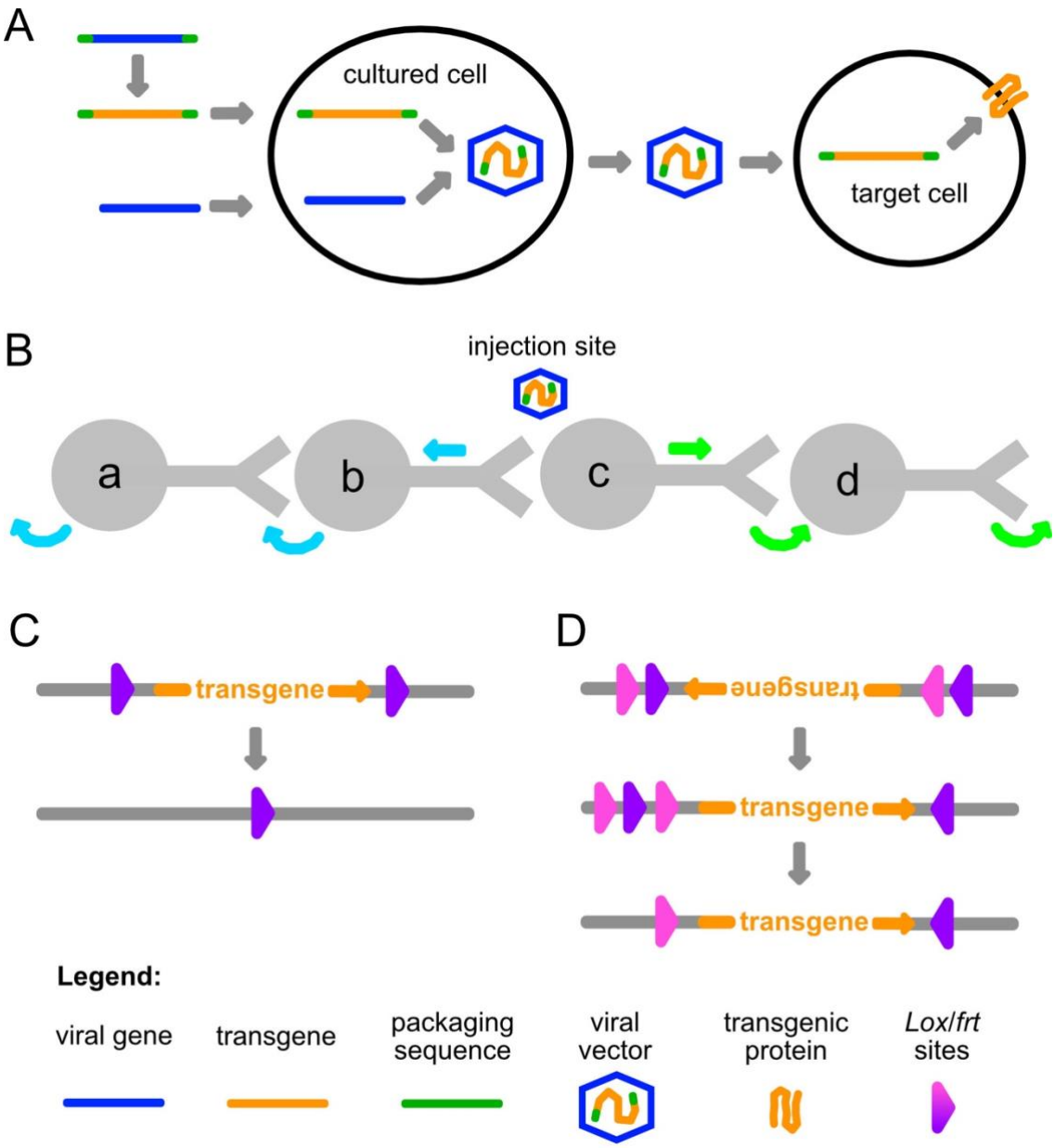

Figure 1.4. *Refer to next page for figure legend*.

Figure 1.4. *Molecular approaches for transgene delivery*. A common method for introducing transgenes into neuronal populations *in vivo* is the use of replication-deficient viral vectors, whose spread is more readily controlled and less immunogenic than replication-competent vectors. Schematic **(A)** depicts the production and application of replication-deficient viral vectors. The use of recombinant DNA technology allows genes necessary for virion replication to be removed from the viral genome and replaced with sequences encoding transgenes of interest, fusing them to signals for viral packaging. Introduction of both the modified viral genome and, via a separate construct, the genes necessary for virion production into cultured cells enables replication-deficient vectors to be assembled and harvested. As replication-deficient vectors cannot spread in the absence of the removed viral genes, they can be used to target transgene delivery selectively to populations of interest. An overview of methods to target neural circuits is shown in **(B)** (developed from concepts in Saleeba et al. (2019)). Many vectors do not undergo transport within neurons, including most AAVs and lentiviruses, meaning they would only transduce cell bodies of population (c) at the injection site. Replication deficient vectors that are retro- or anterogradely transported (blue and green arrows, respectively) can undergo further spread from the injection site or population (c) to transduce populations (b) or (d), respectively; examples include CAV2 and some AAV serotypes. Supplying viral replication genes *in trans* can allow further monosynaptic retro- or anterograde spread; for example, expression of the rabies G protein in population (b) would allow monosynaptic spread of replication-deficient rabies vectors to the upstream population (a). Some protocols also allow the use of replication-competent vectors for polysynaptic spread (e.g., some forms of HSV and rabies vector). Additional control of transgene expression using viral vectors and/or germline transgenic animals can be achieved using recombinase recognition sites such as *Lox* or *frt*, whose positioning and orientation can be utilised for conditional gene deletion **(C)** or expression **(D)** in the presence of the corresponding recombinase/s (developed from concepts in Schnutgen et al. (2003)).

1.3 Transgenic approaches in modern neuroscience

As the nervous system has become amenable to genetic engineering, a variety of genes have been isolated, engineered, and applied specifically for the study of neuronal structures and functions. Such transgenic approaches provide researchers not only with substantial diversity and sophistication in terms of the introduced constructs, but also unparalleled spatiotemporal control over their experimental design. Section 1.3 introduces the main categories of transgenes developed for neuroscientific applications to date, as well as concepts underlying their directed expression in specific cell-types or subcellular structures of interest.

1.3.1 Visualising circuitry

Among the advances made in visualising neural circuitry since the development of silver staining techniques by Golgi and Rámon y Cajal during the late nineteenth century, none have been as revolutionary as the heterologous expression of fluorescent proteins, accompanied by advances in fluorescent and confocal microscopy which enable their imaging. Transgenic studies of the nervous system initially relied on enzymes, such as β-galactosidase, to visualise transgene expression in neurons. However, such approaches were hindered by cumbersome staining protocols using exogenously applied chromogenic substrates, making their application to living tissue impractical. This obstacle was overcome in the early 1990s, when the green fluorescent protein (GFP) gene of the jellyfish *Aequoria victoria* was first cloned, expressed, and visualised in *E. coli* and the nematode worm *Caenorhabditis elegans* (Prasher et al. 1992; Chalfie et al. 1994). Crucially, these studies indicated that GFP fluorescence could be produced in any cell type, independently of other substrates (Chalfie et al. 1994). This was later shown to be due to the GFP chromophore being composed of a cyclic tripeptide, entirely encoded by its polypeptide sequence and formed during posttranslational processing (Ormo et al. 1996). As such, all that is required to visualise GFP in fixed or living cells is exposure to blue light (Chalfie et al. 1994; Okada et al. 1999).

Over the following decades, the discovery and engineering of new GFP-like proteins has produced a vibrant catalogue of genetically encoded fluorophores (Figure 1.5A). Screens of *Aequoria* GFP derivatives, following directed or random mutagenesis, have identified numerous variants with emission spectra in blue, green, and yellow wavelengths (Rodriguez et al. 2017). Various ‘enhanced’ versions of these proteins are also available. Enhanced GFP (EGFP), for

example, includes mutations and codon changes for optimal expression in mammalian cells and compatibility with imaging hardware (Cormack et al. 1996; Zolotukhin et al. 1996). Additional red-shifted variants were also of interest due to the reduced autofluorescence and light scattering of longer wavelength emissions. While these could not be engineered from *Aequoria* GFP, a number of naturally occurring yellow, orange, and red fluorescent proteins have been isolated from other marine species (Miyawaki 2005). The first of these, *Ds*Red, was cloned from the coral *Discosoma striata* in 1999 (Matz et al. 1999). While *Aequoria* GFP typically dimerises only under specific conditions, most other wild-type fluorescent proteins strongly oligomerise, including *Ds*Red, which exists as tetramer (Baird et al. 2000). As this oligomerisation can interfere with cellular processes, particularly where the fluorophore is being used to tag other proteins (see below), developing monomeric derivatives of *Ds*Red became a priority. This led to the creation of monomeric red fluorescent protein 1 (mRFP1) (Campbell et al. 2002), followed by the 'mFruit' series, with emission peaks ranging from yellow (mBanana) to far-red (mPlum) (Shaner et al. 2004; Wang et al. 2004). Despite difficulties concerning cofactor reliance and dim emission intensities, a further push towards near-infrared fluorescent proteins derived from bacterial phytochromes is also underway (Rodriguez et al. 2016; Rodriguez et al. 2017). In all, thousands of fluorescent proteins are now available, the details of which are being actively consolidated in online databases (Lambert 2019).

Given their reliable expression, low toxicity, and ease of visualisation, fluorescent proteins were quickly adopted for studying the nervous system (Okada et al. 1999; Feng et al. 2000). An immediate application was the mapping of neurons and their fine, branching processes, through which fluorescent proteins can spread via cytosolic diffusion (Chalfie et al. 1994). Using selectively trafficked viral vectors to mediate their expression, fluorescent proteins also enable complex interconnected circuitry to be mapped, largely supplanting chemical antero- and retrograde neural tracers developed in the 1970s and 1980s (Saleeba et al. 2019). The use of 'split' fluorescent proteins, specifically reconstituted at synaptic contacts, further enriches potential insights of such circuit tracing studies (Kim et al. 2012). Additionally, the expanding spectrum of fluorescent protein emission profiles allows multiple neurons and pathways to be labelled in a single animal. This is perhaps best exemplified by the *Brainbow* strategy, where stochastic recombination of *Lox/frt* flanked fluorescent proteins is used to label and map individual neurons and their processes with up to 100 distinct colour combinations (Livet et al. 2007; Cai et al. 2013). Understanding protein expression and trafficking within neurons has also been facilitated by fluorescent proteins, which can be fused with endogenous proteins, or used

in isolation, to monitor activity from regulatory DNA associated with a gene of interest (Kallal et al. 2000; Chudakov et al. 2005). Importantly, well-designed fluorescent protein fusion constructs typically do not affect the partner protein's functionality, allowing a variety of native and introduced gene products to be tagged and visualised directly.

Through the development of engineered constructs with dynamic emission spectra or intensities, fluorescent proteins can also facilitate the real-time visualisation of neuronal activity *in vivo*. This approach typically relies on conformational changes in a fusion partner, which affects fluorescent emissions either by shifting the distance between two fluorescent proteins, which can be detected as a change in Förster resonance energy transfer (FRET), or, more often, by conformationally altering the fluorescent protein itself through circular permutation (Figure 1.5B,C) (Lin et al. 2016). Directly measuring voltage changes across the plasma membrane using genetically encoded voltage indicators (GEVIs), which couple fluorescent proteins with ion channel-, phosphatase-, or rhodopsin-derived voltage-sensitive domains, has been a key priority (Wang et al. 2019b). Although the need for plasma membrane localisation, fast kinetics, photostability, and high signal-to-noise ratio (SNR) has made this endeavour technically challenging (Peterka et al. 2011), several GEVIs have been used to detect action potentials *in vivo* (Gong et al. 2015; Bando et al. 2019).

Rather than direct visualisation of voltage changes, the downstream effects of membrane depolarisation have to date proven more reliably detectable. For example, genetically encoded calcium indicators (GECIs), the most commonly used fluorescent sensors, take advantage of conformational changes in the calcium-binding protein, calmodulin, to monitor intracellular calcium fluctuations associated with neural activity. These were initially developed as the FRET-based 'cameleon' fusion constructs (Miyawaki et al. 1997), although 'GCaMP' GECIs, containing a single circularly permuted fluorescent protein, have been much more widely adopted (Chen et al. 2013). Increased intracellular calcium in turn facilitates neurotransmitter release, which can itself be detected using fluorescent proteins sensitive to the differing pH environments within presynaptic vesicles and the synaptic cleft (Figure 1.5D) (Miesenbock et al. 1998). Several methods have also been developed to visualise transmission of individual neurotransmitter species *in vivo*, including G-protein coupled receptor (GPCR)-based fluorescent sensors for dopamine (Patriarchi et al. 2018; Sun et al. 2018), norepinephrine (Feng et al. 2019), and acetylcholine (Jing et al. 2020).

Although fluorescent indicators have not yet reliably matched the precision of patch-clamp electrophysiology for recording activity in individual neurons, they do offer several advantages. These include the ability to take repeated measurements from neurons over extended periods of time, study fine structures such as dendritic spines, and monitor the network dynamics of large populations without highly invasive electrode arrays, all of which can be achieved in conscious, behaving animals using implantable or multiphoton imaging devices (Peterka et al. 2011; Yang et al. 2017). The use of transmitter-specific sensors, and the genetically encodable nature of fluorescent indicators (discussed further below), also allows their targeted expression in circuits of interest. As such, these and future fluorescent protein-based constructs offer opportunities to study the structure and activity of the nervous system with unprecedented detail.

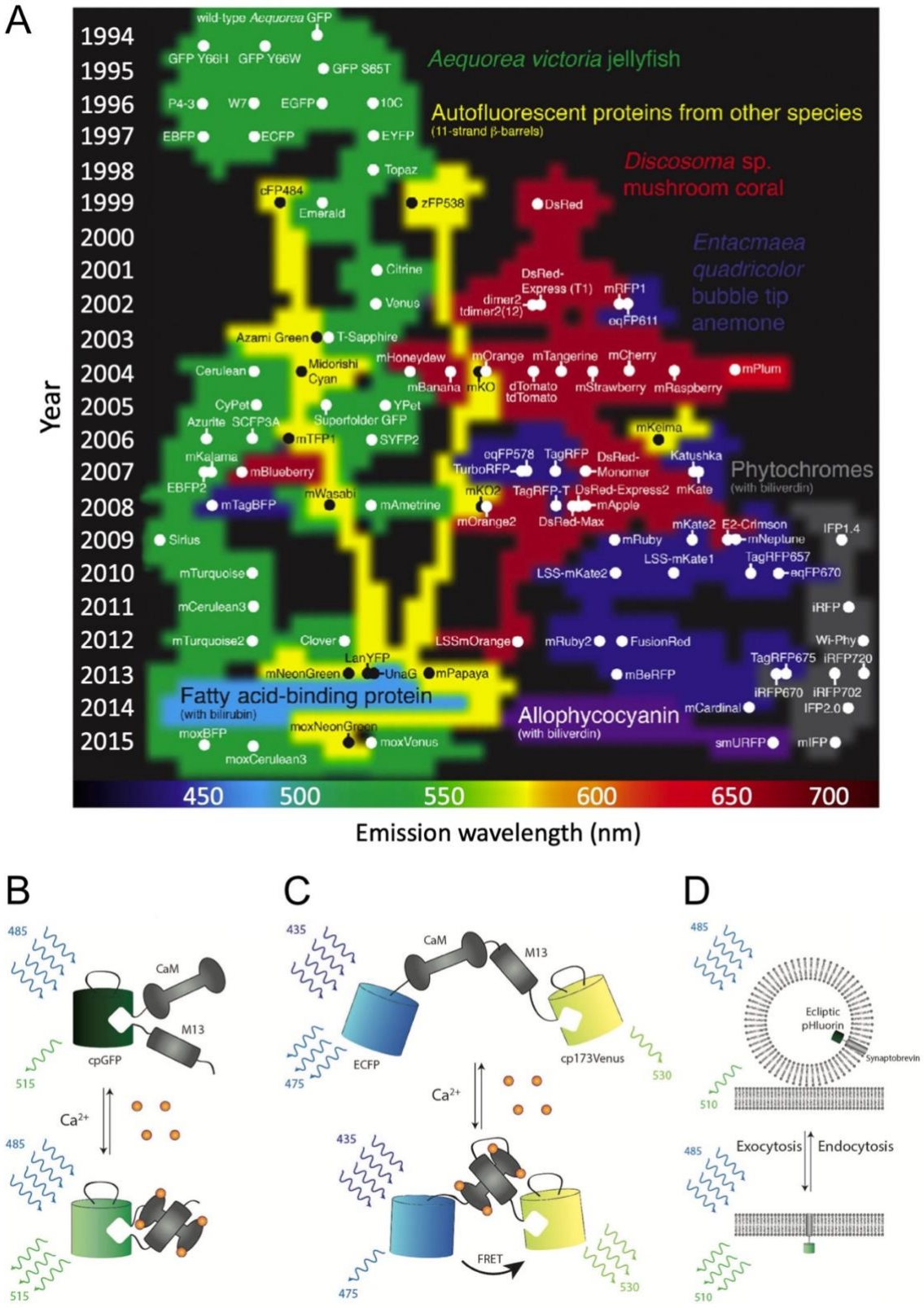

Figure 1.5. *Refer to next page for figure legend*.

Figure 1.5. *Fluorescent proteins and sensors*. Since the cloning of GFP from *A. victoria* in 1992, a range of fluorescent proteins have been discovered and engineered. An illustration of this diversity is provided in **(A)** (adapted from Rodriguez et al. (2017)), with fluorophores graphed according to their peak emission wavelength (x-axis) and year of development as transgenic tools (y-axis). Each protein is also classed based on its source, highlighting the blue to yellow variants developed from wild-type GFP, the yellow to red *Ds*Red derivatives, and the far-red phytochrome-based fluorescent proteins. Several mechanisms have also emerged by which fluorescent proteins can be used to monitor neuronal activity. These rely on fluctuations in emission intensities caused by conformational changes in circularly permuted proteins **(B)** or fusion partners which alter the distance between FRET pairs **(C)**. While the calcium-binding calmodulin (CaM) and M13 proteins are used as an example here, these principles have been applied to many other fusion partners, including enzymes and GPCRs. Aspects of the cellular environment can also affect fluorescent emissions, such as pH differences between the vesicular lumen and synaptic cleft **(D)** (**(B-D)** adapted from Broussard et al. (2014)).

1.3.2 Manipulating activity

While optical readouts from fluorescent protein-based sensors allow the endogenous activity of neural circuitry to be monitored and associated with particular functions, such correlations do not necessarily demonstrate a causal link. It is therefore important to support these observational data with experiments showing that the hypothesised behaviour or physiological process can be induced and disrupted through manipulation of the relevant circuitry (Kim et al. 2017; Wang et al. 2019b). A variety of transgenic approaches are now routinely used in neuroscience to address such questions, by providing targeted manipulation of cell signalling and membrane potential *in vivo*. The defining characteristic of these approaches is their use of introduced genes to make neurons sensitive to otherwise biologically inert stimuli; in the two most commonly used techniques, opto- and chemogenetics, these take the form of light and chemical substances, respectively.

Optogenetics, which involves the use of light-sensitive microbial opsins to alter ion permeability or transport across the neuronal membrane (Figure 1.6A), provides the most direct method for manipulating membrane potential and hence neural activity. The idea that light could be used to control neural activity was proposed as early as 1979 by Francis Crick, although a practical mechanism for this approach would not emerge until several decades later (Yizhar et al. 2011). The first demonstration of optogenetic control over neuronal activity utilised channelrhodopsin-2 (ChR2), an algal cation-conducting opsin (Nagel et al. 2003). On exposure to blue light, which opens the ChR2 pore, Boyden et al. (2005) reliably recorded action potentials in cultured mammalian neurons expressing this transgene. Evidence of ChR2-mediated neuronal depolarisation was soon followed by the first examples of optogenetic hyperpolarisation or inhibition, involving the archaeal ion pumps halorhodopsin (*Np*HR) and archaeorhodopsin-3 (Arch), which drive inward chloride or outward proton transport, respectively (Zhang et al. 2007; Chow et al. 2010). Many more opsins have since been discovered and engineered, varying in their kinetics, spectral sensitivity, ion selectivity, and channel conductance (Mahn et al. 2020). An informative example comes from the anion-conducting channelrhodopsins (ACRs), which have been both engineered from ChR2 (Berndt et al. 2014; Wietek et al. 2014) and found in nature (Govorunova et al. 2015). ACRs have several advantages over *Np*HR and Arch pumps as inhibitory tools, including their generation of much stronger photocurrents and inability to move ions against physiological gradients (Cho et al. 2016).

In contrast to optogenetics, chemogenetic actuators are responsive to chemicals which are otherwise inert in mammalian systems, either due to mutation of native receptors, or heterologous expression of genes from other, usually invertebrate, species. Early chemogenetic tools, such as the GPCR-based Receptors Activated Solely by Synthetic Ligands (RASSLs) (Coward et al. 1998), suffered from high basal activity and off-target ligand binding (Sternson et al. 2014). These were superseded by the Designer Receptors Exclusively Activated by Designer Drugs (DREADDs), created through the directed evolution and engineering of human muscarinic and κ-opioid GPCRs for sensitivity to the drug metabolites clozapine-N-oxide (CNO) and salvinorin B, respectively (Armbruster et al. 2007; Vardy et al. 2015). Both neuronal inhibition and excitation have been demonstrated using DREADDs, according to their G-protein coupling characteristics (Figure 1.6B), making them valuable tools which have gained wide-spread use (Atasoy et al. 2018). This is despite some non-specific ligand binding, which remains an issue but can be accounted for using appropriate experimental controls (discussed further below) (Goutaudier et al. 2019). Invertebrate (Slimko et al. 2002) and engineered mammalian (Magnus et al. 2011; Magnus et al. 2019) ligand-gated ion channels (LGICs) have also been developed for chemogenetic control of neuronal hyper- or depolarisation (Figure 1.6C). The use of invertebrate GPCR systems, particularly the insect neuropeptide allatostatin (Ast) and its receptor (AstR) (Lechner et al. 2002), has provided an additional approach to chemogenetic modulation. While most chemogenetic receptors require their corresponding ligands to be locally or systemically infused, Ngo et al. (2020) capitalised on the genetically encodable nature of Ast for circuit-specific chemogenetic inhibition of AstR-expressing neurons.

A number of advantages and limitations must be considered when employing opto- and chemogenetic tools. Optogenetics provides precise temporal control over neuronal activity in the order of milliseconds to seconds (Boyden 2015). However, invasive fibre optic implants are typically required, with light scattering and absorption limiting the affected tissue volume and potentially causing unintended effects from heating (Yizhar et al. 2011; Owen et al. 2019). The ability to deliver chemogenetic ligands systemically makes this approach less invasive, but limits temporal, and often also spatial, targeting (Atasoy et al. 2018). Measures to control and account for any off-target effects of chemogenetic ligands and their metabolic products are also essential, as highlighted by the conversion of peripherally administered CNO to clozapine (Gomez et al. 2017), a drug known to interact with multiple endogenous receptor systems (Coward 1992). Optogenetics is therefore often best suited to acute manipulations in a defined region of interest, while chemogenetics generally provides more spatial flexibility and is most

appropriate for chronic interventions. Both opto- and chemogenetics are compatible with the fluorescent sensors described above, allowing direct optical readouts of activity from manipulated neurons, although it is important to account for overlap between opsin and sensor spectral properties (Kim et al. 2017).

A major advantage of the tools describe here in Section 1.3 is that they are genetically encoded. As such, their production can be limited to specific cell-types or circuits of interest. This is a significant advance from traditional techniques outlined in Section 1.1. For example, focal lesion methods, stemming from Fluorens' experiments localising the respiratory centre, create permanent damage across multiple neuronal populations and, depending on the approach used, any fibres of passage (Vaidya et al. 2019). Opto- and chemogenetic approaches, in contrast, provide reversible silencing of activity only in neurons expressing these transgenes. Similarly, while electrical stimulation was crucial to early functional mapping studies, delivered currents cannot be restricted to circuitry of interest beyond the level of physical distance from an electrode (Tehovnik 1996). The electrical activity of genetically defined populations, and even their subcellular components such as the axon or dendrites, can be controlled over milliseconds to hours using transgenic approaches. Although pharmacological methods developed from the pioneering work of Dale and Loewi provide specificity at the level of neuronal receptor expression, chemogenetic technologies allow further refinement of the circuitry targeted, with additional temporal precision over neuronal activity offered by optogenetics. As such, the development of techniques for targeting transgene expression to experimentally important neuronal populations and subcellular structures has become a key focus of neuroscience research.

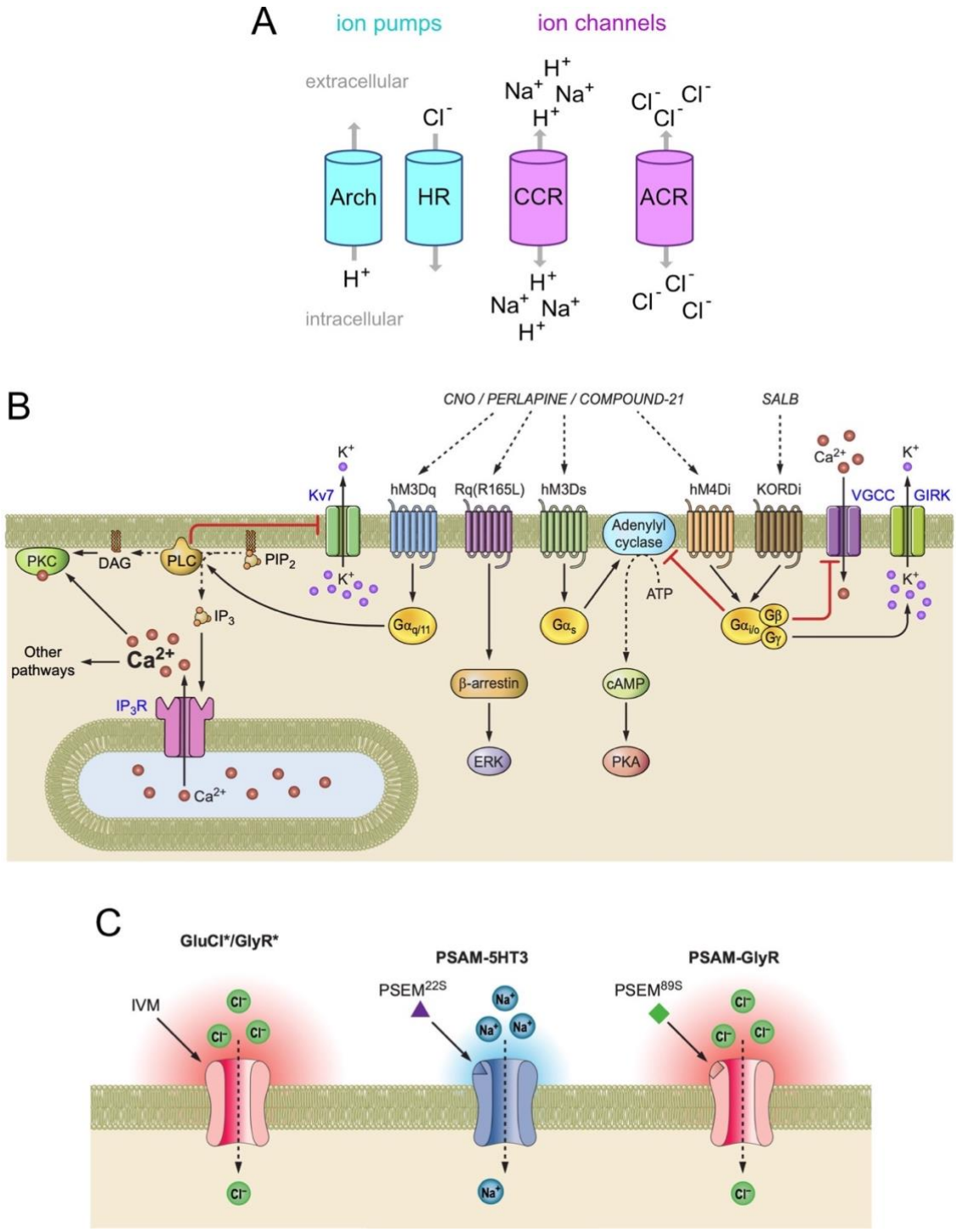

Figure 1.6. *Refer to next page for figure legend*.

Figure 1.6. *Transgenic actuators for manipulating neural activity*. The two most widely adopted types of transgene for altering neural activity are opto- and chemogenetic actuators. Optogenetic actuators, or opsins **(A)**, facilitate ion movement across the neuronal membrane in response to light of specific wavelengths. Some commonly used opsins include the hyperpolarising archaerhodopsin (Arch) and halorhodopsin (HR) ion pumps, and the cation- and anion-conducting channelrhodopsins (CCRs and ACRs), which are generally depolarising and hyperpolarising, respectively. Among chemogenetic actuators, the Designer Receptors Exclusively Activated by Designer Drugs (DREADDs) have been the most widely used. DREADDs are mammalian GPCRs which have undergone directed evolution for activation by otherwise biologically inert drug metabolites, allowing cell-type specific neural activation or inhibition via G-protein-mediated signalling cascades **(B)**. Several ligand-gated ion channels (LGICs) have also been developed for chemogenetic applications **(C)**, including *C. elegans* chloride channels (GluCl/GlyR) activated by the antiparasitic chemical ivermectin (IVM), and the mutated mammalian LGICs called pharmacologically selective actuator modules (PSAMs), which are activated by pharmacologically selective effector molecules (PSEMs) (**(B,C)** adapted from Atasoy et al. (2018)).

1.3.3 Cellular and subcellular localisation

The development of transgenic approaches in neuroscience has facilitated a refinement of functional localisation, from that originating with lesion and stimulation of gross anatomical structures to modern concepts at the level of individual cell types and the circuits they form. This has resulted in the delineation of intermingled, but functionally distinct, populations of neurons (see e.g. Harris et al. (2013); Janak et al. (2015)), as well as the identification of functional networks distributed throughout the brain, such as those comprising memory engrams (Poo et al. 2016). Data gleaned from such studies provide unprecedented insights into how information is processed by the nervous system, while also identifying novel therapeutic targets and strategies. As such, the ongoing development of molecular tools for targeted transgene expression within the nervous system is a key research priority and forms the basis of experiments described in the current thesis.

The first level at which cell-type specific expression can be achieved is through the method of transgene delivery employed. In the context of viral vector-mediated transgene delivery, selective expression in anatomical regions of interest can be achieved through stereotaxic injections to relevant coordinates. This can be extended to target neurons based on their afferent inputs or projection targets, using strategic injections of retro- or anterogradely transported vectors (reviewed in Section 1.2.2). A further degree of targeting is provided by the mechanism of uptake for each viral vector, which results in a preferential transduction of specific cell-types, referred to as cell 'tropism'. For example, cells expressing the AAV receptor (AAVR) are efficiently transduced by AAV vectors (Pillay et al. 2016), while tropism for CAV2 vectors is mediated by the coxsackievirus and adenovirus receptor (CAR) (Soudais et al. 2000). Although the catalogue of naturally occurring viral vector capsids and envelopes allows a variety of cell-types to be transduced, further refinement has been achieved by artificially engineering vectors and their target cells. Altered tropism for CAV2 vectors, for example, has been demonstrated through heterologous expression of CAR in neurons of interest (Li et al. 2018). Similarly, rabies vectors psuedotyped with the avian sarcoma and leukosis virus (ASLV) envelope glycoprotein, 'EnvA', can selectively transduce mammalian neurons of interest through their heterologous expression of the corresponding avian TVA receptor (Wickersham et al. 2007b). An alternative approach, developed by Viviana Gradinaru's laboratory, employs 'barcoded' AAV libraries to screen for capsids with desired target tropism *in vivo* (Deverman et al. 2016; Chan et al. 2017).

Once inside the target cell, an additional layer of control over transgene expression is provided by regulatory DNA sequences. As every cell in the body contains the complete set of an organism's genes, the array of phenotypes observable between different populations is largely a consequence of how gene expression is regulated. An important aspect of gene regulation stems from non-coding DNA elements with which transcription factors interact, such as the promoter region immediately upstream of a gene's coding sequence. In some cases, virally mediated transgene expression can be targeted to genetically defined populations directly through the use of short promoter sequences (Walther et al. 1996). However, given the limited packaging capacity of viral vectors, this approach often fails to incorporate all necessary regulatory elements, leading to non-specific expression. This can be resolved through the development of germline transgenic animals carrying much larger constructs, such as bacterial artificial chromosomes (BACs), in which the transgenic coding sequence is flanked by long sequences of non-coding DNA associated with the gene of interest (Schmidt et al. 2013). Cell-type specific Cre-recombinase expression is a common approach in such transgenic animals (Luo et al. 2020), providing a flexible platform from which to express Cre-dependent transgenic actuators, sensors, or markers delivered via viral vector transduction or genetic cross with a separate transgenic line.

The subcellular localisation of an expressed transgene can have additional consequences for its function and utility. An illustrative example of this is provided by the archaeal *Np*HR and Arch opsins, which exhibit poor membrane trafficking and form intracellular aggregates when expressed in mammalian cells (Gradinaru et al. 2008; Mattis et al. 2011). This expression pattern is suboptimal for several reason, including a reduced capacity to affect ion movement across the plasma membrane, and hence neuronal excitability. Fusion with signal peptide, endoplasmic reticulum export, and membrane trafficking motifs, derived from native mammalian proteins, has generated enhanced versions of *Np*HR and Arch (e*Np*HR3.0 and eArch3.0, respectively) with greatly improved membrane localisation and associated photocurrents (Gradinaru et al. 2010; Mattis et al. 2011). Subcellular localisation has also been a key consideration for GEVI development, where the electric field generated by action potentials rapidly dissipates with distance from the plasma membrane (Peterka et al. 2011). The complex morphology of neurons, comprising structurally, biochemically, and functionally distinct axonal, dendritic, and somatic compartments, further emphasises the need for subcellular targeting of transgene expression in neuroscience. A range of transgenic actuators and sensors have emerged with targeted subcellular expression over recent years, again typically directed by fusion with trafficking motifs

derived from endogenously localised proteins (Rost et al. 2017). Some examples include an axonally targeted DREADD (Stachniak et al. 2014), axonal and dendritic GCaMPs (Mao et al. 2008; Broussard et al. 2018), and soma-localised opsins (Wu et al. 2013; Baker et al. 2016).

The following Chapters describe experiments conducted to develop novel molecular tools for targeted transgene expression across these levels of resolution in the rat brain. The use of short promoter sequences to achieve cell-type specific viral vector transduction of *nucleus incertus* relaxin-3 circuitry, a key modulator of arousal and emerging therapeutic target, is explored in Chapter 2. Data described in Chapter 3 focus on the development of ACRs with directed axonal or somatic trafficking, and their use to functionally dissect closely interrelated autonomic centres in the ventral medulla. Further experiments to deliver recombinase mediated, cell-type specific expression of a novel ACR construct into amygdala neurons projecting to the nucleus of the solitary tract are discussed in Chapter 4. In closing this thesis, Chapter 5 provides an overview of the utility and limitations of the tools developed, with a particular focus on their research applications and relevance to targeted transgenic technologies of the future.

Chapter 2

Targeted viral vector transduction of relaxin-3 neurons in the rat *nucleus incertus* using a novel cell-type specific promoter

2.1 Introduction

States of wakefulness, which broadly influence behaviour and cognitive function, are maintained by basal forebrain, hypothalamic, thalamic and brainstem neurons via a range of chemical and peptide transmitters (Jones 2003). Among these, the neuropeptide, relaxin-3, has emerged as a highly-conserved modulator of arousal in vertebrate species. While primarily located within the brainstem *nucleus incertus* (NI) (Burazin et al. 2002), relaxin-3 neurons are also found in the periaqueductal grey (PAG), pontine raphe nucleus and a region dorsal to the substantia nigra in rat (Tanaka et al. 2005), mouse (Smith et al. 2010) and macaque (Ma et al. 2009b) brain. The vast majority of NI neurons produce γ-aminobutyric acid (GABA), with around one-third of GABAergic NI neurons expressing relaxin-3 (Ma et al. 2007; Ma et al. 2017a). Various other neuropeptides, including cholecystokinin (Kubota et al. 1983; Olucha-Bordonau et al. 2003) and neuromedin B (Chronwall et al. 1985), along with the calcium-binding proteins, calbindin and calretinin (Paxinos 1999; Ma et al. 2007), are also expressed in the NI, indicating a specialised role for relaxin-3 neurons amongst these heterogeneous populations.

The anatomical location and innervation pattern of the NI (Goto et al. 2001; Olucha-Bordonau et al. 2003) suggest relaxin-3 signalling from this nucleus is driven by integrated inputs related to behavioural planning, and in turn, modulates appropriate cognitive activity and responses. For example, blockade of corticotropin-releasing factor-1 (CRF_1) (Walker et al. 2017) or orexin-2 (OX_2) (Kastman et al. 2016) receptors attenuates stress-induced relapse to alcohol-seeking in alcohol-preferring (iP) rats, with NI relaxin-3 neurons expressing receptors for, and being responsive to, these peptides (Ma et al. 2013; Blasiak et al. 2015). 5-HT_{1A} serotonin (Miyamoto et al. 2008) and D_2 dopamine (Kumar et al. 2015) receptors are also expressed by relaxin-3 NI neurons, and have been implicated in anxiety (Kumar et al. 2016) and locomotor (Kumar et al. 2015) behaviour, respectively. These various integrated inputs are conveyed by ascending relaxin-3 projections to mid- and forebrain regions containing neurons expressing relaxin-family peptide receptor 3 (RXFP3) (Ma et al. 2007; Smith et al. 2010).

RXFP3 is the cognate receptor for relaxin-3 (Liu et al. 2003) and triggers $G_{i/o}$-protein-mediated inhibition of cyclic adenosine monophosphate (cAMP) production in response to relaxin-3 binding *in vitro* (Liu et al. 2003; Van der Westhuizen et al. 2005). Similarly, electrophysiological studies of RXFP3 activation in brain slices typically identified membrane hyperpolarisation and

neuronal inhibition (Blasiak et al. 2013; Kania et al. 2017; Ch'ng et al. 2019). As such, relaxin-3 signalling, likely working in conjunction with co-expressed, fast-acting GABA neurotransmission (Ma et al. 2007), appears to promote arousal in part through the selective disinhibition of key neural networks (Ma et al. 2018). One such network, the septohippocampal pathway, contains inhibitory, parvalbumin-positive medial septal neurons and hippocampal somatostatin- and parvalbumin-positive interneurons that express RXFP3 in rat and mouse brain (Haidar et al. 2017; Albert-Gasco et al. 2018a; Haidar et al. 2019; Rytova et al. 2019). Selective blockade or deletion of RXFP3 (Ma et al. 2009a; Haidar et al. 2017; Haidar et al. 2019) in these regions impairs spatial memory and associated hippocampal theta rhythm, to which relaxin-3 NI neurons are strongly phase-locked (Ma et al. 2013). Social recognition is also influenced by relaxin-3 signalling, as RXFP3 agonists, delivered by viral vector-mediated expression in ventral hippocampus (Rytova et al. 2019) or intracerebroventricular infusion (Albert-Gasco et al. 2018b), reduce interactions of rats with novel conspecifics.

Additional pharmacological studies targeting RXFP3 have shown effects on interrelated anxiety (Ryan et al. 2013; Zhang et al. 2015a), feeding (McGowan et al. 2006; Shabanpoor et al. 2012) and motivated (Smith et al. 2014a) behaviours, most likely via actions within limbic and hypothalamic networks (Kania et al. 2017). A key role for this system in innate anxiety is also highlighted by independent relaxin-3 and RXFP3 gene knock-out mouse lines, which display a small, but consistent, decrease in anxiety behaviour (Watanabe et al. 2011; Hosken et al. 2015). Considering these and other described functions, in addition to its discrete expression profile and neuromodulatory nature, the relaxin-3/RXFP3 system offers considerable potential as a therapeutic target (see Smith et al. (2014b), Kumar et al. (2017), Ma et al. (2017b) for review). In advancing our understanding of relaxin-3 neural circuitry, which to date has largely relied on pharmacological and gene knock-out models, we sought to take advantage of modern transgenic approaches. Recent chemo- (Ma et al. 2017a) and opto-genetic (Szonyi et al. 2019) manipulations have provided powerful insights into the ability of NI neurons to fine-tune behavioural responses and memory formation. Our laboratory has also established adeno-associated viral (AAV) vectors for efficient transgene delivery into NI neurons (Callander et al. 2012; Ma et al. 2017a). However, these experiments targeted either GABAergic NI neurons or the entire nucleus, thus affecting multiple populations, including but not limited to, relaxin-3 neurons (Ma et al. 2007; Ma et al. 2015).

The present study therefore aimed to identify a promoter sequence capable of selectively driving transgene expression in relaxin-3 NI neurons following viral vector transduction. Tanaka et al. (2009) are, to our knowledge, the only other investigators to describe a relaxin-3 promoter. Their experiments reported promoter activity from a 1.8 kilobase (kb) sequence, located directly 5' of the mouse relaxin-3 gene, which was upregulated following stimulation of the CRF_1 receptor and downstream cAMP-protein kinase A (PKA) pathway. Although these experiments demonstrated this sequence could drive enhanced green fluorescent protein (EGFP) expression in cultured neuroblastoma cells expressing relaxin-3, they did not determine the cell-type specificity of the observed promoter activity. As such, we assessed the ability of an approximately analogous 1,736 base pair (bp) region of rat genomic DNA to provide cell-type specific transduction of relaxin-3 NI neurons. In addition, we have discovered that tropomyosin receptor kinase A (TrkA), a high-affinity receptor for nerve-growth factor (NGF), is exclusively co-expressed with relaxin-3 in rat NI neurons (see e.g. Sobreviela et al. (1994); and Results). In light of existing evidence for cell-type specific activity from human or mouse TrkA promoter and enhancer elements in neuroblastoma cell lines (Chang et al. 1998; Sacristan et al. 1999) and mouse trigeminal and dorsal root ganglia during development (Ma et al. 2000), we also attempted to achieve targeted AAV transduction of relaxin-3 neurons in rat NI using an 880 bp TrkA promoter sequence.

In contrast to previous data obtained using different experimental conditions, we observed widespread non-specific transduction of neurons in the rat NI and neighbouring dorsal tegmental nuclei, following stereotaxic injection of an AAV vector expressing mCherry using the 880 bp TrkA promoter. However, a similar AAV vector, engineered to express mCherry under the control of the 1,736 bp rat relaxin-3 promoter, was able to transduce relaxin-3 NI neurons with 98% specificity for at least eight weeks following transgene delivery.

2.2 Methods

2.2.1 Animals

All experiments were approved by The Florey Institute of Neuroscience and Mental Health Animal Ethics Committee and conducted in accordance with ethical guidelines provided by the National Health and Medical Research Council of Australia. Sprague-Dawley rats (250-300 g males, Animal Resources Centre, WA, Australia) were single-housed with free access to water and standard chow under ambient conditions (21°C) and a 12 h light:dark cycle (lights on 07:00). Every effort was made to minimise the number of rats used and any stress resulting from the procedures described.

2.2.2 Relaxin-3 and TrkA promoter design

Pairwise alignments of rat genomic sequences (Jul. 2014 (RGSC 6.0/rn6) assembly) (Gibbs et al. 2004; Havlak et al. 2004) with other vertebrate genomes, including mouse (Dec. 2011 (GRCm38/mm10) assembly) (Mouse Genome Sequencing Consortium et al. 2002) and human (Dec. 2011 (GRCh38/hg38) assembly) (Lander et al. 2001), were visualised using the UCSC Genome Browser's chain track feature (Kent et al. 2002). Based on the location of two regions upstream of the relaxin-3 gene, conserved in rodents but not primates, we initially attempted to isolate a 3.5 kb sequence from rat genomic DNA using polymerase chain reaction (PCR). However, 1.8 kb of poorly conserved DNA between these regions was skipped during PCR amplification (Figure 2.1A), resulting in a 1,736 bp relaxin-3 promoter amplicon. Given that the conserved regions of interest were retained, we proceeded to characterise this 1,736 bp sequence. Similar genomic comparisons using the UCSC Genome Browser were performed for the TrkA promoter region, revealing a high degree of sequence conservation in the non-coding region between the closely adjacent TrkA and insulin receptor-related protein (INSRR) genes (Figure 2.1B). Additional consideration was given to incorporate regions of rat genome analogous to minimal promoter and enhancer elements described for mouse (Sacristan et al. 1999; Ma et al. 2000) and human (Chang et al. 1998), resulting in selection of an 880 bp TrkA promoter region for characterisation (synthesised by GenScript (NJ, USA)). Data presented in Figure 2.1 were adapted from BLAT searches (Kent 2002) of each promoter against the rat genome (Jul. 2014 (RGSC 6.0/rn6) assembly) in the UCSC Genome Browser.

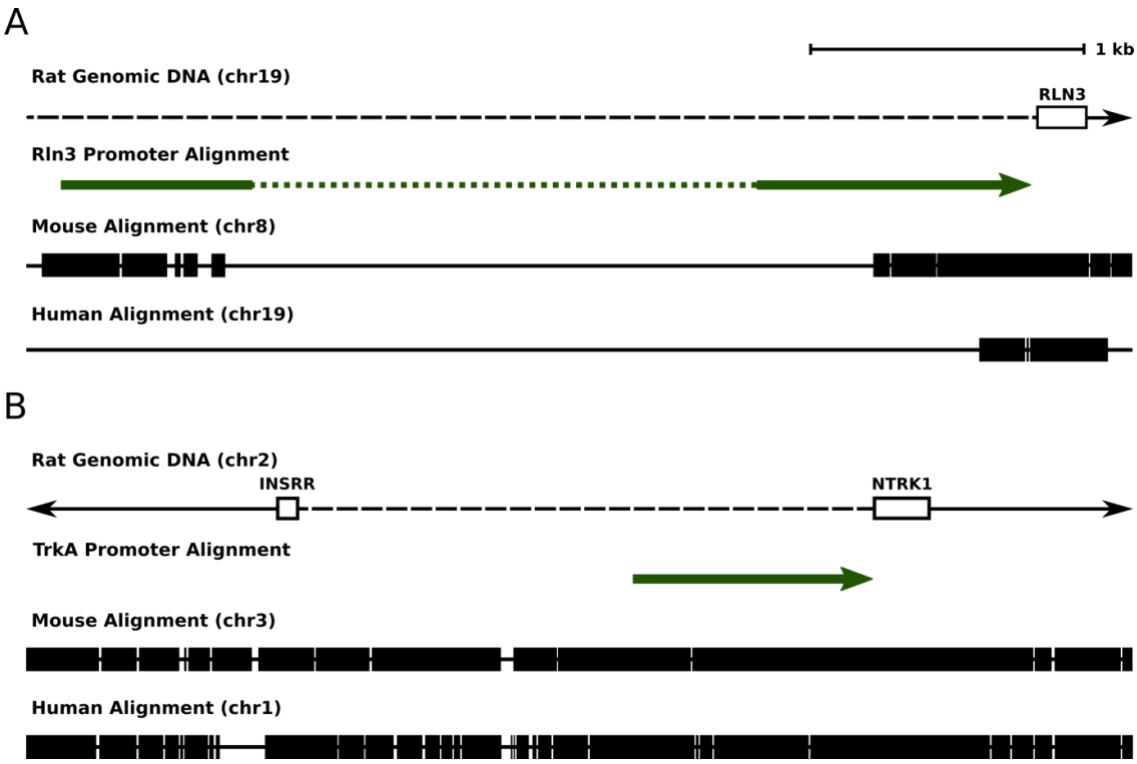

Figure 2.1. *Genomic location and conservation of promoter sequences*. The genomic locations of rat relaxin-3 and TrkA promoter sequences (solid green lines, **(A)** and **(B)** respectively) used in the present study are illustrated, based on BLAST-like alignment tool (BLAT) search against the Jul. 2014 (RGSC 6.0/rn6) Assembly in the University of California Santa Cruz (UCSC) Genome Browser. The first exon and intron of genes within each field is provided as a white box and solid black line, respectively, along with the abbreviated gene name. The orientation (5' to 3') of promoter and gene sequences is reflected by the direction of relevant arrow heads, and non-coding rat genomic DNA is represented by a black dashed line. Regions of the rat genome that are conserved in mouse (Dec. 2011 (GRCm38/mm10) Assembly) and human (Dec. 2011 (GRCh38/hg38) Assembly) genomes are indicated with black boxes in **(A)** and **(B)**, based on UCSC Genome Browser chain track alignment with the rat Jul. 2014 (RGSC 6.0/rn6) Assembly. Gaps between conserved regions are shown as solid black lines. A non-conserved sequence skipped during PCR cloning of the 1,736 bp relaxin-3 promoter used is indicated by the dotted green line in **(A)**. Scale bar, 1 kilobase (kb). Abbreviations: *chr*, chromosome; *INSRR*, Insulin related receptor; *NTRK1*, Neurotrophic receptor kinase 1 (synonymous with TrkA); *RLN3*, Relaxin-3; *TrkA*, Tropomyosin-related kinase A.

2.2.3 Generation of plasmid vectors

Plasmids containing recombinant AAV vector genomes, with mCherry as a marker for promoter activity, were prepared using the Gateway cloning system, as described by White et al. (2011). To facilitate this, a Gateway-compatible AAV backbone plasmid (pAM-Gateway) was created using *Spe*I and *Hin*dIII cut sites to replace CAG promoter and EGFP coding sequences of pAM-DCA-*Eco*RI-EGFP (Callander et al. 2012) with an attR1-R2 cloning cassette. The 1,736 bp rat relaxin-3 promoter sequence was cloned using forward (5'-attB1-CCTGCAAACTTGTCTGTGTAC-3') and reverse (5'-attB5r-CAGCTGAGATGCCTGCGA-3') primers. Additional forward (5'-attB1-GAACGGTTCCCAGCTCACACGTCCG-3') and reverse (5'-attB5r-CGCGGCGGCGCCCGCCTAG-3') primers were used to amplify the 880 bp rat TrkA promoter sequence. pENTR-L1-Rln3-R5 and pENTR-L1-TrkA-R5 plasmids were created by recombination of respective PCR products (50 fmol) with pDONR-P1-P5r. Further recombination steps, involving 10 fmol of either pENTR-L1-Rln3-R5 or pENTR-L1-TrkA-R5, with 10 fmol pENTR-L5-mCherry-L2 and 20 fmol of pAM-Gateway destination vector, produced pAM-Rln3-mCherry and pAM-TrkA-mCherry plasmids. Each recombination reaction used Clonase™ II reagents (Life Technologies, VIC, Australia) and was incubated at 25°C for 16 h. pDONR-P1-P5r, pENTR-L5-mCherry-L2 and plasmid containing attR1-R2 cloning cassette, used in generating pAM-Gateway, were a gift from Dr Melanie White (A*STAR, Singapore). Constructs containing PCR amplified promoter inserts were verified by Sanger sequencing (Australian Genome Research Facility, VIC, Australia).

2.2.4 AAV vector production and titration

Mosaic serotype 1/2 AAV vectors were produced as described (Zolotukhin et al. 1999; Ganella et al. 2013). In brief, genomes from pAM-TrkA-mCherry or pAM-Rln3-mCherry were packaged into AAV1/2 capsids by co-transfection into HEK293FT cells with pDPI and pDPII plasmids (Grimm et al. 2003). Harvested vectors were purified by iodixanol gradient centrifugation and the titre, reported as genomic copies (gc) per ml, was determined using quantitative PCR with primers against the woodchuck hepatitis virus post-transcriptional regulatory element (WPRE) sequence, as described (Ma et al. 2017a).

2.2.5 Stereotaxic injection of colchicine or AAV vectors

Rats were placed in an enclosed chamber and anaesthesia induced by inhalation of 4% isoflurane before transfer to a stereotaxic frame (Kopf Instruments, CA, USA). Anaesthesia was maintained during surgical procedures with 2-3% isoflurane in air, delivered via a rat anaesthetic mask at 200 ml/min. Depth of anaesthesia was verified regularly by lack of eye-blink reflex in response to medial canthus touch and lack of withdrawal response to firm hind paw pinch. Body temperature was maintained throughout surgery with a heat pad. Rats were administered meloxicam intraperitoneally (1.5 mg/kg; Boehringer Ingelheim, MO, USA), and bupivacaine subcutaneously at the top of the scalp (0.5% in sterile water), prior to an incision to expose the skull surface. A burr hole was drilled through the skull based on stereotaxic coordinates (Paxinos et al. 2014) as detailed below.

In studies to maximise the level of peptide and protein accumulation in the soma of NI neurons for the comparative immunohistochemical detection of relaxin-3 and TrkA, a cohort of rats (n = 5) were treated with intracerebroventricular colchicine. An injector needle (29G) attached to polyethylene tubing connected to a 10 µl Hamilton syringe (Harvard Apparatus, MA, USA) mounted on an infusion pump (11-Plus, Harvard Apparatus) was used to deliver colchicine (80 µg in 5 µl sterile saline) at a rate of 1 µl/min to the right lateral cerebral ventricle (AP -0.2 mm, ML +1.5 mm, DV -4 mm from bregma). To minimise reflux of injectate up the cannula, the needle was left in place for 10 min and then withdrawn.

In separate cohorts of rats, promoter activity was characterised by stereotaxic injection of AAV vectors into NI. Prior to injection, AAV1/2-Rln3-mCherry (1.86×10^{11} gc/ml) or AAV1/2-TrkA-mCherry (2.04×10^{11} gc/ml) was mixed with an AAV1/2-CAG-EGFP vector (as described by Callander et al. (2012); 9.08×10^{10} gc/ml), to allow visualisation of total viral vector spread from the injection site, as reflected by EGFP expression driven by the non-specific CAG promoter. These values reflect the final titre of each vector when injected and account for dilution caused by mixing. Rats (n = 3 per group) received 0.4 µl bilateral injections of one of these viral vector mixtures, delivered into the NI at 0.1 µl/min using a pulled glass pipette attached to a 1 µl syringe. The coordinates used for injections were: AP -2.5 mm; ML $\pm$ 0.1 mm; DV -6.5 mm from lambda; incisor bar -12.5 mm. To minimise reflux, the pipette was left in place for 10 min after each injection, raised 1 mm and held in place for a further one min, before being slowly withdrawn.

Following colchicine or viral vector delivery, the incision was sutured, swabbed with providone iodine, and rats regained consciousness in a warm chamber. Rats were euthanised 24 h following colchicine infusion, whereas those that received viral vector injections were treated with meloxicam for a further 2 d following surgery, and maintained for 8 wk prior to sacrifice.

2.2.6 Histology and Immunostaining

Rats were euthanised by intraperitoneal injection of pentobarbitone (100 mg/kg) before transcardial perfusion with 300 ml of ice-cold phosphate-buffered saline (PBS, 0.1 M, pH 7.4) followed by 400 ml of 4% paraformaldehyde in PBS (PFA). Dissected brains were fixed in ice-cold 4% PFA for a further 1-2 h before undergoing cryoprotection by submersion in a 30% sucrose/PBS solution at 4°C for 3 d.

For immunostaining and assessment of viral vector transduction in NI, coronal sections (40 µm) from bregma -10.4 mm to -8.4 mm (Paxinos et al. 2014) were collected free-floating in PBS. Sections were transferred to blocking buffer (10% v/v normal horse serum (NHS) in PBS with 0.1% Triton-X) and incubated for 1 h at room temperature with agitation. NHS blocked sections from colchicine-treated rats were incubated in PBS containing mouse anti-relaxin-3 (1:5; HK4-144-10 (Kizawa et al. 2003; Tanaka et al. 2005; Ma et al. 2007)) and rabbit anti-TrkA (1:10,000; kindly provided by Dr Louis Reichardt, UCSF, CA, USA; (Clary et al. 1994; Sobreviela et al. 1994; Holtzman et al. 1995)) antibodies with 2% NHS and 0.1% Triton-X at 4˚C for 72 h. Some sections were incubated with *only* the mouse anti-relaxin-3 antiserum or the rabbit anti-TrkA antisera to check for non-specific interactions in the double-label studies. Coronal NI sections from rats that received AAV vector injections were incubated in PBS containing mouse anti-relaxin-3 (1:5; HK4-144-10) and rabbit anti-red fluorescent protein (1:1,000; Rockland Immunochemicals, PA, USA) antibodies with 2% NHS and 0.1% Triton-X for 24 h at 4°C.

Sections were washed 3 × 10 min in PBS following primary antibody incubations. Sections were incubated in PBS containing Alexa Fluor-594-conjugated donkey anti-rabbit and Alexa Fluor-647-conjugated donkey anti-mouse antibodies (1:500 each; Jackson ImmunoResearch, PA, USA) as well as bis-benzimide H (Hoechst) 33342 (1 µg/ml; Sigma-Aldrich, NSW, Australia) for 1 h at room temperature. Sections were washed 3 × 5 min in PBS, slide-mounted and coverslipped with Dako fluorescence mounting medium (Agilent Technologies, CA, USA).

In studies to visualise NI-transduced neuronal projections in the medial septum (MS), 40 µm coronal sections from bregma +1.56 mm to 0.00 mm were collected and blocked with NHS as described. Following incubation in PBS containing 1:500 mouse anti-mCherry (Developmental Studies Hybridoma Bank, University of Iowa, IA, USA) and 1:500 rabbit anti-GABA (Sigma-Aldrich) antibodies, with 2% NHS, 0.1% Triton-X and 0.5% thimerosal (Sigma-Aldrich) for 72 h at room temperature, sections were washed 3 × 10 min in PBS. A further 2 h incubation at room temperature in PBS solution containing 1:500 Alexa-594-conjugated donkey anti-mouse and Alexa-647 conjugated donkey anti-rabbit antibodies (Jackson ImmunoResearch) as well as bis-benzimide H (Hoechst) 33342 (1 µg/ml) preceded 3 × 5 min washes in PBS and slide-mounting as described.

2.2.7 Imaging and quantitative analysis

An LSM 780 Zeiss Axio Imager 2 laser scanning confocal microscope (Carl Zeiss AG, Germany) was used to acquire images. To assess promoter activity in NI neurons, relaxin-3-immunoreactivity (IR) (Alexa Fluor-647) and mCherry-IR (Alexa Fluor-594), as well as Hoechst nuclear stain (to assist with cell counting) and innate EGFP, were imaged using a 20× air objective lens in every third section from bregma -9.00 mm to -9.84 mm for each rat. Centred on the midline directly ventral to the fourth ventricle, 1.57 mm × 1.19 mm images were collected using a stitching stage and Zen Black software (Carl Zeiss AG). Planes were collected at 3 µm intervals through the z-axis and used to produce maximum projection images in Fiji software (Schindelin et al. 2012), where manual cell counts and colocalisation analysis of fluorescent soma were also performed. Percentages calculated for the specificity and efficiency of viral vector transduction (see Section 2.3.1 for further descriptions) are reported as mean ± standard error of the mean (SEM). High magnification images of relaxin-3-IR (Alexa Fluor-647) and TrkA-IR (Alexa Fluor-594) in NI, or mCherry-IR (Alexa Fluor-594), GABA-IR (Alexa Fluor-627), innate EGFP and Hoechst nuclear stain in MS, were collected using a 63× oil immersion objective lens, with images collected at 2 µm intervals through the z-axis. All microscopy data in figures presented are maximum intensity z-stack projections.

2.3 Results

Established and emerging transgenic techniques offer powerful approaches to understanding neural circuit structure and function. Such techniques have been applied in recent molecular and behavioural studies utilising viral vector injections for targeted NI expression in wild-type or transgenic rodents (Ma et al. 2017a; Szonyi et al. 2019). However, these experiments affected multiple, heterogeneous populations of NI neurons (Ma et al. 2007; 2015), highlighting the need for more selective methods of transgene expression. In the present study, we sought to identify a promoter sequence capable of selectively driving transgene expression in relaxin-3 NI neurons following AAV vector transduction. In addition to a conserved region upstream of the rat relaxin-3 gene coding sequence, we also characterised the activity of a promoter region for the TrkA receptor, which is selectively co-expressed with relaxin-3 in NI neurons. The promoter activity of each sequence, as reflected by mCherry expression in transduced neurons, was characterised against immunolabelling for the relaxin-3 peptide. Co-injection of a separate, EGFP-expressing vector allowed relaxin-3 and TrkA promoter activity to be compared with the constitutive CAG promoter, while also facilitating visualisation of AAV vector spread outside the NI.

2.3.1 Targeted transduction of rat relaxin-3 NI neurons using a novel relaxin-3 promoter

In these studies, data were collected from rats (n = 3) displaying neuronal transduction by AAV1/2-Rln3-mCherry and AAV1/2-CAG-EGFP distributed bilaterally throughout the NI (Figure 2.2F), with data excluded from rats in which off-target or limited spread of transduction was observed. Neurons displaying fluorescence in individual optical wavelength channels for EGFP, mCherry-IR or relaxin-3-IR were counted, with further counts of neurons containing EGFP and/or mCherry-IR in addition to relaxin-3-IR also performed (Table 2.1). The specificity (proportion of transduced cells expressing relaxin-3) and efficiency (proportion of total relaxin-3 population transduced) of each promoter was calculated from these cell counts (Table 2.2, Figure 2.2G). Similar transduction efficiencies were observed between AAV1/2-Rln3-mCherry and AAV1/2-CAG-EGFP vectors, with a majority of relaxin-3-IR NI neurons displaying EGFP (73 ± 8%) and/or mCherry-IR (70.1 ± 2%) fluorescence. As expected, non-specific transduction by AAV1/2-CAG-EGFP was evident throughout the NI and in regions of some neighbouring nuclei (e.g. DTg, Figure 2.2B), leading to relaxin-3-IR detection in only 30 ± 5% of EGFP expressing neurons. Importantly, this viral vector spread outside the NI was only reflected by CAG promoter-driven EGFP expression, with mCherry expression under the control of the Rln3 promoter limited to the NI

(Figure 2.2F). Of the total number of neurons transduced by AAV1/2-Rln3-mCherry, virtually all (98 ± 1%) were found to contain relaxin-3-IR (Figure 2.2G). This was despite non-specific transduction of closely adjacent NI neurons by AAV1/2-CAG-EGFP (Figure 2.2C-E), indicating that the targeted mCherry expression was dependent on promoter activity rather than viral vector tropism.

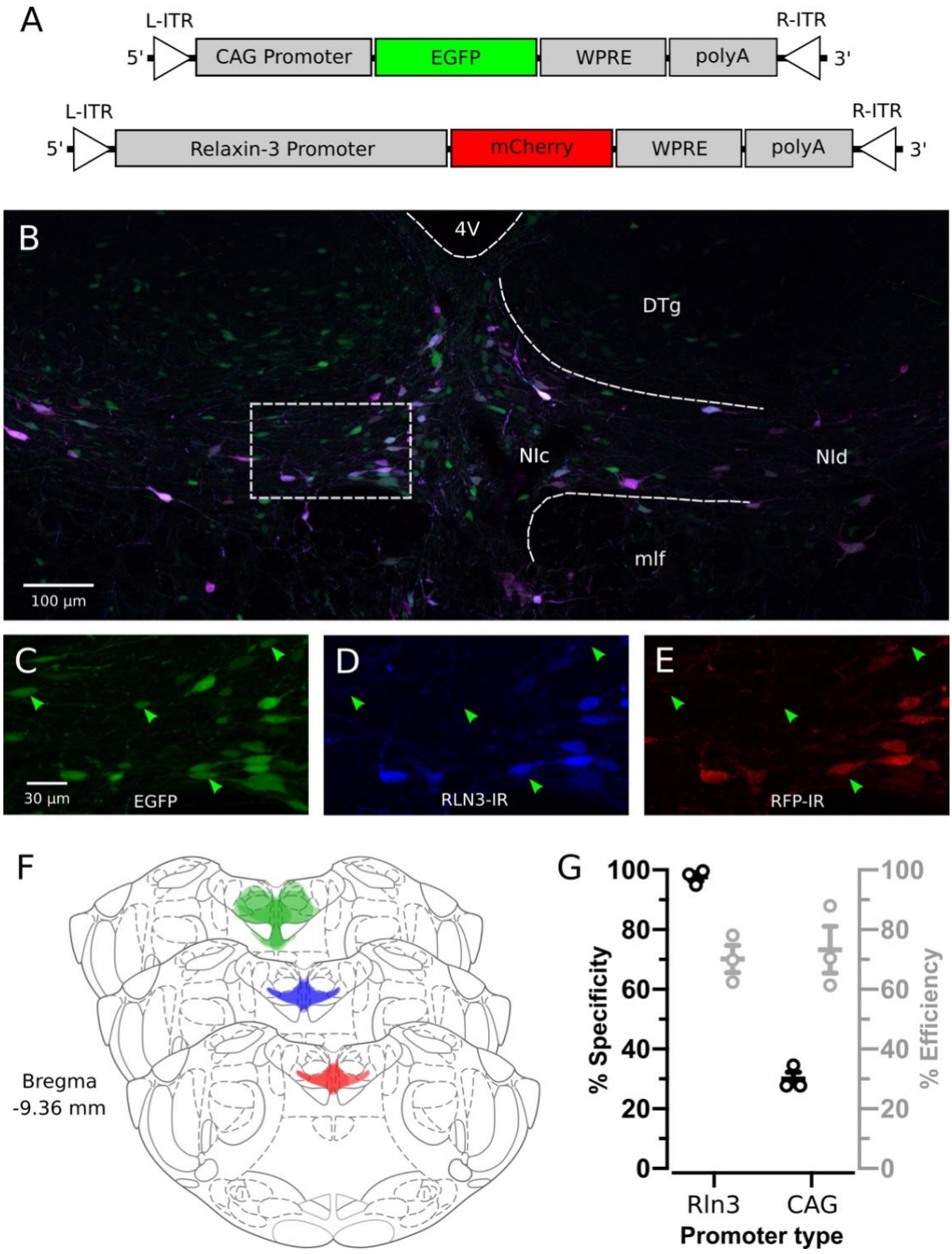

Figure 2.2. *Refer to next page for figure legend.*

Figure 2.2. *Neuronal transduction by AAV1/2-Rln3-mCherry*. **(A)** Schematic design of recombinant AAV genomes for AAV1/2-CAG-EGFP and AAV1/2-Rln3-mCherry vectors (*L-ITR*, left inverted terminal repeat; *WPRE*, woodchuck hepatitis virus post-transcriptional regulatory element; *polyA*, SV40 poly A sequence; *R-ITR*, right inverted terminal repeat). **(B)** Representative image of innate fluorescence produced by EGFP (green) and fluorescence produced by mCherry (red) and relaxin-3 (blue) immunoreactivity, eight weeks after stereotaxic injection of AAV1/2-CAG-EGFP and AAV1/2-Rln3-mCherry vectors targeting NI (*4V*, fourth ventricle; *DTg*, dorsal tegmental nucleus; *mlf*, medial longitudinal fasciculus; *NIc*, NI *pars compacta*; *NId*, NI *pars dissipata*). **(C-E)** Individual fluorescence channels from **(B)** are illustrated at higher magnification**.** Transduced neurons lacking relaxin-3 immunoreactivity (RLN3-IR) are indicated by green arrowheads (i.e., AAV1/2-CAG-EGFP transduced only). Note there are no AAV1/2-Rln3-mCherry-transduced neurons in the field that do not contain RLN3-IR (*RFP-IR*, red fluorescent protein (mCherry) immunoreactivity). **(F)** Distribution of neurons transduced by AAV1/2-CAG-EGFP (green) or AAV1/2-Rln3-mCherry (red) vectors, with RLN3-IR (blue) at bregma -9.36 mm in the rats (n = 3) used in the analysis. **(G)** Quantification of promoter specificity (proportion of transduced neurons containing RLN3-IR (black circles)) and efficiency (proportion of total RLN3-IR neurons transduced (grey circles)). Data points for each variable represent individual rats (n = 3) and bars represent mean ± SEM.

Table 2.1. *Summary of NI cell counts.*

Rat ID	RLN3-IR	RFP-IR	RLN3 + RFP	EGFP	RLN3 + EGFP
27	702	2689	305	2879	515
28	776	2249	271	2405	470
29	697	1548	126	2462	373
Mean (TrkA)	*725*	*2162*	*234*	*2582*	*453*
09	783	576	547	1597	552
30	704	552	550	2238	619
31	636	403	397	1407	390
Mean (Rln3)	*708*	*510*	*498*	*1747*	*520*

Figures represent total cell counts from each rat, with manual counts accumulated over every third section from bregma levels -9.00 mm to -9.84 mm (sections cut at 40 µm). Rats 27, 28 and 29 received injections containing AAV1/2-TrkA-mCherry, whereas rats 09, 30 and 31 received injections containing AAV1/2-Rln3-mCherry (*RLN3-IR*, relaxin-3 immunoreactivity, *RFP-IR*, red fluorescent protein (mCherry) immunoreactivity, *RLN3 + RFP*, co-labelling for relaxin-3 and mCherry immunoreactivity, *RLN3 + EGFP*, fluorescence signal for relaxin-3 immunoreactivity and EGFP).

Table 2.2. *Calculated promoter specificity and efficiency.*

Rat ID	Specificity (RFP, %)	Efficiency (RFP, %)	Specificity (EGFP, %)	Efficiency (EGFP, %)
27	11.3	43.4	17.9	73.4
28	12.0	34.9	19.5	60.6
29	8.1	18.1	15.2	53.5
Mean (TrkA)	*10.5*	*32.1*	*17.5*	*62.5*
09	95.0	69.9	34.6	70.5
30	99.6	78.1	27.7	87.9
31	98.5	62.4	27.7	61.3
Mean (Rln3)	*97.7*	*70.1*	*30.0*	*73.2*

Specificity (proportion of AAV transduced neurons containing relaxin-3 immunoreactivity) and efficiency (proportion of total relaxin-3 population transduced) as calculated from cell counts in Table 2.1 (*RFP*, statistics for AAV vectors expressing mCherry under experimental TrkA or Rln3 promoter, *EGFP*, statistics for co-injected AAV1/2-CAG-EGFP in each rat/cohort).

2.3.2 AAV1/2-Rln3-mCherry transduction identifies direct NI relaxin-3 neuron input to GABAergic medial septum circuitry

Multiplex *in situ* hybridisation studies have shown that *Rxfp3* mRNA is strongly co-expressed with vesicular GABA transporter (*vGAT*) mRNA in MS neurons (Albert-Gasco et al. 2018a; Haidar et al. 2019). In studies to build on these findings and demonstrate the utility of AAV1/2-Rln3-mCherry in mapping networks formed by relaxin-3 NI neurons, we labelled coronal sections through the MS of rats used in the analysis of promoter specificity for GABA- and mCherry-IR (n = 2 rats; Figure 2.3). Staining of MS sections for relaxin-3 was not undertaken, given the exclusive expression of mCherry in relaxin-3 NI neurons observed. Large fibres containing EGFP emanating from neurons transduced by the control AAV1/2-CAG-EGFP vector were densely concentrated in the medial septum/diagonal band complex (MS/DB; Figure 2.3A), consistent with neural tract-tracing studies of NI (Goto et al. 2001; Olucha-Bordonau et al. 2003; Ma et al. 2009a); confirming that ascending efferent projections from the NI pass through and/or terminate in the MS/DB. In a subset of these MS/DB EGFP fibres, red fluorescence resulting from AAV1/2-Rln3-mCherry transduced NI neurons was also present (Figure 2.3C), confirming relaxin-3 NI neurons send direct projections to the MS/DB. High-magnification confocal images in MS also revealed fine structures containing EGFP and mCherry-IR fluorescence, indicative of potential axon terminals or boutons (Figure 2.3B-D). Of particular note, given existing evidence for RXFP3 mRNA expression by vGAT mRNA-positive MS neurons, many of the putative relaxin-3 NI (mCherry-positive) nerve terminals were observed in close apposition to MS neurons containing GABA-IR (Figure 2.3C).

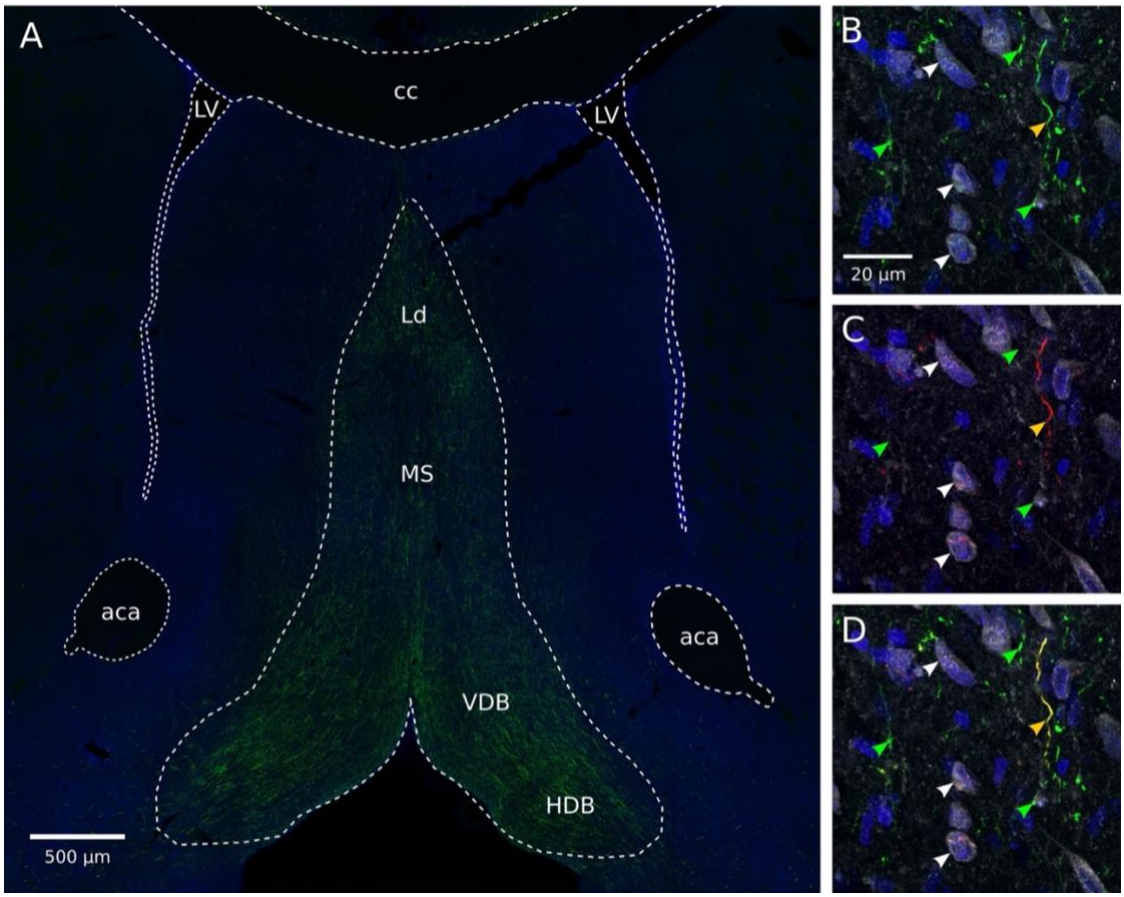

Figure 2.3. *Visualisation of AAV1/2-Rln3-mCherry transduced NI projections, with close apposition to GABAergic neuronal soma in the medial septum*. Fluorescent protein expression was visualised in efferent fibres projecting from transduced NI neurons to the medial septum/diagonal band complex (MS/DB) of rats which received AAV1/2-Rln3-mCherry and AAV1/2-CAG-EGFP injections (**(A)**; EGFP, *green*; mCherry-IR, *red*; Hoechst nuclear stain, *blue*; representative image from n = 2 rats). **(B-D)** In addition to larger fibres passing through the MS which contained both mCherry-IR and EGFP (yellow arrowhead), or EGFP alone (green arrowheads), fine processes and potential terminals from transduced NI neurons were observed in close apposition to neuronal soma containing GABA-IR (*white*; putative contacts indicated by white arrowheads). Representative images of merged (**D**) or separate non-specific EGFP (**B**) and relaxin-3 promoter driven mCherry-IR (**C**) channels highlight the ability of this approach to provide targeted mapping of fibres and terminals projecting from transduced relaxin-3 NI neurons. Abbreviations: *aca*, anterior commissure, anterior part; *cc*, corpus callosum; *HDB*, nucleus of the horizontal limb of the diagonal band; *IR*, immunoreactivity; *Ld*, lambdoid septal zone; *LV*, lateral ventricle; *MS*, medial septum; *VDB*, nucleus of the vertical limb of the diagonal band.

2.3.3 TrkA is co-expressed with relaxin-3 in rat NI neurons

In parallel to studies characterising the relaxin-3 promoter, we investigated whether a TrkA promoter could be used for targeted transduction of relaxin-3 neurons. Dense immunostaining of TrkA has previously been detected in the clearly distinguishable neurons that comprise the rat NI, despite the fact that this anatomical structure was incorrectly identified as the *prepositus hypoglossal nucleus* in that report (see Fig. 11, Sobreviela et al. (1994)). The *prepositus hypoglossal nucleus* also expresses dense TrkA mRNA and immunoreactivity (Gibbs et al. 1994; Sobreviela et al. 1994), but it is clearly distinct and distinguishable from the NI. In extending and clarifying these earlier studies, we performed dual immunohistochemistry for TrkA and relaxin-3 to assess their degree of co-expression in NI neurons (n = 5 rats). As expected, immunofluorescence detection revealed TrkA immunoreactive neurons throughout the NI (Figure 2.4B) and most, if not all, of these neurons also displayed relaxin-3 immunofluorescence (Figures 2.4A, 2.4C). Furthermore, an overlay of TrkA and relaxin-3 immunofluorescence staining in separate, adjacent sections revealed an identical neuronal co-distribution, despite some differences in the subcellular distribution of the immunoreactive materials (Figure 2.4D-F). This co-expression is consistent with identified roles for NGF/TrkA signalling in supporting the survival and function of key projection-neuron networks, such as cholinergic basal forebrain and GABAergic septohippocampal systems (Rocamora et al. 1996; Conner et al. 2009), and provided the basis for studies of TrkA promoter specificity in rat NI.

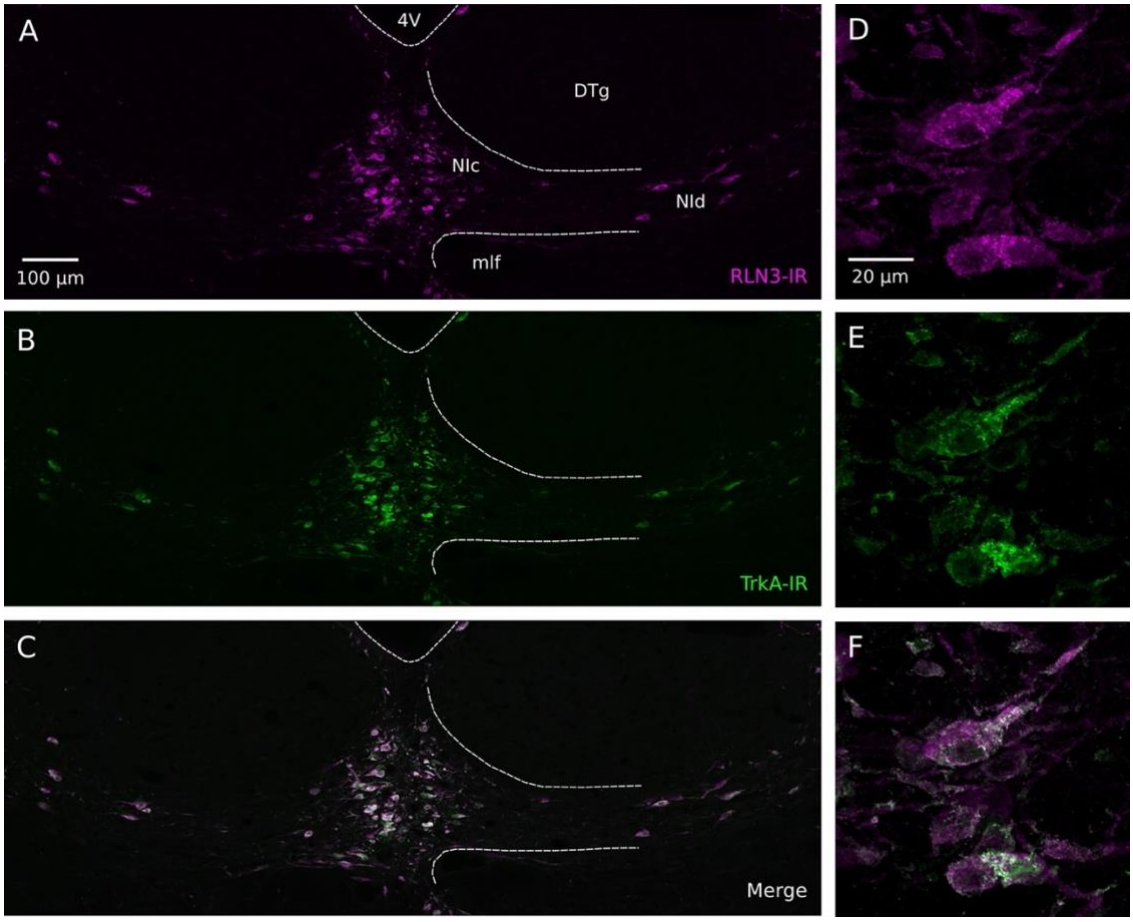

Figure 2.4. *Co-expression of relaxin-3 and TrkA immunoreactivity in rat NI*. Overview of immunofluorescence for relaxin-3 (RLN3) (**A**, magenta) and TrkA (**B**, green) in the NI, with a merged image revealing the strong co-expression and resultant overlap of channels (**C**, white). High magnification images of individual (**D**, **E**) and merged (**F**) relaxin-3 and TrkA immunoreactivity show differences in the subcellular distribution of these co-expressed gene products in NI neurons. Abbreviations: *4V*, fourth ventricle; *DTg*, dorsal tegmental nucleus; *IR*, immunoreactivity; *mlf*, medial longitudinal fasciculus; *NIc*, NI *pars compacta*; *NId*, NI *pars dissipata*.

2.3.4 TrkA promoter drives non-specific transgene expression in dorsal pons of adult rats

As described for rats receiving AAV1/2-Rln3-mCherry injections, inclusion of data from rats co-injected with AAV1/2-TrkA-mCherry and AAV1/2-CAG-EGFP in the final analyses (Figure 2.5, n = 3) was dependent on successful bilateral transduction by these vectors throughout the NI. No significant difference was observed in the efficiency of relaxin-3 NI neuronal transduction by AAV1/2-CAG-EGFP in these rats (63 ± 6%; *P* = 0.33 (Student's t-test)) compared to the Rln3 promoter cohort. However, due to some variation in spread of injected vectors to regions surrounding the NI, the calculated specificity for AAV1/2-CAG-EGFP in this group (18 ± 1%, Figure 2.5G) was slightly lower. A similar distribution of non-specifically transduced neurons in NI and adjacent regions was observed for AAV1/2-TrkA-mCherry (Figures 2.5B, 2.5F), resulting in only 11 ± 1% of mCherry-IR neurons containing relaxin-3-IR. Differences in TrkA and CAG promoter activity within the NI (Figures 2.5C-E) resulted in a relatively low calculated efficiency as well, with AAV1/2-TrkA-mCherry transducing around one-third (32 ± 8%) of relaxin-3-IR NI neurons. Additional TrkA immunolabelling (data not shown) confirmed widespread transduction of neurons lacking TrkA immunoreactivity by AAV1/2-TrkA-mCherry in these rats.

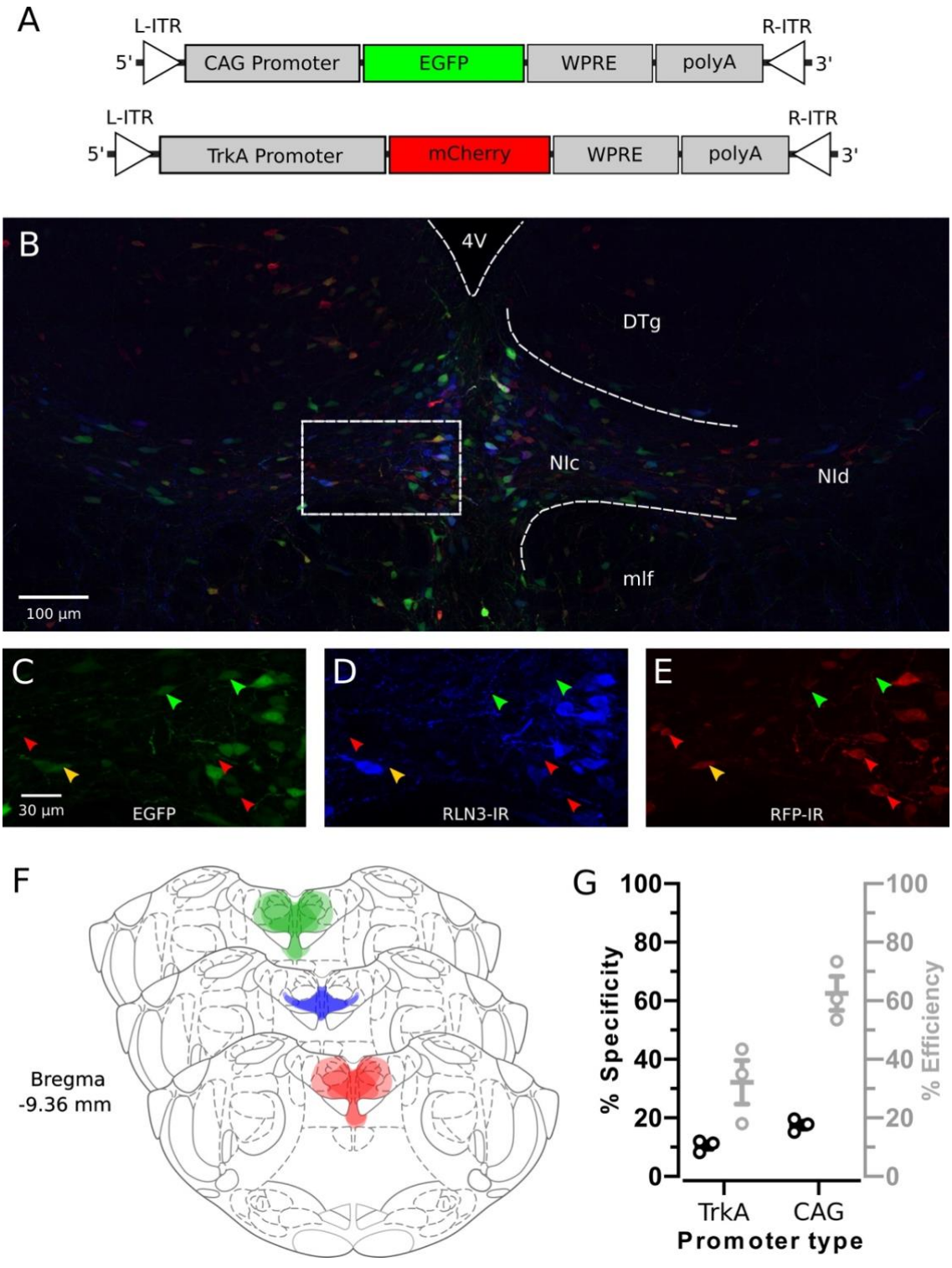

Figure 2.5. *Refer to next page for figure legend.*

Figure 2.5. *Neuronal transduction by AAV1/2-TrkA-mCherry*. **(A)** Schematic design of recombinant AAV genomes for AAV1/2-CAG-EGFP and AAV1/2-TrkA-mCherry vectors (*L-ITR*, left inverted terminal repeat; *WPRE*, woodchuck hepatitis virus post-transcriptional regulatory element; *polyA*, SV40 poly A sequence; *R-ITR*, right inverted terminal repeat). **(B)** Representative image of innate fluorescence detected from EGFP (green), together with fluorescent immunoreactivity for mCherry (red) and relaxin-3 (blue), eight weeks after stereotaxic injection of AAV1/2-CAG-EGFP and AAV1/2-TrkA-mCherry vectors targeting NI (*4V*, fourth ventricle; *DTg*, dorsal tegmental nucleus; *mlf*, medial longitudinal fasciculus; *NIc*, NI *pars compacta*; *NId*, NI *pars dissipata*). **(C-E)** Individual fluorescence channels from **(B)** illustrated at higher magnification, revealing neurons lacking relaxin-3 immunoreactivity (RLN3-IR) transduced by AAV1/2-CAG-EGFP only (green arrowheads), AAV1/2-TrkA-mCherry only (mCherry - red fluorescent protein immunoreactivity (RFP-IR); red arrowheads), and both AAV1/2-CAG-EGFP and AAV1/2-TrkA-mCherry (yellow arrowhead). **(F)** Distribution of neurons transduced by AAV1/2-CAG-EGFP (green) or AAV1/2-TrkA-mCherry (red) vectors, compared to the distribution of RLN3-IR (blue) at bregma -9.36 mm, in rats used in the analysis (n = 3). **(G)** Quantification of promoter specificity (proportion of transduced neurons containing RLN3-IR; black circles) and efficiency (proportion of total RLN3-IR neurons transduced; grey circles). Data points for each variable represent individual rats (n = 3) and bars represent mean ± SEM.

2.5 Discussion

Ascending relaxin-3 neurons form abundant connections with key mid- and forebrain targets. In the rat, these connections are likely maintained by retrograde NGF signalling via TrkA (Harrington et al. 2013), in light of the observed selective expression of TrkA with relaxin-3. Previous reports of cell-type specific transgene expression using TrkA promoter elements in other species and contexts (Chang et al. 1998; Sacristan et al. 1999; Ma et al. 2000) suggested this approach could allow targeted viral vector transduction of rat TrkA/relaxin-3 NI neurons. However, an AAV vector engineered to express mCherry under the control of an 880 bp TrkA promoter sequence failed to provide cell-type specific expression in rat NI. In contrast, using a previously uncharacterised 1,736 bp relaxin-3 promoter sequence, we were able to efficiently transduce relaxin-3 NI neurons with 98% specificity.

Several technical obstacles must be overcome to successfully use promoter sequences to achieve cell-type specific transgene expression from a viral vector. Viral vectors have a limited packaging capacity, with AAV vectors failing to incorporate recombinant genomes larger than ~4.7 kb (Wu et al. 2010). Feasible promoter candidates must therefore be restricted to several kilobases or less, depending on the vector used. As a result, loss of regulatory elements such as histone binding sites, located potentially tens of kilobases upstream from the gene coding sequence of interest, can be a major impediment to this experimental approach. Cell-type specific promoters also need to be able to suppress expression driven by the AAV inverted terminal repeat (ITR) sequences. These ITRs, which are essential for AAV genome packaging, can drive transgene expression independently of other promoter elements (Flotte et al. 1993). Furthermore, high viral vector titres can reduce transduction specificity by increasing the number of genomic copies introduced to a cell, thus amplifying any weak, non-specific promoter activity (Kakava-Georgiadou et al. 2019). As alternative vector titres or volumes were not tested, this is an important consideration for the use of these and similar vectors in future studies. The potential for variations in transcription factor expression and/or epigenetic modifications due to cellular environment and context is also a key consideration when validating the suitability of promoters for their intended applications.

One or more of these factors may have led to the non-specific activity observed for the 880 bp rat TrkA promoter. Previous studies have identified a minimal promoter region of ~150 bp,

directly upstream of human (Chang et al. 1998) and mouse (Sacristan et al. 1999) TrkA coding sequences, which provided cell-type specific transgene expression in cultured neuroblastoma cells following transient transfection. A conserved TrkA enhancer was also shown to provide cell-type specific transgene expression from a pronuclear-injected plasmid construct, independently of the minimal promoter, in trigeminal and dorsal root ganglia of P0 mouse pups (Ma et al. 2000). Although the 880 bp rat TrkA promoter region used in our AAV1/2-TrkA-mCherry vector contained regions analogous to these human and mouse minimal promoter and mouse enhancer sequences, with 59%, 96% and 87% sequence identity, respectively, we were unable to replicate the targeted expression reported *in vitro* and in P0 mice. In addition to targeting neurons in the adult rat brainstem, rather than developing mouse ganglia or cell culture, our recombinant AAV genomes by necessity contain ITR sequences that were absent from the plasmids used in earlier studies. The incorporation of further sequence 5' to the 880 bp promoter trialled may capture elements sufficient to provide cell-type specific expression, but as mentioned, would eventually be limited by the AAV vector packaging capacity.

However, the AAV1/2-Rln3-mCherry vector, containing a 1,736 bp rat relaxin-3 promoter region, provided highly targeted transduction of relaxin-3 NI neurons. Transgene expression mediated by this vector was localised to the NI, where 98% of mCherry transduced neurons also contained relaxin-3 immunoreactivity. This was despite non-specific transduction of DTg and closely adjacent, non-relaxin-3 neurons in NI by co-injected AAV1/2-CAG-EGFP, emphasising that the specificity of the AAV1/2-Rln3-mCherry vector was achieved through promoter-mediated control of transgene expression and not viral vector tropism. Notably, one outcome that was apparently due to AAV1/2 vector tropism was a consistent transduction efficiency of around 70% of relaxin-3 NI neurons (with the exception of AAV1/2-TrkA-mCherry). Although alternative approaches, such as equivalent transgenic mouse or rat lines, may increase this efficiency, a purely viral vector-based methodology offers highly flexible options in targeting particular relaxin-3 neuron populations at specific time points during the lifespan of rats or mice. In the future, it will also be of interest to investigate the use of the relaxin-3 promoter vector to study the function of the smaller and more dispersed relaxin-3 neuron populations in the pontine raphe, PAG and dorsal to substantia nigra. Detailed analysis of the neurochemistry of transduced relaxin-3 neurons and their efferent connections, as demonstrated here in the MS/DB, will be valuable in determining the implications of targeted functional studies, that extend those using constitutively active promoters (Ma et al. 2017a; Szonyi et al. 2019).

The future utility of a relaxin-3-specific promoter is wide-ranging in nature. In the current study, targeted transgene expression was validated eight weeks after viral vector injection, indicating this approach would be suitable for physiological and behavioural studies within similar, if not potentially longer, time frames. New AAV constructs designed to include the relaxin-3 promoter would be able to accommodate at least 1.6 kb of transgene coding sequence. Many transgenes commonly used in modern neuroscience, including genetically-encoded calcium indicators (around 1.3 kb; Tian et al. (2009)) and fluorescently-tagged opsins (around 1.6 kb; Boyden et al. (2005)), could readily be expressed directly from an AAV vector under this relaxin-3 promoter. An AAV1/2 capsid was used here, as we have previously established its favourable tropism towards NI neurons (Callander et al. 2012), but other vectors such as lentivirus could be explored as a means of increasing packaging capacity for transgene cargo. Additional AAV packaging space could also be gained through the use of condensed polyadenylation and posttranscriptional regulatory elements (Choi et al. 2014), and further refinement of the relaxin-3 promoter itself. Although beyond the scope of this study, determining the particular motifs that confer cell-type specificity may allow engineering of a more compact promoter, improving transgene packaging capacity as well as promoter compatibility with transcriptional amplification strategies (Liu et al. 2008). Furthermore, such endeavours could also provide insights into relaxin-3 gene regulation, similar to those reported in response to CRF signalling (Tanaka et al. 2009).

In conclusion, following transduction by an injected AAV vector targeting the NI, we observed widespread non-specific mCherry transgene expression driven by an 880 bp TrkA promoter sequence in the adult rat brainstem. Differences in cell context, species and/or method of transgene delivery may explain discrepancies between our data and previous reports of selective expression driven from analogous promoter or enhancer regions in neuroblastoma cell lines and developing mouse nervous system. Notably, we also identified a novel cell-type specific relaxin-3 promoter, capable of transducing relaxin-3 NI neurons with 98% specificity for at least 8 weeks after AAV vector injection. Future studies utilising this promoter should lead to further insights into the molecular mechanisms that regulate relaxin-3 gene expression. Importantly, this newly characterised promoter sequence also represents a versatile tool for targeted studies of relaxin-3 circuitry in ongoing preclinical research.

Chapter 3

Directed subcellular opsin trafficking: differential physiological effects following optogenetic inhibition of neurons in the preBötzinger complex

3.1 Introduction

The need for rapid and efficient electrochemical communication has led neurons to evolve highly complex morphologies. A principal characteristic of this morphology is the polarisation of neurons into structurally, biochemically, and functionally distinct somatodendritic and axonal compartments. Polarisation begins early in neuronal development, with accumulation of cytoskeletal elements, recruitment of vesicles, and activity of particular enzymes occurring in one of the several nascent, morphologically indistinct processes, called neurites (Kunda et al. 2001; Shi et al. 2003; Yoshimura et al. 2005; Arimura et al. 2007). Though the underlying mechanisms by which this occurs are not well understood, it is thought to be determined by secreted factors, such as neurotrophins, as well as interactions with the extracellular matrix and processes from other neurons and glia, *in vivo* (Yogev et al. 2017); however, in the absence of such cues, polarisation still occurs stochastically in cultured neurons (Banker et al. 1977; Dotti et al. 1988).

Once designated, the growth of this neurite, destined to become an axon, far exceeds that of its counterparts, which, through a combination of feedback mechanisms, are prevented from becoming axons themselves and will instead mature into dendrites (Andersen et al. 2000; Arimura et al. 2007). This differential growth is facilitated by remodelling of the actin cytoskeleton (Bradke et al. 1999; Garvalov et al. 2007) and posttranslational modifications that stabilise axonal microtubules (Janke et al. 2011), which have an almost exclusively 'positive' orientation (Burton et al. 1981; Heidemann et al. 1981). In contrast, dendritic microtubules are less stable and have a mixed (Baas et al. 1988) or predominantly 'negative' (Stone et al. 2008) alignment. Biased transport of vesicles containing molecular cargo along these cytoskeletal networks by kinesin and dynein motors, which typically move towards the plus or minus end of microtubules, respectively (Vale 2003), also plays a crucial role in the development and maintenance of neuronal polarity (Nirschl et al. 2017; Kelliher et al. 2019).

After entering the axon or dendrite, further control over delivery of vesicular cargo is provided at the level of fusion with the plasma membrane. During synthesis in the endoplasmic reticulum and Golgi network, axonal and dendritic proteins are sorted into separate vesicles (Bonifacino 2014), coated with specific tethers and SNAREs that determine where each vesicle can fuse with the plasma membrane (Jahn et al. 2006; Bentley et al. 2016). Given that vesicles containing axonal proteins are created in, and therefore cannot be excluded from, the somatodendritic

compartment, their selective fusion with the axonal membrane provides an essential mechanism for polarised expression; though for some proteins, this can also be mediated by rapid endocytosis from the dendritic membrane (Sampo et al. 2003).

Once delivered to their appropriate destination, proteins must be prevented from randomly diffusing through the plasma membrane or cytosol. In some instances, this can be achieved by anchoring proteins to cytoskeletal scaffolding (MacGillavry et al. 2011). However, the most important structure in maintaining distinct somatodendritic and axonal compartments is the axon initial segment (AIS) (Rasband 2010). The AIS forms in the proximal axon, soon after differentiation from the dendrites, and is organised around the scaffold protein ankyrin G (AnkG) (Ogawa et al. 2008). The accumulation of specific proteins at the AIS, including ion channel species crucial to action potential generation (Zhou et al. 1998) and a fasciulated microtubule network (Sobotzik et al. 2009), is dependent on AnkG. This dense accumulation of protein in the AIS provides a physical barrier to diffusion (Kobayashi et al. 1992; Nakada et al. 2003), and also filters vesicles prior to their entering the axon (Song et al. 2009). Knockout or knockdown of the AnkG gene has been shown to cause morphological and molecular de-differentiation of the axon, both *in vitro* (Hedstrom et al. 2008) and *in vivo* (Sobotzik et al. 2009).

Though essential for proper neuronal function, the distinct biochemical environments resulting from polarised, subcellular gene expression can complicate the outcome and interpretation of preclinical transgenic experiments. An important example of this has recently been demonstrated in the field of optogenetics (Wiegert et al. 2016). By introducing microbial genes for light sensitive ion channels or pumps (opsins) to neurons, optogenetic approaches allow neuroscientists to artificially stimulate or inhibit neural activity on millisecond timescales in conscious, behaving animals. This technique relies on ion gradients, maintained by endogenously expressed pumps in the neuronal plasma membrane, to create a hyper- or depolarising current when the opsin channel is opened by exposure to light (Rajasethupathy et al. 2016). However, such ion gradients are not necessarily consistent between or within individual neurons.

The gradient of chloride (Cl^-) ions across the neuronal membrane, for example, is determined by a balance of K^+/Cl^- (KCC2) and $Na^+/K^+/Cl^-$ (NKCC1) cotransporters, which move Cl^- out of or into the cytosol, respectively (Blaesse et al. 2009). In immature neurons, NKCC1 is more abundantly expressed than KCC2 (Kaila et al. 2014). This concentrates Cl^- inside the neuron, causing

membrane depolarisation by Cl^--conducting receptors, such as $GABA_A$ and glycine (Obata et al. 1978; Yamada et al. 2004). As the neuron develops, KCC2 becomes more abundantly expressed than NKCC1 (Stein et al. 2004; Delpy et al. 2008), shifting the Cl^- gradient to be higher outside the cell. Stimulation of $GABA_A$ (Rivera et al. 1999) or glycine (Ehrlich et al. 1999) receptors therefore typically causes membrane hyperpolarisation in the mature mammalian central nervous system. Furthermore, KCC2 is excluded from the axon and selectively expressed in the somatodendritic membrane (Hubner et al. 2001; Baldi et al. 2010), resulting in higher Cl^- concentrations inside the axon than in the soma or dendrites (Price et al. 2006). This variation in Cl^- concentrations has led to unanticipated complications when applying anion conducting opsins as inhibitory (hyperpolarising) tools for neuroscience research.

Among the most widely adopted anion conducting opsins are those isolated from the cryptophyte alga *Guillardia theta* (Govorunova et al. 2015), particularly *G. theta* anion channel rhodopsin 1 (G*t*ACR1) and 2 (*Gt*ACR2). *Gt*ACRs are transmembrane proteins spanned by a tunnel, gated at several points by electropositive residues, which selectively permit anion passage following photon-induced conformational changes (Kim et al. 2018; Li et al. 2019). Relative to previously established 'inhibitory' opsins, such as *Natronomonas pharaonis* halorhodopsin (*Np*HR; Zhang et al. (2007)) and archaerhodopsin-3 (Arch; Chow et al. (2010)), which are ion pumps, *Gt*ACRs deliver much stronger photocurrents at lower light intensities (Govorunova et al. 2015), making them potent tools for neuronal inhibition.

However, due to variations in intracellular Cl^- concentrations, the somatodendritic membrane alone appears to be hyperpolarised by *Gt*ACRs. When activated in the axonal membrane, *Gt*ACRs have been found to elicit membrane depolarisation by allowing Cl^- efflux from the axon, causing neurotransmitter release and antidromic spiking (Mahn et al. 2016; Malyshev et al. 2017). *Gt*ACRs have to date been characterised in mature neurons and animals, and their application to studies of neuronal or nervous system development would presumably also be affected by varying intracellular Cl^- environments. In the present study, we sought to optimise the utility of *Gt*ACRs as optogenetic tools by directing their expression selectively to the somatic or axonal membrane. In addition to providing uniform hyper- or depolarisation, we hypothesised such targeted subcellular expression would also prove valuable in functionally dissecting closely interconnected neural circuitry *in vivo*. Given its faster kinetics (Govorunova et al. 2015), we focus here on *Gt*ACR2, rather than *Gt*ACR1.

Many previous attempts to achieve targeted subcellular expression of chemo- and optogenetic receptors have yielded fruitful results. Such directed expression typically relies on fusing a short trafficking motif, isolated from an endogenously localised protein, to the intracellular C-terminus of the introduced receptor. For example, a 65-amino acid sequence, derived from the voltage-gated potassium channel Kv2.1 (Lim et al. 2000), has been widely used in restricting transgene expression to the soma. Truncation of this trafficking motif from Kv2.1, which normally localises to the soma and proximal dendrites, results in non-specific expression across dendritic, somatic, and axonal membranes of cultured neurons (Lim et al. 2000). Fusion constructs incorporating this Kv2.1 motif have mimicked expression of the native channel, providing targeted, somatic opsin expression in mouse retinal ganglion cells (Wu et al. 2013) and cortical neurons (Baker et al. 2016).

The feasibility of targeting transgene expression to the axon has also been demonstrated. To selectively express the chemogenetic hM4Di receptor in the axonal membrane, Stachniak et al. (2014) fused this protein with a trafficking motif from the synaptic adhesion and signalling molecule, neurexin 1α (Nrxn1α). Neurexins are packaged in synaptic protein transport vesicles (STVs) and carried by kinesin-like protein KIF1A throughout neurons, though this transport is biased towards the axon (Neupert et al. 2015). Once inside the axon, STVs selectively fuse with the axonal membrane adjacent to synapses, from which neurexins reach the active zone by lateral diffusion (Neupert et al. 2015). This selective transport of neurexins is mediated by a C-terminal PDZ recognition motif (Fairless et al. 2008), which, as shown by Stachniak et al. (2014), also has the capacity to direct axonal expression of transgenic fusion constructs.

This chapter describes two novel *Gt*ACR2-fusion constructs, developed for selective expression in the somatic or axonal membrane through incorporation of the Kv2.1 or Nrxn1α trafficking motif, respectively. Following initial histological characterisation in cultured mouse hippocampal neurons, the trafficking and function of these constructs was assessed in viral vector-transduced rat ventral respiratory column (VRC) neurons *in vivo*. VRC circuitry was selected as a particularly apt system for such characterisation, given its well established role as a central pattern generator of respiratory drive (Del Negro et al. 2018) and its connections with neighbouring cardiovascular nuclei in the medulla (Habler et al. 1994). These close anatomical connections are mirrored by the physiological coupling of respiratory and cardiovascular function across vertebrates (Taylor et al. 1999). Examples of such coupling include respiratory sinus arrhythmia (RSA), which describes the increase and decrease in heart rate that occurs during inspiration and

expiration, respectively (Angelone et al. 1964), as well as the respiratory modulation of sympathetic nerve activity which generates blood pressure oscillations known Traube-Hering (TH) waves (Killip 1962).

Though the physiological significance of such cardiorespiratory coupling remains contentious, with hypothesized roles including optimisation of cardiac efficiency and respiratory gas exchange (Hayano et al. 1996; Dick et al. 2009; Ben-Tal et al. 2012), these phenomena have clear clinical relevance. Aberrant sympatho- and cardiorespiratory coupling have been linked to heart failure and hypertension (Garcia et al. 2013; Menuet et al. 2017; Elstad et al. 2018), among other conditions. The persistence of sympatho- and cardiorespiratory coupling following removal or manipulation of peripheral inputs, for example through vagotomy (Adrian et al. 1932; Haselton et al. 1989), artificial ventilation (Daly 1991; Shykoff et al. 1991) and/or in the working heart-brainstem preparation (WHBP) (Pickering et al. 2006; Simms et al. 2009), indicate central mechanisms play a key role in maintaining this synchrony. However, the underlying neural circuitry remains poorly understood. Expressing the described *Gt*ACR2 fusion constructs in VRC neurons therefore not only offers a clear indication of their functionality (i.e. through their effects on breathing), but also a potential method for mapping local network connections with cardiac and sympathetic nuclei through subcellular optogenetic manipulation.

3.2 Methods

3.2.1 Animals

All experiments were approved by The University of Melbourne Animal Research Ethics and Biosafety Committees or The Florey Institute of Neuroscience and Mental Health Animal Ethics Committee, and conducted in accordance with the Code of Practice for the Care and Use of Animals for Scientific Purposes published by the Australian National Health and Medical Research Council. C57BL/6J mouse colonies, which supplied studies involving cultured hippocampal neurons, were housed in individually ventilated cages on a 12 h light-dark cycle (lights on 07:00). Mice were time-mated overnight, with visualisation of a vaginal plug the following morning considered as embryonic day (E) 0.5. Optogenetic experiments utilised male Sprague Dawley rats, housed in open-top cages under a 12 h light-dark cycle (lights on 06:30). Mouse and rat cages were maintained at 22 ± 1 ˚C, and all animals had *ad libitum* access to water and standard chow.

3.2.2 Plasmid design and generation

Subcellular trafficking in neurons was assessed using plasmid and AAV vectors, developed for expression of *Gt*ACR2 fused with a fluorescent tag alone, or the Kv2.1 or Nrxn1α trafficking motif. To express *Gt*ACR2 from an AAV vector, the *Gt*ACR2-EYFP coding sequence was ligated from pFUGW-h*Gt*ACR2-EYFP (Addgene plasmid #67877; Govorunova et al. (2015)); a gift from Prof John Spudich (The University of Texas, TX, USA)) into pAM-CAG-tdTomato (kindly provided by Dr Verena Wimmer, Walter and Eliza Hall Institute, VIC, Australia) using *Bam*HI and *Hin*dIII sites, creating pAM-CAG-*Gt*ACR2-EYFP (Figure 3.1A). The EYFP tag for this construct is fused to the *Gt*ACR2 intracellular C-terminus via a linker containing three alanine residues, as originally cloned and functionally characterised by Govorunova et al. (2015). Further AAV vectors were designed for bicistronic expression of *Gt*ACR2, fused to either a 65 amino acid Kv2.1 or 55 amino acid Nrxn1α trafficking motif, with cytosolic mCherry to allow clear visualisation of transduced neurons and facilitate subcellular identification of *Gt*ACR2 channel localisation. The Kv2.1-fusion construct included a monomeric, ultra-stable green fluorescent protein (muGFP) tag (Scott et al. 2018) between *Gt*ACR2 and Kv2.1 sequences, mimicking the design of previously characterised opsin-Kv2.1 fusion constructs (Wu et al. 2013; Baker et al. 2016), with four alanine residues linking muGFP to the *Gt*ACR2 C-terminus. For the Nrxn1α-fusion construct, three alanine

residues linked a haemagglutinin (HA) tag to the C-terminus of *Gt*ACR2, with the Nrxn1α motif in turn fused to the C-terminus of this HA tag. This design is analogous to that used by Stachniak et al. (2014) for axonal expression of, and functional inhibition by, the hM4Di receptor. pUC57 plasmids, containing synthetic *Gt*ACR2-HA-Nrxn1α-P2A-mCherry, *Gt*ACR2-muGFP-P2A-mCherry, or Kv2.1 trafficking motif coding sequences, were provided by Genscript (NJ, USA). Incorporation of these sequences into AAV vector plasmid backbones was achieved using the Gateway™ cloning system. Forward (5'-attB1-TCTAGAGCCACCATGGCCTC) and reverse (5'-attB2-AAGCTTTTACTTGTACAGCTCGTCC) primers facilitated polymerase chain reaction (PCR) amplification of *Gt*ACR2-muGFP-P2A-mCherry for recombination with pDONR-P1-P2 (Thermo Fisher Scientific, VIC, Australia), producing pENTR-L1-*Gt*ACR2-muGFP-P2A-mCherry-L2 plasmid. pENTR-L1-*Gt*ACR2-muGFP-P2A-mCherry-L2 was recombined with the pAAV-Gateway destination vector (Addgene plasmid #32617; (White et al. 2011); a gift from Dr Melanie White, A*STAR, Singapore), which also contains the constitutively active CAG promoter sequence, to produce pAAV-CAG-*Gt*ACR2-muGFP-P2A-mCherry (Figure 3.1B). An introduced *Bam*HI restriction site was used to ligate the Kv2.1 trafficking motif between muGFP and P2A coding sequences of pAAV-CAG-*Gt*ACR2-muGFP-P2A-mCherry, creating pAAV-CAG-*Gt*ACR2$^{Kv2.1}$-P2A-mCherry (Figure 3.1C). Additional forward (5'-attB5-ATGGCCTCCCAGGTCGTG) and reverse (5'-attB2-TTACTTGTACAGCTCGTCCATG) primers were used in PCR amplification of *Gt*ACR2-HA-Nrxn1α-P2A-mCherry. Recombination of this PCR product with pDONR-P5-P2 produced pENTR-L5-*Gt*ACR2-HA-Nrxn1α-P2A-mCherry-L2. Subsequent recombination of pENTR-L1-Ef1α-R5 and pENTR-L5-*Gt*ACR2-HA-Nrxn1α-P2A-mCherry-L2 plasmids with the destination vector, pAM-Gateway (Wykes et al. 2020), resulted in pAM-Ef1α-*Gt*ACR2^{nrxn}-P2A-mCherry (Figure 3.1D), which expresses *Gt*ACR2^{nrxn} and mCherry under the constitutively active Ef1α promoter. pDONR P5-P2 and pENTR-L1-Ef1α-R5 plasmids were gifts from Dr Melanie White (A*STAR, Singapore). *Bam*HI, *Hin*dIII and T4 Ligase enzymes were sourced from Promega (NSW, Australia) or New England BioLabs (VIC, Australia). All primers were synthesised by Sigma-Aldrich (NSW, Australia), and PCR performed using Vent® DNA polymerase (New England BioLabs). Recombination reactions were incubated at 25 °C for 16 h, using Clonase™II reagents (Life Technologies, VIC, Australia). Plasmids containing PCR amplified inserts were verified by Sanger sequencing (Australian Genome Research Facility, VIC, Australia).

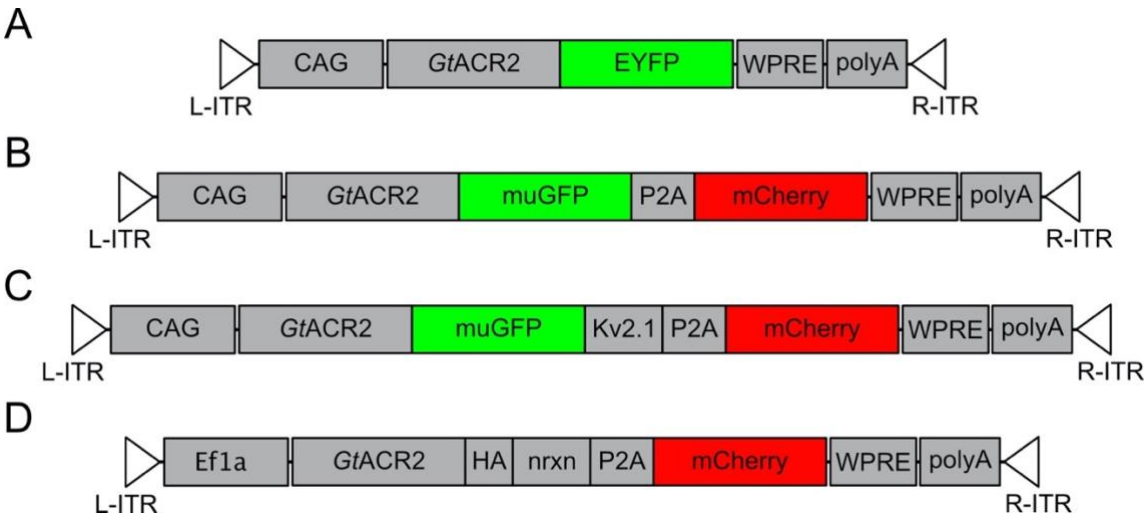

Figure 3.1 *Schematic representation of viral vectors genomes developed in this chapter.* Viral vector genomes, as packaged into AAV1/2 vector capsids*, from **(A)** pAM-CAG-*Gt*ACR2-EYFP, **(B)** pAAV-CAG-*Gt*ACR2-muGFP-P2A-mCherry, **(C)** pAAV-CAG-*Gt*ACR2$^{Kv2.1}$-P2A-mCherry, or **(D)** pAM-Ef1α-*Gt*ACR2^{nrxn}-P2A-mCherry plasmids (*CAG*, cytomegalovirus/chicken β-actin synthetic promoter; *Ef1*α, elongation factor 1α promoter; *EYFP*, enhanced yellow fluorescent protein; *HA*, haemagglutinin tag; *L-ITR*, left inverted terminal repeat; *muGFP*, monomeric ultra-stable green fluorescent protein; *P2A*, porcine teschovirus-1 2A self-cleaving peptide; *polyA*, simian virus 40 poly A sequence; *R-ITR*, right inverted terminal repeat; *WPRE*, woodchuck hepatitis virus post-transcriptional regulatory element). *pAAV-CAG-*Gt*ACR2-muGFP-P2A-mCherry was used in the present study for cloning and *in vitro* transfection, however AAV vectors were not produced from this plasmid directly or used *in vivo*.

3.2.3 AAV vector production

Recombinant AAV vector genomes were packaged into mosaic 1/2 serotype capsids, as described (Zolotukhin et al. 1999; Ganella et al. 2013). In brief, pAM-CAG-*Gt*ACR2-EYFP was co-transfected with pHelper and pAAV-RC plasmids (Stratagene, CA, USA) into AAV293 cells (Agilent Technologies, CA, USA), and pAAV-CAG-*Gt*ACR2$^{Kv2.1}$-P2A-mCherry or pAM-Ef1α-*Gt*ACR2^{nrxn}-P2A-mCherry was co-transfected with pDPI and pDPII plasmids (Grimm et al. 2003) into 293FT cells (Thermo Fisher Scientific). Following purification of harvested vectors by iodixanol gradient centrifugation, quantitative PCR, using primers against the woodchuck hepatitis virus post-transcriptional regulatory element (WPRE) sequence (as described by Ma et al. (2017a)), was used to determine vector titre as genomic copies (gc)/ml.

3.2.4 Neuronal cultures and immunocytochemistry

Dissociated primary hippocampal enriched neuronal cultures were prepared from E17.5 mouse embryos of both sexes, as described (Baker et al. 2015). Following decapitation, single-cell suspensions were plated on poly-D-lysine and laminin-coated 25 mm coverslips at a density of 2.5-3.5 x 10^4 cells/coverslip. At 7 days *in vitro* (DIV), cells were transfected with 500 ng of either pAAV-CAG-GtACR2-muGFP-P2A-mCherry or pAAV-CAG-GtACR2$^{Kv2.1}$-P2A-mCherry using Lipofectamine 2000 (Thermo Fisher Scientific), as described (Gordon et al. 2011). At DIV 14, cells were fixed by 20 min incubation in phosphate buffered saline (PBS) solution containing 4 % (w/v) paraformaldehyde (PFA) and immunocytochemistry (ICC) performed. In preparation for ICC, coverslips were immersed in PBS containing 50 mM NH_4Cl for 10 min, briefly washed with PBS and permeabilised for 5 min in PBS containing 0.1 % (v/v) Triton X-100 and 1 % (v/v) bovine serum albumin (BSA), before further PBS washes and blocking for 1 h in 1 % BSA/PBS solution. Blocked coverslips were incubated for 2 h in 1 % BSA/PBS containing the primary antibodies, rabbit anti-Microtubule Associated Protein 2 (MAP2; 1:200) (AB5622, Merck Millipore, VIC, Australia) and mouse anti-mCherry (1:100) (3A11, Developmental Studies Hybridoma Bank, University of Iowa, IA, USA). Coverslips were then washed with PBS and incubated for 1 h in 1 % BSA/PBS containing donkey anti-mouse Alexa-594 (1:200) (Jackson Laboratory, ME, USA) and donkey anti-rabbit Alexa-647 (1:500) (Thermo Fisher Scientific) conjugated antibodies with 1 µg/ml bis-benzimide H (Hoechst) 33342 (Sigma-Aldrich). Further PBS washes and rinsing in distilled water preceded slide mounting of coverslips using Dako fluorescence mounting medium (Agilent Technologies). Rabbit anti-MAP2 antibody was a gift from A/Prof Clare Parish

(The Florey Institute, VIC, Australia). Fixation and all ICC incubations were performed at room temperature, with coverslips contained in a dark humidified chamber during antibody incubations.

3.2.5 Stereotaxic injections

Rats were placed in an enclosed chamber and lightly anesthetised by inhalation of isoflurane (Rhodia Australia Pty. Ltd., VIC, Australia), prior to intramuscular (i.m.) injection of ketamine (60 mg/kg; Lyppard, VIC, Australia) mixed with medetomidine (250 µg/kg; Pfizer Animal Health, NSW, Australia). Once deeply anesthetised, as determined by lack of pedal withdrawal and corneal reflexes, rats were placed in a stereotaxic frame (RWD Life Science, GD, China), with the nose ventro-flexed (incisor bar -15 mm). During surgery, body temperature was maintained at 37.5 ˚C with a heat pad (TC-1000 Temperature Controller, CWE Inc., PA, USA). To expose the dorsal brainstem, a midline incision was made over the occipital bone, portions of which were removed with a dental drill, and the atlanto-occipital membrane opened. Glass micropipettes (~30 µm external tip diameter) were loaded with injectate, and a silver wire, connected to an electrophysiology amplifier (NeuroLog system, Digitimer Ltd., UK), inserted to enable recording of neuronal activity. Using a 20 ˚ angled approach (tip pointing forward, rostro-caudal axis), the pipette was lowered into the brainstem 1.5 mm lateral from the midline, to record extracellular multiunit activity. The column of robust inspiratory-locked neuronal activity along the ventral brainstem was mapped, to find the most rostral point. This coordinate was used to define injections targeting the preBötzinger complex (preBötC) of the VRC (typically between 0.0 and 0.3 mm rostral, 1.4 ± 0.3 mm ventral to the *calamus scriptorius*). Fifty nl injections of AAV1/2-CAG-GtACR2-EYFP (5.61-9.65 x 10^{11} gc/ml, n = 3 rats), AAV1/2-CAG-GtACR2$^{Kv2.1}$-P2A-mCherry (8.83 x 10^{11} gc/ml, n = 9 rats), or AAV1/2-Ef1α-GtACR2^{nrxn}-P2A-mCherry (2.42 x 10^{10} gc/ml, n = 4 rats) were made bilaterally in the respiratory column using a picospritzer (World Precision Instruments, FL, USA). In a separate cohort of rats, to facilitate extracellular multiunit activity recordings during optogenetic manipulations, bilateral 50 nl injections of AAV1/2-CAG-GtACR2-EYFP (n = 2 rats) were made into the respiratory column via burr holes drilled through the dorsal surface of the occipital bone (ML = ±1.5 mm from midline, AP = -3.6 mm from interaural line, DV = -7.0 (±0.5) mm from brain surface, pipette tip angled 20 ˚ caudally; incisor bar -15 mm). For all injections, reflux of injectate up the injection track was minimised by leaving the pipette in place for 2 min before it was slowly withdrawn. Sterile sutures were used to close each wound, prior to subcutaneous administration of meloxicam (1mg/kg, Metacam, Boehringer Ingelheim, NSW,

Australia), intraperitoneal injection of Hartmann's solution (Baxter Healthcare, NSW, Australia) for fluid replacement, and anaesthesia reversal with atipamazole (1 mg/kg, i.m., Antisedan, Pfizer Animal Health).

3.2.6 Optogenetic experiments

Following at least 3 weeks recovery from stereotaxic surgery, anaesthesia was again induced by inhalation of isoflurane (Rhodia Australia Pty. Ltd.) in an enclosed chamber. Rats were transferred to a stereotaxic frame (incisor bar +3 mm; RWD Life Science), where anaesthesia was maintained with 3-3.5 % isoflurane, delivered in oxygen (800 ml/min) through an anaesthetic mask. Body temperature was maintained at 37.5 ˚C with a TC-1000 heat pad (CWE Inc.). For diaphragm electromyography (dEMG) recordings, a lateral abdominal incision was made and two nylon-insulated stainless-steel wire electrodes (0.25 mm insulated diameter) ending with suture pads (0.7 × 1.0 × 3.2 mm, Plastics One, VA, USA) placed in the costal diaphragm, 3–4 mm apart. The femoral artery and vein of one leg were cannulated for measurement of arterial pressure and drug administration, respectively (PE10 tubing (ID 0.28 x OD 0.61 mm) connected to PE50 (0.17 x 1.45 mm)). Isoflurane anaesthesia was gradually replaced by 1.2 mg/kg intravenous urethane, following which rats were tracheotomised, and oxygen (100%) directed over the tracheotomy cannula. The arterial catheter, connected to a Statham Gould (P23 Db) pressure transducer, and the dEMG electrode wires, were coupled to a pre-amplifier (NeuroLog System, Digitimer Ltd., UK) and connected to a data acquisition system (Cambridge Electronic Design, UK; 0.5-1 kHz band-pass filter, 5 kHz sampling rate used for dEMG recordings). Arterial pressure and dEMG were recorded using Spike2 software (Cambridge Electronic Design). To perform optogenetic experiments, the optical fibres (200 µm diameter, RWD Life Science), were secured to a manipulator on the stereotaxic frame and lowered through the dorsal surface of the skull through burr holes made in the occipital bone centred approximately 1 mm rostral to the occipital suture, and ±1.8 mm lateral from the midline. Output intensity from the optical fibres was determined using a PM100D Meter (Thorlabs, NJ, USA). Physiological responses to *Gt*ACR2 stimulation were investigated by probing the brainstem at various AP levels between the occipital suture and up to 2.5 mm rostral to this point, where light (473 nm, 15-20 mW) was delivered continuously, or in 5 ms pulses at 10, 20, or 50 Hz, at 0.5 mm increments moving ventrally from the medulla surface. In a separate cohort of rats, extracellular multiunit activity was recorded during optogenetic manipulations. For these experiments the brainstem was accessed via the atlanto-occipital membrane with visual

observation of the dorsal brainstem surface. The optical fibres were angled at 20˚ with the tip projecting caudally whilst the glass recording micropipette (~3 µm tip diameter) was angled at 20˚ with the tip projecting rostrally. The glass pipette was filled with 4 M NaCl and connected, via a silver wire, to an electrophysiology amplifier (NeuroLog System; 10 kHz sampling rate used to record action potentials, other parameters as above). Once the optical fibres were positioned in the medulla so as to elicit the maximal physiological response to *Gt*ACR2 activation (continuous illumination), the micropipette was used to localise and monitor nearby, respiratory-locked phasic activity.

3.2.7 Histology

At the conclusion of optogenetic stimulations, rats were transcardially perfused with 1 ml/g ice-cold PBS, followed by 1 ml/g of 4 % PFA. Dissected brains were post-fixed in 4 % PFA overnight at 4 ˚C, then transferred to a 20 % (w/v) sucrose solution (4 ˚C, 48 h) for cryoprotection. Forty µm thickness coronal sections were cut through the medulla, from the pyramidal decussations to the level of the facial nucleus (VIIn) using a cryostat, and collected free-floating for immunohistochemistry (IHC), as described (Chen et al. 2010; Sevigny et al. 2012; Menuet et al. 2014). Chicken anti-GFP (1:5000; AB13970, Abcam, VIC, Australia), rabbit anti-*Ds*Red (1:5000; Cat. No. 632496, Takara Bio USA, CA, USA), and goat anti-choline acetyltransferase (ChAT; 1:1000; AB144P, Merck-Millipore) were used as primary antibodies. These markers were visualised using AlexaFluor-488-conjugated donkey anti-chicken, Cy3-conjugated donkey anti-rabbit, and Cy5-conjugated donkey anti-goat secondary antibodies (1:500 each; Jackson Laboratory).

3.2.8 Imaging

To map the location of transduced neurons through the medulla, whole sections were imaged using a Zeiss Axio Imager M2 epifluorescent microscope (Carl Zeiss AG, BW, Germany). Tiled images of immunofluorescence were obtained using a 10 × air objective lens and automated stage, with collected frames stitched and exported using Zen Blue software (Carl Zeiss AG). Representative, high resolution images of cultured hippocampal and transduced VRC neurons were collected using an LSM 780 Zeiss Axio Imager 2 laser scanning confocal microscope and Zen Black software (Carl Zeiss AG). Confocal images were acquired using a 20 × air objective lens, with planes through the entire z-axis of each sample imaged at 2 µm intervals. Excitation

wavelengths and emission filter parameters for each fluorophore were as follows: Hoechst 33342, 405 nm (410-496 nm); muGFP/Alexa488, 488 nm (493-579 nm); Cy3, 561 nm (561-624 nm); Alexa-594, 561 nm (588-650 nm); Alexa-647/Cy5, 633 nm (653-755 nm). Further processing, including the generation z-axis maximum projection images, was performed with Fiji software (Schindelin et al. 2012).

3.2.9 Data analysis

Sorting of data from extracellular multiunit activity recordings was performed using Spike2 software (Cambridge Electronic Design). A series of templates were generated according to the waveform characteristics of events across the recording, with a minimum of eight similar spikes in a series of 400 required to create a new template. Individual spikes were then matched to these templates based on their waveform shape. Heart rate, mean arterial pressure, and respiratory frequency data were derived from arterial pressure and dEMG recordings using Spike2 software (Cambridge Electronic Design). Relevant data preceding, during, and following optogenetic stimulations for each rat were exported at 100 Hz sampling frequency into Excel (Microsoft Corporation, WA, USA), where these data were normalised as the percentage difference relative to 'baseline' values for each parameter (taken as the average value during the 20 s immediately prior to laser onset). Normalised data were transferred to Prism (GraphPad Software, CA, USA) and graphed as the mean ± 95 % confidence interval. Further analysis of TH waves and RSA in rats expressing *Gt*ACR2^{nrxn} was performed in Spike2 software (Cambridge Electronic Design). Waveform averages of systolic arterial pressure and heart rate values from 10 breaths prior to, during, and following laser stimulation were generated for each rat, to characterise the effect of optogenetic manipulation on TH waves and RSA, respectively. RSA and TH wave amplitude in rats expressing *Gt*ACR2^{nrxn}, as well as between-group differences in heart rate, mean arterial pressure, and missed breaths (calculated as the baseline respiratory frequency multiplied by apnoea duration) during laser stimulation, were graphed using Prism software (GraphPad Software), where one-way ANOVA tests were also performed.

3.3 Results

3.3.1 Fusion with Kv2.1 motif does not provide somatic localisation of *Gt*ACR2 *in vitro*

The ability of the Kv2.1 motif to provide somatic GtACR2 expression was initially characterised in cultured mouse hippocampal neurons. Transfection of neurons using plasmid vectors, rather than AAV vector-transduction, was used to achieve sparse labelling *in vitro* and allow clear visualisation of individual neurons. Following transfection with pAAV-CAG-*Gt*ACR2-muGFP-P2A-mCherry, muGFP expression was visible throughout cultured neurons, including the dendritic arbor and soma, identified by labelling with MAP2 immunoreactivity, and axonal projections, which are morphologically distinct from dendrites and lack MAP2 immunoreactivity (Figures 3.2A, 3.2C, 3.2D; representative neuron from n = 2 cultures). In neurons transfected with pAAV-CAG-*Gt*ACR2$^{Kv2.1}$-P2A-mCherry, muGFP fluorescence was also distributed throughout each compartment (Figures 3.2B, 3.2E, 3.2F; representative neuron from n = 2 cultures), despite fusion with the Kv2.1 trafficking motif. There did not appear to be any differences in subcellular trafficking between these two constructs *in vitro*.

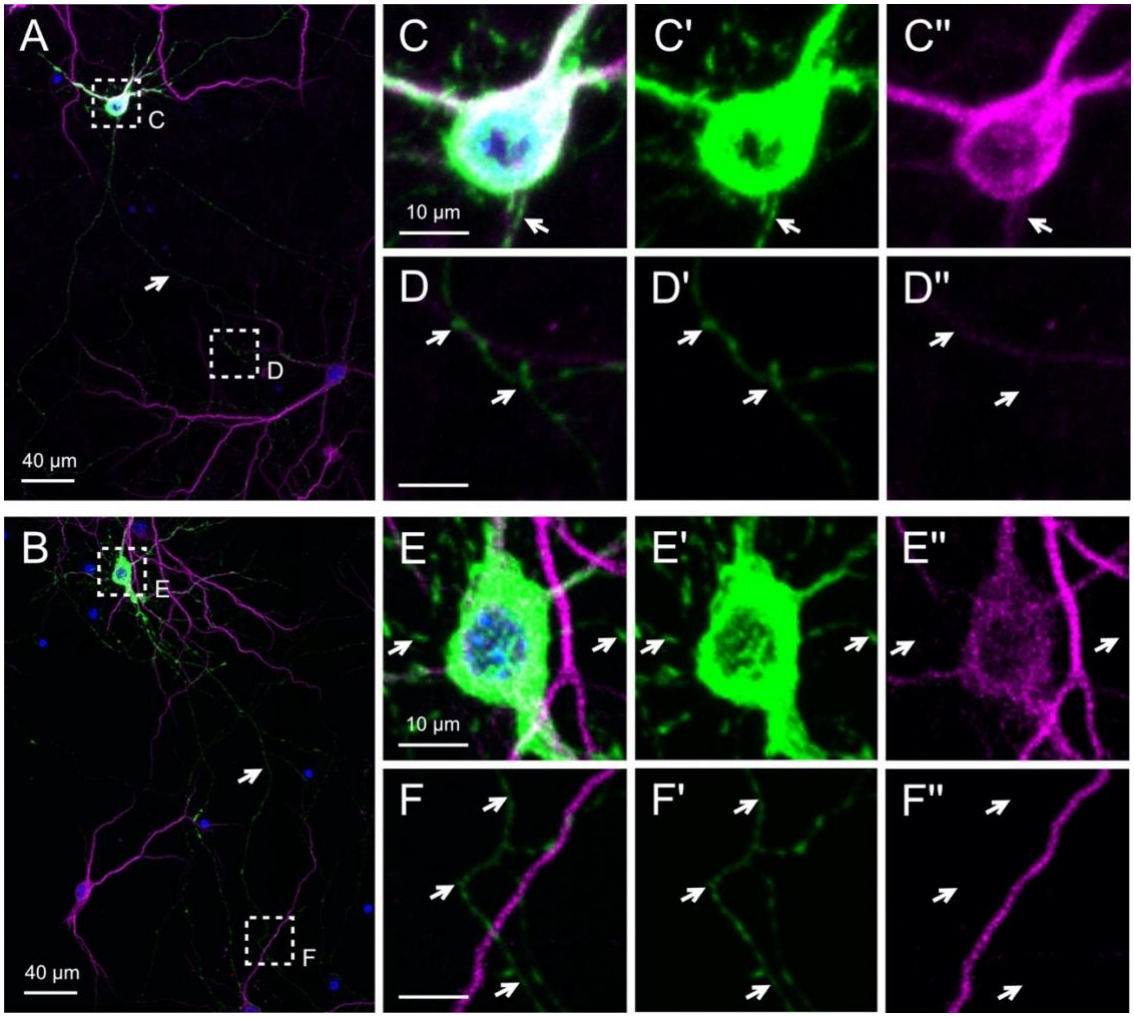

Figure 3.2 *Kv2.1 motif-fusion does not prevent axonal GtACR2 expression in vitro*. Representative cultured hippocampal neurons, expressing **(A)** *Gt*ACR2-muGFP following transfection with pAAV-CAG-*Gt*ACR2-muGFP-P2A-mCherry (n = 2 cultures), or **(B)** *Gt*ACR2$^{Kv2.1}$ following transfection with pAAV-CAG-*Gt*ACR2$^{Kv2.1}$-P2A-mCherry (n = 2 cultures). Fluorescent muGFP signal (green) from both *Gt*ACR2-muGFP and *Gt*ACR2$^{Kv2.1}$ was present throughout transfected neurons, including the soma and dendrites (labelled with MAP2 immunoreactivity (magenta); overlaid MAP2 immunoreactivity and muGFP fluorescence shown in white), as well as axon (lacking MAP2 immunoreactivity and indicated by arrowheads). Nuclei stained with Hoechst 33342 are shown in blue. Higher resolution images of merged fluorescent channels, illustrating somatic and axonal expression of *Gt*ACR2-muGFP and *Gt*ACR2$^{Kv2.1}$, are provided in **(C,D)** and **(E,F)**, respectively, as well as individual channels for muGFP **(C'-F')** and MAP2 **(C''-F'')** immunoreactivity in these fields.

3.3.2 *Gt*ACR2$^{Kv2.1}$ is expressed in axons *in vivo*, and shows enhanced neuronal expression

To assess axonal trafficking of *Gt*ACR2 constructs *in vivo*, images were collected from facial nucleus (VIIn) in rats with AAV vector injections targeting the VRC. VIIn lies rostral to the VRC in the medulla, and is known to be innervated by VRC neurons (Yang et al. 2018). Dense innervation of VIIn by immunofluorescently labelled axons was observed in rats which received AAV1/2-CAG-*Gt*ACR2-EYFP injections targeting the VRC (Figure 3.3A; representative image from n = 3 rats). This was also the case in rats that received VRC injections of AAV1/2-CAG-*Gt*ACR2$^{Kv2.1}$-P2A-mCherry (Figure 3.3B; representative image from n = 9 rats).

Robust immunofluorescent labelling of VRC neurons with EYFP, muGFP, and/or mCherry was observed in both of these cohorts following transduction with AAV1/2-CAG-*Gt*ACR2-EYFP (Figure 3.4A; representative image from n = 3 rats) or AAV1/2-CAG-*Gt*ACR2$^{Kv2.1}$-P2A-mCherry (Figure 3.4B; representative image from n = 9 rats), as well as in rats that received AAV1/2-Ef1α-*Gt*ACR2^{nrxn}-P2A-mCherry injections (Figure 3.4C; representative image from n = 4 rats). At higher magnification, *Gt*ACR2-EYFP immunofluorescence appeared highly dispersed (Figure 3.4A'), such that it was difficult to visualise individual soma at the injection site. In contrast, fluorescent signal from muGFP allowed neuronal boundaries to be easily defined following transduction with AAV1/2-CAG-*Gt*ACR2$^{Kv2.1}$-P2A-mCherry (Figure 3.4B'), suggesting *Gt*ACR2$^{Kv2.1}$ was more efficiently expressed by VRC neurons than *Gt*ACR2-EYFP. Fluorescent signal from muGFP was also distinct from cytosolic mCherry expression (Figure 3.4B), indicating efficient P2A-mediated cleavage. Cytosolic mCherry immunofluorescence alone was used to identify neurons transduced with AAV1/2-Ef1α-*Gt*ACR2^{nrxn}-P2A-mCherry (Figure 3.4C), as IHC attempts made here to visualise *Gt*ACR2^{nrxn} directly in transduced neurons, using antibodies against its fused HA tag, were unsuccessful. However, mCherry production demonstrates that the AAV1/2-Ef1α-*Gt*ACR2^{nrxn}-P2A-mCherry vector efficiently transduced VRC neurons, where mRNA encoding *Gt*ACR2^{nrxn} must also have been expressed. Physiological responses to laser delivery in these rats (see Section 3.3.5 below) also suggest *Gt*ACR2^{nrxn} was functional and expressed in the neuronal membrane.

Although AAV vector injections used the rostral locus of phasic, inspiratory-locked neuronal activity to target the preBötC in the VRC, spread of neuronal transduction was also evident outside this region. This primarily affected the nucleus ambiguus (NAmb), which borders the VRC dorsally, with more variable spread to the neighbouring intermediate reticular nucleus (IRt)

and ventrolateral medulla (VLM). A similar distribution of transduced neurons was observed between each cohort of rats (Figures 3.4D-F).

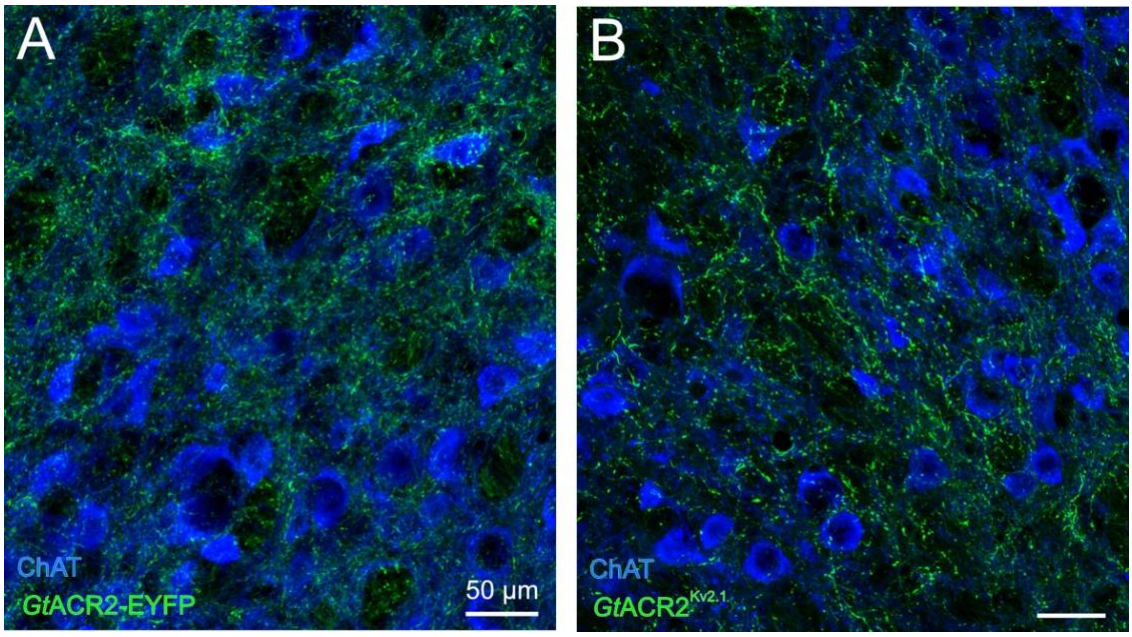

Figure 3.3 *Kv2.1 motif-fusion does not prevent axonal GtACR2 expression in vivo*. Following transduction of VRC column neurons, axonal expression of *Gt*ACR2 constructs was assessed in projections innervating VIIn (marked with ChAT immunoreactivity in blue). Axonal trafficking of both *Gt*ACR2-EYFP (**(A)**, representative image from n = 3 rats) and *Gt*ACR2$^{Kv2.1}$ (**(B)**, representative image from n = 9 rats) from transduced VRC was evident, indicating fusion with the Kv2.1 motif did not prevent axonal *Gt*ACR2 expression *in vivo*.

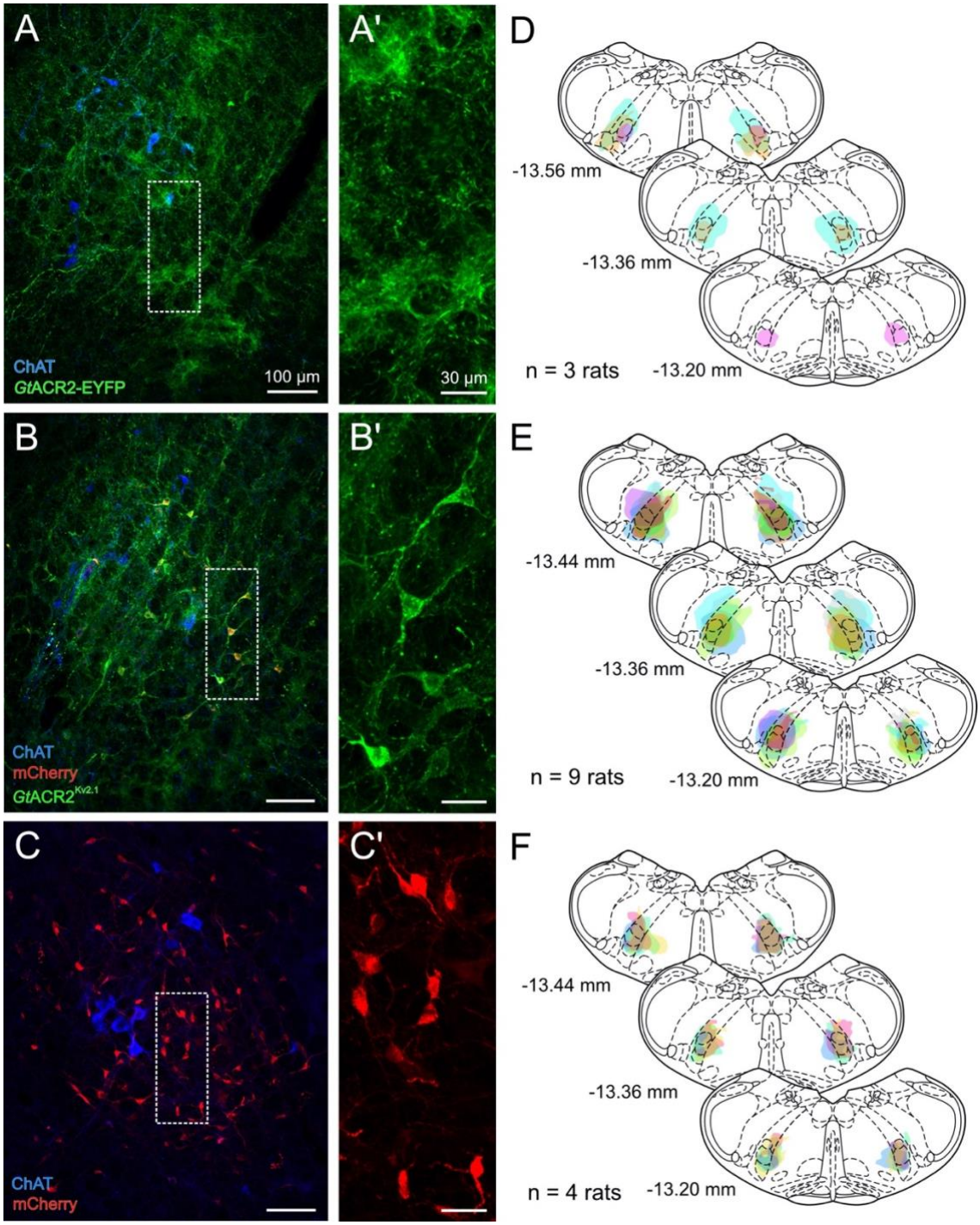

Figure 3.4 *Refer to next page for figure legend*

Figure 3.4 *Histological profile and distribution of viral vector transduction in rat medulla.* Neurons in the VRC and neighbouring nuclei, including NAmb (labelled with ChAT-IR (blue)), expressing **(A)** *Gt*ACR2-EYFP following transduction with AAV1/2-CAG-*Gt*ACR2-EYFP (representative image from n = 3 rats), **(B)** *Gt*ACR2$^{Kv2.1}$ and mCherry following transduction with AAV1/2-CAG-*Gt*ACR2$^{Kv2.1}$-P2A-mCherry (representative image from n = 9 rats), or **(C)** mCherry following transduction with AAV1/2-Ef1α-*Gt*ACR2^{nrxn}-P2A-mCherry (representative image from n = 4 rats). *Gt*ACR2-EYFP appeared highly dispersed at the injection site, making individual neurons difficult to visualise in processed tissue. A higher resolution image of *Gt*ACR2-EYFP expression is provided in **(A')**. Fusion with the Kv2.1 motif appeared to improve neuronal expression of *Gt*ACR2, as highlighted by green fluorescence from *Gt*ACR2$^{Kv2.1}$ clearly defining neuronal boundaries at higher magnification in **(B')**. *Gt*ACR2$^{Kv2.1}$ expression was also distinct from cytosolic mCherry, indicating efficient P2A-mediated cleavage. Due to technical difficulties, *Gt*ACR2^{nrxn} could not be labelled directly via its HA tag *in vivo*. However, cytosolic filling with mCherry **(C')** and physiological responses to laser delivery (see Figures 3.7, 3.8) indicate *Gt*ACR2^{nrxn} was expressed in the neuronal membrane following efficient P2A-mediated cleavage. Mapping of cell bodies labelled with EYFP-, muGFP-, and/or mCherry-immunoreactivity showed a similar spread of transduced VRC neurons between animals which received AAV1/2-CAG-*Gt*ACR2-EYFP (n = 3, **(D)**), AAV1/2-CAG-*Gt*ACR2$^{Kv2.1}$-P2A-mCherry (n = 9, **(E)**), or AAV1/2-Ef1α-*Gt*ACR2^{nrxn}-P2A-mCherry (n = 4, **(F)**). Some vector leak and transduction of neurons outside the VRC, particularly in NAmb, VLM, and IRt, was also present in all groups. (AP level indicated in millimetres from bregma; note that mapping is not provided for every rat at each AP level shown).

3.3.3 *Gt*ACR2-mediated photoinhibition of VRC neurons associated with apnoea, bradycardia, and depressor responses

The effect of each *Gt*ACR2 variant on respiratory and cardiovascular function was investigated in urethane anesthetised rats. Optical fibres were used to probe and identify the location in each rat where the strongest physiological response to light (473 nm, 15-20 mW) was elicited, which was found to correspond approximately with the coordinates targeted by AAV vector injections (with the exception of *Gt*ACR2^{nrxn}; see Section 3.3.5 below).

To confirm *Gt*ACR2 was inhibitory in VRC neurons, extracellular multiunit activity recordings were made during laser delivery in rats expressing *Gt*ACR2-EYFP (n = 2; Figure 3.5, representative traces). Continuous illumination was used for these recordings, as artefacts associated with laser triggering were observed in the extracellular recording electrode when 10-50 Hz laser delivery was attempted. At laser onset, rhythmic bursts in extracellular multiunit spiking activity from VRC neurons were immediately inhibited (Figure 3.5A), though some of this activity spontaneously recovered prior to the laser being switched off. Interestingly, when units were grouped according to their waveform characteristics, it was possible to segregate a subset of units that recovered activity during photoinhibition (Figure 3.5B) from those that remained inactive (Figure 3.5C). This spontaneous recovery of neuronal firing was associated with a resumption of dEMG activity (breathing; Figure 3.5D), which also ceased immediately in response to photoinhibition. A gradual decrease in heart rate was observed in response to photoinhibition (Figure 3.5E), with blood pressure unaffected or increasing slightly (maximum pressure increase of 15 mmHg in one rat; data not shown). These cardiovascular changes were maintained throughout photoinhibition and did not fully recover until it was removed.

In a separate cohort of rats expressing *Gt*ACR2-EYFP, physiological responses to 5 ms laser pulses at 10, 20, or 50 Hz, as well as continuous illumination, were assessed. Of these, photoinhibition at 50 Hz was found to provide the strongest cardiovascular and respiratory responses (Figure 3.6A; representative traces from n = 3 rats; data for other frequencies not shown). Upon 50 Hz laser onset, rhythmic dEMG activity from breathing was immediately replaced with tonic activity, which in some cases subsided until electrocardiogram (ECG) signal alone was detected (Figure 3.6A). Following 8.9 (± 9.2) s of apnoea, rhythmic dEMG activity gradually recovered, despite continued laser delivery (Figures 3.6A, 3.6D). Gradual decreases in both heart rate and blood pressure, which stabilised at 70-80% below baseline values, were also seen during

photoinhibition (Figure 3.6D). While blood pressure increased slightly upon recovery of respiration, neither heart rate nor blood pressure recovered to baseline values until photoinhibition was removed (Figure 3.6D).

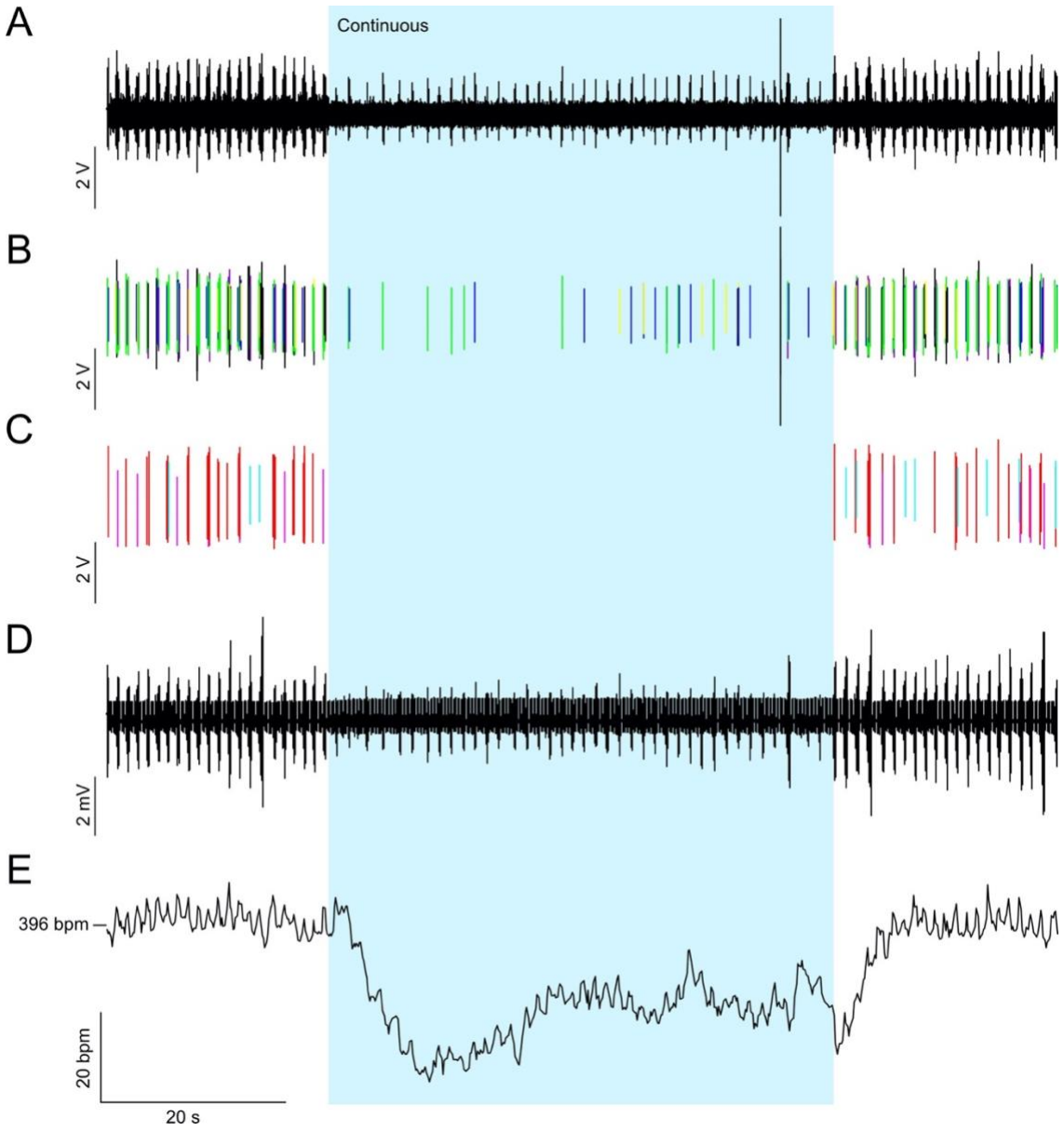

Figure 3.5 *Refer to next page for figure legend*

Figure 3.5 *GtACR2-EYFP inhibits VRC neurons and affected multiple populations*. In a separate cohort of rats (n = 2, representative traces depicted) to those described in Figures 3.4 and 3.6, the effect of *Gt*ACR2-EYFP activation was assessed using extracellular multiunit activity recordings. Laser onset was associated with an immediate disruption to rhythmic bursting activity from VRC neurons **(A),** although this activity was able to partially recover despite continued photoinhibition. Grouping of individual units from these recordings, based on their waveform characteristics, revealed that a particular subset **(B)** were associated with this recovery of bursting activity during photoinhibition. A second subset of units **(C)** remained inactive for the duration of photoinhibition, but quickly resumed firing once the laser was switched off. It seems likely that the units shown in **(B)** were responsible for the observed inhibition of dEMG activity **(D)**, which also recovered during photoinhibition, while those depicted in **(C)** may have been associated with cardiac effects **(E)** that did not recover to baseline levels until photoinhibition was removed.

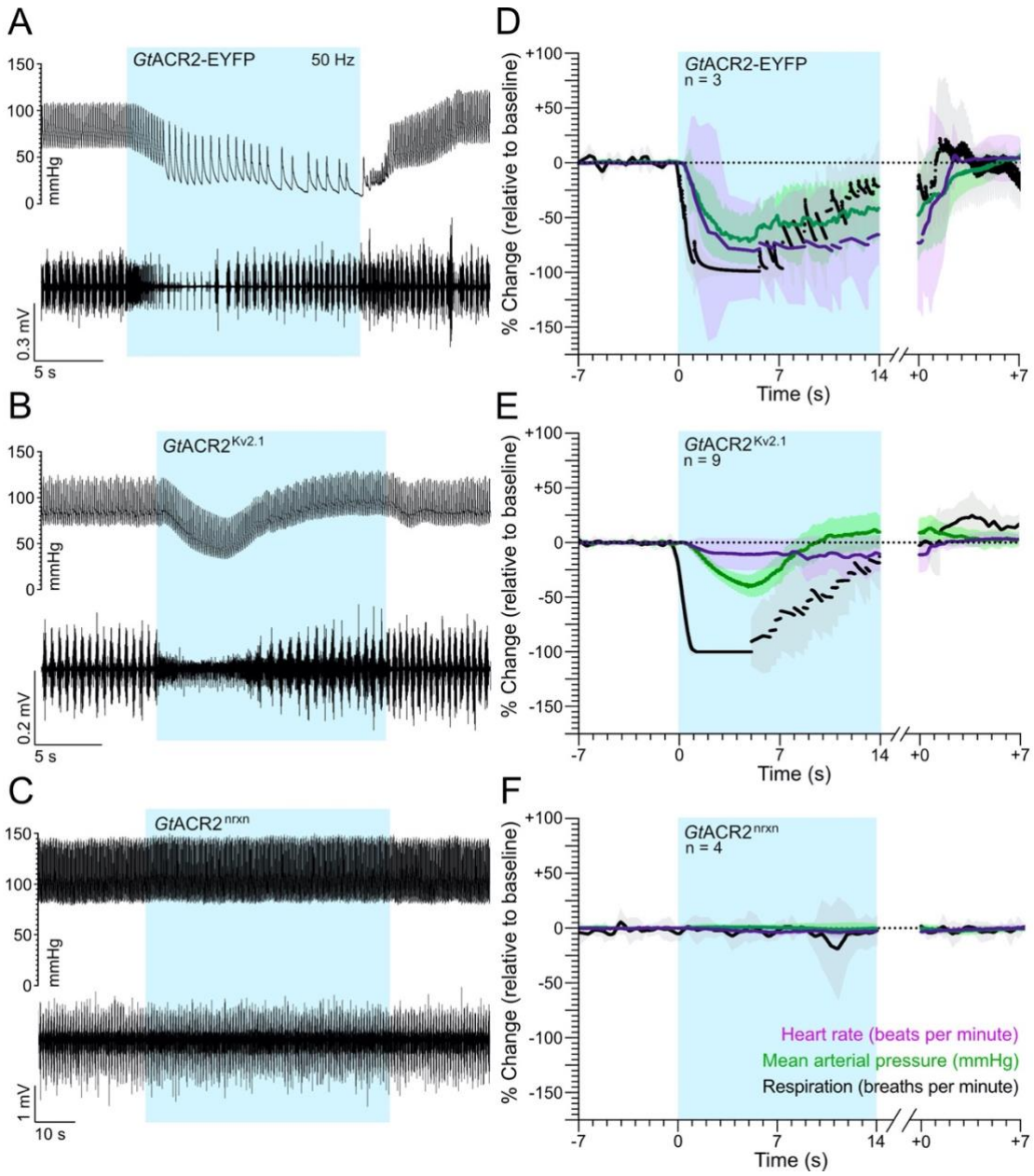

Figure 3.6 *Refer to next page for figure legend*

Figure 3.6 *Physiological responses to photoinhibition in rats expressing GtACR2-EYFP, GtACR2$^{Kv2.1}$, or GtACR2^{nrxn}.* Blood pressure and dEMG traces showing physiological responses to 50 Hz photoinhibition of VRC neurons (period of laser delivery shown in blue) are depicted for rats expressing *Gt*ACR2-EYFP (representative traces from n = 3 rats, **(A)**), *Gt*ACR2$^{Kv2.1}$ (representative traces from n = 9 rats, **(B)**), or *Gt*ACR2^{nrxn} (representative traces from n = 4 rats, **(C)**). To illustrate the effect of photoinhibition across all rats in each group, heart rate (beats per minute, magenta), mean arterial pressure (mmHg, green), and respiratory frequency (breaths per minute, black) were normalised as a percentage change from the average value of baseline recordings in the 20 seconds immediately prior to laser onset, and graphed as the mean ± 95 % confidence interval for rats expressing *Gt*ACR2-EYFP (n = 3, **(D)**), *Gt*ACR2$^{Kv2.1}$ (n = 9, **(E)**), or *Gt*ACR2^{nrxn} (n = 4, **(F)**). As photoinhibition duration varied slightly between animals, data recorded more than 14 seconds after laser onset is excluded (indicated by a break in the x-axis prior to laser being switched off). While the respiratory responses between rats expressing *Gt*ACR2-EYFP and *Gt*ACR2$^{Kv2.1}$ were similar, cardiac responses were significantly reduced in rats expressing *Gt*ACR2$^{Kv2.1}$. This effect on heart rate during photoinhibition is also likely to account for the different blood pressure responses between these groups **(D, E)**, with respiratory modulation of sympathetic activity seeming much more apparent in rats expressing *Gt*ACR2$^{Kv2.1}$. While there were no significant effects on breathing or blood pressure in rats expressing *Gt*ACR2^{nrxn}, there was a slight decrease in heart rate during 50 Hz laser delivery (see also Figure 3.7).

3.3.4 Fusion with Kv2.1 motif alters cardiovascular, but not respiratory, effects of *Gt*ACR2 in VRC neurons

When optical fibres were used to probe VRC coordinates in rats expressing GtACR2$^{Kv2.1}$, 50 Hz laser delivery was again found to have the largest physiological impact (Figure 3.6B; representative traces from n = 9 rats). Onset of photoinhibition at this frequency immediately disrupted rhythmic dEMG activity (breathing), which was replaced for 8.6 (± 2.0) s by tonic and/or a complete loss of dEMG activity. This apnoea was similar to that seen in rats expressing *Gt*ACR2-EYFP, with no significant difference between the number of breaths missed in each group (P = 0.43, one-way ANOVA; Figure 3.7A). Following apnoea, rhythmic dEMG activity again spontaneously recovered, prior to removal of photoinhibition (Figures 3.6B, 3.6E). Blood pressure also gradually decreased from the laser onset. However, unlike in *Gt*ACR2-EYFP-expressing rats, this depressor response was significantly smaller (P = < 0.01, Figure 3.7B) and reversed in phase with the recovery of breathing to slightly exceed baseline levels, until photoinhibition ceased and blood pressure returned to baseline (Figure 3.6E). Variations in heart rate also occurred during photoinhibition in rats expressing *Gt*ACR2$^{Kv2.1}$. Again, these responses differed from rats expressing *Gt*ACR2-EYFP, being both smaller in magnitude (P = < 0.01, Figure 3.7C) and, despite typically causing bradycardia, also inducing tachycardia in two rats (total n = 9 rats; Figures 3.6E, 3.8C).

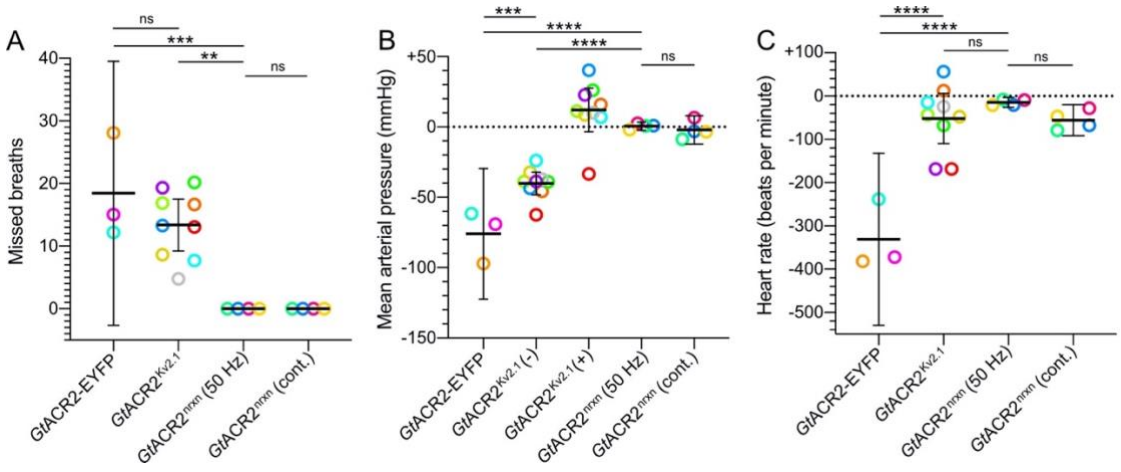

Figure 3.7 *Between-group analysis of maximum physiological responses to activation of GtACR2 variants expressed in VRC neurons*. To compare physiological responses elicited by different *Gt*ACR2 variants *in vivo*, the number of missed breaths (**(A)**, calculated as the baseline respiratory frequency multiplied by apnoea duration), as well as maximum changes in **(B)** mean arterial pressure and **(C)** heart rate, were plotted for each rat. The colour of data points for each rat corresponds to mapping data presented in Figures 3.4D-F. The initial decrease and subsequent increase in blood pressure seen during laser delivery in rats expressing *Gt*ACR2$^{Kv2.1}$ are graphed and denoted as (-) and (+), respectively. Physiological responses to both 50 Hz and continuous illumination (see Figure 3.8) in rats expressing GtACR2^{nrxn} are graphed and indicated with (50 Hz) or (cont.) notation. Error bars reflect mean ± 95 % confidence interval. Notation used to indicate statistical significance between groups (one-way ANOVA) are as follows: *ns* = not significant; ** P = < 0.01; *** P = < 0.001; **** P = <0.0001.

3.3.5 *Gt*ACR2^{nrxn} expression in VRC neurons does not alter breathing or blood pressure, but may affect cardiac function

Given 50 Hz stimulation of *Gt*ACR2-EYFP and *Gt*ACR2$^{Kv2.1}$ elicited the strongest physiological responses, this frequency was also used initially to probe the medulla for functional responses in rats expressing *Gt*ACR2^{nrxn}. Though respiration and blood pressure appeared unaffected during 50 Hz laser delivery in these rats (Figures 3.6C, 3.6F), a slight decrease in heart rate (15 ± 11 bpm) was observed (Figure 3.7C, n = 4 rats). During continuous illumination, this bradycardia trended towards a larger decrease of 56 (± 36) bpm (Figures 3.7C, 3.8A-B). However, no significant differences were found between photoinhibition using 50 Hz or continuous illumination across any of the physiological parameters measured in rats expressing *Gt*ACR2^{nrxn} (Figure 3.7). The bradycardia recorded in rats expressing *Gt*ACR2^{nrxn} was significantly smaller than that seen in rats expressing *Gt*ACR2-EYFP (P = < 0.01), instead being closer to that observed in those expressing *Gt*ACR2$^{Kv2.1}$ (P = 0.75, Figure 3.7C). Regardless of the *Gt*ACR2 variant expressed, these changes in heart rate did not return to baseline values until removal of photoinhibition (Figures 3.6, 3.8).

As noted in Section 3.3.3, the strongest physiological responses in rats expressing *Gt*ACR2-EYFP and *Gt*ACR2$^{Kv2.1}$ were seen when fibre optics were positioned at approximately the same coordinates to those used for AAV vector injections. This was not the case in rats expressing *Gt*ACR2^{nrxn}, where the maximum decrease in heart rate appeared to occur at coordinates roughly 1 mm rostral to those seen for *Gt*ACR2-EYFP and *Gt*ACR2$^{Kv2.1}$. These observations were based on the stereotaxic coordinates of optical fibres recorded during each experiment, as multiple fibre entries and difficulties visualising fibre tracts prevented the precise histological mapping of optical fibre positions in processed tissue.

As no apnoea occurred in rats expressing GtACR2^{nrxn}, further analysis was conducted to assess potential changes in sympatho- and cardiorespiratory coupling during photoinhibition. Analysis of waveform averages for heart rate and systolic arterial pressure across 10 breaths, taken either prior to or following laser delivery, typically showed a decrease in both heart rate and blood pressure during inspiration (Figure 3.8C; representative traces from n = 4 rats). These observations, inverse to those normally described for TH waves and RSA, are most likely the result of urethane anaesthesia (Bouairi et al. 2004). Anaesthesia may also have affected the amplitude of TH waves and heart rate variability, which were relatively small and did not show

any significant changes resulting from *Gt*ACR2^{nrxn} stimulation (Figures 3.8D-E). However, a change in sinus arrhythmia phase, such that the heart rate maxima and minima occurred mid-way through expiration and inspiration, respectively, was observed during laser delivery in a subset of rats with higher heart rate variability (Figure 3.8C; heart rate trace representative for n = 2 of 4 rats); no such changes were seen for TH waves.

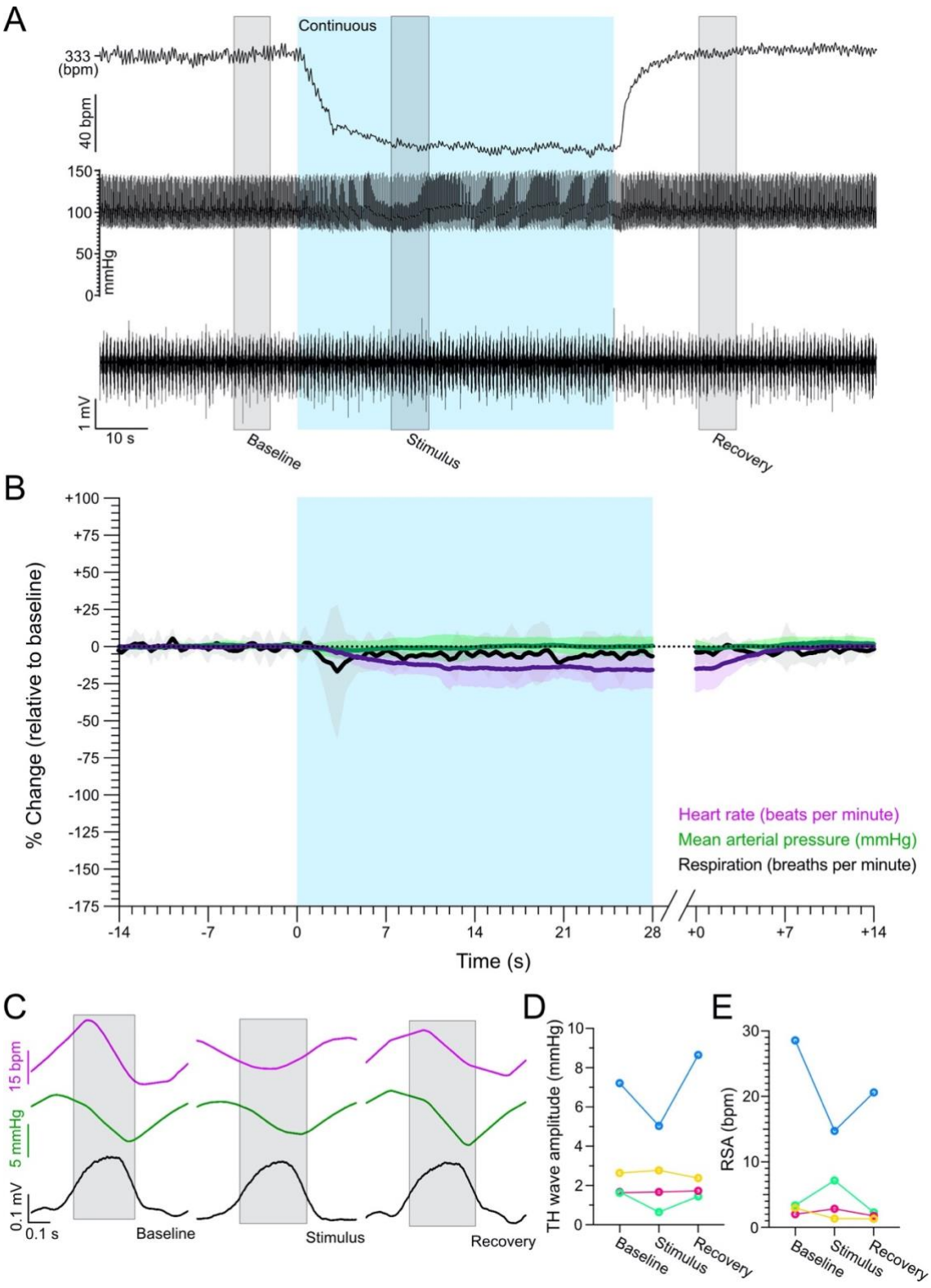

Figure 3.8 *Refer to next page for figure legend*

Figure 3.8 *Continuous laser delivery increases cardiac effects in rats expressing GtACR2^{nrxn}*. **(A)** Representative heart rate, blood pressure, and dEMG traces showing a specific increase in bradycardia during continuous laser delivery (blue) in rats expressing *Gt*ACR2^{nrxn} (n = 4; see Figures 3.4, 3.6 for expression and 50 Hz data). To illustrate the effect of continuous *Gt*ACR2^{nrxn} stimulation across all rats (n = 4), heart rate (beats per minute, magenta), mean arterial pressure (mmHg, green), and respiratory frequency (breaths per minute, black) were normalised as a percentage change from the average value of baseline recordings in the 20 seconds immediately prior to laser onset, and graphed in **(B)** as the mean ± 95 % confidence interval. As photoinhibition duration varied slightly between animals, data recorded more than 28 seconds after laser onset is excluded (indicated by a break in the x-axis prior to laser offset). Continuous illumination led to a further decrease in heart rate to that seen with 50 Hz laser delivery (Figure 3.6F; see also Figure 3.7C), while respiratory frequency also decreased slightly, and blood pressure remained unaffected. **(C)** Representative traces showing waveform averages of heart rate (magenta), systolic arterial pressure (green), and dEMG activity (black) over 10 breaths taken during baseline, laser stimulus, and recovery periods, as indicated with shaded boxes in **(A)**. Inspiration is indicated for each period with a shaded box in **(C)**. Both heart rate and blood pressure decreased during inspiration, likely as a result of urethane anaesthesia. This pattern of cardiac activity was disrupted during laser delivery in a subset of rats with higher heart rate variability (n = 2), suggesting *Gt*ACR2^{nrxn} activity may have affected cardiorespiratory coupling. No such disruption was seen in blood pressure fluctuations (TH waves), and no significant changes in the amplitude of TH waves **(D)** or RSA **(E)** were observed (one-way ANOVA, P = > 0.9 across all comparisons). The colour of data points for each rat in **(D)** and **(E)** corresponds to that shown for mapping data in Figure 3.4F.

3.4 Discussion

In attempting to direct selective somatic or axonal expression, and in doing so elicit consistent hyper- or depolarising effects while providing a means to map closely interconnected neural circuitry, fusion constructs between *Gt*ACR2 and Kv2.1 or Nrxn1α trafficking motifs were developed and characterised. Though the Kv2.1 motif did not prevent axonal *Gt*ACR2 expression *in vitro* or *in vivo*, neuronal expression of *Gt*ACR2$^{Kv2.1}$ appeared to be enhanced relative to *Gt*ACR2-EYFP in transduced VRC neurons. Although technical considerations prevented the histological characterisation of *Gt*ACR2^{nrxn} expression *in vivo*, it is interesting to note that rats expressing each *Gt*ACR2 variant exhibited distinct physiological responses to photoinhibition. While rats expressing *Gt*ACR2-EYFP displayed apnoea, as well as large decreases in heart rate and blood pressure, expression of *Gt*ACR2$^{Kv2.1}$ or *Gt*ACR2^{nrxn} appeared to be associated specifically with the respiratory or cardiac aspects of this response, respectively. These findings may be explained by a preferential distribution of *Gt*ACR2 to particular subcellular domains and/or cell types that was not sufficiently binary to detect histologically.

The injection protocol used here was designed to specifically target the preBötC within the VRC. The preBötC is a core component of rhythmogenic inspiratory circuitry, composed of multiple neurochemically distinct populations. Prominent among these are a group of excitatory rhythmogenic neurons, crucial to respiration and characterised by their expression of glutamate and somatostatin (Tan et al. 2008; Cui et al. 2016), as well as inhibitory, glycinergic neurons that modulate breathing and can induce apnoea, but are not rhythmogenic (Sherman et al. 2015). Although several other gene products have been identified in preBötC (see Del Negro et al. (2018) for review), a specific marker for this region has yet to be identified. As viral vectors developed here for expression of the described *Gt*ACR2 constructs were designed for generic neuronal expression, rather than cell-type specific transduction, a variety of preBötC cell-types are likely to have been affected by photoinhibition in the present study. This expected heterogeneity among transduced preBötC neurons is reflected in extracellular multiunit activity recordings, where some units were able to recovery activity during *Gt*ACR2-EYFP-mediated photoinhibition while others were not. Each of these groups likely underlies the observed respiratory and cardiac responses to photoinhibition, respectively.

A model that may explain the circuitry involved in these physiological responses is presented in Figure 3.9. Both *Gt*ACR2-EYFP and *Gt*ACR2$^{Kv2.1}$ expression was associated with immediate

apnoea at laser onset, with respiratory activity recovering after approximately nine seconds and before removal of photoinhibition. Photoinhibition of excitatory preBötC neurons would account for this response, although the spontaneous recovery of breathing was somewhat unexpected. Previous chemogenetic studies targeting excitatory preBötC neurons induced apnoea such that animals required mechanical ventilation for at least 40 minutes before breathing recovered (Tan et al. 2008). An explanation for this discrepancy lies in a potentially stronger hyperpolarisation from the potassium channels, and/or other effects of second messenger pathways, activated via the allatostatin receptor system employed by these authors (Birgul et al. 1999; Lechner et al. 2002). If this assumption is true, then input from other brainstem regions contributing to rhythmic respiratory activity, which would have been suppressed using the allatostatin system, may be sufficient to override weaker *Gt*ACR2-mediated inhibition in this population of neurons.

Manipulation of a separate, inhibitory population of preBötC neurons may underlie the cardiac responses that were associated with photoinhibition. Inhibitory input from preBötC to NAmb could contribute to increases in heart rate, such as those seen with respiratory sinus arrhythmia, by decreasing vagal cardiac parasympathetic activity. Removing preBötC inhibition to NAmb by optogenetically inhibiting this circuitry could explain the bradycardia typically observed here. However, the reason for such large differences in cardiac responses to photoinhibition in rats expressing *Gt*ACR2-EYFP, as opposed to *Gt*ACR2$^{Kv2.1}$ or *Gt*ACR2^{nrxn}, is unclear. Although axonal *Gt*ACR2 expression was still evident following fusion with the Kv2.1 trafficking motif, there may have been differences in subcellular enrichment of *Gt*ACR2 expression between each construct that caused these distinct cardiac responses to photoinhibition (discussed further below).

Finally, the decreases in blood pressure seen during photoinhibition were most likely a product of removing excitatory input from preBötC to the rostral VLM (RVLM), in the case of *Gt*ACR2$^{Kv2.1}$ expression, or a combination of reduced RVLM input and a substantially reduced cardiac output due to bradycardia in rats expressing *Gt*ACR2-EYFP. This is also supported by the increases in blood pressure that occurred with the recovery of breathing during photoinhibition in rats expressing *Gt*ACR2-EYFP or *Gt*ACR2$^{Kv2.1}$, likely reflecting increased sympathetic activity through coupling with respiratory drive.

While a small volume was used for viral vector injections targeting preBötC in the present study, transduced neurons were also present in some surrounding nuclei. These included varying

amounts of viral vector spread to the NAmb dorsally, VLM ventrally, rostral ventral respiratory group (rVRG) caudally, and the surrounding IRt. NAmb neurons are a key source of parasympathetic vagal tone to the heart (Nosaka et al. 1979), the rVRG contains inspiratory premotor neurons (Yamada et al. 1988), and the VLM is a key modulator of sympathetic output (Kumagai et al. 2012). The IRt has also recently been shown to influence sympathetic activity (Toor et al. 2019). As such, photoinhibition in one or more of these populations outside the preBötC could have influenced the observed physiological responses. However, given the concentration of transduced neurons in the VRC and overall physiological responses to photoinhibition, it is reasonable to credit preBötC/VRC neurons as the primary source of the observed effects. Molecular approaches, such as those described in the preceding and subsequent chapters, in addition to modifications of the injection volume and/or protocol, may enable more refined targeting of preBötC transduction in future studies. Techniques such as single-cell transcriptomic sequencing of functionally defined populations may be required to facilitate the identification of promoter candidates capable of distinguishing specific autonomic nuclei of interest, which would be especially valuable in this context.

The observed physiological responses were also likely impacted by *Gt*ACR2 expression in axonal projections. Potential ramifications of this are complicated by the reported depolarising effects of *Gt*ACR2 on the axonal membrane (Mahn et al. 2016; Malyshev et al. 2017), an issue which we sought to alleviate in the present study. Despite incorporating the Kv2.1 motif, which previously provided somatically localised opsin expression in mouse retinal ganglion cells (Wu et al. 2013) and cortical neurons (Baker et al. 2016), axonal *Gt*ACR2$^{Kv2.1}$ expression was evident both *in vitro* and *in vivo*. However, *Gt*ACR2$^{Kv2.1}$ appeared to be more efficiently expressed by neurons than *Gt*ACR2-EYFP *in vivo*. Overexpression of these *Gt*ACR2 constructs following transfection of hippocampal neurons may have obscured this effect *in vitro*.

It is interesting to note that this pattern of *Gt*ACR2 expression has been replicated in two independent studies that emerged concurrent with the present study. These reports describe two constructs analogous to *Gt*ACR2$^{Kv2.1}$, both of which exhibited enhanced neuronal expression, with some axonal localisation, in mouse cortical neurons (Mahn et al. 2018; Messier et al. 2018). However, electrophysiological recordings by these authors revealed that fusion with the Kv2.1 motif reduced axonal *Gt*ACR2 expression to the extent that axons containing these constructs were significantly less likely to produce action potentials when illuminated, compared to axons containing *Gt*ACR2 fused to a fluorescent tag only. As each construct carried

a different fluorescent tag, the use of muGFP here is unlikely to have affected *Gt*ACR2 trafficking. These results indicate that while *Gt*ACR2-Kv2.1 fusion constructs are not entirely excluded from the axon, their expression is sufficiently 'somatically enriched' to minimise the depolarising effects of *Gt*ACR2 in the axonal membrane. It seems likely that such a reduction in axonal *Gt*ACR2 expression following Kv2.1 motif fusion also occurred in the present study, causing a significantly reduced cardiac response to photoinhibition. Although the exact mechanism by which this occurred is unclear, involvement of axons innervating NAmb seems likely.

A selective axonal enrichment of *Gt*ACR2^{nrxn} is also supported by the present study. In contrast to *Gt*ACR2-EYFP and *Gt*ACR2$^{Kv2.1}$, both of which are expected to have been expressed in the somatic membrane of VRC neurons and induced immediate apnoea upon stimulation, breathing was unaffected in rats expressing *Gt*ACR2^{nrxn}. However, laser delivery in rats expressing *Gt*ACR2^{nrxn} caused a consistent reduction in heart rate, which aligns with the hypothesis that axonal *Gt*ACR2 expression mediated cardiac responses. The lesser magnitude of this response, and increased laser output from 50 Hz to continuous illumination required to elicit it, may be due to relatively low membrane expression levels of *Gt*ACR2^{nrxn} compared to *Gt*ACR2-EYFP and *Gt*ACR2$^{Kv2.1}$, but does suggests this expression could be selective to the axon. In addition, the strongest bradycardia in rats expressing *Gt*ACR2^{nrxn} was elicited at coordinates roughly 1 mm rostral to those at which the most profound physiological responses were observed in rats expressing *Gt*ACR2-EYFP or *Gt*ACR2$^{Kv2.1}$, an effect that could be explained by trafficking of *Gt*ACR2^{nrxn} away from the soma. It is important to note that additional experiments, to control for potential effects of laser delivery and tissue heating – which can have significant functional consequences (Owen et al. 2019) – are required to validate that the observed bradycardia was truly due to *Gt*ACR2^{nrxn} activity. However, these data give a promising indication that *Gt*ACR2^{nrxn} is selectively trafficked to the axonal membrane, and clearly show the respiratory and blood pressure responses in rats expressing *Gt*ACR2-EYFP and *Gt*ACR2$^{Kv2.1}$ were not influenced by such factors.

With breathing unaffected in rats expressing *Gt*ACR2^{nrxn}, it was also possible to assess effects on TH waves and RSA in these animals. Laser delivery did not have a significant effect on sympatho- or cardiorespiratory coupling reflected by these variables, although this outcome may have been influenced by urethane anaesthesia. Urethane has been reported to invert the pattern of cardiorespiratory coupling (Bouairi et al. 2004), as observed here, and may also have resulted in a reduced amplitude of TH waves and RSA. It is interesting to note that in a subset of rats with

higher heart rate variability, the pattern of RSA appeared to be altered during laser delivery. This suggests *Gt*ACR2^{nrxn} activation may have impacted circuitry underlying cardiorespiratory coupling, in addition to impairing central maintenance of heart rate.

It will be important in future studies to assess the described physiological responses to each *Gt*ACR2 construct in the absence of complications arising from anaesthesia. Alternative approaches that could achieve this include experimentation in conscious animals or the WHBP. As optogenetic interventions offer precise temporal control, it would be feasible to briefly perturb key autonomic functions without causing undue stress in conscious rats monitored via telemetry. Such an approach would allow clear insight into how the affected circuitry modulates autonomic function and coupling mechanisms under physiological conditions. A detailed understanding of this circuit architecture and its peripheral outputs could be gleaned from studies in the WHBP, where decerebration also removes the need for anaesthesia.

In conclusion, data presented in this chapter provide evidence for the successful enrichment of *Gt*ACR2 expression in somatic and axonal membranes *in vivo,* following fusion with Kv2.1 or Nrxn1α trafficking motifs, respectively. Activation of *Gt*ACR2$^{Kv2.1}$ in rat VRC circuitry primarily impacted respiratory activity, while *Gt*ACR2^{nrxn} selectively affected cardiac function, with non-localised *Gt*ACR2-EYFP eliciting both respiratory and cardiac responses. This differentiation suggests *Gt*ACR2$^{Kv2.1}$ and *Gt*ACR2^{nrxn} were trafficked to distinct subcellular compartments, although technical considerations necessitate further studies to distinguish the specific neuronal populations involved in these responses. Importantly, data produced using the *Gt*ACR2$^{Kv2.1}$ vector developed here are consistent with observations reported in relation to analogous constructs, developed independently from and concurrent with these experiments, showing improved neuronal expression and somatic enrichment of *Gt*ACR2 following fusion with the Kv2.1 trafficking motif. These constructs offer a solution for consistent membrane hyper- or depolarisation using *Gt*ACR2, while also providing useful tools in dissociating complex functions regulated by closely interconnected nuclei – an important step towards understanding the underlying neural circuitry.

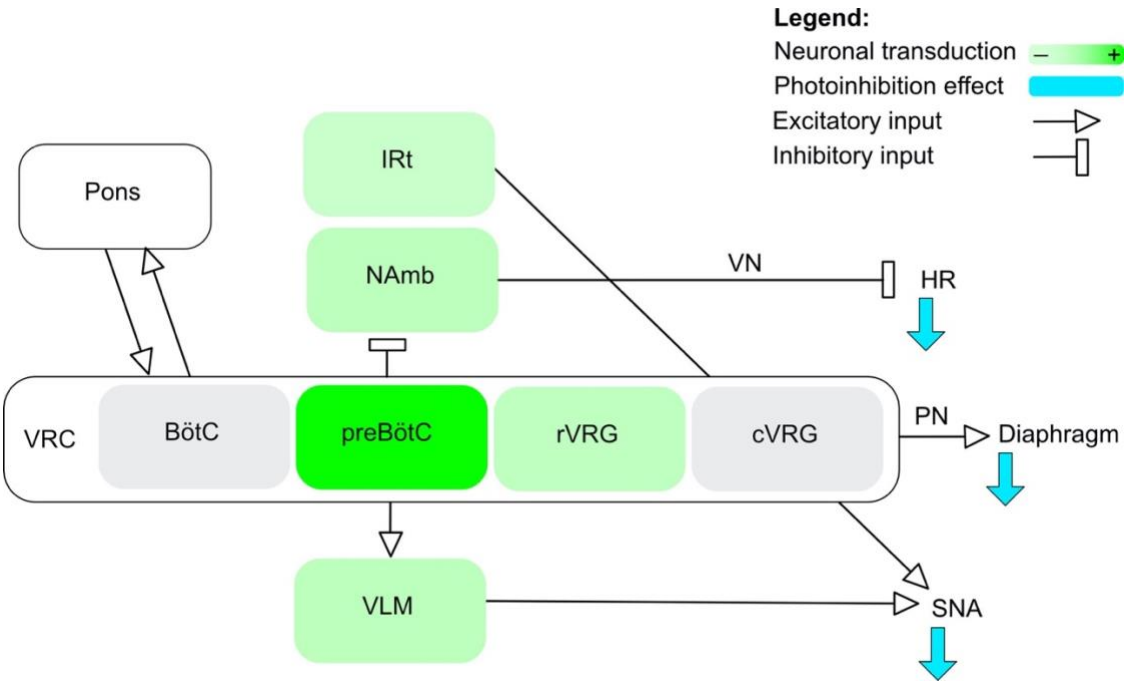

Figure 3.9 *Hypothesised circuitry underlying physiological responses to VRC photoinhibition*. In the present study, photoinhibition of VRC neurons expressing *Gt*ACR2-EYFP was associated with apnoea, bradycardia, and depressor responses. Transduced neurons were concentrated in the preBötC, with some spread caudally to the rVRG; photoinhibition of these inspiratory VRC neurons would prevent central respiratory drive to the diaphragm via the phrenic nerve (PN), resulting in apnoea. We hypothesise respiratory effects were primarily due to photoinhibition of excitatory preBötC neurons. Breathing recovered despite continued photoinhibition, suggesting reciprocal connections between respiratory nuclei in the VRC and pons may have been capable of overriding *Gt*ACR2-mediated photoinhibition in this population. Expiratory Bötzinger complex (BötC) and caudal ventral respiratory group (cVRG) populations were not directly affected by photoinhibition. The decrease in heart rate (HR) is thought to be due to photoinhibition in a separate, inhibitory population of preBötC neurons, effectively disinhibiting NAmb neurons and increasing parasympathetic output to the heart via the vagus nerve (VN). A combination of decreased sympathetic nerve activity (SNA) through removal of respiratory drive and reduced cardiac output also explain the depressor effect. While respiratory responses to photoinhibition were maintained in rats expressing *Gt*ACR2$^{Kv2.1}$, cardiac responses were significantly reduced. Though the underlying mechanism is unclear, reduced axonal expression of *Gt*ACR2$^{Kv2.1}$ seems likely to be involved. Consistent with this hypothesis, cardiac rather than respiratory responses to photoinhibition were elicited in rats expressing *Gt*ACR2^{nrxn}. Note that populations in IRt, NAmb, and VLM, which also contained some transduced neurons, may have been directly affected by photoinhibition and influenced the observed physiological responses.

Chapter 4

Selective viral vector transduction of central amygdala neurons projecting to the nucleus of the solitary tract in rat

4.1 Introduction

Nervous systems allow organisms to dynamically integrate and respond to stimuli. Alongside those originating in the external environment, such as olfactory, gustatory, tactile, auditory, and visual stimuli, which can be classed as 'exteroceptive', the body's internal state must also be closely monitored. This is achieved through 'interoceptive' inputs, including visceromotor, nociceptive, thermal, metabolic, and hormonal signals, conveyed to the central nervous system (CNS) either by spinal or cranial nerves, or directly through circulating factors (Critchley et al. 2013). The CNS in turn coordinates appropriate behavioural and physiological responses through efferent projections to various peripheral effector organs and the release of hormones (Pace-Schott et al. 2019). The nature of these responses has become particularly sophisticated in mammals, where highly developed limbic and cortical structures broadly facilitate the valence coding, storage, and retrieval of information (Preston et al. 2013; Namburi et al. 2016). Thus, emotional and cognitive experience, which shapes behaviour and visceral function, can itself be modulated by internal state.

This concept of reciprocal modulation between cognition, affect, and peripheral physiology is encapsulated by the neurovisceral integration (NVI) model, developed by Thayer, Lane and colleagues (Thayer et al. 2000, 2009b; Smith et al. 2017). Under the NVI model, a hierarchy of nested, bidirectional integration loops within a 'central autonomic network' (CAN) are proposed to optimise energy expenditure according to present and anticipated future metabolic needs based on physiological state and, at higher levels, emotional status and conscious deliberation, facilitating goal-directed behaviour and survival (Smith et al. 2017). The core components of the CAN, as defined by Benarroch (1993) and in ascending order, include the nucleus of the solitary tract (NST), the parabrachial nucleus (PBN), the periaqueductal gray (PAG) and hypothalamus, the amygdala, and the insular, medial prefrontal (mPFC), and other subregions of the cerebral cortex. In addition to functional characteristics, further described below, retrograde labelling of these regions using transneuronal viral tracers injected into the rat myocardium (Ter Horst et al. 1997), stomach wall (Yang et al. 1999; Rinaman et al. 2000; 2004), associated stellate and celiac ganglia, or adrenal gland (Westerhaus et al. 2001) also supports their postulated role as CAN nodes within the NVI model.

A variety of afferent sources supply the CAN, including chemoreceptors that respond to local and circulating factors, and stretch-sensitive receptors in the walls of hollow organs (Critchley

et al. 2013; Pace-Schott et al. 2019). These afferents mainly convey signals related to physiological status and autonomic visceral function, entering the CNS via glossopharyngeal and vagal terminations in the NST (Torvik 1956; Beckstead et al. 1979; Adachi et al. 1984). The NST also receives some exteroceptive inputs, with gustatory information being a notable example (May et al. 2006). These afferent signals are integrated by the NST to coordinate medullary reflexes across multiple organ systems (Machado et al. 1997; Travagli et al. 2006; Zoccal et al. 2014), and are also relayed from the NST to all other CAN regions (Benarroch 1993). Additional visceral afferents enter the CNS via the spinal cord; however, these have a more prominent role in signalling tissue damage and are primarily relayed through the thalamus (Grundy 2002; Critchley et al. 2013), which is not considered part of the CAN (Benarroch 1993; Smith et al. 2017).

Information from the viscera is further integrated with exteroceptive inputs in the pontine PBN, which forms a key component of circuitry modulating respiratory and cardiovascular function, thermoregulation, and ingestive behaviour (Smotherman et al. 2006; Davern 2014; Campos et al. 2016; Yahiro et al. 2017). The midbrain hypothalamus and PAG provide the first point of substantial convergence between visceral and somatic motor coordination (Smith et al. 2017); for example, both PAG and hypothalamus drive aggressive and defensive behaviours (Lin et al. 2011; Wang et al. 2015; Falkner et al. 2019; Lefler et al. 2020) and are linked to associated cardiovascular responses (Carrive 1993; DiMicco et al. 1996). Behavioural and autonomic activity is also coordinated with the endocrine system at this level via the hypothalamus (Smith et al. 2006). The amygdala plays a critical role in subliminally orienting attention toward, and assigning negative (aversive) or positive (appetitive) valence to, salient stimuli (Mulckhuyse et al. 2010; Fernando et al. 2013). Perceptual representations of the body's internal state are produced in the insular cortex (Ceunen et al. 2016), which also serves as the main locus of integration between viscerosensory information supplied by the NST and additional nociceptive and visceromotor inputs conveyed from spinal afferents via the thalamus (Critchley et al. 2013). Finally, conceptual interpretations of perceived inputs, based on previous experience, are thought to be generated in other cortical regions, including the mPFC (Smith et al. 2017).

In addition to the 'bottom-up' perspective used here to introduce the CAN, each of the nodes listed share strong reciprocal connections, facilitating ongoing integration, feedback, and adjustment of network activity, as well as descending central modulation of autonomic function (Benarroch 1993; Smith et al. 2017). CAN innervation and modification of sympathetic and

parasympathetic output from neurons of the ventrolateral medulla (VLM), dorsal motor nucleus of vagus (10N), and nucleus ambiguus (NAmb) ultimately give rise to this descending control (Critchley et al. 2013). Heart rate variability (HRV), primarily driven by parasympathetic output from NAmb, has been posited as an accessible, direct index of CAN output (Thayer et al. 2009a; Smith et al. 2017). A reduction in HRV under threatening or uncertain circumstances, for example, is thought to arise from the removal of tonic mPFC inhibition of the amygdala, disinhibiting direct amygdaloid projections to the medulla (Thayer et al. 2009b). Though this effect facilitates acute energy mobilisation and survival, such circuitry also provides a potential mechanism underlying cardiovascular comorbidities associated with chronic stress and anxiety (Cohen et al. 2015), illustrating how a comprehensive understanding of CAN architecture and function may provide insight into the aetiology of, and potential therapeutic remedies to, a variety of pathologies involving close interactions between psychological and physiological processes.

Amongst structures comprising the CAN, the amygdala has emerged as a major hub for orchestrating emotional and physiological components of behavioural responses. Some of the most compelling evidence for this association stems from patients with temporal lobe epilepsy, where case reports of electrical stimulation or lesion implicate the amygdala in producing anxious or fearful experiences and behaviour, as well as sympathetic arousal reflected by pupil dilation, sweating, altered respiratory rhythms and cyanosis, tachycardia, and pressor responses (Chapman et al. 1954; 1957; Masaoka et al. 2003; Dlouhy et al. 2015). Thus, along with its well-established role in learning, primarily involving the basolateral nucleus (BLA) which mediates valence coding of experiences as aversive or rewarding (Janak et al. 2015), the amygdala also appears to modulate visceral activity. Although numerous preclinical experiments have assessed the effects of electrically or chemically manipulating the amygdala on cardiovascular and respiratory function, there has been considerable variation in the nature of observed responses between and within studies. These differences likely reflect confounding factors arising from variation in anaesthesia and stimulus parameters used, the affected regions and neuronal populations, and species studied (Mogenson et al. 1973; Faiers et al. 1975; Gelsema et al. 1987; Iwata et al. 1987).

Evidence also exists for amygdaloid regulation of ingestive behaviour and gastrointestinal function. Electrical stimulation of the amygdala has been shown to affect vagally-mediated gastric motility (Shealy et al. 1957; Fennegan et al. 1966; Liubashina et al. 2002; Lyubashina

2004). Similarly, electrical and chemical amygdala stimulation has been associated with increased gastric acid secretion and the development of gastric ulcers and haemorrhages, which are prevented by vagotomy (Shealy et al. 1957; Henke 1980; Hernandez et al. 1990). Neurons in the amygdala are activated by intraperitoneal delivery of acetic acid (Nakagawa et al. 2003), and their lesion abolishes conditioned aversion to environments associated with this noxious visceral stimulus (Tanimoto et al. 2003). Furthermore, NST neurons responsive to gastric or intestinal distension are modulated by stimulation of the amygdala (Zhang et al. 2003), as are taste-sensitive NST neurons (Li et al. 2002; Cho et al. 2003; Kang et al. 2010). In the latter case, this influence of the amygdala on NST neurons is thought to enhance discrimination of palatable and aversive gustatory stimuli (Cho et al. 2003; Kang et al. 2010). Though amygdala lesion does not affect conditioned taste aversion (Reilly et al. 2005; Andre et al. 2007), chemo- and optogenetic studies suggest a role in appetite suppression, in part through afferent PBN input (Carter et al. 2013; Zseli et al. 2018).

These described visceral functions appear to be primarily mediated by direct axonal projections from the amygdala to the medulla. The γ-aminobutyric acid (GABA)-expressing central nucleus (CeA) serves as the main output source from the amygdala (Ehrlich et al. 2009), establishing long-range connections with other CAN regions, including the NST. Efferent projections from the CeA to NST have been demonstrated in rats using anterograde tracers delivered to CeA (van der Kooy et al. 1984; Danielsen et al. 1989; Zahm et al. 1999; Saha et al. 2000; Chiou et al. 2014) and fluorescent dyes retrogradely transported from the NST (van der Kooy et al. 1984; Veening et al. 1984; Gray et al. 1987a; Thompson et al. 1989). Similar findings in mouse (Gasparini et al. 2020), rabbit (Schwaber et al. 1980; 1982), cat (Hopkins et al. 1978; Onai et al. 1987), and macaque (Price et al. 1981) demonstrate that this innervation of NST by CeA neurons is well conserved across species. Diffusion magnetic resonance imaging (MRI)-based tractography also supports the likely existence of this pathway in humans (Arrigo et al. 2017).

The neurochemical composition of CeA populations projecting to the NST (referred to here as CeA→NST neurons) has been investigated through further tracing and immunohistochemical studies. In addition to GABA, CeA→NST neurons express the neuropeptides somatostatin (SST), corticotropin-releasing factor, neurotensin, substance P (SP), and vasoactive intestinal peptide, as well as the enzyme nitric oxide synthase (Higgins et al. 1983; Gray et al. 1987a; Saha et al. 2000; Batten et al. 2002; Saha et al. 2002), and 5-HT_{1A}, 5-HT_{1B} serotonergic (Saha et al. 2010), and α_{2A} adrenergic (Glass et al. 2002), receptors. Close apposition of anterogradely-labelled CeA

axons to NST neurons expressing sst_{2A}, neurokinin-1, and $GABA_A$ receptors further support a role for SST, SP, and GABA signalling in this pathway (Batten et al. 2002; Saha et al. 2002). An absence of immunoreactivity for met-enkephalin and galanin in CeA→NST neurons was also noted by Gray et al. (1987a), with the latter neuropeptide instead expressed by CeA neurons projecting to the PAG (Gray et al. 1987b; Steinberg et al. 2020). If gene products capable of selectively demarcating CeA→NST neurons exist, they have to date remained elusive. For example, SST CeA populations project not only to NST, but also to PAG, VLM, substantia nigra (SN), and bed nucleus of the stria terminalis (BNST) (Bowman et al. 2013; Penzo et al. 2014; Steinberg et al. 2020).

Rather than neurochemical phenotype, which may orchestrate overarching behavioural responses (Fadok et al. 2017), specific modalities mediated by CeA subpopulations appear to be defined more so by their projection target. Two lines of evidence support this hypothesis. Firstly, dual retrograde tracing and single-axon reconstruction studies indicate that individual projection targets are innervated by essentially distinct CeA efferent populations, with collaterals being sparse where present (Thompson et al. 1989; Veinante et al. 2003; Viviani et al. 2011; Han et al. 2017). The apparently contradictory observations of Xu et al. (2016) likely resulted from their highly sensitive molecular approach, which may not differentiate primary projection targets from their sparse collaterals. Secondly, functional studies indicate that different aspects of responses mediated by the CeA are achieved through projections to particular downstream targets. Behavioural (freezing) responses to fear-conditioned stimuli in rodents, for example, are mediated through projections to the PAG, whereas concomitant cardiovascular responses likely result from separate projections innervating the medulla (LeDoux et al. 1988; Viviani et al. 2011).

To facilitate a clearer understanding of this circuitry, the present chapter aimed to establish a method for targeted viral vector transduction of rat CeA→NST neurons, while also validating a novel adeno-associated viral (AAV) vector, developed here for Cre-recombinase-dependent expression of the *Guillardia theta* anion channel rhodopsin 2-Kv2.1 motif fusion construct (*Gt*ACR2$^{Kv2.1}$) introduced in Chapter 3. This construct was designed for localised somatic expression, to avoid inconsistencies in membrane polarisation upon *Gt*ACR2 activation arising from variations in somatodendritic and axonal intracellular chloride environments (Mahn et al. 2016), and to provide a tool for interrogating closely interconnected neural circuity. Despite not being exclusively localised to the soma, *Gt*ACR2$^{Kv2.1}$ was found to exhibit enhanced neuronal expression, while analogous constructs have been reported to significantly reduce *Gt*ACR2-

mediated axonal depolarisation (Mahn et al. 2018; Messier et al. 2018). Cre-dependent regulation of *Gt*ACR2$^{Kv2.1}$ production therefore offers a versatile approach for cell-type specific photoinhibition of neural circuitry, including CeA→NST neurons, in conscious, behaving animals.

4.2 Methods

4.2.1 Animals

All procedures were approved by the University of Melbourne Animal Research Ethics and Biosafety Committees and conducted in accordance with the Code of Practice for the Care and Use of Animals for Scientific Purposes published by the Australian National Health and Medical Research Council. Experiments involved adult male Sprague Dawley rats, housed under a 12 h light-dark cycle (lights on 06:30) at 22 ± 1 ˚C with *ad libitum* access to water and standard chow.

4.2.2 Plasmid and viral vectors

To achieve Cre-dependent expression, *Gt*ACR2$^{Kv2.1}$ was incorporated into pAAV-hSyn-DIO-(hCAR)$_{off}$-(ChETA-mRuby2)$_{on}$-W3SL plasmid (Addgene plasmid #111391; Li et al. (2018); a gift from Prof Adam Kepecs (Cold Spring Harbor Laboratory, NY, USA)), replacing the ChETA-mRuby2 coding sequence. The resulting vector expresses the human coxsackievirus and adenovirus receptor (hCAR) in transduced neurons prior to Cre-mediated recombination, providing enhanced tropism for canine adenovirus 2 (CAV2) vectors, as described by (Li et al. 2018). Following recombination, hCAR is replaced by *Gt*ACR2$^{Kv2.1}$ expression. *Gt*ACR2$^{Kv2.1}$ was amplified by polymerase chain reaction (PCR) from pAAV-CAG-*Gt*ACR2$^{Kv2.1}$-P2A-mCherry (Chapter 3) using Forward (5'-GTAGTAGCTAGCCACCATGGCCTCCCAG) and reverse (5'-CATCATTTAATTAAAACCGCGTAGCCTCTGGAAAATC) primers. These primers included *Nhe*I and *Pac*I adaptor sequences, respectively, which were used to ligate *Gt*ACR2$^{Kv2.1}$ into the pAAV-hSyn-DIO-(hCAR)$_{off}$-(ChETA-mRuby2)$_{on}$-W3SL plasmid, following excision of ChETA-mRuby2 using these enzymes, resulting in pAAV-hSyn-DIO-(hCAR)$_{off}$-(*Gt*ACR2$^{Kv2.1}$)$_{on}$-W3SL plasmid. Co-transfection of this construct with pDPI and pDPII plasmids (Grimm et al. 2003) into AAV293 cells (Agilent Technologies, CA, USA) preceded harvesting and iodixanol gradient purification (as described by Zolotukhin et al. (1999) and Ganella et al. (2013)) of AAV1/2-hSyn-DIO-(hCAR)$_{off}$-(*Gt*ACR2$^{Kv2.1}$)$_{on}$-W3SL vector. Titration of the purified vector was performed as described by Ma et al. (2017a), using forward (5'-CATTCTCGGACACAAACTGGAGTACAAC) and reverse (5'-GTCTGCTAGTTGAACGGAACCATCTTC) primers targeting the monomeric ultrastable green fluorescent protein (muGFP) coding sequence, rather than WPRE (which is replaced here by W3SL). All primers were synthesised by Bioneer Pacific (VIC, Australia). Vent® DNA polymerase, *Nhe*I, and *Pac*I enzymes were procured from New England Biolabs (VIC, Australia). T4 DNA ligase

was supplied by Promega (NSW, Australia). Sanger sequencing (Australian Genome Research Facility, VIC, Australia) was used to verify the PCR amplified insert. AAV-DJ-hSyn-FLEX-mGFP-2A-Syp-mRuby (Beier et al. 2015) was purchased from the Stanford Vector Core Facility (Stanford University, CA, USA; Reference No. GVVC-AAV-100). CAV2-Cre (Hnasko et al. 2006) and CAV2-CreGFP (Uematsu et al. 2017) vectors were supplied by the PVM Vector Core (Institute of Molecular Genetics of Montpellier, France).

4.2.3 Stereotaxic injections

Rats (200-300 g) were lightly anesthetised by inhalation of isoflurane (Rhodia Australia Pty. Ltd., VIC, Australia) in an enclosed chamber, prior to intramuscular (i.m.) injection of ketamine (60 mg/kg; Lyppard, VIC, Australia) mixed with medetomidine (250 µg/kg; Pfizer Animal Health, NSW, Australia). Once deeply anesthetised, as determined by lack of pedal withdrawal and corneal reflexes, rats were placed in a stereotaxic frame (RWD Life Science, GD, China). Body temperature was maintained at 37.5 ˚C during surgery with a heat pad (TC-1000 Temperature Controller, CWE Inc., PA, USA). A midline incision was made along the scalp, and burr holes drilled through the skull to allow access to stereotaxic coordinates targeting the amygdala. Two 75 nl injections of either AAV-DJ-hSyn-FLEX-mGFP-2A-Syp-mRuby (6.42×10^{12} gc/ml, n = 9 rats) or AAV1/2-hSyn-DIO-$(hCAR)_{off}$-$(GtACR2^{Kv2.1})_{on}$-W3SL (2.34×10^{11} gc/ml, n = 4 rats) were delivered bilaterally via a glass micropipette (~30 µm external tip diameter) connected to a picospritzer (World Precision Instruments, FL, USA). The coordinates used for these injections, relative to bregma (AP, ML) and brain surface (DV), were: Site #1: AP - 2.20 mm, ML ± 3.90 mm, DV -7.20 mm; Site #2: AP - 2.80 mm, ML ± 4.00 mm, DV - 7.20 mm; pipette angled 0 ˚, head flat. To minimise reflux of injectate up the injection track, the pipette was left in place for 2 min after each injection, before being was slowly withdrawn. The wound was closed using sterile sutures, prior to subcutaneous administration of meloxicam (1mg/kg, Metacam, Boehringer Ingelheim, NSW, Australia), intraperitoneal (i.p.) injection of Hartmann's solution (Baxter Healthcare, NSW, Australia) for fluid replacement, and anaesthesia reversal with atipamezole (1 mg/kg, i.m., Antisedan, Pfizer Animal Health).

Following two weeks recovery, rats were anaesthetised and placed in a stereotaxic frame (RWD Life Science) as described, with nose ventro-flexed (incisor bar -15 mm). The dorsal brainstem was exposed by a midline incision over the occipital bone, portions of which were removed with a dental drill, and opening of the atlanto-occipital membrane. Two 50 nl injections of either

CAV2-CreGFP or CAV2-Cre (2.00×10^{10} gc/ml, both vectors) were delivered to the NST of each rat via a glass micropipette (~30 µm external tip diameter) connected to a picospritzer (World Precision Instruments). Coordinates for these injections, which targeted either the caudal or rostral NST, were: Caudal site #1: AP - 0.25 mm, ML 0.00 mm, DV -0.43 mm; Caudal site #2: AP + 0.73 mm, ML + 0.55 mm, DV - 0.21 mm; Rostral site #1: AP + 1.62 mm, ML + 1.00 mm, DV - 0.53 mm; Rostral site #2: AP + 2.15 mm, ML + 1.30 mm, DV - 0.74 mm (coordinates relative to obex (AP, ML) and brainstem surface (DV), pipette angled 20 ˚ rostrally). Injections lateral to the midline were made unilaterally (left side). The wound was closed, and meloxicam (Boehringer Ingelheim), Hartmann's solution (Baxter Healthcare), and atipamezole (Pfizer Animal Health) delivered as described. Rats were maintained for a further 6 weeks prior to sacrifice.

4.2.4 Histology

Rats were deeply anaesthetised via inhalation of isoflurane or urethane injection (1.2 mg/kg, i.p.) and sacrificed by transcardial perfusion with 1 ml/g ice cold phosphate buffered saline (PBS), followed by 1 ml/g of 4 % (w/v) paraformaldehyde (PFA) in PBS. Dissected brains were post-fixed in 4 % PFA overnight at 4 ˚C, then transferred to a 20 % (w/v) sucrose solution (4 ˚C, 48 h) for cryoprotection. A cryostat was used to collect free-floating coronal sections (40 µm) through the brainstem, from the pyramidal decussation to the level of the trigeminal nucleus, and the forebrain, from the merger of anterior and inferior horns of the lateral ventricle caudally, to that of the lateral and third ventricles rostrally. Immunohistochemistry (IHC) was performed as previously described (Chen et al. 2010; Sevigny et al. 2012; Menuet et al. 2014). Forebrain sections from rats that received AAV-DJ-hSyn-FLEX-mGFP-2A-Syp-mRuby were incubated with chicken anti-GFP (1:5000; AB13970, Abcam, VIC, Australia) and rabbit anti-*Ds*Red (1:5000; Cat. No. 632496, Takara Bio USA, CA, USA) primary antibodies. Brainstem sections from these rats were incubated with the same primary antibodies, in addition to mouse anti-tyrosine hydroxylase (TH) (1:5000; MAB318, Merk Millipore, VIC, Australia). AlexaFluor-488-conjugated donkey anti-chicken, Cy3-conjugated donkey anti-rabbit, and Cy5-conjugated donkey anti-mouse secondary antibodies (1:500 each; Jackson Laboratory) were used to visualise each marker, respectively. Where rats received AAV1/2-hSyn-DIO-$(hCAR)_{off}$-$(GtACR2^{Kv2.1})_{on}$-W3SL, chicken anti-GFP (1:5000; AB13970, Abcam) was applied to brainstem and forebrain sections, with mouse anti-TH (1:5000; MAB318, Merk Millipore) and goat anti-choline acetyltransferase (ChAT; 1:1000; AB144P, Merck-Millipore) primary antibodies also included for brainstem sections. AlexaFluor-488-conjugated donkey anti-chicken, Cy3-conjugated donkey anti-mouse,

and Cy5-conjugated donkey anti-goat (1:500 each; Jackson Laboratory) secondary antibodies were applied to fluorescently label these markers. Bis-benzimide H (Hoechst) 33342 (1 µg/ml; Sigma-Aldrich, NSW, Australia) was included as a nuclear counterstain in all secondary antibody incubations.

4.2.5 Imaging

Immunofluorescent labelling was imaged using an LSM 780 Zeiss Axio Imager 2 laser scanning confocal microscope (Carl Zeiss AG, Oberkochen, Germany). In rats that received injections of AAV-DJ-hSyn-FLEX-mGFP-2A-Syp-mRuby to the amygdala and CAV2-CreGFP or CAV2-Cre to the NST, mGFP/CreGFP- (AlexaFluor-488), Syp-mRuby- (Cy3), and TH- (Cy5) immunoreactivity was imaged. Where AAV1/2-hSyn-DIO-$(hCAR)_{off}$-$(\textit{Gt}ACR2^{Kv2.1})_{on}$-W3SL and CAV2-Cre were injected to the amygdala and NST, respectively, immunoreactivity for muGFP (AlexaFluor-488), TH (Cy3), and ChAT (Cy5) was imaged. All immunolabelling was accompanied by Hoechst 33342 nuclear staining. Each fluorophore was imaged using excitation wavelength and emission filter parameters as follows: Hoechst 33342, 405 nm (410-496 nm); GFP/AlexaFluor-488, 488 nm (499-552 nm); Syp-mRuby/Cy3, 561 nm (561-624 nm); Cy5, 633 nm (638-759 nm). Tiled epi-fluorescent scans using a 10 × air objective lens, automated stitching stage, and Zen Black software (Carl Zeiss AG) were used to image whole coronal sections in rats that received amygdala AAV-DJ-hSyn-FLEX-mGFP-2A-Syp-mRuby injections. Affinity Designer software (Serif, UK) was used to manually trace mGFP-labelled fibres from imaged coronal sections and map them to Paxinos and Watsons's rat brain atlas (Paxinos et al. 2014). Confocal images were also collected from regions of interest in rats where CAV2 vector injections targeted the rostral NST, with either AAV-DJ-hSyn-FLEX-mGFP-2A-Syp-mRuby or AAV1/2-hSyn-DIO-$(hCAR)_{off}$-$(\textit{Gt}ACR2^{Kv2.1})_{on}$-W3SL injected to the amygdala. These images were acquired using a 20 × air objective lens, automated stitching stage, and Zen Black software (Carl Zeiss AG), with maximum projection images, from planes imaged at 2 µm intervals through the entire z-axis, generated in Fiji software (Schindelin et al. 2012).

4.3 Results

4.3.1 CAV2 vector injections to rostral, but not caudal, NST efficiently transduces CeA efferents

To establish a protocol for cell-type specific transduction of CeA→NST neurons, AAV-DJ-hSyn-FLEX-mGFP-2A-Syp-mRuby (Figure 4.1A) was delivered via bilateral injections to the amygdala, with midline or unilateral CAV2-CreGFP injections made at sites targeting either the caudal or rostral NST (Figure 4.1B). This vector combination provides labelling of CeA efferent neurons with membrane bound GFP (mGFP) and synaptophysin-mRuby (Syp-mRuby) fluorophores in the presence of Cre-recombinase, which must be delivered by retrograde CAV2 vector transport from terminals innervating the NST. While mGFP is expressed throughout the neuronal membrane following co-transduction of CeA efferents, Syp-mRuby provides putative labelling of presynaptic sites in these neurons (Beier et al. 2015; Lerner et al. 2015). CreGFP immunofluorescence, which localises primarily to the nucleus and soma (Kaspar et al. 2002; Li et al. 2018), was used here to validate CAV2 vector injection sites in the NST.

Fluorescent signal from GFP-immunoreactive cell bodies at coordinates targeted by the more caudal NST injections (Figures 4.1C, 4.1D; representative images from n = 3 rats) indicated that CAV2-CreGFP was delivered primarily to medial (SolM), commissural (SolC), and intermediate (SolIM) regions. Additional somatic labelling in the area postrema (AP), 10N, and dorsolateral NST (SolDL) reflected limited CAV2-CreGFP spread to these neighbouring areas, likely including some reflux along the injection tract. At NST levels rostral to these injection sites, sparse labelling of fibres with GFP and Syp-mRuby immunoreactivity (Figures 4.1E, 4.1F; representative images from n = 3 rats) was observed. A similar pattern of immunoreactivity in the CeA and stria terminalis (Figure 4.1G; representative image from n = 3 rats) suggested that although some co-transduction of CeA neurons with AAV-DJ-hSyn-FLEX-mGFP-2A-Syp-mRuby and CAV2-CreGFP had occurred, it was relatively inefficient in these animals.

In rats that received CAV2-CreGFP injections targeting rostral NST coordinates (Figure 4.2A), GFP-immunofluorescent cell bodies were concentrated in SolM, SolIM, and dorsomedial (SolDM) regions, again with limited spread to neighbouring areas including 10N (Figures 4.2B, 4.2C; representative images from n = 2 rats). Clear GFP- and Syp-mRuby-immunoreactivity in CeA cell bodies, as well as fibres innervating the NST (data not shown), indicated efficient co-transduction of CeA efferent neurons following CAV2 vector injection to these rostral

coordinates. To remove the potential for confounding CreGFP-immunoreactivity when mapping mGFP-expressing CeA fibres innervating NST, injections of CAV2-Cre were performed in a second cohort of rats using these validated coordinates (n = 4 rats; Figure 4.2A). Different densities of labelling, with similar distributions, were observed in two of these rats compared to the others; the highest density labelling is described first.

Dense labelling of neuronal cell bodies with mGFP- and Syp-mRuby-immunoreactivity in the medial division of the CeA (CeM) was evident ipsilateral to the CAV2-Cre NST injection sites in these rats (Figure 4.2D; representative image for n = 2 rats). Consistent with previous tracing studies (van der Kooy et al. 1984; Danielsen et al. 1989; Chiou et al. 2014), only sparse labelling was present in the contralateral CeM (Figure 4.2E; representative image for n = 2 rats). Prominent mGFP- and Syp-mRuby-immunoreactivity was also present in fibres coursing through the ipsilateral stria terminalis (Figure 4.2F; representative image from n = 2 rats). The abundant expression of Syp-mRuby in this fibre tract, likely reflecting its trafficking along the axon, indicates that this construct should not be used in isolation as a pre-synaptic marker. Instead, Syp-mRuby appears to serve more so as an 'axonal' marker, with further evidence, such as proximity to a labelled post-synaptic molecule, required to indicate synaptic localisation. For this reason, further characterisation of Syp-mRuby expression in CeA→NST neurons was not performed here. Similar patterns of expression were seen in the remaining two rats that received CAV2-Cre injections to rostral NST. However, substantially fewer CeM neurons were transduced (Figure 4.2G; representative data from n = 2 rats), with an associated decrease in the density of mGFP/Syp-mRuby-labelled fibres.

The first two rats of this cohort, which exhibited robust transduction of CeA→NST neurons (Figure 4.2D), received CAV2-Cre injections on the day this vector was thawed from -80 ˚C storage. The injections in the second two rats, that showed an apparent reduction in transduction efficiency (Figure 4.2G), were made after the same CAV2-Cre aliquot had been stored for 2 days at 4 ˚C or on ice. Therefore, the reduction in transduction efficiency may reflect a temperature-dependent decrease in CAV2 vector infectious titre following short-term storage at this higher temperature. It should be noted that the CAV2-CreGFP vector was also stored and used over several days at 4 ˚C or on ice and appeared to be associated with a similarly reduced transduction efficiency in these rats. Despite these differences in transduction efficiency, a consistent distribution of labelled CeM neurons and fibres innervating the NST (Figures 4.2H-J; representative images for n = 2 rats with most robust CeA→NST transduction efficiency; see

also Section 4.3.2 below) was observed across all six rats that received CAV2 vector injections to the rostral NST.

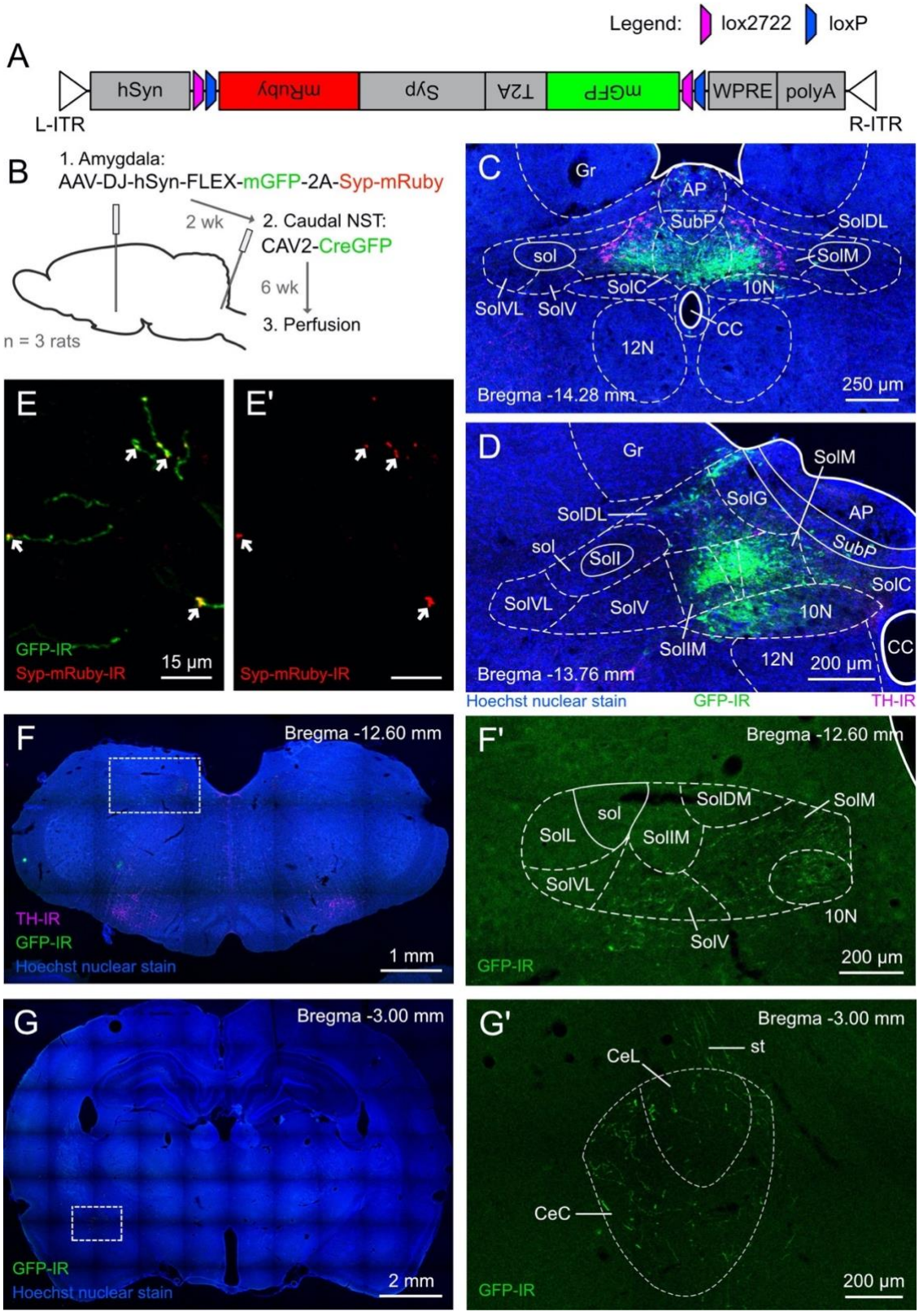

Figure 4.1. *Refer to next page for figure legend.*

Figure 4.1. *CAV2 vector injections to caudal NST sparsely transduce CeA efferents.* **(A)** Schematic representation of the viral vector genome for AAV-DJ-hSyn-FLEX-mGFP-2A-Syp-mRuby, used here to validate CAV2 vector NST injection coordinates and map the distribution of CeA→NST fibres. In the presence of Cre-recombinase, neurons transduced with this AAV vector express membrane bound GFP (mGFP), which provides labelling throughout the neuronal membrane, and synaptophysin-mRuby (Syp-mRuby), that putatively labels presynaptic sites. The experimental design followed is summarised in **(B)**. Bilateral injections of AAV-DJ-hSyn-FLEX-mGFP-2A-Syp-mRuby to the amygdala were made in rats (n = 3) two weeks prior delivery of CAV2-CreGFP at two sites in caudal NST, after which rats were maintained for a further six weeks before transcardial perfusion and histological processing. Midline **(C)** and unilateral **(D)** subpostremal NST injection sites were validated using presumptive CreGFP-immunoreactive cell bodies (green), which predominantly localised to medial (SolM), intermediate (SolIM), and commissural (SolC) subregions (TH-immunoreactivity shown in magenta; Hoechst nuclear stain shown in blue). Sparse labelling of GFP- (green) and Syp-mRuby- (red) immunoreactive fibres was also observed in caudal NST, with a representative image from SolM (Bregma -13.36 mm) depicted in **(E)** (examples of Syp-mRuby immunoreactivity indicated by arrow heads; Syp-mRuby immunoreactivity alone also provided in **(E')**). Similar sparse labelling of fibres in rostral NST **(F)** (GFP- and TH- immunoreactivity shown in green and magenta, respectively, with Hoechst 33342 nuclear stain shown in blue), as well as CeA and stria terminalis **(G)** (GFP-immunoreactivity shown in green, Hoechst nuclear stain shown in blue) indicated limited co-transduction of CeA→NST neurons in these rats. Higher magnification images of GFP-immunoreactivity in ipsilateral NST, as well as CeA and stria terminalis, are shown in **(F')** and **(G')**, respectively. All images depict representative data from n = 3 rats. *Abbreviations*: *AP*, area postrema; *CC*, central canal; *CeC*, central amygdaloid nucleus, capsular part; *CeL*, central amygdaloid nucleus, lateral division; *Gr*, gracile nucleus; *hSyn*, human synapsin 1 promoter; *IR*, immunoreactivity; L-*ITR*, left inverted terminal repeat; *polyA*, human growth hormone polyadenylation signal; *R-ITR*, right inverted terminal repeat; *sol*, solitary tract - nucleus of the solitary tract (*Sol*) subregions: *SolC*, commissural part; *SolDL*, dorsolateral part; *SolDM*, dorsomedial part, *SolG*, gelatinous part; *SolI*, interstitial prat; *SolIM*, intermediate part; *SolL*, lateral part; *SolM*, medial part; *SolV*, ventral part; *SolVL*, ventrolateral part – *st*, stria terminalis; *SubP*, subpostrema area; *T2A*, *Thosea asigna* virus 2A self-cleaving peptide; *WPRE*, woodchuck hepatitis virus post-transcriptional regulatory element; *10N*, dorsal motor nucleus of vagus; *12N*, hypoglossal nucleus.

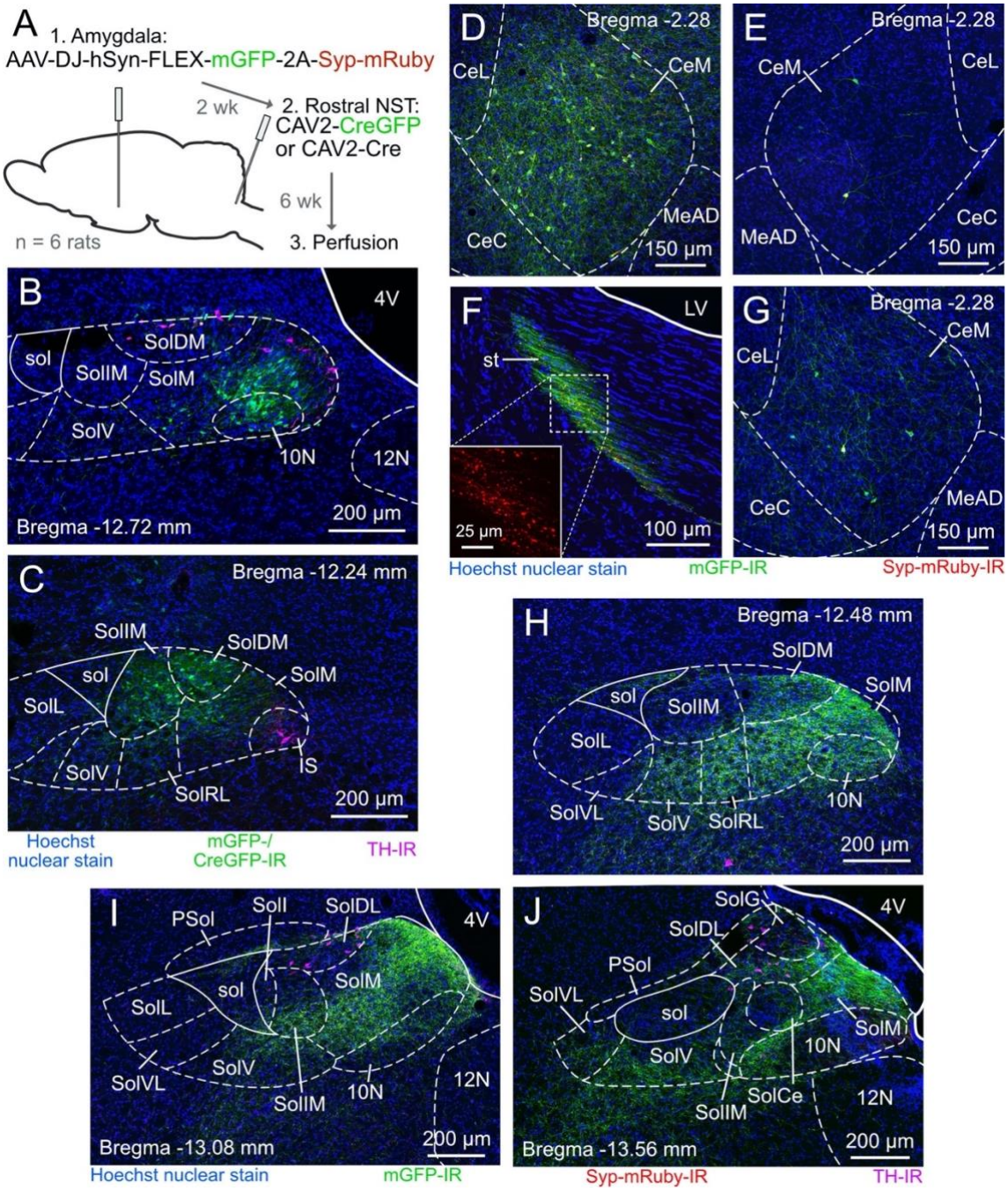

Figure 4.2. *Refer to pages 120-121 for figure legend.*

Figure 4.2. *Robust, cell-type specific transduction of CeA→NST neurons following CAV2 injections to rostral NST.* **(A)** To assess the efficacy of CeA→NST neuronal transduction following CAV2 vector delivery to rostral NST, a separate cohort of rats (n = 6) received bilateral AAV-DJ-hSyn-FLEX-mGFP-2A-Syp-mRuby injections targeting the amygdala. Two weeks later, CAV2-CreGFP (n = 2 rats) or CAV2-Cre (n = 4 rats) was delivered unilaterally to two sites in the rostral NST. Rats were maintained for a further six weeks prior to transcardial perfusion and histological processing. To validate these coordinates, the rostral NST was imaged for GFP-immunoreactive cell bodies (green; presumed CreGFP expression from injected CAV2 vector), which were found localised in dorsomedial (SolDM), intermediate (SolIM), and medial (SolM) subregions (**(B, C)**; TH-immunoreactivity shown in magenta; Hoechst nuclear stain shown in blue; representative images from n = 2 rats). Transduced cell bodies were also present in some neighbouring regions, most notably the dorsal motor nucleus of vagus (10N). **(D)** Injection of Cre-expressing CAV2 vectors to rostral NST was associated with robust transduction of cell bodies expressing mGFP (green) and Syp-mRuby (red) in the ipsilateral CeA, specifically its medial division (CeM) (Hoechst nuclear stain shown in blue; representative image for n = 2 rats which received CAV2-Cre injections on the day this vector was thawed from - 80 ˚C storage; data in E, F, and H-J are from the same animal as that shown here in D). **(E)** Sparse transduction of neurons in the contralateral CeM was also observed (representative image for n = 2 rats, as described in D). **(F)** Immunoreactivity for both mGFP (green) and Syp-mRuby (red) was readily visualised in the stria terminalis fibre tract, indicating that Syp-mRuby labels both axons of passage and presynaptic sites (representative image from n = 2 rats, as described in D). **(G)** The injection of CAV2 vectors following storage at 4 ˚C or on ice resulted in substantially reduced transduction efficacy, as illustrated in ipsilateral CeM here from a rat injected 48 hrs after initial thawing of CAV2-Cre from - 80 ˚C storage (representative image for n = 4 rats; CAV2-CreGFP injections were also made after vector storage at 4 ˚C; fluorescent markers as described for D). Examples of transduced CeA fibres (showing immunoreactivity for mGFP (green) and Syp-mRuby (red)) innervating the NST are depicted in **(H-J)** (representative images for n = 2 rats, as described in D; TH-immunoreactivity shown in magenta; Hoechst nuclear stain shown in blue).

Figure 4.2 (continued). *Abbreviations*: Central amygdaloid nucleus (*Ce*) subregions; *CeC*, capsular part; *CeL*, lateral division; *CeM*, medial division – *IR*, immunoreactivity; *IS*, inferior salivatory nucleus; *LV*, lateral ventricle; *MeAD*, medial amygdala, anterodorsal part; *sol*, solitary tract – nucleus of the solitary tract (*Sol*) subregions; *PSol*, parasolitary nucleus; *SolCe*, central part; *SolDL*, dorsolateral part; *SolDM*, dorsomedial part; *SolG*, gelatinous part; *SolL*, lateral part; *SolM*, medial part; *SolI*, interstitial part; *SolIM*, intermediate part; *SolRL*, rostrolateral part; *SolV*, ventral part; *SolVL*, ventrolateral part – *st*, stria terminalis; *4V*, fourth ventricle; *10N*, dorsal motor nucleus of vagus; *12N*, hypoglossal nucleus.

4.3.2 Mapping of CeA→NST efferents exiting the amygdala and innervating the brainstem

In rats that received CAV2-Cre vector injections to the rostral NST, mapping of mGFP-immunoreactive cell bodies and fibres revealed a distribution broadly consistent with that described in previous tracing studies (van der Kooy et al. 1984; Danielsen et al. 1989; Zahm et al. 1999; Saha et al. 2000) (Figures 4.3, 4.4; representative mapping for n = 4 rats). Efferent fibres emanating from transduced CeM neurons were either funnelled caudally to exit the amygdala via the stria terminalis (Figure 4.3F), or followed a more dispersed, anteromedial trajectory into the ventral amygdalofugal (VAF) pathway (Figure 4.3B). Those efferents entering the stria terminalis proceeded caudally before following this fibre tract dorsally (Figure 4.3H) and looping back in a rostral direction, passing dorsal to their transduced soma in the amygdala (Figures 4.3C-E). During their ventral descent, which primarily followed the medial boundary of the internal capsule, efferents exited the stria terminalis via the sublenticular extended amygdala, where they intermingled with mGFP-labelled amygdalofugal fibres rostral to CeA (Figure 4.3A). These interspersed fibres projected caudally past the amygdala in a loose formation along the medial border of the internal capsule, gradually concentrating in the lateral hypothalamus to continue their path caudally within the medial forebrain bundle (Figures 4.3G-I). Notable deviations from these described pathways included relatively sparse fibres travelling ventrally from the caudal pole of the CeA towards the basomedial amygdala (Figures 4.3E, 4.3F) and amygdalopiriform transition area (Figures 4.3H, 4.3I), as well as a collection of fibres proceeding dorsally from those entering the medial forebrain bundle to innervate the mediodorsal thalamic nucleus (Figures 4.3H, 4.3I). Regions immediately rostral and caudal to those illustrated in Figure 4.3 were not mapped in the present study.

Mapping in these animals was resumed in the pontine brainstem, where punctate mGFP-immunoreactivity surrounding the trigeminal nucleus indicated transection of CeA efferents taking a direct caudal trajectory (Figure 4.4A). Labelled fibres continued towards the medulla by passing through the reticular formation (Figures 4.4B, 4.4C), before reaching the most rostral extent of the NST (Figure 4.4D). At this level, a subset of CeA efferents appeared to move dorsally, densely innervating the rostral NST, while other fibres continued to travel caudally within the reticular formation. This pattern of NST innervation by CeA efferents rising from the reticular formation continued along the rostro-caudal extent of the NST, being most pronounced at NST levels rostral to the merger of the central canal and fourth ventricle. Particularly dense innervation was observed in ventral and medial NST subregions, especially SolM, but also SolIM,

SolDM, rostrolateral (SolRL), ventral (SolV), and SolC nuclei (Figures 4.2H-J, 4.4D-J; representative data for n = 4 rats). Sparse fibres were seen extending ventrally into autonomic control regions including NAmb, ventral respiratory column (VRC), and rostral ventrolateral medulla (RVLM) (Figures 4.4F-H), and also appeared to continue caudally through the reticular formation towards the cervical spinal cord (Figure 4.4J).

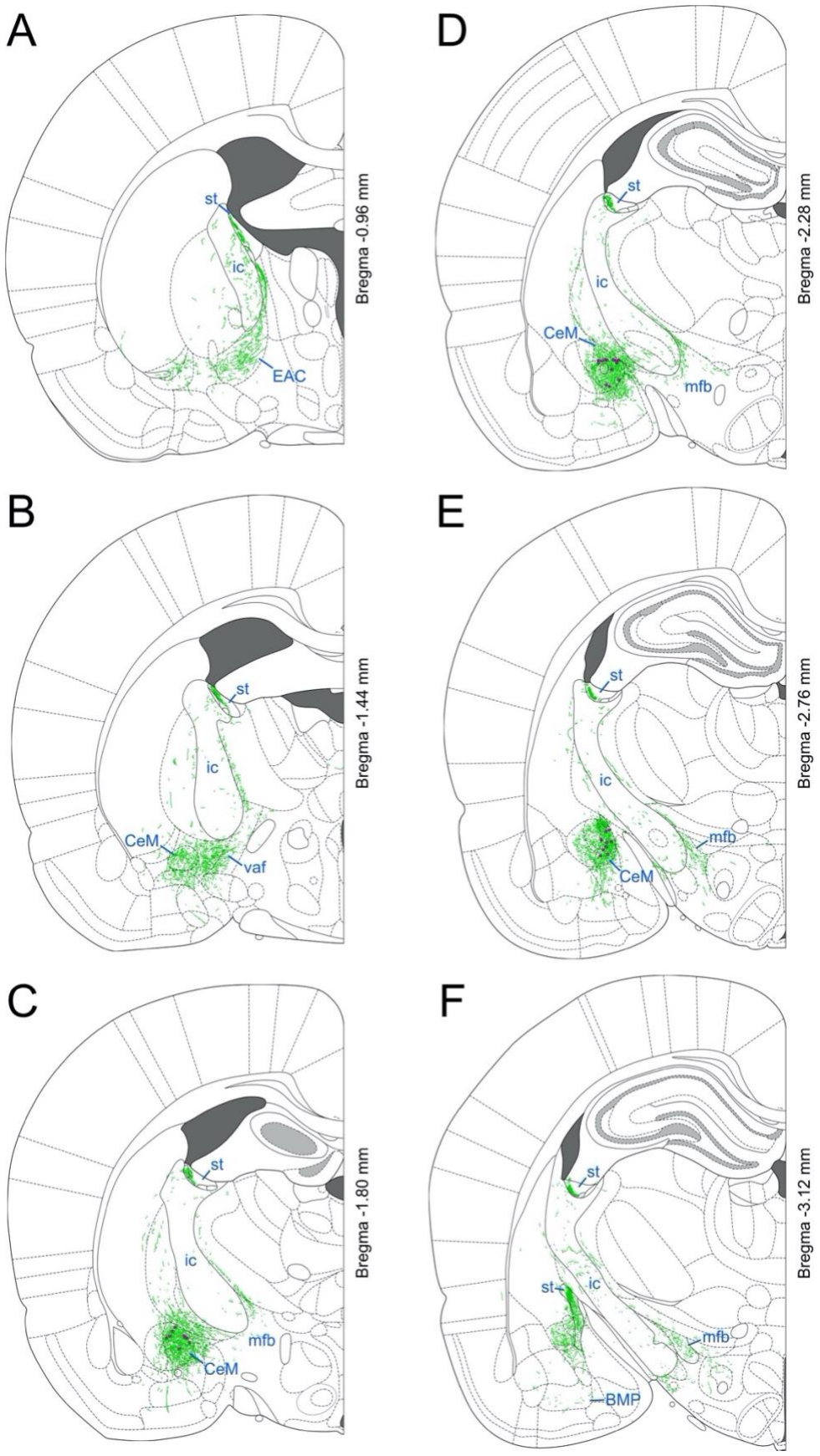

Figure 4.3. *Mapping of efferent fibres exiting the amygdala from transduced cell bodies in CeA* (*continued next page).*

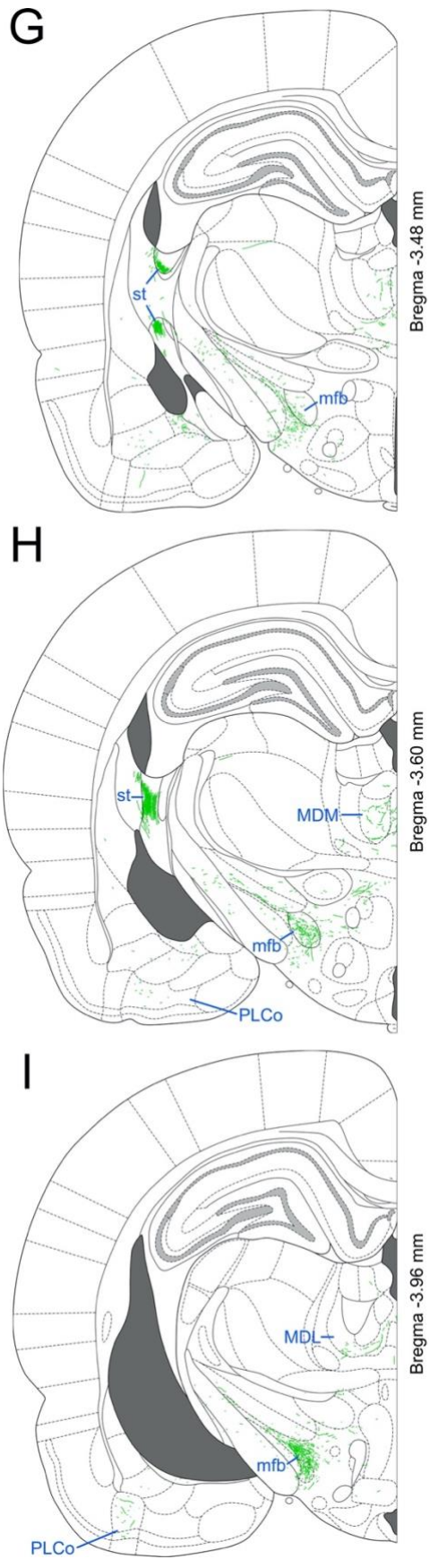

Figure 4.3 (continued). Imaging of coronal sections, taken from rats which received AAV-DJ-hSyn-FLEX-mGFP-2A-Syp-mRuby and CAV2-Cre injections to the amygdala and rostral NST, respectively (n = 4, as per Figure 4.2; representative data shown from one rat; corresponding brainstem mapping from this rat is depicted in Figure 4.4), were used to map the distribution of transduced cell bodies (magenta dots) in CeA, and the path followed by their efferent projections (green lines), ipsilateral to NST injection sites. Transduced efferent fibres originating from stria terminalis and VAF pathways were seen to intermingle rostral to the amygdala **(A, B)**. Transduced cell bodies were present specifically in CeM **(C-E)**, with concentrated fibres passing dorsally through the stria terminalis and along the medially boundary of the internal capsule at these levels. Fibres entering the stria terminalis, which courses caudally and dorsally before proceeding rostrally, as well as fibres gathering in the lateral hypothalamus, were observed at more caudal levels **(F-H)**. Descending efferents passing through the lateral hypothalamus continued caudally through the medial forebrain bundle **(I)**. Sparse labelling of fibres deviating from these paths were also present, most notably to the thalamus (G-I), basomedial amygdala (C-F) and amygdalopiriform transition area (I). This pattern of transduced cell bodies and efferent fibres, though much sparser, was also present in contralateral structures (data not shown). Abbreviated regions of interest (detailed next page) are annotated in blue.

Figure 4.3 (continued). *Abbreviations*: *BMP*, basomedial amygdaloid nucleus, posterior part; *CeM*, central amygdaloid nucleus, medial division; *EAC*, sublenticular extended amygdala, central part; *ic*, internal capsule; *MDL*, mediodorsal thalamic nucleus, lateral part; *MDM*, mediodorsal thalamic nucleus, medial part; *mfb*, medial forebrain bundle; *PLCo*, posterolateral cortical amygdaloid nucleus; *st*, stria terminalis; *vaf*, ventral amygdalofugal pathway.

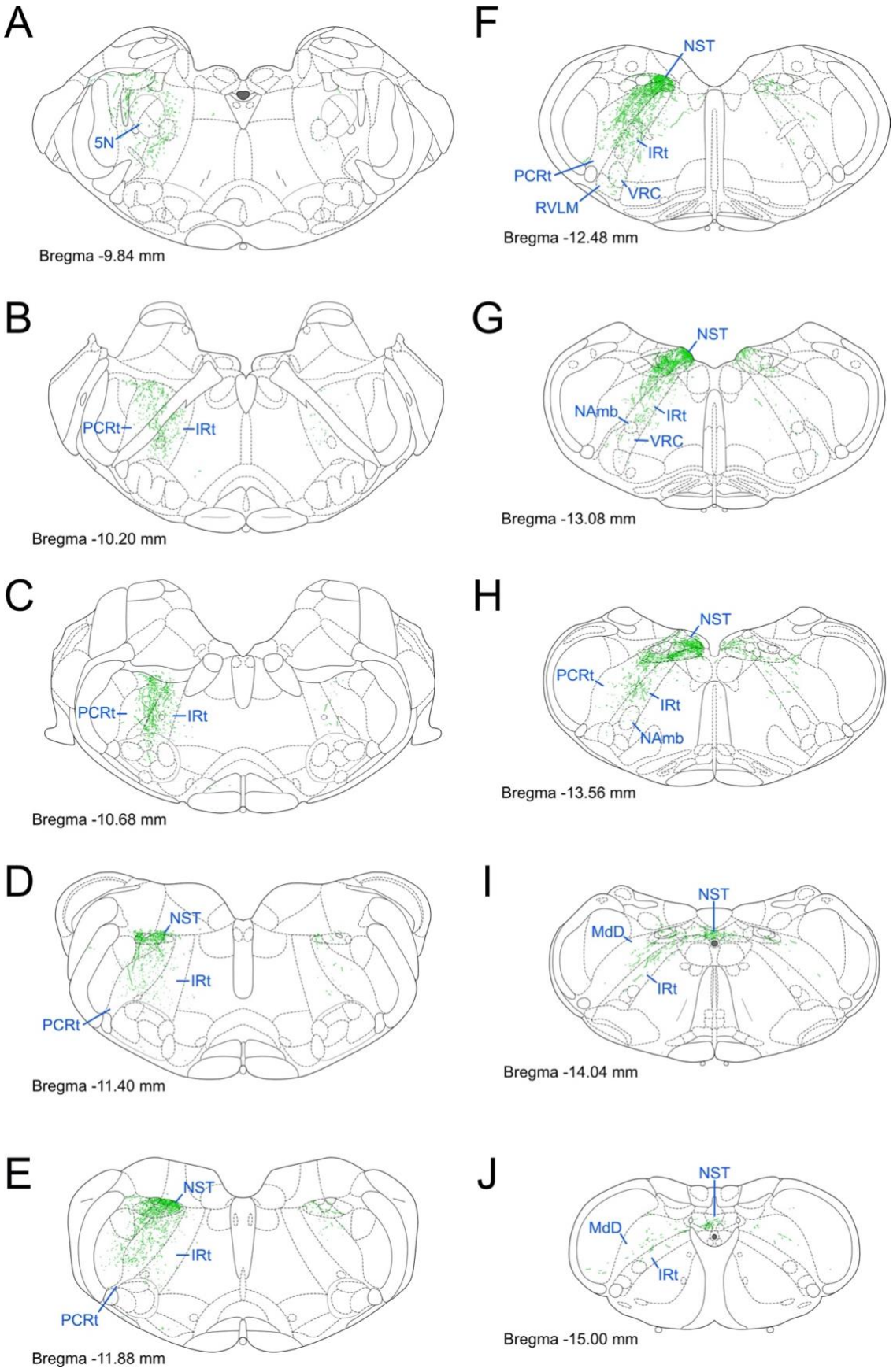

Figure 4.4. *Refer to next page for figure legend.*

Figure 4.4. *Mapping of transduced CeA efferent fibres innervating the brainstem*. Imaging of coronal sections, taken from rats which received AAV-DJ-hSyn-FLEX-mGFP-2A-Syp-mRuby and CAV2-Cre injections to the amygdala and rostral NST, respectively (n = 4, as per Figure 4.2; representative data shown from one rat; corresponding forebrain mapping from this rat is depicted in Figure 4.3), were used to map the distribution of transduced CeA efferent fibres (green lines) innervating the brainstem. Punctate fibres surrounding the trigeminal nucleus indicated a direct caudal trajectory that largely avoided this nucleus **(A)**. These fibres continued caudally through the reticular formation **(B, C)** before reaching the most rostral pole of the NST **(D)**. At this point, transduced fibres appeared to move dorsally from the reticular formation to densely innervate the NST. While a subset of fibres continued through the reticular formation, many appeared to continue branching dorsally to enter the NST, where especially dense innervation was seen in rostral, ventral, and medial regions **(E-G)**. The density of NST innervation gradually diminished through more caudal levels **(H-J)**, with some efferents continuing through the reticular formation towards the cervical spinal cord **(J)**. This pattern of innervation was most pronounced ipsilateral to NST injection coordinates, with spare labelling in the corresponding contralateral structures also present. Abbreviated regions of interest are annotated in blue: *IRt*, intermediate reticular nucleus; *MdD*, medullary reticular nucleus, dorsal part; *NAmb*, nucleus ambiguus; *NST*, nucleus of the solitary tract; *PCRt*, parvicellular reticular nucleus; *RVLM*, rostral ventrolateral medulla; *VRC*, ventral respiratory column; *5N*, trigeminal nucleus.

4.3.3 Conditional, but not soma-localised, expression of *Gt*ACR2$^{Kv2.1}$ in CeA→NST neurons

Having established a protocol for cell-type specific transduction of CeA→NST neurons, this approach was used to characterise the novel AAV1/2-hSyn-DIO-(hCAR)$_{off}$-(*Gt*ACR2$^{Kv2.1}$)$_{on}$-W3SL vector (Figure 4.5A), developed here for Cre-recombinase dependent expression of the *Gt*ACR2$^{Kv2.1}$ fusion construct introduced in Chapter 3. Prior to Cre-mediated recombination, neurons transduced with this vector are expected to express the hCAR cell-surface adhesion molecule, which provides enhanced tropism for CAV2 vectors by facilitating their endocytosis and retrograde axonal transport (Salinas et al. 2009; Li et al. 2018). To validate Cre-dependent *Gt*ACR2$^{Kv2.1}$ expression from this vector, rats (n = 4) received bilateral amygdala injections of AAV1/2-hSyn-DIO-(hCAR)$_{off}$-(*Gt*ACR2$^{Kv2.1}$)$_{on}$-W3SL two weeks prior to unilateral delivery of CAV2-Cre to the rostral NST, following which, rats were maintained for a further six weeks before perfusion and tissue processing (Figure 4.5B).

Immunoreactivity against the *Gt*ACR2$^{Kv2.1}$ muGFP tag revealed a similar distribution of expression to that described in rats which received AAV-DJ-hSyn-FLEX-mGFP-2A-Syp-mRuby injections (Figure 4.2). Labelled cell bodies were concentrated specifically in CeM ipsilateral to the CAV2-Cre injection coordinates (Figure 4.5C), with only sparse labelling in the contralateral CeM (Figure 4.5D). These data, which reflect the pattern of predominantly ipsilateral NST innervation by CeA neurons (detailed above; see also Section 4.4), provide evidence validating the Cre-dependent nature of *Gt*ACR2$^{Kv2.1}$ expression from AAV1/2-hSyn-DIO-(hCAR)$_{off}$-(*Gt*ACR2$^{Kv2.1}$)$_{on}$-W3SL. Consistent with observations made in transduced respiratory column neurons (Chapter 3), inclusion of the Kv2.1 motif again failed to limit *Gt*ACR2$^{Kv2.1}$ to the soma *in vivo*, with fluorescent signal clearly demarcating transduced CeA efferent axons in the ipsilateral stria terminalis (Figure 4.5E) and NST (Figure 4.5F). It is important to note that the CAV2-Cre vector aliquot used in this cohort of rats had been stored at 4 ˚C prior to injection, which may have resulted in a loss of infectious titre and suboptimal expression in the present study, as postulated in Section 4.3.1 above. Given this, as well as the robust CAV2 vector transduction of CeA→NST neurons seen with AAV-DJ-hSyn-FLEX-mGFP-2A-Syp-mRuby (Figure 4.2), a detailed assessment of potential effects from hCAR transgene expression on vector tropism was not performed in the present study.

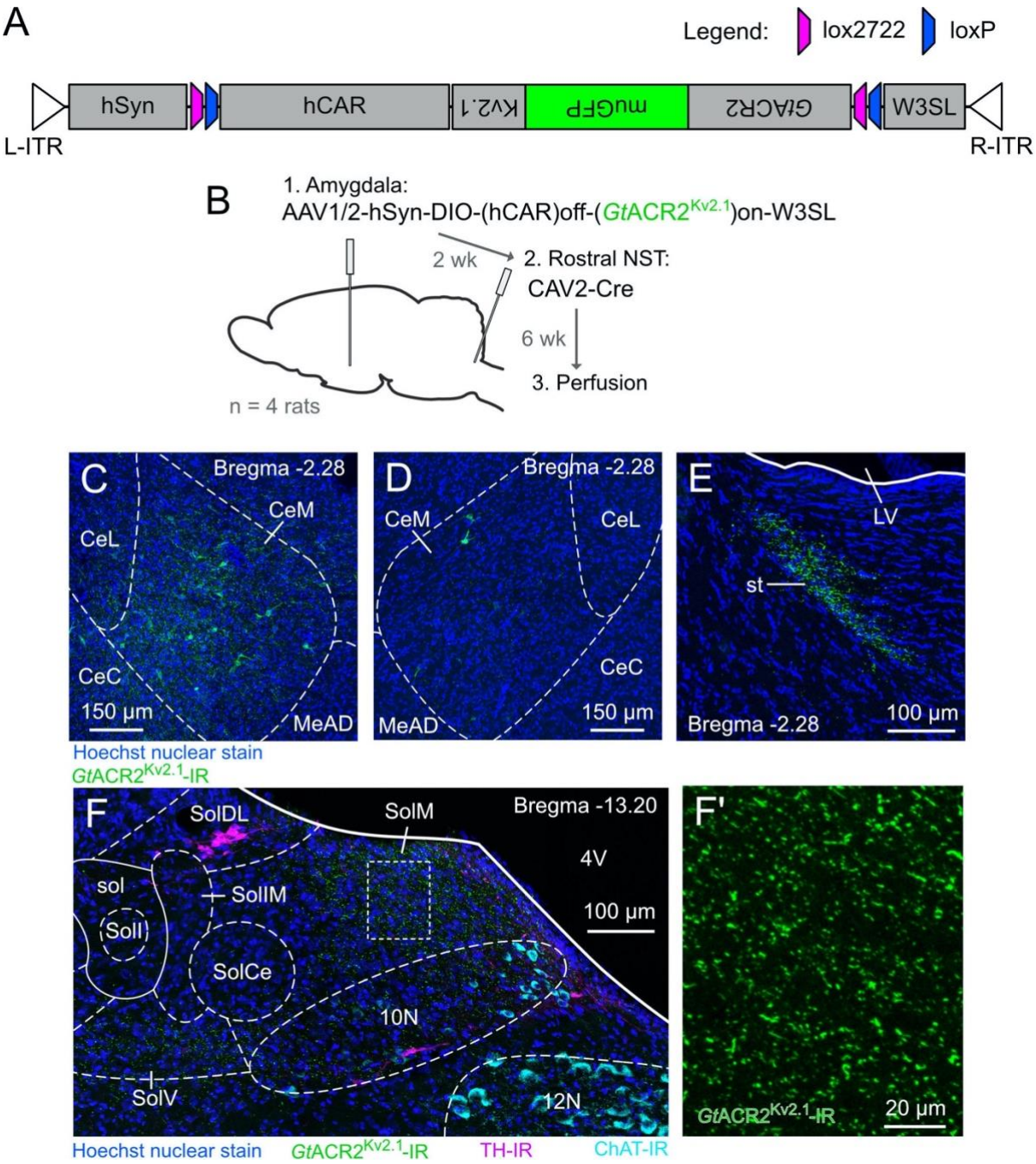

Figure 4.5. *Refer to next page for figure legend.*

Figure 4.5. *Cell-type specific, but not soma localised, GtACR2$^{Kv2.1}$ expression in CeA→NST neurons*. **(A)** Schematic representation of the AAV1/2-hSyn-DIO-(hCAR)$_{off}$-(*Gt*ACR2$^{Kv2.1}$)$_{on}$-W3SL vector genome, developed here for conditional expression of *Gt*ACR2$^{Kv2.1}$ in the presence of Cre-recombinase. Prior to Cre-mediated recombination, neurons transduced with this vector produce the hCAR receptor, providing enhanced tropism for CAV2 vectors. **(B)** To validate Cre-dependent *Gt*ACR2$^{Kv2.1}$ expression *in vivo*, AAV1/2-hSyn-DIO-(hCAR)$_{off}$-(*Gt*ACR2$^{Kv2.1}$)$_{on}$-W3SL was injected bilaterally to the amygdala in rats (n = 4), with CAV2-Cre delivered unilaterally to the rostral NST two weeks later. Six weeks after CAV2 vector injections to the rostral NST rats underwent transcardial perfusion, prior to tissue processing for IHC. Immunolabelling of muGFP (green) revealed transduced cell bodies were concentrated in CeM ipsilateral to NST injection sites **(C)**, with only sparse labelling in the contralateral CeM **(D)**, indicating Cre-dependent, cell-type specific expression of *Gt*ACR2$^{Kv2.1}$ in CeA→NST neurons. Immunoreactivity against muGFP was also clearly visible in the ipsilateral stria terminalis **(E)**, indicating trafficking of *Gt*ACR2$^{Kv2.1}$ along CeA axons coursing through this fibre tract. Labelling of fibres innervating the NST with muGFP-immunoreactivity **(F)** (see also higher magnification image of muGFP-immunoreactivity alone in **(F')**) suggests that axonal *Gt*ACR2$^{Kv2.1}$ trafficking persists even in long-range projections to distant targets. Images are representative for n = 4 rats, and all include Hoechst nuclear stain (blue) in addition to muGFP-immunoreactivity (green). In NST (F), TH- (magenta) and ChAT- (cyan) immunolabelling is also shown. *Abbreviations*: central amygdaloid nucleus (*Ce*) subregions; *CeC*, capsular part; *CeL*, lateral division; *CeM*, medial division – *GtACR2*, *Guillardia theta* anion channel rhodopsin 2; *hCAR*, human coxsackievirus and adenovirus receptor; *hSyn*, human synapsin 1 promoter; *IR*, immunoreactivity; *Kv2.1*, Kv2.1 potassium channel trafficking motif; *L-ITR*, left inverted terminal repeat; *MeAD*, medial amygdala, anterodorsal part; *muGFP*, monomeric ultrastable green fluorescent protein; *LV*, lateral ventricle; *R-ITR*, right inverted terminal repeat; *sol*, solitary tract – nucleus of the solitary tract (*Sol*) subregions; *SolCe*, central part; *SolDL*, dorsolateral part; *SolM*, medial part; *SolI*, interstitial part; *SolIM*, intermediate part; *SolV*, ventral part – *st*, stria terminalis; *W3SL*, condensed woodchuck hepatitis virus post-transcriptional regulatory element (WPRE) and simian virus 40 polyadenylation signal sequence; *4V*, fourth ventricle; *10N*, dorsal motor nucleus of vagus; *12N*, hypoglossal nucleus.

4.4 Discussion

The primary aims of experiments described in this chapter were (1) to validate and characterise Cre-recombinase dependent production of *Gt*ACR2$^{Kv2.1}$ expression from a novel AAV vector, and, in facilitating in this, (2) to establish a protocol for cell-type specific transgene expression in CeA→NST neurons. In addressing the latter aim, robust transduction of CeA efferent neurons with AAV-DJ-hSyn-FLEX-mGFP-2A-Syp-mRuby was observed following delivery of Cre-expressing CAV2 vectors to the rostral, but not caudal, NST. Partial mapping of mGFP-immunoreactive CeA→NST efferent fibres showed their transition from stria terminalis and ventral amygdalofugal tributaries into the medial forebrain bundle, moving caudally to eventually flow through the brainstem reticular formation and supply the ipsilateral NST, with especially prominent innervation at rostral and medial levels. Immunoreactive fibres deviating from this route were sparse where present. Similar distributions of labelling in rats receiving the novel AAV1/2-hSyn-DIO-(hCAR)$_{off}$-(*Gt*ACR2$^{Kv2.1}$)$_{on}$-W3SL to CeA provide evidence for Cre-dependent production of *Gt*ACR2$^{Kv2.1}$ from this vector *in vivo*. However, as observed in transduced respiratory column neurons (Chapter 3), fusion with the Kv2.1 trafficking motif failed to prevent axonal expression of *Gt*ACR2 in CeA→NST neurons.

Though transduction of CeA→NST neurons was much more robust following CAV2 vector delivery to rostral, as opposed to caudal, NST, it is unclear the extent to which this reflects the topography of CeA terminals in the NST. While the CAR receptor that mediates CAV2 vector internalisation is endogenously expressed by many neurons in presynaptic boutons, it is also present in the axon and soma (Zussy et al. 2016), suggesting endocytosis can occur away from presynaptic sites – a point highlighted by CAV2 vector transduction of neurons at the site of injection.

However, the efficiency of CAV2 entry from sites other than the presynaptic membrane has not been established (Del Rio et al. 2019). Data presented here may therefore reflect more efficient CAV2 vector uptake from CeA efferents terminating primarily in the rostral NST, with sparse collaterals targeting more caudal regions. Alternatively, it could be that the dense plexus of CeA fibres in rostral NST simply provided a greater surface area over which entry could occur, even if many of these projections actually terminate in less densely innervated NST regions caudally. Although retrograde labelling of CeA→NST neurons with True Blue is also strongest following rostral rather than caudal NST injection (van der Kooy et al. 1984), this tracer is known to be

taken up by fibres of passage (Sawchenko et al. 1981), presenting a similar obstacle to the accurate mapping of terminal fields.

The use of Syp-Ruby expression to clarify the distribution of synapses formed by CeA→NST neurons in the present study also proved problematic, as this marker was readily visualised in fibres of passage traversing the stria terminalis fibre tract. Although Syp-mRuby has been referred to as a putative presynaptic marker in the literature (Lerner et al. 2015), the extent to which this assumption has been verified is unclear. While synaptophysin does concentrate in presynaptic terminals, it is first synthesised and processed in the soma and undergoes vesicular axonal transport to reach this location (Tixier-Vidal et al. 1988; Okada et al. 1995). Such trafficking appeared to be reflected by observations made in the present study, indicating that Syp-mRuby may be suitable as an axonal marker, but should not be used in isolation to identify presynaptic sites. Alternative approaches, such as the use of trans-synaptic fluorescent markers (Kim et al. 2012), high resolution imaging with dual pre- and post-synaptic labelling, and/or electrophysiological approaches, will therefore be required to accurately map the distribution of synaptic contacts formed by CeA→NST neurons in future studies.

If the observed distribution of NST innervation were to correlate with an abundance of synaptic contacts, this would suggest a primary connection of CeA efferents with NST gustatory and gastrointestinal circuitry. Cranial nerves conveying gustatory information densely innervate the rostral and medial NST (May et al. 2006), where neuronal activity, reflected by immunolabelling for the immediate early gene c-Fos, is significantly increased following oral exposure to a variety of tastants (Harrer et al. 1996; DiNardo et al. 1997; Yamamoto et al. 2000; Emond et al. 2001; Chan et al. 2004). Direct intragastric infusion or gavage (Yamamoto et al. 2000; Emond et al. 2001; Schwarz et al. 2010) and gastric distension (Vrang et al. 2003; Bonnet et al. 2013) also increase c-Fos labelling in the medial NST, but with a somewhat more caudal distribution. However, mice lacking P2X genes necessary for taste sensation are reported to retain a preference for monosodium glutamate (MSG) flavoured water, at least in part through activity in the rostral NST (Stratford et al. 2011), indicating this region is activated by both oral and post-ingestive cues.

In contrast, respiratory (Bonham et al. 1990; Dobbins et al. 1994) and cardiovascular (Ciriello 1983; Chan et al. 2000) circuitry lies in more caudal, lateral, and commissural NST regions, as does afferent innervation from related carotid body chemoreceptor afferents (Finley et al.

1992). Although caudolateral NST regions showed relatively light labelling with CeA fibres following CAV2 vector delivery to rostral NST, these efferents may still have a direct or indirect influence on cardiovascular and pulmonary function. Indeed, despite the predominance of CeA innervation to gustatory- and gastrointestinal-related NST regions, studies manipulating the amygdala have to date largely focused on cardiovascular function. While data produced from these experiments are complicated by factors including the use of anaesthesia and limited target specificity (Faiers et al. 1975; Iwata et al. 1987), they do suggest a role for CeA in modulating cardiovascular activity, including baroreflex function (Yamanaka et al. 2018) (discussed further below). Importantly, the distribution of CeA efferents within NST following CAV2 vector delivery to rostral coordinates is consistent with that resulting from anterograde tracing studies (van der Kooy et al. 1984; Danielsen et al. 1989). This indicates that the concentration of transduced CeA fibres in rostromedial NST regions observed here reflects the biological nature of this pathway, rather than simply being an artefact of the injection coordinates used.

It will also be of interest in future studies to comprehensively map the anatomical distribution of CeA→NST efferent fibres and determine the full extent of any collateral projections. Anterograde tracing studies (Krettek et al. 1978; van der Kooy et al. 1984; Rosen et al. 1991; Zahm et al. 1999) have shown that CeA efferents proceeding caudally from the medial forebrain bundle innervate and pass the substantia nigra laterally, before tracing a dorsomedial path around the superior cerebellar peduncle into the mesopontine tegmentum, from which numerous branching collaterals enter the PAG. Those fibres continuing through the pontine tegmental field densely innervate the PBN before turning ventrally and dividing to pass the trigeminal motor nucleus, as described here. The CeA also densely innervates the BNST rostrally (Dong et al. 2001), a structure with which it shares many characteristics, including descending projection targets and neurochemical phenotype, as part of the 'central extended amygdala' (Gray et al. 1987a; Becker et al. 2008). While the stria terminalis serves as the major source of CeA efferent input to BNST (Sun et al. 1991), single-axon reconstruction (Veinante et al. 2003) and antidromic spiking (Nagy et al. 2008) experiments provide evidence of direct brainstem innervation from CeA efferents passing through both this fibre tract and the shorter VAF pathway.

Given the paucity of evidence for significant innervation of collateral targets by CeA outputs (Thompson et al. 1989; Veinante et al. 2003; Viviani et al. 2011; Han et al. 2017), one would expect any revealed by further mapping of CeA→NST fibres to be sparse where present. Targets

of sparse collateral innervation indicated here include the thalamus, ventrolateral medulla, and spinal cord. Innervation of the thalamus and lateral habenula by CeA projections has been previously described by Rosen et al. (1991). Though delivery of chemical tracers to the cervical spinal cord has failed to produce retrograde staining in the rat CeA (Schwanzel-Fukuda et al. 1984; Nudo et al. 1988), small populations of CeA neurons have been labelled using this approach in macaque (Mizuno et al. 1985), cat (Sandrew et al. 1986), mouse (Liang et al. 2011), and a number of other mammalian species (Nudo et al. 1988). CeA efferents are also known to innervate RVLM (Cassell et al. 1989; Takayama et al. 1990; Bowman et al. 2013), and, consistent with data presented here, dual retrograde labelling has shown CeA neurons supplying RVLM and NST to be essentially separate populations (Thompson et al. 1989). Thus, mapping of transduced CeA→NST fibres here suggests a pattern of predominantly ipsilateral innervation to a principal projection target with very limited collateralisation, consistent with previous descriptions of CeA efferent populations.

Applying the molecular approach developed here in future experiments will make understanding the functional role of CeA→NST neurons, and that of any collateral branches formed, a much more tractable endeavour. Exchange of AAV-DJ-hSyn-FLEX-mGFP-2A-Syp-mRuby for vectors expressing alternative transgene cargoes, such as genetically encoded calcium indicators and chemo- or optogenetic receptors, would facilitate a range of targeted insights into the activity of CeA→NST circuitry and its physiological and behavioural significance. Though efforts have been made to elucidate how cardiovascular function is modulated by CeA activity, research to date has been hampered by a reliance on electrical or chemical stimulation – which provide limited specificity regarding the affected circuitry – as well as the use of anaesthesia. Issues raised by the presence of anaesthesia were addressed directly by Iwata et al. (1987), who showed that tachycardia and pressor responses elicited by electrical stimulation of CeA in conscious rats were inverted to bradycardia and depressor effects when these same rats were tested under anaesthesia.

Despite similarly limited target specificity, lesion studies have shed some light of the nature of CeA activity in modulating cardiovascular function under defensive or stressful conditions. Lesion to the CeA or lateral hypothalamus, through which CeA→NST fibres transit, selectively affects cardiovascular, but not behavioural, responses to aversive stimuli in rats (LeDoux et al. 1988; Roozendaal et al. 1990). Recent evidence from Waki and colleagues also suggests a role for the CeA in baroreflex resetting under specific emotional and behavioural states, including

physical exercise (Yamanaka et al. 2018; Kim et al. 2020). However, the potential for the CeA to modulate ingestive behaviour and gastrointestinal function has received much less attention, particularly considering its dense innervation of the rostromedial NST and other relevant CAN regions (Krettek et al. 1978; Veening et al. 1984). Cell-type specific transduction and manipulation of CeA→NST activity, for example using AAV1/2-hSyn-DIO-$(hCAR)_{off}$-$(GtACR2^{Kv2.1})_{on}$-W3SL as described here, offers a flexible approach for clarifying and building on previous studies through the targeted functional dissection of this circuitry in conscious, behaving animals.

Localised expression of *Gt*$ACR2^{Kv2.1}$ observed here in CeM ipsilateral to CAV2-Cre NST injection sites provides strong evidence for the successful validation of Cre-dependent expression from AAV1/2-hSyn-DIO-$(hCAR)_{off}$-$(GtACR2^{Kv2.1})_{on}$-W3SL *in vivo*. While sparse labelling of neurons was also present in the contralateral CeM, this is consistent with the small proportion of CeA efferents known to innervate contralateral targets, including NST (Danielsen et al. 1989; Rosen et al. 1991; Sun et al. 1991), as well as the distribution of neurons transduced by AAV-DJ-hSyn-FLEX-mGFP-2A-Syp-mRuby under analogous conditions here. Nonetheless, it would be ideal to confirm a complete absence of expression from AAV1/2-hSyn-DIO-$(hCAR)_{off}$-$(GtACR2^{Kv2.1})_{on}$-W3SL in animals lacking any Cre-recombinase production with future studies, given the off-target 'leaky' expression that can occur from recombinase-dependent AAV vectors (Fischer et al. 2019). The characterisation of hCAR expression from AAV1/2-hSyn-DIO-$(hCAR)_{off}$-$(GtACR2^{Kv2.1})_{on}$-W3SL, which is reported to facilitate 'tropism-free' neuronal transduction by CAV2 vectors (Li et al. 2018), will also be of interest for utilising this vector to target other neuronal populations. Given their robust transduction in the absence of exogenous CAR expression, as demonstrated here in rats that received AAV-DJ-hSyn-FLEX-mGFP-2A-Syp-mRuby, it appears CeA→NST neurons naturally express sufficient levels of CAR for efficient CAV2 vector uptake and transport.

Consistent with observations made in Chapter 3 using transfected rodent hippocampal neurons *in vitro* and transduced respiratory column neurons *in vivo*, fusion of *Gt*ACR2 with the Kv2.1 motif again failed to provide somatic localisation here. Analogous fusion constructs between *Gt*ACR2 and the Kv2.1 trafficking motif, developed independently by Mahn et al. (2018) and (Messier et al. 2018), are reported to significantly reduce, but not completely prevent, axonal expression of this opsin, with an associated decrease in *Gt*ACR2-mediated membrane depolarisation and neurotransmitter release. Although this precedent suggests similarly

reduced axonal expression of *Gt*ACR2$^{Kv2.1}$ should be expected here, additional immunohistochemical and electrophysiological studies are required to demonstrate this. However, to the extent that this remains an issue, the likelihood of illuminating and depolarising *Gt*ACR2$^{Kv2.1}$-transduced axons is particularly low in the context of somatic CeA→NST photoinhibition, given the distant terminations and limited collateralisation of these neurons. Stronger photocurrents and enhanced neuronal expression of *Gt*ACR2 following fusion with the Kv2.1 motif were also described by Mahn et al. (2018) and Messier et al. (2018), with the latter observation also apparent in respiratory column neurons expressing *Gt*ACR2$^{Kv2.1}$ (Chapter 3). As such, while potential effects of axonal depolarisation will remain an important consideration, experiments described here and in Chapter 3 illustrate the value of Cre-dependent *Gt*ACR2$^{Kv2.1}$ expression as an effective method of cell-type specific optogenetic inhibition.

In conclusion, data presented in this chapter demonstrate an efficient approach for cell-type specific viral vector transduction of rat CeA→NST neurons, while also validating Cre-recombinase dependent *Gt*ACR2$^{Kv2.1}$ expression from a novel AAV vector. Though *Gt*ACR2$^{Kv2.1}$ expression is not exclusively somatic, data presented in the previous chapter and published literature support the efficacy of this construct as a potent mediator of neuronal photoinhibition. As such, the conditional expression of *Gt*ACR2$^{Kv2.1}$ described here provides a versatile approach for selective inhibition of neuronal populations of interest *in vivo*. Expression of *Gt*ACR2$^{Kv2.1}$ and other transgenic actuators in CeA→NST circuitry, using the methods developed here, offers a powerful approach to understanding how physiological process are influenced by emotional and cognitive status to facilitate goal-directed behaviour, how dysregulation of this pathway may underlie related disease states, and the potential utility of this system as a therapeutic target.

Chapter 5

General discussion

5.1 Introduction

Since their inception during the late twentieth-century, transgenic technologies have provided unprecedented insight into nervous system structure and function. The circuits and fine processes formed by neurons can now be mapped *in vivo* through expression of fluorescent proteins (Livet et al. 2007), obviating a reliance on chromogenic substrates, chemical tracers, and tissue fixation to visualise this architecture. Integrating fluorescent proteins with fusion partners that undergo conformational changes also allows the activity of neural networks to be optically monitored (Wang et al. 2019b), complementing and expanding on electrode-based recording techniques. The gross manipulation of brain activity with electrodes has been largely supplanted by optogenetics, which provides temporally precise stimulation or inhibition of specific neural populations expressing microbial opsins (Kim et al. 2017). Pharmacological approaches to understanding brain function have also been refined through the selective expression of chemogenetic receptor systems in circuitry of interest (Atasoy et al. 2018). These transgenic markers, sensors, and actuators are at the forefront of modern neuroscience, and continue to provide innovative approaches in this field of research.

Beyond the intrinsic utility of these tools, their genetically encodable nature provides the additional capacity for targeted cellular and subcellular expression. As a result, multiple levels of control can be implemented over where and when a transgene is expressed. The selective introduction of transgenes into a neuronal population of interest can be mediated by viral vectors based on their method of delivery, mechanism of uptake, and transport between neurons (Saleeba et al. 2019). Transgene expression within the neuron can in turn be controlled through association with non-coding DNA elements, including gene-specific promoter sequences and recognition sites for microbial recombinases (Luo et al. 2020; Nectow et al. 2020). Once a transgene is expressed in the target population, further control over its subcellular localisation can be achieved through fusion with trafficking motifs derived from endogenous proteins (Rost et al. 2017).

Given the scientific and therapeutic value of understanding neural contributions to behaviour and physiology at the level of defined cell-types and circuits, the development of novel molecular tools for targeted transgene expression has become a major focus of contemporary neuroscience research. Several such tools are described in this thesis, spanning both cellular and subcellular levels of resolution. The following discussion provides a review of the tools

developed, including considerations and caveats concerning their use, in addition to their potential future applications alongside emerging targeted and non-invasive transgenic technologies.

5.2 Research outcomes

Experiments described in the preceding Chapters highlight several novel approaches for targeted transgene expression in neural structures of interest. These include a promoter sequence capable of driving transgene expression selectively in relaxin-3 neurons of the *nucleus incertus* (NI; Chapter 2), and a viral vector- and recombinase-based strategy for transduction of central amygdala (CeA) neurons projecting to the nucleus of the solitary tract (NST; Chapter 4). While further validation is required, functional data presented in Chapter 3 indicate that differential subcellular trafficking of the inhibitory *Gt*ACR2 opsin fusion constructs I developed was also achieved. Examples of poorly targeted expression, such as the non-specific tropomyosin receptor kinase A (TrkA) promoter activity shown in Chapter 2, and the heterogeneity of respiratory column and neighbouring neurons transduced in Chapter 3, were also observed. The applications and lessons offered by these outcomes are explored below.

5.2.1 Novel strategies for cell-type specific transgene expression

As outlined previously, there are many levels at which transgene expression can be targeted in the nervous system, including to defined neural populations of interest. One characteristic commonly used to delineate populations, and that is especially relevant in the context of pharmaceutical development, is the expression of specific gene products. This level of expression was the focus of Chapter 2, which detailed the development of a promoter-based approach for adeno-associated viral (AAV) vector-mediated transgene expression in a key subpopulation of NI neurons, characterised by their expression of the neuropeptide, relaxin-3. In attempting to selectively transduce relaxin-3 NI neurons, promoter elements from the rat genome that are endogenously associated with the expression of either relaxin-3, or the co-expressed TrkA receptor, were tested. Cell-type specific transduction was assessed by developing recombinant AAV vectors, expressing mCherry under either the relaxin-3 or TrkA promoter, which were delivered to the rat NI by stereotaxic injection. Despite evidence of cell-type specific TrkA promoter activity in other systems (Chang et al. 1998; Sacristan et al. 1999; Ma et al. 2000), this promoter proved ineffective for targeted expression in transduced TrkA-

/relaxin-3-expressing rat NI neurons, highlighting both the complexity of gene regulation under differing conditions and the importance of validating promoter activity in novel experimental contexts. However, targeted expression was achieved using a 1,736 base pair (bp) relaxin-3 promoter sequence to drive transgene expression.

Several routes towards an improved understanding of the relaxin-3 arousal system and its therapeutic potential are possible using this cell-type specific promoter in future studies. The development of further viral vectors, and particularly AAV vectors, expressing transgenic markers, sensors, or actuators directly from the relaxin-3 promoter should provide highly targeted expression. However, this approach is limited by the need to produce individual vectors for each transgene one wishes to express. Given the diverse catalogue of recombinase-dependent transgenic constructs and animals currently available, an alternative strategy is to develop vectors expressing Cre or other recombinases under the relaxin-3 promoter. Although much more flexible, this method also introduces potential sources of off-target expression, including 'leaky' expression from recombinase-dependent constructs (Fischer et al. 2019). Any weak non-specific activity from the relaxin-3 promoter would also likely be amplified with this approach, due to the use of constitutively active promoters in the corresponding recombinase-dependent constructs, which can theoretically be activated by a single recombinase molecule (see e.g. Kakava-Georgiadou et al. (2019)). The production of future constructs would benefit from the identification of specific elements within the 1,736 bp relaxin-3 promoter that are responsible for its cell-type specific activity, as this could facilitate the development of condensed and hybridised derivative promoters that provide strong, targeted expression while occupying minimal space within a limited viral vector packaging capacity. This is especially relevant to the development of new AAV vectors, where total packaging capacity is restricted to around 4,700 bp (Wu et al. 2010). Validation of the relaxin-3 promoter in populations outside the NI, and in species other than rat, will also be of interest moving forward. It is important to note that, subsequent to the publication of data in Chapter 2, a transgenic line of mice expressing a Cre-GFP fusion construct from the relaxin-3 locus has been described (Nasirova et al. 2020). This study both complements the viral vector-based technique developed here in rats and provides a template from which CRISPR-mediated germline editing could be applied to target relaxin-3 circuitry in other species.

A further approach to cell-type specific transgene expression was illustrated in Chapter 4, where CeA neurons were selectively transduced based on their axonal projection to an efferent target,

rather than a particular genetic marker. This choice reflects a biological, and not simply methodological, distinction; while ascending relaxin-3 fibres serve a coherent 'arousal' function via multiple targets (Smith et al. 2014b), the role of CeA subpopulations, for example in mediating autonomic as opposed to behavioural responses to emotive stimuli, are much more readily defined by projection target than neurochemical phenotype (LeDoux et al. 1988; Viviani et al. 2011). In order to achieve selective transgene expression in CeA→NST neurons, CeA neurons were locally transduced with AAV vectors containing transgene cargos whose expression was dependent on Cre-mediated recombination. Activation of transgene expression in CeA→NST neurons was then facilitated by uptake and retrograde transport of Cre-expressing canine adenovirus 2 (CAV2) vectors from injection sites in the rostral NST, resulting in cell-type specific transduction. With the use of recombinase-mediated expression in this strategy, it is again essential to control for leaky expression from such vectors. Another caveat to this approach is that the neural populations transduced may be biased by viral vector tropism, depending on the whether or not the cell-surface molecules required for vector uptake are endogenously expressed (Sun et al. 2019). Where biased transduction does occur, heterologous expression of receptors involved in vector uptake can be used to alter tropism in the target population, as demonstrated by Li et al. (2018) using heterologous coxsackievirus and adenovirus receptor (CAR) expression for enhanced CAV2 transduction. While robust transduction of CeA→NST neurons was observed here both with and without heterologous CAR expression, suggesting minimal bias introduced by AAV or CAV2 tropism, this is an important consideration for future studies where alternative vector combinations may be employed.

As highlighted in Chapter 3, more precise methods for targeted transgene expression are required in future studies of the preBötzinger complex (preBötC) and surrounding autonomic nuclei. Either of the general strategies outlined above may offer a solution. Indeed, our laboratory is currently investigating the possibility of targeting preBötC neurons through retrograde recombinase delivery from specific efferent targets, as per the approach used to selectively transduce CeA→NST neurons. Although genetic markers capable of distinguishing preBötC neurons from neighbouring populations are currently lacking (Del Negro et al. 2018), these may be identifiable using methods such as single-cell transcriptome sequencing in functionally demarcated populations. Genetic markers discovered in this process could serve as candidates either for the development of cell-type specific promoters and transgenic animal lines or vector tropism-based strategies, though the latter approach applies to a much smaller pool of genes. Should these techniques, utilising perhaps one or two characteristics of a target

population, prove insufficient for cell-type specific expression, the required selectivity may be achieved using an emerging platform for 'intersectional' targeting. Intersectional strategies, which promise ever more precise transgene delivery based on multiple characteristics of the target population, are discussed in Section 5.3 below.

5.2.2 Subcellular localisation of *Gt*ACR2 fusion constructs

While the strategies detailed above centre on targeting transgene expression to cell-types of interest, another major focus of this project has been the directed subcellular localisation of expressed transgenes, and particularly that of the chloride-conducting opsin, *Gt*ACR2. Experiments described in Chapters 3 and 4 sought to selectively express *Gt*ACR2 in the somatic or axonal membrane, through fusion with trafficking motifs derived from the voltage-gated potassium channel, Kv2.1, or neurexin 1α (Nrxn1α), respectively, to create *Gt*ACR2$^{Kv2.1}$ and *Gt*ACR2^{nrxn}. These aims served to both mitigate conflicting effects of *Gt*ACR2-mediated hyperpolarisation and depolarisation of somatodendritic and axonal membranes, respectively, which arise from varying intracellular chloride concentrations between these compartments (Mahn et al. 2016; Malyshev et al. 2017), and to provide tools for the functional dissection of closely interconnected neural circuitry. Fusion of *Gt*ACR2 with the Kv2.1 trafficking motif appeared to provide enhanced neuronal *Gt*ACR2 expression compared to the original *Gt*ACR2-EYFP, although selective somatic localisation was not observed, with axonal *Gt*ACR2$^{Kv2.1}$ expression present in cultured mouse hippocampal neurons *in vitro* (Chapter 3), and rat respiratory column and CeA→NST neurons *in vivo* (Chapters 3 and 4, respectively). However, altered trafficking was suggested by physiological responses to photoinhibition of transduced respiratory column neurons in anesthetised rats, where *Gt*ACR2$^{Kv2.1}$ expression was associated with similar apnoea but significantly reduced cardiovascular effects, relative to those in rats expressing *Gt*ACR2-EYFP. This may reflect a preferential somatic trafficking of *Gt*ACR2$^{Kv2.1}$, rather than exclusive compartmental localisation, sufficient to alter the physiological response to photoinhibition. Technical difficulties prevented the direct detection of *Gt*ACR2^{nrxn}, which was designed for targeted axonal expression. Further work is required to overcome this. However, when expressed in respiratory column neurons in anesthetised rats, *Gt*ACR2^{nrxn} was associated with a small but specific effect on cardiac function, in direct contrast to the primarily respiratory effects of *Gt*ACR2$^{Kv2.1}$. As such, this selective and complimentary dissociation of the physiological responses to *Gt*ACR2-EYFP photoinhibition supports the differential subcellular trafficking of *Gt*ACR2$^{Kv2.1}$ and *Gt*ACR2^{nrxn} *in vivo*.

Building from these data, the subcellular expression of *Gt*ACR2$^{Kv2.1}$ may be further elucidated in future studies, with two publications characterising independently developed fusion constructs between *Gt*ACR2 and the Kv2.1 trafficking motif having already emerged (Mahn et al. 2018; Messier et al. 2018). Although axonal expression was not eliminated in either study, fusion of *Gt*ACR2 with the Kv2.1 trafficking motif was associated with enhanced somatic photocurrents and a reduction in optically induced neurotransmitter release from mouse cortical neurons expressing these constructs, when compared to *Gt*ACR2 constructs with a fluorescent tag alone (Mahn et al. 2018; Messier et al. 2018). These results indicate an 'enrichment' of *Gt*ACR2 expression in the somatic membrane that is mediated by fusion with the Kv2.1 trafficking motif, providing stronger photoinhibition with minimal axonal depolarisation. As the design of *Gt*ACR2$^{Kv2.1}$ does not differ substantially from the constructs described by Mahn et al. (2018) and Messier et al. (2018), a similar somatic enrichment of expression would be expected here, and is consistent with the physiological responses to photoinhibition reported in Chapter 3. Future use of *Gt*ACR2$^{Kv2.1}$ and analogous constructs should be carefully designed to account for factors that may affect residual axonal expression and its implications, including transduction titres, promoters, and other parameters determining expression levels, as well as the light source and intensity used, which may be optimised for somatic photoinhibition.

Further characterisation of *Gt*ACR2^{nrxn} will also be essential moving forward. While data presented in Chapter 3 support the selective axonal expression of this construct, additional evidence is required to prove this is the case. If *Gt*ACR2^{nrxn} is trafficked in a similar fashion to Nrxn1α, it would be present in vesicles throughout the intracellular environment, which then selectively fuse with the axonal membrane (Neupert et al. 2015), making *in vivo* axonal localisation difficult to determine histologically. The addition of an extracellular N-terminal tag to *Gt*ACR2^{nrxn} offers the most feasible approach to determine cell-surface expression using immunocytochemistry in non-permeabilised, cultured neurons, as described by Stachniak et al. (2014) for hM4D^{nrxn}. The reduced complexity of neurons in a cultured monolayer would also facilitate selective illumination of the soma, dendrites, or axon, which, accompanied by patch-clamp electrophysiology, could provide insights as to the cell-surface expression of *Gt*ACR2^{nrxn} and consequences of its activation. A similar approach may be possible in acute slices or *in vivo*, using a combination of sparse viral vector transduction and holographic or two-photon illumination of subcellular components (Packer et al. 2013; Emiliani et al. 2015). Data from such

studies will be both valuable and necessary in establishing *Gt*ACR2^{nrxn} as a reliable tool for selective optogenetic manipulation of membrane potential in the axon.

Several alternative strategies for subcellular optogenetic manipulation may further refine or improve on results obtained using *Gt*ACR2$^{Kv2.1}$ or *Gt*ACR2^{nrxn}. Fusion of *Gt*ACR2 with alternative trafficking motifs, for example that derived from the kainate receptor subunit 2 (KA2) N-terminus and used by Shemesh et al. (2017) for somatic opsin expression, could be explored as a means of improving localisation. A more detailed understanding of the mechanisms driving compartment-specific expression, and the extent to which they are captured by isolated protein trafficking motifs, may also be necessary in this regard. For example, compartment-specific transcriptomes have been identified within neurons, the development of which appears ultimately to depend on trafficking mechanisms mediated by RNA-binding protein interactions with elements encoded in mRNA transcripts (Buxbaum et al. 2015; Turner-Bridger et al. 2020). As such, engineering transgenes at the level of the mRNA transcript, rather than, or in addition to, expressed protein, could facilitate or enhance localised somatic, axonal, or dendritic expression. An example of this is provided by Hayashi-Takagi et al. (2015), who used a combination of protein fusion and mRNA trafficking to target heterologous GTPase expression to dendritic spines. The presence of transcripts for endogenous ion-conducting receptors and channels at pre- and post-synaptic sites (Hafner et al. 2019; Pushpalatha et al. 2019; Engel et al. 2020) indicates this strategy would be compatible with localised opsin expression in the neuronal membrane. Any remaining paradoxical effects of *Gt*ACR2 activation caused by varying chloride environments may also be alleviated in future studies through the use of other actuators, including potassium-conducting channels. Given that efficient potassium-mediated photoinhibition of AAV vector-transduced mammalian neurons has been recently demonstrated (Alberio et al. 2018; Sierra et al. 2018), such constructs provide an alternative platform from which subcellular optogenetic inhibition may be achieved.

5.3 Intersectional targeting strategies

An exciting area of development in this field, and one that will impact future applications of both the cell-type specific expression strategies and subcellular optogenetic tools described here, is that of intersectional targeting. Instead of focusing on one or two features of a neural population, such as the expression of a gene of interest or connection with a particular projection target – as shown here with relaxin-3 and CeA→NST neurons, respectively –

intersectional strategies target multiple features for transgene expression in ever more precisely defined populations. Intersectional strategies can describe any combination of targeting mechanisms that allow selective access to a population of interest, including the use of viral vector tropism, injection site, and trafficking, as well as promoters and recombinases, to define the expression target. Negative selection markers can also be incorporated to this process, such as the use of small non-coding RNAs to silence off-target transgene expression (Xie et al. 2011). Alongside these approaches, dedicated systems of multiplexed 'genetic switches', as detailed below, have been developed for streamlined intersectional targeting. The different combinations of features targeted by intersectional strategies, and particularly systems involving genetic switches, can be conceptualised in terms of Boolean logic, where transgene expression is determined by 'AND', 'OR', and 'NOT' operations (Figure 5.1A-C).

Strategies that have emerged to date for intersectional targeting via genetic switches involve either recombinase- or CRISPR-mediated DNA editing. Early iterations of recombinase-based genetic switches used two STOP cassettes to prevent translation, each flanked by recognition sites for independent recombinases (e.g. Cre and Flp) (Figure 5.1D). In the presence of each recombinase, the corresponding STOP cassette is excised, with the removal of both cassettes necessary for transgene expression (Dymecki et al. 2010). By crossing lines of transgenic mice engineered for promoter derived, cell-type specific recombinase expression, Madisen et al. (2015) used this STOP cassette approach to selectively label parvalbumin-expressing GABAergic neurons. A further example is provided by Yetman et al. (2019), who targeted genetically defined interneuron subtypes by employing viral vector-mediated Flp delivery in Cre-expressing mouse driver lines. Instead of STOP cassette excision, the 'intronic recombinase sites enabling combinatorial targeting' (INTRSECT) strategy allows transgene reading frames, created through the insertion of artificial introns containing recombinase recognition sites, to be flipped between sense- and antisense-orientations (Figure 5.1E,F) (Fenno et al. 2014; 2020). Transgene expression can currently be determined by up to three cellular features using INTRSECT, with this approach primarily limited by the availability of recombinases with non-overlapping activity at established recognition sites. An alternative, recombinase-free strategy is described by Garcia-Marques et al. (2019), involving the suppression of functional transgene expression using sequences that are selectively removed with CRISPR/Cas9-based editing. In this fashion, various elements of a transgenic construct can be interrupted by a theoretically 'unlimited' number of sites (Figure 5.1G,H), each being targeted for removal through the expression of a unique guide RNA.

With ever more data shedding light on the genetic and structural nature of neural circuits, a process being accelerated by connectome and single-cell transcriptome sequencing studies, intersectional targeting of transgene expression is becoming increasingly relevant. However, several important caveats need to be considered when using these approaches. First among these, it must be emphasised that the specificity of transgene expression should always be thoroughly validated. Although the use of multiple checkpoints suggests intersectional approaches would provide increased specificity with each additional layer of regulation, some degree of off-target expression may persist. This is particularly the case where promoters, which rarely achieve complete specificity, are used to drive expression. Total coverage of the target population is also unlikely with any given targeting mechanism, an issue which may be compounded by intersectional strategies and lead to increasingly reduced transduction efficiencies. The potential for cellular aberrations and toxicity caused by expression of multiple transgenes should also be carefully monitored, particularly in the context of recombinase overexpression (Gangoda et al. 2012; Janbandhu et al. 2014) and off-target Cas9 activity (Zhang et al. 2015b; Han et al. 2020). Given the use of appropriate experimental controls to account for these factors, intersectional strategies offer a powerful approach for the delivery of highly targeted, cell-type specific transgene expression that is likely to gain widespread adoption moving forward.

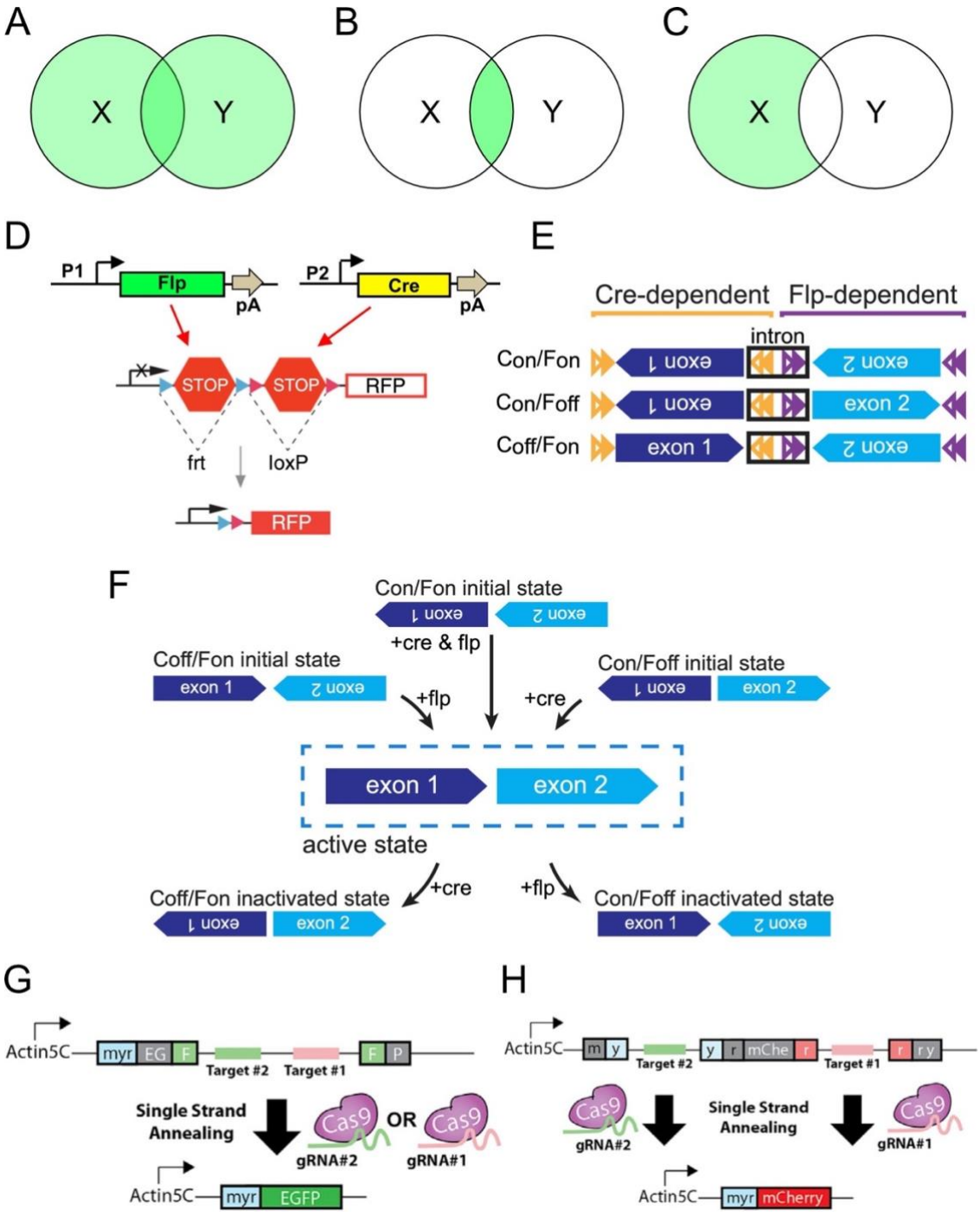

Figure 5.1. *Refer to next page for figure legend.*

Figure 5.1. *Intersectional approaches for cell-type specific transgene expression*. Cell populations targeted by intersectional techniques can be defined in several ways using Boolean operations. For example, cells may be targeted according to the presence of either feature X OR feature Y **(A)**, the presence of both feature X AND feature Y **(B)**, or the presence of feature X but NOT feature Y **(C)**. The number of features and type of operations applicable to their targeting will depend on the circuitry of interest and intersectional approach used for selective transgene expression. Intersectional targeting can be facilitated through the use of recombinase- or CRISPR-mediated 'genetic switches.' An early approach to recombinase-based intersectional targeting is shown in **(D)** (adapted from Madisen et al. (2015) and Yetman et al. (2019)). In this example, expression of a red fluorescent protein (RFP) transgene is suppressed by two upstream STOP codons, one flanked by *frt* sites and the other by *LoxP* sites. RFP expression occurs only after each STOP codon is selectively excised by the corresponding Flp or Cre recombinase, whose expression in turn can be controlled by factors such as promoter (P1/P2) activity and viral vector transduction. The more recently developed 'intronic recombinase sites enabling combinatorial targeting' (INTRSECT) strategy offers an alternative approach, whereby artificially constructed transgene reading frames are flipped in or out of sense-orientation using inserted introns containing recombinase recognition sites (such as *lox* (yellow arrows) or *frt* (purple arrows) variants). Three example configurations are illustrated in **(E)** and **(F)** (adapted from Fenno et al. (2020)), showing how transgene configuration can be moved to an active state in the presence of Cre AND Flp (C_{on}/F_{on}), Cre but NOT Flp (C_{on}/F_{off}), and Flp but NOT Cre (C_{off}/F_{on}). In addition to introducing NOT operations, multiple introns and additional recombinases can be employed to make INTRSECT a versatile, multiplexed platform for intersectional targeting. Selective guide RNA (gRNA) rather than recombinase expression can be used to manipulate multiplexed genetic switches, created through the disruption of various elements within a transgenic construct by corresponding gRNA recognition sites or 'targets', using CRISPR-based editing. Two example configurations are shown in **(G)** and **(H)** (adapted from Garcia-Marques et al. (2019)), where CRISPR/Cas9-mediated transgene reconstitution is directed by independently expressed gRNAs. A virtually unlimited number of sites can be introduced in this way for conditional transgene expression, depending on the desired features designated for intersectional targeting.

5.4 Emerging technologies for non-invasive neuronal manipulation

A notable limitation of most established techniques for manipulating and imaging neural activity is their reliance on invasive procedures. In the context of transgenic approaches, this includes aspects of both transgene delivery, for example the stereotaxic injection of viral vectors, and methods for accessing genetically modified circuitry, such as the implantation of cannulae or optical fibres. The tissue damage, infection risk, and other complications arising from surgical procedures or the use of long-term implants restricts the applications of transgenic technologies in research and presents an obstacle to their translational potential. Local vector injection or stimulus delivery also limits the area over which transgenic interventions can be applied, an issue of particular importance in larger species, including humans. Given that transgenic tools for imaging neural activity are based on changes in fluorescence, typically at wavelengths easily scattered and absorbed by biological tissues over relatively short distances, the development of real-time, non-invasive imaging techniques at the circuit level are not feasible in the near future. However, spatially and temporally precise, non-invasive genetic modification and manipulation of neural activity is a realistic short-term prospect, with several distinct approaches explored in recent studies.

Non-invasive transgene expression has been available for many years in the form of germline transgenic animals. An alternative route currently gaining interest is the systemic delivery of viral vectors by intravenous (i.v.) administration. Given their safety record (Hudry et al. 2019), as well as the ability of some serotypes, including AAV9 (Foust et al. 2009) and AAVHSC variants (Ellsworth et al. 2019), to cross the blood-brain barrier, studies exploring this approach largely focus on AAV vectors. The relatively low transduction efficiency (around 10 % of neurons or less in most brain regions) following i.v. injection of these naturally evolved serotypes has spurred the development of enhanced AAV capsids, using methods including *in silico* design (Hudry et al. 2018), protein engineering (Choudhury et al. 2016), and *post hoc* tissue screening of mutant AAV libraries (Deverman et al. 2016). Of these approaches, the latter, termed CREATE (Cre recombination–based AAV targeted evolution) by its authors, has yielded the most robust results, with transduction efficiencies of up to 90 % demonstrated by the resultant ‘AAV-PHP’ vectors (Chan et al. 2017; Kumar et al. 2020). However, transduction efficiencies between brain regions vary substantially for all peripherally available AAV serotypes identified to date. This variation in tropism may prove valuable in combination with the intersectional targeting mechanisms discussed in Section 5.3, which will be essential both for transgene expression in

the intended circuitry and repression in peripheral organs such as the liver, where varying levels of transduction are also seen (Challis et al. 2019). In addition to bearing similar or lower associated costs, systemically delivered AAV vectors also have the potential for direct clinical applications, making them an increasingly popular alternative to transgenic animal lines (Bedbrook et al. 2018; Li et al. 2020).

Several modalities for non-invasive manipulation of genetically modified neurons have also emerged from recent studies, with the most common approach to date being the use of magnetic fields to active so-called magneto- or thermogenetic actuators. The genetically encoded actuators associated with this method are typically derived from heat-sensitive transient receptor potential (TRP) cation channels of the vanilloid subfamily (TRPV channels), with a magnetic interface provided either through fusion with ferritin (Stanley et al. 2016; Wheeler et al. 2016) or proximity to magnetic nanoparticles (Chen et al. 2015; Munshi et al. 2017) (Figure 5.2A,B) – although the plausibility and efficacy of the former has been a subject of controversy in the literature (Meister 2016; Barbic 2019; Wheeler et al. 2020). Upon exposure to an alternating magnetic field, hysteretic ferritin or nanoparticle heating is used to activate the heterologously expressed TRPV construct, leading to cellular and behavioural responses within seconds (Chen et al. 2015; Stanley et al. 2016; Wheeler et al. 2016; Munshi et al. 2017). Magnetogenetic tools derived from mechanoreceptors (Figure 5.2C) have also been validated *in vitro*, though the strong magnetic field gradient required to activate them presents a challenge to their application *in vivo* (Gahl et al. 2018; Christiansen et al. 2019). Similarly, direct thermogenetic activation of a heterologously expressed snake TRP channel using infrared radiation has been shown by Ermakova et al. (2017) – however, the application of this approach in mammals will require channels with higher activation thresholds to avoid *in vivo* desensitisation.

Chemo- and optogenetic technologies have been adapted for non-invasive manipulation as well, in part through the use of focused ultrasound. Rao et al. (2019), for example, employed an alternating magnetic field to induce the release of clozapine-N-oxide (CNO) from heat-sensitive liposomes loaded with magnetic nanoparticles (Figure 5.2D), allowing non-invasive chemogenetic manipulation of neurons expressing designer receptors exclusively activated by designed drugs (DREADDs) with an approximately 20 s latency. Non-invasive chemogenetics has also been achieved using focused ultrasound for localised blood-brain barrier-opening, allowing more efficient entry of systemically delivered, DREADD-expressing AAV9 vectors, with which

brain circuitry can be transduced and subsequently manipulated by intraperitoneal CNO injection (Szablowski et al. 2018). The thermal or mechanical consequences of acoustic energy delivered by focused ultrasound may also prove valuable for non-invasively manipulating deep brain structures, either directly or via heterologous expression of 'sonogenetic' receptors (Rabut et al. 2020). Indeed, focused ultrasound has already been used to non-invasively stimulate channelrhodopsin-2 (ChR2) by targeting mechanoluminescent nanoparticles in the brain's vasculature (Wu et al. 2019) (Figure 5.2E). An alternative approach for nanoparticle-mediated optogenetics is demonstrated by Chen et al. (2018), who used up-conversion of near-infrared light to activate ChR2 in several brain regions (Figure 5.2F). Direct transcranial activation of the red-shifted 'ChRmine' opsin, expressed either by stereotaxic or i.v. AAV vector injection, has also been shown at depths of up to 7 mm in mice (Chen et al. 2020).

It is worth noting that many of the studies mentioned above used stereotaxic injection of viral vectors, nanoparticles, and/or liposomes prior to the application of non-invasive stimulation techniques. Further examples of entirely non-invasive neuronal manipulations should be enabled by the use of engineered viral vectors, as demonstrated by Chen et al. (2020) using an AAV-PHP serotype, and/or ultrasound-mediated blood-brain barrier-opening to allow access of systemically circulating particles, as used by Szablowski et al. (2018). The cell-type specific tropism and millimetric level of spatial resolution afforded by these approaches, respectively, provide additional layers at which circuitry can be targeted using intersectional strategies (Li et al. 2020; Meng et al. 2020). Important considerations for future studies will also include the extent of any unintended biological effects or damage induced by the techniques described, as well as the potential for immune responses to systemically delivered agents, which may be more likely, given the substantially greater volumes involved and exposure levels, relative to localised injections. However, these preliminary studies indicate a variety of non-invasive approaches will be available for neuronal manipulation in the near future, providing previously unimaginable experimental and therapeutic access to the nervous system.

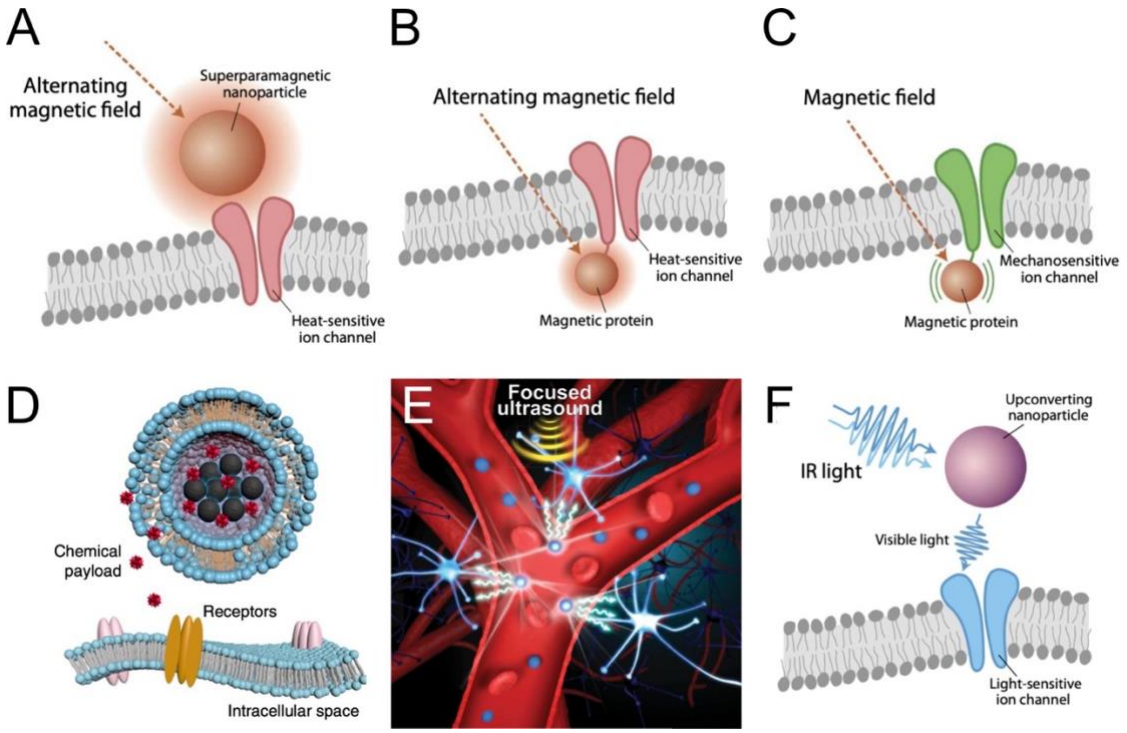

Figure 5.2. *Methods for non-invasive manipulation of neural activity*. A variety of strategies have been developed for non-invasive manipulation of neural activity using transgenic actuators. Heat-sensitive ion channels can be activated by hysteretic heating of nearby nanoparticles **(A)**, or fusion with magnetic proteins such as ferritin **(B)**, through exposure to an alternating magnetic field. Magnetic fields can also be used to activate mechanosensitive ion channels to which a magnetic protein is fused **(C)**. Indirect chemogenetic stimulation, through the release of chemical ligands from nanoparticle-impregnated, heat-sensitive liposomes, can also be achieved using alternating magnetic fields **(D)** (nanoparticles shown in black, ligand or 'chemical payload' shown in red). Opsin-expressing neurons have been non-invasively stimulated using focused ultrasound to generate light from circulating mechanoluminescent nanoparticles **(E)**, or nanoparticle-mediated up-conversion of transcranial infrared (IR) light to visible light **(F)**. **A-C, F** are adapted from Rivnay et al. (2017); **D** and **E** are adapted from Rao et al. (2019) and Wu et al. (2019), respectively.

5.5 Future directions and concluding remarks

Several novel tools and strategies for targeted cellular and subcellular neuronal transgene expression are identified by experiments described in this thesis. Among the applications for these tools, the further mapping and functional dissection of relaxin-3 NI and CeA→NST circuitry using promoter- and recombinase-based strategies detailed in Chapters 2 and 4, respectively, is directly feasible through the constructs and approaches developed. Data presented in Chapter 3 also support the directed enrichment of somatic *Gt*ACR2$^{Kv2.1}$ and axonal *Gt*ACR2^{nrxn}, providing enhanced optogenetic tools for the efficient manipulation and investigation of these heterogeneous cellular structures and their role in circuitry contributing to physiology and behaviour. Additional studies applying and further validating these fusion constructs in other systems and species will be of great interest.

Paired with the diverse catalogue of transgenic markers, sensors, and actuators currently available, along with the development of new technologies for non-invasive neuronal manipulation, the cell-type specific targeting strategies outlined here offer powerful approaches to understand the composition and function of neural circuits. While targeting CeA→NST neurons through the approach described in Chapter 4 requires stereotaxic injections, due to the need for localised CAV2 vector delivery to select for NST-projecting efferents, its use to express transgenes enabling non-invasive manipulation of neural activity would facilitate temporally precise insights under naturalistic conditions and behaviours without any external equipment or tethers. This can also be achieved in the short-term using established chemogenetic approaches, though without the same temporal resolution. Existing techniques for optogenetic manipulation and optical monitoring of neural activity can also be immediately applied to investigate potential roles for CeA→NST neurons in modulating autonomic and behavioural responses to emotive stimuli, aided by the ongoing development of miniaturised, flexible, and implantable interfaces (Won et al. 2020). This is particularly true of the *Gt*ACR2 constructs developed in Chapters 3 and 4, with cell-type specific *Gt*ACR2$^{Kv2.1}$ expression already demonstrated here. These same methods apply to investigating the role of NI, and perhaps also global, relaxin-3 circuitry in modulating arousal and related functions, using the promoter-based strategy described in Chapter 2.

The tools and techniques developed here are also compatible with intersectional targeting strategies outlined in Section 5.3. In this way, further refinement of relaxin-3 NI circuitry

transduction, for example based on co-expression with other genes or projection targets of interest, would be possible using promoter driven recombinase, guide RNA, and/or marker, sensor, or actuator expression. Intersectional strategies may also prove necessary for targeted expression where the relaxin-3 promoter is used in conjunction with a systemically delivered viral vector. Although the high degree of specificity reported in Chapter 2 suggests cell-type specific promoter activity would be seen outside the NI as well, promoter specificity following AAV vector transduction has been reported to vary by as much as 60 % depending on the brain region assessed (Chan et al. 2017). If such regional variability were found with the relaxin-3 promoter, it may be possible to correct this using intersectional methods to suppress off-target expression. The CeA→NST targeting strategy developed in Chapter 4 is itself a basic form of viral vector- and recombinase-based intersectional targeting, which may be elaborated on using multiplexed INTRSECT- or CRISPR-based methods. Naturally, these and other intersectional techniques can also be used for targeted *Gt*ACR2$^{Kv2.1}$ and *Gt*ACR2^{nrxn} expression in precisely defined circuits of interest. Intersectional strategies would be especially useful in building upon the physiological observations reported in Chapter 3, through more refined targeting of *Gt*ACR2 construct expression and photoinhibition in preBötC and associated circuitry.

In closing, experiments described in this thesis provide valuable and diverse contributions to the expanding toolset for targeted cellular and subcellular transgene expression. Their application in future studies offer many opportunities to understand how defined neural circuits contribute to cognition and behaviour, from which novel therapeutic strategies for a variety of neuropsychiatric conditions may be developed.

References

Ablondi F (1998) Automata, living and non-living: Descartes' mechanical biology and his criteria for life. *Biol Philos* 13: 179-186.

Acar F, Naderi S, Guvencer M, Ture U, and Arda MN (2005) Herophilus of Chalcedon: a pioneer in neuroscience. *Neurosurgery* 56: 861-867.

Adachi A, Shimizu N, Oomura Y, and Kobashi M (1984) Convergence of hepatoportal glucose-sensitive afferent signals to glucose-sensitive units within the nucleus of the solitary tract. *Neurosci Lett* 46: 215-218.

Adrian ED, Bronk DW, and Phillips G (1932) Discharges in mammalian sympathetic nerves. *J Physiol* 74: 115-133.

Afshar A, Steensma DP, and Kyle RA (2019) Andreas Vesalius and De Fabrica. *Mayo Clin Proc* 94: e67-e68.

Akli S, Caillaud C, Vigne E, Stratfordperricaudet LD, Poenaru L, Perricaudet M, Kahn A, and Peschanski MR (1993) Transfer of a foreign gene into the brain using adenovirus vectors. *Nat Genet* 3: 224-228.

Alberio L, Locarno A, Saponaro A, Romano E, Bercier V, Albadri S, Simeoni F, Moleri S, et al. (2018) A light-gated potassium channel for sustained neuronal inhibition. *Nat Methods* 15: 969-976.

Albert-Gasco H, Ma S, Ros-Bernal F, Sanchez-Perez AM, Gundlach AL, and Olucha-Bordonau FE (2018a) GABAergic neurons in the rat medial septal complex express relaxin-3 receptor (RXFP3) mRNA. *Front Neuroanat* 11: 133.

Albert-Gasco H, Sanchez-Sarasua S, Ma S, Garcia-Diaz C, Gundlach AL, Sanchez-Perez AM, and Olucha-Bordonau FE (2018b) Central relaxin-3 receptor (RXFP3) activation impairs social recognition and modulates ERK-phosphorylation in specific GABAergic amygdala neurons. *Brain Struct Funct* 224: 453-469.

Andersen SS, and Bi GQ (2000) Axon formation: a molecular model for the generation of neuronal polarity. *Bioessays* 22: 172-179.

Andre JS, and Reilly S (2007) Effects of central and basolateral amygdala lesions on conditioned taste aversion and latent inhibition. *Behav Neurosci* 121: 1363-1363.

Angelone A, and Coulter NA, Jr. (1964) Respiratory sinus arrhythemia: a frequency dependent phenomenon. *J Appl Physiol* 19: 479-482.

Arimura N, and Kaibuchi K (2007) Neuronal polarity: from extracellular signals to intracellular mechanisms. *Nat Rev Neurosci* 8: 194-205.

Armbruster BN, Li X, Pausch MH, Herlitze S, and Roth BL (2007) Evolving the lock to fit the key to create a family of G protein-coupled receptors potently activated by an inert ligand. *Proc Natl Acad Sci U S A* 104: 5163-5168.

Arraez-Aybar LA, Navia-Alvarez P, Fuentes-Redondo T, and Bueno-Lopez JL (2015) Thomas Willis, a pioneer in translational research in anatomy (on the 350th anniversary of Cerebri anatome). *J Anat* 226: 289-300.

Arrigo A, Mormina E, Calamuneri A, Gaeta M, Marino S, Milardi D, Anastasi GP, and Quartarone A (2017) Amygdalar and hippocampal connections with brainstem and spinal cord: A diffusion MRI study in human brain. *Neuroscience* 343: 346-354.

Atasoy D, and Sternson SM (2018) Chemogenetic tools for causal cellular and neuronal biology. *Physiol Rev* 98: 391-418.

Baars BJ, and Gage NM. (2010) *Cognition, brain, and consciousness,* Academic Press.

Baas PW, Deitch JS, Black MM, and Banker GA (1988) Polarity orientation of microtubules in hippocampal neurons: uniformity in the axon and nonuniformity in the dendrite. *Proc Natl Acad Sci U S A* 85: 8335-8339.

Baird GS, Zacharias DA, and Tsien RY (2000) Biochemistry, mutagenesis, and oligomerization of DsRed, a red fluorescent protein from coral. *Proc Natl Acad Sci U S A* 97: 11984-11989.

Baker CA, Elyadat YM, Parra A, and Bolton MM (2016) Cellular resolution circuit mapping with temporal-focused excitation of soma targeted channelrhodopsin. *Elife* 5.

Baker G, and Morris KJ. (1996) *Decartes' dualism,* Routledge: London.

Baker K, Gordon SL, Grozeva D, van Kogelenberg M, Roberts NY, Pike M, Blair E, Hurles ME, et al. (2015) Identification of a human synaptotagmin-1 mutation that perturbs synaptic vesicle cycling. *J Clin Invest* 125: 1670-1678.

Baldi R, Varga C, and Tamas G (2010) Differential distribution of KCC2 along the axo-somato-dendritic axis of hippocampal principal cells. *Eur J Neurosci* 32: 1319-1325.

Ball CS (1996) The early history of the compound microscope. *Bios* 37: 51-60.

Bando Y, Sakamoto M, Kim S, Ayzenshtat I, and Yuste R (2019) Comparative evaluation of genetically encoded voltage indicators. *Cell Rep* 26: 802-813 e804.

Banker GA, and Cowan WM (1977) Rat hippocampal neurons in dispersed cell culture. *Brain Res* 126: 397-342.

Barbara JG, Broussolle E, Poirier J, and Clarac F (2012) Figures and institutions of the neurological sciences in Paris from 1800 to 1950. Part II: Neurophysiology. *Rev Neurol (Paris)* 168: 106-115.

Barbic M (2019) Possible magneto-mechanical and magneto-thermal mechanisms of ion channel activation in magnetogenetics. *Elife* 8: e45807.

Batten TF, Gamboa-Esteves FO, and Saha S (2002) Evidence for peptide co-transmission in retrograde- and anterograde-labelled central nucleus of amygdala neurones projecting to NTS. *Auton Neurosci* 98: 28-32.

Becker JA, Befort K, Blad C, Filliol D, Ghate A, Dembele D, Thibault C, Koch M, et al. (2008) Transcriptome analysis identifies genes with enriched expression in the mouse central extended amygdala. *Neuroscience* 156: 950-965.

Beckstead RM, and Norgren R (1979) An autoradiographic examination of the central distribution of the trigeminal, facial, glossopharyngeal, and vagal nerves in the monkey. *J Comp Neurol* 184: 455-472.

Bedbrook CN, Deverman BE, and Gradinaru V (2018) Viral strategies for targeting the central and peripheral nervous systems. *Annu Rev Neurosci* 41: 323-348.

Beier KT, Steinberg EE, DeLoach KE, Xie S, Miyamichi K, Schwarz L, Gao XJ, Kremer EJ, et al. (2015) Circuit architecture of VTA dopamine neurons revealed by systematic input-output mapping. *Cell* 162: 622-634.

Ben-Tal A, Shamailov SS, and Paton JF (2012) Evaluating the physiological significance of respiratory sinus arrhythmia: looking beyond ventilation-perfusion efficiency. *J Physiol* 590: 1989-2008.

Benarroch EE (1993) The central autonomic network: functional organization, dysfunction, and perspective. *Mayo Clin Proc* 68: 988-1001.

Benson KR (2001) T. H. Morgan's resistance to the chromosome theory. *Nat Rev Genet* 2: 469-474.

Bentivoglio M, Cotrufo T, Ferrari S, Tesoriero C, Mariotto S, Bertini G, Berzero A, and Mazzarello P (2019) The original histological slides of Camillo Golgi and his discoveries on neuronal structure. *Front Neuroanat* 13: 3.

Bentley M, and Banker G (2016) The cellular mechanisms that maintain neuronal polarity. *Nat Rev Neurosci* 17: 611-622.

Berg P, Baltimore D, Boyer HW, Cohen SN, Davis RW, Hogness DS, Nathans D, Roblin R, et al. (1974) Potential biohazards of recombinant DNA molecules. *Science* 185: 303.

Berg P, Baltimore D, Brenner S, Roblin RO, and Singer MF (1975) Summary statement of the Asilomar conference on recombinant DNA molecules. *Proc Natl Acad Sci U S A* 72: 1981-1984.

Berg P, and Singer MF (1995) The recombinant DNA controversy: twenty years later. *Proc Natl Acad Sci U S A* 92: 9011-9013.

Berg P, and Mertz JE (2010) Personal reflections on the origins and emergence of recombinant DNA technology. *Genetics* 184: 9-17.

Berndt A, Lee SY, Ramakrishnan C, and Deisseroth K (2014) Structure-guided transformation of channelrhodopsin into a light-activated chloride channel. *Science* 344: 420-424.

Bertucci P (2016) Shocking subjects: human experiments and the material culture of medical electricity in eighteenth-century England. *Clio Med* 95: 111-138.

Birgul N, Weise C, Kreienkamp HJ, and Richter D (1999) Reverse physiology in drosophila: identification of a novel allatostatin-like neuropeptide and its cognate receptor structurally related to the mammalian somatostatin/galanin/opioid receptor family. *EMBO J* 18: 5892-5900.

Blaesse P, Airaksinen MS, Rivera C, and Kaila K (2009) Cation-chloride cotransporters and neuronal function. *Neuron* 61: 820-838.

Blasiak A, Blasiak T, Lewandowski MH, Hossain MA, Wade JD, and Gundlach AL (2013) Relaxin-3 innervation of the intergeniculate leaflet of the rat thalamus - neuronal tract-tracing and in vitro electrophysiological studies. *Eur J Neurosci* 37: 1284-1294.

Blasiak A, Siwiec M, Grabowiecka A, Blasiak T, Czerw A, Blasiak E, Kania A, Rajfur Z, et al. (2015) Excitatory orexinergic innervation of rat nucleus incertus - Implications for ascending arousal, motivation and feeding control. *Neuropharmacology* 99: 432-447.

Blomer U, Naldini L, Kafri T, Trono D, Verma IM, and Gage FH (1997) Highly efficient and sustained gene transfer in adult neurons with a lentivirus vector. *J Virol* 71: 6641-6649.

Bonham AC, and McCrimmon DR (1990) Neurones in a discrete region of the nucleus tractus solitarius are required for the Breuer-Hering reflex in rat. *J Physiol* 427: 261-280.

Bonifacino JS (2014) Adaptor proteins involved in polarized sorting. *J Cell Biol* 204: 7-17.

Bonnet MS, Ouelaa W, Tillement V, Trouslard J, Jean A, Gonzalez BJ, Gourcerol G, Dallaporta M, et al. (2013) Gastric distension activates NUCB2/nesfatin-1-expressing neurons in the nucleus of the solitary tract. *Regul Pept* 187: 17-23.

Bouairi E, Neff R, Evans C, Gold A, Andresen MC, and Mendelowitz D (2004) Respiratory sinus arrhythmia in freely moving and anesthetized rats. *J Appl Physiol* 97: 1431-1436.

Bowman BR, Kumar NN, Hassan SF, McMullan S, and Goodchild AK (2013) Brain sources of inhibitory input to the rat rostral ventrolateral medulla. *J Comp Neurol* 521: 213-232.

Boyden ES, Zhang F, Bamberg E, Nagel G, and Deisseroth K (2005) Millisecond-timescale, genetically targeted optical control of neural activity. *Nat Neurosci* 8: 1263-1268.

Boyden ES (2015) Optogenetics and the future of neuroscience. *Nat Neurosci* 18: 1200-1201.

Boyer H (2009) Wonderful life: an interview with Herb Boyer. [Interview by Jane Gitschier]. *PLoS Genet* 5: e1000653.

Bradke F, and Dotti CG (1999) The role of local actin instability in axon formation. *Science* 283: 1931-1934.

Broca P (2011) Remarks on the seat of spoken language, followed by a case of aphasia (1861). *Neuropsychol Rev* 21: 227-229.

Broussard GJ, Liang R, and Tian L (2014) Monitoring activity in neural circuits with genetically encoded indicators. *Front Mol Neurosci* 7: 97.

Broussard GJ, Liang Y, Fridman M, Unger EK, Meng G, Xiao X, Ji N, Petreanu L, et al. (2018) In vivo measurement of afferent activity with axon-specific calcium imaging. *Nat Neurosci* 21: 1272-1280.

Burazin TCD, Bathgate RAD, Macris M, Layfield S, Gundlach AL, and Tregear GW (2002) Restricted, but abundant, expression of the novel rat gene-3 (R3) relaxin in the dorsal tegmental region of brain. *J Neurochem* 82: 1553-1557.

Burton PR, and Paige JL (1981) Polarity of axoplasmic microtubules in the olfactory nerve of the frog. *Proc Natl Acad Sci U S A* 78: 3269-3273.

Buxbaum AR, Haimovich G, and Singer RH (2015) In the right place at the right time: visualizing and understanding mRNA localization. *Nat Rev Mol Cell Biol* 16: 95-109.

Cai D, Cohen KB, Luo T, Lichtman JW, and Sanes JR (2013) Improved tools for the Brainbow toolbox. *Nat Methods* 10: 540-547.

Callander GE, Ma S, Ganella DE, Wimmer VC, Gundlach AL, Thomas WG, and Bathgate RAD (2012) Silencing relaxin-3 in nucleus incertus of adult rodents: A viral vector-based approach to investigate neuropeptide function. *PLoS One* 7: e42300.

Cambiaghi M, and Sandrone S (2014) Robert Bartholow (1831-1904). *J Neurol* 261: 1649-1650.

Campbell RE, Tour O, Palmer AE, Steinbach PA, Baird GS, Zacharias DA, and Tsien RY (2002) A monomeric red fluorescent protein. *Proc Natl Acad Sci U S A* 99: 7877-7882.

Campos CA, Bowen AJ, Schwartz MW, and Palmiter RD (2016) Parabrachial CGRP neurons control meal termination. *Cell Metab* 23: 811-820.

Capecchi MR (2005) Gene targeting in mice: functional analysis of the mammalian genome for the twenty-first century. *Nat Rev Genet* 6: 507-512.

Carrive P (1993) The periaqueductal gray and defensive behavior: functional representation and neuronal organization. *Behav Brain Res* 58: 27-47.

Carter ME, Soden ME, Zweifel LS, and Palmiter RD (2013) Genetic identification of a neural circuit that suppresses appetite. *Nature* 503: 111-114.

Cassell MD, and Gray TS (1989) The amygdala directly innervates adrenergic (C1) neurons in the ventrolateral medulla in the rat. *Neurosci Lett* 97: 163-168.

Cavero I, Guillon JM, and Holzgrefe HH (2017) Reminiscing about Jan Evangelista Purkinje: a pioneer of modern experimental physiology. *Adv Physiol Educ* 41: 528-538.

Cederbaum SD, Fareed GC, Lovett MA, and Shapiro LJ (1984) Recombinant DNA in medicine. *West J Med* 141: 210-222.

Ceunen E, Vlaeyen JW, and Van Diest I (2016) On the origin of interoception. *Front Psychol* 7: 743.

Ch'ng SS, Fu J, Brown RM, Smith CM, Hossain MA, McDougall SJ, and Lawrence AJ (2019) Characterization of the relaxin family peptide receptor 3 system in the mouse bed nucleus of the stria terminalis. *J Comp Neurol*: doi: 10.1002/cne.24695.

Chalfie M, Tu Y, Euskirchen G, Ward WW, and Prasher DC (1994) Green fluorescent protein as a marker for gene-expression. *Science* 263: 802-805.

Challis RC, Ravindra Kumar S, Chan KY, Challis C, Beadle K, Jang MJ, Kim HM, Rajendran PS, et al. (2019) Systemic AAV vectors for widespread and targeted gene delivery in rodents. *Nat Protoc* 14: 379-414.

Chan CY, Yoo JE, and Travers SP (2004) Diverse bitter stimuli elicit highly similar patterns of Fos-like immunoreactivity in the nucleus of the solitary tract. *Chem Senses* 29: 573-581.

Chan KY, Jang MJ, Yoo BB, Greenbaum A, Ravi N, Wu WL, Sanchez-Guardado L, Lois C, et al. (2017) Engineered AAVs for efficient noninvasive gene delivery to the central and peripheral nervous systems. *Nat Neurosci* 20: 1172-1179.

Chan RK, Jarvina EV, and Sawchenko PE (2000) Effects of selective sinoaortic denervations on phenylephrine-induced activational responses in the nucleus of the solitary tract. *Neuroscience* 101: 165-178.

Chang AC, and Cohen SN (1974) Genome construction between bacterial species in vitro: replication and expression of Staphylococcus plasmid genes in Escherichia coli. *Proc Natl Acad Sci U S A* 71: 1030-1034.

Chang BB, Persengiev SP, de Diego JG, Sacristan MP, Zanca DM, and Kilpatrick DL (1998) Proximal promoter sequences mediate cell-specific and elevated expression of the favorable prognosis marker TrkA in human neuroblastoma cells. *J Biol Chem* 273: 39-44.

Chapman WP, Schroeder HR, Geyer G, Brazier MA, Fager C, Poppen JL, Solomon HC, and Yakovlev PI (1954) Physiological evidence concerning importance of the amygdaloid

nuclear region in the integration of circulatory function and emotion in man. *Science* 120: 949-950.

Chapman WP, Singh MM, Schroeder HR, and Fager C (1957) Temporal lobe epilepsy: brief review; responses on electrical stimulation of the amygdaloid region in six patients. *Am J Med* 23: 107-119.

Chen D, Bassi JK, Walther T, Thomas WG, and Allen AM (2010) Expression of angiotensin type 1A receptors in C1 neurons restores the sympathoexcitation to angiotensin in the rostral ventrolateral medulla of angiotensin type 1A knockout mice. *Hypertension* 56: 143-150.

Chen R, Romero G, Christiansen MG, Mohr A, and Anikeeva P (2015) Wireless magnetothermal deep brain stimulation. *Science* 347: 1477-1480.

Chen R, Gore F, Nguyen QA, Ramakrishnan C, Patel S, Kim SH, Raffiee M, Kim YS, et al. (2020) Deep brain optogenetics without intracranial surgery. *Nat Biotechnol*.

Chen S, Weitemier AZ, Zeng X, He L, Wang X, Tao Y, Huang AJY, Hashimotodani Y, et al. (2018) Near-infrared deep brain stimulation via upconversion nanoparticle-mediated optogenetics. *Science* 359: 679-684.

Chen TW, Wardill TJ, Sun Y, Pulver SR, Renninger SL, Baohan A, Schreiter ER, Kerr RA, et al. (2013) Ultrasensitive fluorescent proteins for imaging neuronal activity. *Nature* 499: 295-300.

Chiou RJ, Kuo CC, and Yen CT (2014) Comparisons of terminal densities of cardiovascular function-related projections from the amygdala subnuclei. *Auton Neurosci* 181: 21-30.

Cho YK, Li CS, and Smith DV (2003) Descending influences from the lateral hypothalamus and amygdala converge onto medullary taste neurons. *Chem Senses* 28: 155-171.

Cho YK, and Li D. 2016. 'Optogenetics: basic concepts and their development.' in A. Kianianmomeni (ed.), *Optogenetics* (Humana Press: New York, NY).

Choi JH, Yu NK, Baek GC, Bakes J, Seo D, Nam HJ, Baek SH, Lim CS, et al. (2014) Optimization of AAV expression cassettes to improve packaging capacity and transgene expression in neurons. *Mol Brain* 7: 17.

Choudhury SR, Harris AF, Cabral DJ, Keeler AM, Sapp E, Ferreira JS, Gray-Edwards HL, Johnson JA, et al. (2016) Widespread central nervous system gene transfer and silencing after systemic delivery of novel AAV-AS vector. *Mol Ther* 24: 726-735.

Chow BY, Han X, Dobry AS, Qian X, Chuong AS, Li M, Henninger MA, Belfort GM, et al. (2010) High-performance genetically targetable optical neural silencing by light-driven proton pumps. *Nature* 463: 98-102.

Christiansen MG, Senko AW, and Anikeeva P (2019) Magnetic strategies for nervous system control. *Annu Rev Neurosci* 42: 271-293.

Chronwall BM, Skirboll LR, and O'Donohue TL (1985) Demonstration of a pontine-hippocampal projection containing a ranatensin-like peptide. *Neurosci Lett* 53: 109-114.

Chudakov DM, Lukyanov S, and Lukyanov KA (2005) Fluorescent proteins as a toolkit for in vivo imaging. *Trends Biotechnol* 23: 605-613.

Ciriello J (1983) Brainstem projections of aortic baroreceptor afferent fibers in the rat. *Neurosci Lett* 36: 37-42.

Clary DO, Weskamp G, Austin LR, and Reichardt LF (1994) TrkA cross-linking mimics neuronal responses to nerve growth factor. *Mol Biol Cell* 5: 549-563.

Cobb M (2014) Oswald Avery, DNA, and the transformation of biology. *Curr Biol* 24: R55-60.

Cohen BE, Edmondson D, and Kronish IM (2015) State of the art review: depression, stress, anxiety, and cardiovascular disease. *Am J Hypertens* 28: 1295-1302.

Cohen SN, Chang AC, and Hsu L (1972) Nonchromosomal antibiotic resistance in bacteria: genetic transformation of Escherichia coli by R-factor DNA. *Proc Natl Acad Sci U S A* 69: 2110-2114.

Cohen SN, Chang AC, Boyer HW, and Helling RB (1973) Construction of biologically functional bacterial plasmids in vitro. *Proc Natl Acad Sci U S A* 70: 3240-3244.

Cohen SN (2013) DNA cloning: a personal view after 40 years. *Proc Natl Acad Sci U S A* 110: 15521-15529.

Conner JM, Franks KM, Titterness AK, Russell K, Merrill DA, Christie BR, Sejnowski TJ, and Tuszynski MH (2009) NGF is essential for hippocampal plasticity and learning. *J Neurosci* 29: 10883-10889.

Cormack BP, Valdivia RH, and Falkow S (1996) FACS-optimized mutants of the green fluorescent protein (GFP). *Gene* 173: 33-38.

Costantini F, and Lacy E (1981) Introduction of a rabbit β-globin gene into the mouse germ line. *Nature* 294: 92-94.

Coward DM (1992) General pharmacology of clozapine. *Br J Psychiatry*: 5-11.

Coward P, Wada HG, Falk MS, Chan SD, Meng F, Akil H, and Conklin BR (1998) Controlling signaling with a specifically designed Gi-coupled receptor. *Proc Natl Acad Sci U S A* 95: 352-357.

Critchley HD, and Harrison NA (2013) Visceral influences on brain and behavior. *Neuron* 77: 624-638.

Crivellato E, and Ribatti D (2007) Soul, mind, brain: Greek philosophy and the birth of neuroscience. *Brain Res Bull* 71: 327-336.

Crystal RG (2014) Adenovirus: the first effective in vivo gene delivery vector. *Hum Gene Ther* 25: 3-11.

Cui Y, Kam K, Sherman D, Janczewski WA, Zheng Y, and Feldman JL (2016) Defining preBotzinger complex rhythm- and pattern-generating neural microcircuits in vivo. *Neuron* 91: 602-614.

Dale HH, and Dudley HW (1929) The presence of histamine and acetylcholine in the spleen of the ox and the horse. *J Physiol* 68: 97-123.

Dale HH (1937) Transmission of nervous effects by acetylcholine: Harvey Lecture, May 20, 1937. *Bull N Y Acad Med* 13: 379-396.

Daly MD (1991) Some reflex cardioinhibitory responses in the cat and their modulation by central inspiratory neuronal-activity. *J Physiol (London)* 439: 559-577.

Danielsen EH, Magnuson DJ, and Gray TS (1989) The central amygdaloid nucleus innervation of the dorsal vagal complex in rat: a Phaseolus vulgaris leucoagglutinin lectin anterograde tracing study. *Brain Res Bull* 22: 705-715.

Davern PJ (2014) A role for the lateral parabrachial nucleus in cardiovascular function and fluid homeostasis. *Front Physiol* 5: 436.

de Castro F, Lopez-Mascaraque L, and De Carlos JA (2007) Cajal: lessons on brain development. *Brain Res Rev* 55: 481-489.

De Palma A, and Pareti G (2011) Bernstein's long path to membrane theory: radical change and conservation in nineteenth-century German electrophysiology. *J Hist Neurosci* 20: 306-337.

DeFelipe J (2015) The dendritic spine story: an intriguing process of discovery. *Front Neuroanat* 9: 14.

Deiters VS, and Guillery RW (2013) Otto Friedrich Karl Deiters (1834-1863). *J Comp Neurol* 521: 1929-1953.

Del Negro CA, Funk GD, and Feldman JL (2018) Breathing matters. *Nat Rev Neurosci* 19: 351-367.

Del Rio D, Beucher B, Lavigne M, Wehbi A, Gonzalez Dopeso-Reyes I, Saggio I, and Kremer EJ (2019) CAV-2 vector development and gene transfer in the central and peripheral nervous systems. *Front Mol Neurosci* 12: 71.

Delpy A, Allain AE, Meyrand P, and Branchereau P (2008) NKCC1 cotransporter inactivation underlies embryonic development of chloride-mediated inhibition in mouse spinal motoneuron. *J Physiol* 586: 1059-1075.

Deverman BE, Pravdo PL, Simpson BP, Kumar SR, Chan KY, Banerjee A, Wu WL, Yang B, et al. (2016) Cre-dependent selection yields AAV variants for widespread gene transfer to the adult brain. *Nat Biotechnol* 34: 204-209.

Devos Y, Maeseele P, Reheul D, Van Speybroeck L, and De Waele D (2008) Ethics in the societal debate on genetically modified organisms: a (re)quest for Sense and Sensibility. *J Agr Environ Ethic* 21: 29-61.

Dick TE, Baekey DM, Paton JF, Lindsey BG, and Morris KF (2009) Cardio-respiratory coupling depends on the pons. *Respir Physiol Neurobiol* 168: 76-85.

DiMicco JA, Stotz-Potter EH, Monroe AJ, and Morin SM (1996) Role of the dorsomedial hypothalamus in the cardiovascular response to stress. *Clin Exp Pharmacol Physiol* 23: 171-176.

DiNardo LA, and Travers JB (1997) Distribution of fos-like immunoreactivity in the medullary reticular formation of the rat after gustatory elicited ingestion and rejection behaviors. *J Neurosci* 17: 3826-3839.

Dlouhy BJ, Gehlbach BK, Kreple CJ, Kawasaki H, Oya H, Buzza C, Granner MA, Welsh MJ, et al. (2015) Breathing inhibited when seizures spread to the amygdala and upon amygdala stimulation. *J Neurosci* 35: 10281-10289.

Dobbins EG, and Feldman JL (1994) Brainstem network controlling descending drive to phrenic motoneurons in rat. *J Comp Neurol* 347: 64-86.

Dong HW, Petrovich GD, and Swanson LW (2001) Topography of projections from amygdala to bed nuclei of the stria terminalis. *Brain Res Rev* 38: 192-246.

Dotti CG, Sullivan CA, and Banker GA (1988) The establishment of polarity by hippocampal neurons in culture. *J Neurosci* 8: 1454-1468.

Dymecki SM, Ray RS, and Kim JC (2010) Mapping cell fate and function using recombinase-based intersectional strategies. *Method Enzymol* 477: 183-213.

Eccles J (1965) The synapse. *Sci Am* 212: 56-66.

Eccles J (1976) From electrical to chemical transmission in the central nervous system. *Notes Rec R Soc Lond* 30: 219-230.

Ehrlich I, Lohrke S, and Friauf E (1999) Shift from depolarizing to hyperpolarizing glycine action in rat auditory neurones is due to age-dependent Cl- regulation. *J Physiol (London)* 520: 121-137.

Ehrlich I, Humeau Y, Grenier F, Ciocchi S, Herry C, and Luthi A (2009) Amygdala inhibitory circuits and the control of fear memory. *Neuron* 62: 757-771.

Elder JT, Spritz RA, and Weissman SM (1981) Simian virus-40 as a eukaryotic cloning vehicle. *Annu Rev Genet* 15: 295-340.

Ellsworth JL, Gingras J, Smith LJ, Rubin H, Seabrook TA, Patel K, Zapata N, Olivieri K, et al. (2019) Clade F AAVHSCs cross the blood brain barrier and transduce the central nervous system in addition to peripheral tissues following intravenous administration in nonhuman primates. *PLoS One* 14: e0225582.

Elstad M, O'Callaghan EL, Smith AJ, Ben-Tal A, and Ramchandra R (2018) Cardiorespiratory interactions in humans and animals: rhythms for life. *Am J Physiol Heart Circ Physiol* 315: H6-H17.

Emiliani V, Cohen AE, Deisseroth K, and Hausser M (2015) All-optical interrogation of neural circuits. *J Neurosci* 35: 13917-13926.

Emond M, Schwartz GJ, and Moran TH (2001) Meal-related stimuli differentially induce c-Fos activation in the nucleus of the solitary tract. *Am J Physiol Regul Integr Comp Physiol* 280: R1315-1321.

Engel KL, Arora A, Goering R, Lo HG, and Taliaferro JM (2020) Mechanisms and consequences of subcellular RNA localization across diverse cell types. *Traffic* 21: 404-418.

Ermakova YG, Lanin AA, Fedotov IV, Roshchin M, Kelmanson IV, Kulik D, Bogdanova YA, Shokhina AG, et al. (2017) Thermogenetic neurostimulation with single-cell resolution. *Nat Commun* 8: 15362.

Fadok JP, Krabbe S, Markovic M, Courtin J, Xu C, Massi L, Botta P, Bylund K, et al. (2017) A competitive inhibitory circuit for selection of active and passive fear responses. *Nature* 542: 96-100.

Fagerstrom T, Dixelius C, Magnusson U, and Sundstrom JF (2012) Stop worrying; start growing. *EMBO Reports* 13: 493-497.

Faiers AA, Calaresu FR, and Mogenson GJ (1975) Pathway mediating hypotension elicited by stimulation of the amygdala in the rat. *Am J Physiol* 228: 1358-1366.

Fairless R, Masius H, Rohlmann A, Heupel K, Ahmad M, Reissner C, Dresbach T, and Missler M (2008) Polarized targeting of neurexins to synapses Is regulated by their C-terminal sequences. *J Neurosci* 28: 12969-12981.

Falkner L, Wei D, Song A, Li WW, Chen I, Feng JE, and Lin D (2019) PAG neurons encode a simplified action-selective signal during aggression. *bioRxiv*: p.745067.

Fearing F (1929) A study in the history of the theories of reflex action. *Psychol Rev* 36: 375-388.

Feldberg W, and Malcolm JL (1959) Experiments on the site of action of tubocurarine when applied via the cerebral ventricles. *J Physiol (London)* 149: 58-77.

Feldberg W, and Myers RD (1965) Changes in temperature produced by micro-injections of amines into the anterior hypothalamus of cats. *J Physiol* 177: 239-245.

Feng G, Mellor RH, Bernstein M, Keller-Peck C, Nguyen QT, Wallace M, Nerbonne JM, Lichtman JW, et al. (2000) Imaging neuronal subsets in transgenic mice expressing multiple spectral variants of GFP. *Neuron* 28: 41-51.

Feng J, Zhang C, Lischinsky JE, Jing M, Zhou J, Wang H, Zhang Y, Dong A, et al. (2019) A genetically encoded fluorescent sensor for rapid and specific in vivo detection of norepinephrine. *Neuron* 102: 745-761 e748.

Fennegan FM, and Puiggari MJ (1966) Hypothalamic and amygdaloid influence on gastric motility in dogs. *J Neurosurg* 24: 497-504.

Fenno LE, Mattis J, Ramakrishnan C, Hyun M, Lee SY, He M, Tucciarone J, Selimbeyoglu A, et al. (2014) Targeting cells with single vectors using multiple-feature Boolean logic. *Nat Methods* 11: 763-U116.

Fenno LE, Ramakrishnan C, Kim YS, Evans KE, Lo M, Vesuna S, Inoue M, Cheung KYM, et al. (2020) Comprehensive dual- and triple-feature intersectional single-vector delivery of diverse functional payloads to cells of behaving mammals. *Neuron* 107: 1-18.

Fernando AB, Murray JE, and Milton AL (2013) The amygdala: securing pleasure and avoiding pain. *Front Behav Neurosci* 7: 190.

Ferrier D (1874) On the localisation of the functions of the brain. *Br Med J* 2: 766-767.

Ferrier D (1875) Experiments on the brain of monkeys - No. I. *Proc R Soc Lond* 23: 409-430.

Finger S. (1994) *Origins of neuroscience: a history of explorations into brain function,* Oxford University Press.

Finley JC, and Katz DM (1992) The central organization of carotid body afferent projections to the brainstem of the rat. *Brain Res* 572: 108-116.

Fischer KB, Collins HK, and Callaway EM (2019) Sources of off-target expression from recombinase-dependent AAV vectors and mitigation with cross-over insensitive ATG-out vectors. *Proc Natl Acad Sci U S A* 116: 27001-27010.

Flotte TR, Afione SA, Solow R, Drumm ML, Markakis D, Guggino WB, Zeitlin PL, and Carter BJ (1993) Expression of the cystic fibrosis transmembrane conductance regulator from a novel adeno-associated virus promoter. *J Biol Chem* 268: 3781-3790.

Foust KD, Nurre E, Montgomery CL, Hernandez A, Chan CM, and Kaspar BK (2009) Intravascular AAV9 preferentially targets neonatal neurons and adult astrocytes. *Nat Biotechnol* 27: 59-65.

Fritsch G, and Hitzig E (2009) Electric excitability of the cerebrum (Uber die elektrische Erregbarkeit des Grosshirns). *Epilepsy Behav* 15: 123-130.

Gahl TJ, and Kunze A (2018) Force-mediating magnetic nanoparticles to engineer neuronal cell function. *Front Neurosci* 12: 299.

Ganella DE, Callander GE, Ma S, Bye CR, Gundlach AL, and Bathgate RAD (2013) Modulation of feeding by chronic rAAV expression of a relaxin-3 peptide agonist in rat hypothalamus. *Gene Ther* 20: 703-716.

Gangoda L, Doerflinger M, Lee YY, Rahimi A, Etemadi N, Chau D, Milla L, O'Connor L, et al. (2012) Cre transgene results in global attenuation of the cAMP/PKA pathway. *Cell Death Dis* 3: e365.

Garcia AJ, 3rd, Koschnitzky JE, Dashevskiy T, and Ramirez JM (2013) Cardiorespiratory coupling in health and disease. *Auton Neurosci* 175: 26-37.

Garcia-Marques J, Yang CP, Espinosa-Medina I, Mok K, Koyama M, and Lee T (2019) Unlimited genetic switches for cell-type-specific manipulation. *Neuron* 104: 227-238 e227.

Garvalov BK, Flynn KC, Neukirchen D, Meyn L, Teusch N, Wu X, Brakebusch C, Bamburg JR, et al. (2007) Cdc42 regulates cofilin during the establishment of neuronal polarity. *J Neurosci* 27: 13117-13129.

Gasparini S, Howland JM, Thatcher AJ, and Geerling JC (2020) Central afferents to the nucleus of the solitary tract in rats and mice. *J Comp Neurol*.

Gelsema AJ, McKitrick DJ, and Calaresu FR (1987) Cardiovascular responses to chemical and electrical stimulation of amygdala in rats. *Am J Physiol* 253: R712-718.

Gest H (2004) The discovery of microorganisms by Robert Hooke and Antoni Van Leeuwenhoek, fellows of the Royal Society. *Notes Rec R Soc Lond* 58: 187-201.

Gibbs RA, Weinstock GM, Metzker ML, Muzny DM, Sodergren EJ, Scherer S, Scott G, Steffen D, et al. (2004) Genome sequence of the Brown Norway rat yields insights into mammalian evolution. *Nature* 428: 493-521.

Gibbs RB, and Pfaff DW (1994) In situ hybridization detection of trkA mRNA in brain: distribution, colocalization with p75NGFR and up-regulation by nerve growth factor. *J Comp Neurol* 341: 324-339.

Glass MJ, Colago EEO, and Pickel VM (2002) Alpha-2A-adrenergic receptors are present on neurons in the central nucleus of the amygdala that project to the dorsal vagal complex in the rat. *Synapse* 46: 258-268.

Goff SP, and Berg P (1976) Construction of hybrid viruses containing SV40 and lambda phage DNA segments and their propagation in cultured monkey cells. *Cell* 9: 695-705.

Gomes MD, Moscovici M, and Engelhardt E (2015) Andreas Vesalius as a renaissance innovative neuroanatomist: his 5th centenary of birth. *Arq Neuro-Psiquiat* 73: 155-158.

Gomez JL, Bonaventura J, Lesniak W, Mathews WB, Sysa-Shah P, Rodriguez LA, Ellis RJ, Richie CT, et al. (2017) Chemogenetics revealed: DREADD occupancy and activation via converted clozapine. *Science* 357: 503-507.

Gong YY, Huang C, Li JZ, Grewe BF, Zhang YP, Eismann S, and Schnitzer MJ (2015) High-speed recording of neural spikes in awake mice and flies with a fluorescent voltage sensor. *Science* 350: 1361-1366.

Gordon JW, Scangos GA, Plotkin DJ, Barbosa JA, and Ruddle FH (1980) Genetic transformation of mouse embryos by microinjection of purified DNA. *Proc Natl Acad Sci U S A* 77: 7380-7384.

Gordon SL, Leube RE, and Cousin MA (2011) Synaptophysin Is required for synaptobrevin retrieval during synaptic vesicle endocytosis. *J Neurosci* 31: 14032-14036.

Goto M, Swanson LW, and Canteras NS (2001) Connections of the nucleus incertus. *J Comp Neurol* 438: 86-122.

Goutaudier R, Coizet V, Carcenac C, and Carnicella S (2019) DREADDs: the power of the lock, the weakness of the key. Favoring the pursuit of specific conditions rather than specific ligands. *eNeuro* 6.

Govorunova EG, Sineshchekov OA, Janz R, Liu X, and Spudich JL (2015) Natural light-gated anion channels: a family of microbial rhodopsins for advanced optogenetics. *Science* 349: 647-650.

Gradinaru V, Thompson KR, and Deisseroth K (2008) eNpHR: a Natronomonas halorhodopsin enhanced for optogenetic applications. *Brain Cell Biol* 36: 129-139.

Gradinaru V, Zhang F, Ramakrishnan C, Mattis J, Prakash R, Diester I, Goshen I, Thompson KR, et al. (2010) Molecular and cellular approaches for diversifying and extending optogenetics. *Cell* 141: 154-165.

Gray TS, and Magnuson DJ (1987a) Neuropeptide neuronal efferents from the bed nucleus of the stria terminalis and central amygdaloid nucleus to the dorsal vagal complex in the rat. *J Comp Neurol* 262: 365-374.

Gray TS, and Magnuson DJ (1987b) Galanin-like immunoreactivity within amygdaloid and hypothalamic neurons that project to the midbrain central gray in rat. *Neurosci Lett* 83: 264-268.

Greenblatt SH (1995) Phrenology in the science and culture of the 19th century. *Neurosurgery* 37: 790-804; discussion 804-795.

Grimm D, Kay MA, and Kleinschmidt JA (2003) Helper virus-free, optically controllable, and two-plasmid-based production of adeno-associated virus vectors of serotypes 1 to 6. *Mol Ther* 7: 839-850.

Gross CG (1998) Galen and the squealing pig. *Neuroscientist* 4: 216-221.

Grundy D (2002) Neuroanatomy of visceral nociception: vagal and splanchnic afferent. *Gut* 51 Suppl 1: i2-5.

Haase AT (1986) Pathogenesis of lentivirus infections. *Nature* 322: 130-136.

Habler HJ, Janig W, and Michaelis M (1994) Respiratory modulation in the activity of sympathetic neurones. *Prog Neurobiol* 43: 567-606.

Hafner AS, Donlin-Asp PG, Leitch B, Herzog E, and Schuman EM (2019) Local protein synthesis is a ubiquitous feature of neuronal pre- and postsynaptic compartments. *Science* 364: eaau3644.

Haidar M, Guevremont G, Zhang C, Bathgate RAD, Timofeeva E, Smith CM, and Gundlach AL (2017) Relaxin-3 inputs target hippocampal interneurons and deletion of hilar relaxin-3 receptors in “floxed-RXFP3" mice impairs spatial memory. *Hippocampus* 27: 529-546.

Haidar M, Tin K, Zhang C, Nategh M, Covita J, Wykes AD, Rogers J, and Gundlach AL (2019) Septal GABA and glutamate neurons express RXFP3 mRNA and depletion of septal RXFP3 impaired spatial search strategy and long-term reference memory in adult mice. *Front Neuroanat* 13: 30.

Han HA, Pang JKS, and Soh BS (2020) Mitigating off-target effects in CRISPR/Cas9-mediated in vivo gene editing. *J Mol Med (Berl)* 98: 615-632.

Han W, Tellez LA, Rangel MJ, Jr., Motta SC, Zhang X, Perez IO, Canteras NS, Shammah-Lagnado SJ, et al. (2017) Integrated control of predatory hunting by the central nucleus of the amygdala. *Cell* 168: 311-324 e318.

Harlow JM (1993) Recovery from the passage of an iron bar through the head. *Hist Psychiatry* 4: 274-281.

Harrer MI, and Travers SP (1996) Topographic organization of Fos-like immunoreactivity in the rostral nucleus of the solitary tract evoked by gustatory stimulation with sucrose and quinine. *Brain Res* 711: 125-137.

Harrington AW, and Ginty DD (2013) Long-distance retrograde neurotrophic factor signalling in neurons. *Nat Rev Neurosci* 14: 177-187.

Harris KD, and Mrsic-Flogel TD (2013) Cortical connectivity and sensory coding. *Nature* 503: 51-58.

Hartl DL, and Orel V (1992) What did Gregor Mendel think he discovered? *Genetics* 131: 245-253.

Haselton JR, and Guyenet PG (1989) Central respiratory modulation of medullary sympathoexcitatory neurons in rat. *Am J Physiol* 256: R739-750.

Havlak P, Chen R, Durbin KJ, Egan A, Ren Y, Song XZ, Weinstock GM, and Gibbs RA (2004) The Atlas genome assembly system. *Genome Res* 14: 721-732.

Hayano J, Yasuma F, Okada A, Mukai S, and Fujinami T (1996) Respiratory sinus arrhythmia. A phenomenon improving pulmonary gas exchange and circulatory efficiency. *Circulation* 94: 842-847.

Hayashi-Takagi A, Yagishita S, Nakamura M, Shirai F, Wu YI, Loshbaugh AL, Kuhlman B, Hahn KM, et al. (2015) Labelling and optical erasure of synaptic memory traces in the motor cortex. *Nature* 525: 333-338.

Hedstrom KL, Ogawa Y, and Rasband MN (2008) AnkyrinG is required for maintenance of the axon initial segment and neuronal polarity. *J Cell Biol* 183: 635-640.

Heidemann SR, Landers JM, and Hamborg MA (1981) Polarity orientation of axonal microtubules. *J Cell Biol* 91: 661-665.

Heinrichs A (2009) Stains and fluorescent dyes. *Nat Cell Biol* 11: S7-S7.

Henke PG (1980) The centromedial amygdala and gastric pathology in rats. *Physiol Behav* 25: 107-112.

Hernandez DE, Salaiz AB, Morin P, and Moreira MA (1990) Administration of thyrotropin-releasing-hormone into the central nucleus of the amygdala Induces gastric-lesions in rats. *Brain Res Bull* 24: 697-699.

Hershey AD, and Chase M (1952) Independent functions of viral protein and nucleic acid in growth of bacteriophage. *J Gen Physiol* 36: 39-56.

Higgins GA, and Schwaber JS (1983) Somatostatinergic projections from the central nucleus of the amygdala to the vagal nuclei. *Peptides* 4: 657-662.

Hillarp NA, Fuxe K, and Dahlstro.A (1966) Demonstration and mapping of central neurons containing dopamine, noradrenaline, and 5-hydroxytryptamine and their reactions to psychopharmaca. *Pharmacol Rev* 18: 727-&.

Hnasko TS, Perez FA, Scouras AD, Stoll EA, Gale SD, Luquet S, Phillips PE, Kremer EJ, et al. (2006) Cre recombinase-mediated restoration of nigrostriatal dopamine in dopamine-deficient mice reverses hypophagia and bradykinesia. *Proc Natl Acad Sci U S A* 103: 8858-8863.

Holtzman DM, Kilbridge J, Li YW, Cunningham ET, Lenn NJ, Clary DO, Reichardt LF, and Mobley WC (1995) TrkA expression in the CNS - Evidence for the existence of several novel NGF-responsive CNS neurons. *J Neurosci* 15: 1567-1576.

Hopkins DA, and Holstege G (1978) Amygdaloid projections to the mesencephalon, pons and medulla oblongata in the cat. *Exp Brain Res* 32: 529-547.

Hosken IT, Sutton SW, Smith CM, and Gundlach AL (2015) Relaxin-3 receptor (Rxfp3) gene knockout mice display reduced running wheel activity: implications for role of relaxin-3/RXFP3 signalling in sustained arousal. *Behav Brain Res* 278: 167-175.

Hubner CA, Stein V, Hermans-Borgmeyer I, Meyer T, Ballanyi K, and Jentsch TJ (2001) Disruption of KCC2 reveals an essential role of K-Cl cotransport already in early synaptic inhibition. *Neuron* 30: 515-524.

Hudry E, Andres-Mateos E, Lerner EP, Volak A, Cohen O, Hyman BT, Maguire CA, and Vandenberghe LH (2018) Efficient gene transfer to the central nervous system by single-stranded Anc80L65. *Mol Ther Methods Clin Dev* 10: 197-209.

Hudry E, and Vandenberghe LH (2019) Therapeutic AAV gene transfer to the nervous system: a clinical reality. *Neuron* 102: 263.

Hughes A (1955) Studies in the history of microscopy. *J R Microsc Soc* 75: 1-22.

Huxley A (2002) From overshoot to voltage clamp. *Trends Neurosci* 25: 553-558.

Ideker RE, Kong W, and Pogwizd S (2009) Purkinje fibers and arrhythmias. *Pacing Clin Electrophysiol* 32: 283-285.

Iwata J, Chida K, and Ledoux JE (1987) Cardiovascular-responses elicited by stimulation of neurons in the central amygdaloid nucleus in awake but not anesthetized rats resemble conditioned emotional responses. *Brain Res* 418: 183-188.

Jahn R, and Scheller RH (2006) SNAREs--engines for membrane fusion. *Nat Rev Mol Cell Biol* 7: 631-643.

Janak PH, and Tye KM (2015) From circuits to behaviour in the amygdala. *Nature* 517: 284-292.

Janbandhu VC, Moik D, and Fassler R (2014) Cre recombinase induces DNA damage and tetraploidy in the absence of loxP sites. *Cell Cycle* 13: 462-470.

Janke C, and Bulinski JC (2011) Post-translational regulation of the microtubule cytoskeleton: mechanisms and functions. *Nat Rev Mol Cell Biol* 12: 773-786.

Jing M, Li Y, Zeng J, Huang P, Skirzewski M, Kljakic O, Peng W, Qian T, et al. (2020) An optimized acetylcholine sensor for monitoring in vivo cholinergic activity. *Nat Methods*.

Jones BE (2003) Arousal systems. *Front Biosci* 8: s438-451.

Jones EG (1994) The neuron doctrine 1891. *J Hist Neurosci* 3: 3-20.

Jones ML (2001) To fix, to harden, to preserve-fixation: a brief history. *J Histotechnol* 24: 155-162.

Kaila K, Price TJ, Payne JA, Puskarjov M, and Voipio J (2014) Cation-chloride cotransporters in neuronal development, plasticity and disease. *Nat Rev Neurosci* 15: 637-654.

Kakava-Georgiadou N, Bullich-Vilarrubias C, Zwartkruis MM, Luijendijk MCM, Garner KM, and Adan RAH (2019) Considerations related to the use of short neuropeptide promoters in viral vectors targeting hypothalamic neurons. *Sci Rep* 9: 11146.

Kallal L, and Benovic JL (2000) Using green fluorescent proteins to study G-protein-coupled receptor localization and trafficking. *Trends Pharmacol Sci* 21: 175-180.

Kang Y, and Lundy RF (2010) Amygdalofugal influence on processing of taste information in the nucleus of the solitary tract of the rat. *J Neurophysiol* 104: 726-741.

Kania A, Gugula A, Grabowiecka A, de Avila C, Blasiak T, Rajfur Z, Lewandowski MH, Hess G, et al. (2017) Inhibition of oxytocin and vasopressin neuron activity in rat hypothalamic paraventricular nucleus by relaxin-3-RXFP3 signalling. *J Physiol (London)* 595: 3425-3447.

Kaplitt MG, Leone P, Samulski RJ, Xiao X, Pfaff DW, Omalley KL, and During MJ (1994) Long-term gene expression and phenotypic correction using adeno-associated virus vectors in the mammalian brain. *Nat Genet* 8: 148-154.

Kaspar BK, Vissel B, Bengoechea T, Crone S, Randolph-Moore L, Muller R, Brandon EP, Schaffer D, et al. (2002) Adeno-associated virus effectively mediates conditional gene modification in the brain. *Proc Natl Acad Sci U S A* 99: 2320-2325.

Kastman HE, Blasiak A, Walker L, Siwiec M, Krstew EV, Gundlach AL, and Lawrence AJ (2016) Nucleus incertus Orexin2 receptors mediate alcohol seeking in rats. *Neuropharmacology* 110: 82-91.

Kelliher MT, Saunders HA, and Wildonger J (2019) Microtubule control of functional architecture in neurons. *Curr Opin Neurobiol* 57: 39-45.

Kent WJ (2002) BLAT--the BLAST-like alignment tool. *Genome Res* 12: 656-664.

Kent WJ, Sugnet CW, Furey TS, Roskin KM, Pringle TH, Zahler AM, and Haussler D (2002) The human genome browser at UCSC. *Genome Res* 12: 996-1006.

Keros T, Borovecki F, Jemersic L, Konjevic D, Roic B, and Balatinec J (2010) The centenary progress of molecular genetics. A 100th anniversary of T. H. Morgan's discoveries. *Coll Antropol* 34: 1167-1174.

Keynes R (2005) J.Z. and the discovery of squid giant nerve fibres. *J Exp Biol* 208: 179-180.

Killip T, 3rd (1962) Oscillation of blood flow and vascular resistance during Mayer waves. *Circ Res* 11: 987-993.

Kim CK, Adhikari A, and Deisseroth K (2017) Integration of optogenetics with complementary methodologies in systems neuroscience. *Nat Rev Neurosci* 18: 222-235.

Kim J, Zhao T, Petralia RS, Yu Y, Peng HC, Myers E, and Magee JC (2012) mGRASP enables mapping mammalian synaptic connectivity with light microscopy. *Nat Methods* 9: 96-U139.

Kim J, Yamanaka K, Tsukioka K, and Waki H (2020) Potential role of the amygdala and posterior claustrum in exercise intensity-dependent cardiovascular regulation in rats. *Neuroscience* 432: 150-159.

Kim YS, Kato HE, Yamashita K, Ito S, Inoue K, Ramakrishnan C, Fenno LE, Evans KE, et al. (2018) Crystal structure of the natural anion-conducting channelrhodopsin GtACR1. *Nature* 561: 343-348.

Kinch MS (2015) An overview of FDA-approved biologics medicines. *Drug Discov Today* 20: 393-398.

Kirshner HS, Casey PF, Henson J, and Heinrich JJ (1989) Behavioral features and lesion localization in Wernickes' aphasia. *Aphasiology* 3: 169-176.

Kizawa H, Nishi K, Ishibashi Y, Harada M, Asano T, Ito Y, Suzuki N, Hinuma S, et al. (2003) Production of recombinant human relaxin 3 in AtT20 cells. *Regul Pept* 113: 79-84.

Kobayashi K, Inoue K, Tanabe S, Kato S, Takada M, and Kobayashi K (2017) Pseudotyped lentiviral vectors for retrograde gene delivery into target brain regions. *Front Neuroanat* 11.

Kobayashi T, Storrie B, Simons K, and Dotti CG (1992) A functional barrier to movement of lipids in polarized neurons. *Nature* 359: 647-650.

Koelle GB (1950) The histochemical differentiation of types of cholinesterases and their localizations in tissues of the cat. *J Pharmacol Exp Ther* 100: 158-179.

Koeppen AH (2004) Wallerian degeneration: history and clinical significance. *J Neurol Sci* 220: 115-117.

Krettek JE, and Price JL (1978) Amygdaloid projections to subcortical structures within the basal forebrain and brainstem in the rat and cat. *J Comp Neurol* 178: 225-254.

Kubota Y, Inagaki S, Shiosaka S, Cho HJ, Tateishi K, Hashimura E, Hamaoka T, and Tohyama M (1983) The distribution of cholecystokinin octapeptide-like structures in the lower brain stem of the rat: an immunohistochemical analysis. *Neuroscience* 9: 587-604.

Kumagai H, Oshima N, Matsuura T, Iigaya K, Imai M, Onimaru H, Sakata K, Osaka M, et al. (2012) Importance of rostral ventrolateral medulla neurons in determining efferent sympathetic nerve activity and blood pressure. *Hypertens Res* 35: 132-141.

Kumar JR, Rajkumar R, Farooq U, Lee LC, Tan FC, and Dawe GS (2015) Evidence of D2 receptor expression in the nucleus incertus of the rat. *Physiol Behav* 151: 525-534.

Kumar JR, Rajkumar R, Lee LC, and Dawe GS (2016) Nucleus incertus contributes to an anxiogenic effect of buspirone in rats: Involvement of 5-HT1A receptors. *Neuropharmacology* 110: 1-14.

Kumar JR, Rajkumar R, Jayakody T, Marwari S, Hong JM, Ma S, Gundlach AL, Lai MKP, et al. (2017) Relaxin' the brain: a case for targeting the nucleus incertus network and relaxin-3/RXFP3 system in neuropsychiatric disorders. *Br J Pharmacol* 174: 1061-1076.

Kumar SR, Miles TF, Chen X, Brown D, Dobreva T, Huang Q, Ding X, Luo Y, et al. (2020) Multiplexed Cre-dependent selection yields systemic AAVs for targeting distinct brain cell types. *Nat Methods* 17: 541-550.

Kunda P, Paglini G, Quiroga S, Kosik K, and Caceres A (2001) Evidence for the involvement of Tiam1 in axon formation. *J Neurosci* 21: 2361-2372.

Ladino LD, Rizvi S, and Tellez-Zenteno JF (2018) The Montreal procedure: the legacy of the great Wilder Penfield. *Epilepsy Behav* 83: 151-161.

Lambert TJ (2019) FPbase: a community-editable fluorescent protein database. *Nat Methods* 16: 277-278.

Lander ES, Linton LM, Birren B, Nusbaum C, Zody MC, Baldwin J, Devon K, Dewar K, et al. (2001) Initial sequencing and analysis of the human genome. *Nature* 409: 860-921.

Lanska DJ, and Lanska JR (2013) Juan Valverde de Hamusco's unauthorized reproduction of a brain dissection by Andreas Vesalius. *Neurology* 80: 852-856.

Lavail JH, Winston KR, and Tish A (1973) A method based on retrograde intraaxonal transport of protein for identification of cell bodies of origin of axons terminating within the CNS. *Brain Res* 58: 470-477.

Lazar RM, and Mohr JP (2011) Revisiting the contributions of Paul Broca to the study of aphasia. *Neuropsychol Rev* 21: 236-239.

Lechner HA, Lein ES, and Callaway EM (2002) A genetic method for selective and quickly reversible silencing of mammalian neurons. *J Neurosci* 22: 5287-5290.

LeDoux JE, Iwata J, Cicchetti P, and Reis DJ (1988) Different projections of the central amygdaloid nucleus mediate autonomic and behavioral correlates of conditioned fear. *J Neurosci* 8: 2517-2529.

Lefler Y, Campagner D, and Branco T (2020) The role of the periaqueductal gray in escape behavior. *Curr Opin Neurobiol* 60: 115-121.

Lerner TN, Shilyansky C, Davidson TJ, Evans KE, Beier KT, Zalocusky KA, Crow AK, Malenka RC, et al. (2015) Intact-brain analyses reveal distinct information carried by SNc dopamine subcircuits. *Cell* 162: 635-647.

Li C, and Samulski RJ (2020) Engineering adeno-associated virus vectors for gene therapy. *Nat Rev Genet* 21: 255-272.

Li CS, Cho YK, and Smith DV (2002) Taste responses of neurons in the hamster solitary nucleus are modulated by the central nucleus of the amygdala. *J Neurophysiol* 88: 2979-2992.

Li H, Huang CY, Govorunova EG, Schafer CT, Sineshchekov OA, Wang M, Zheng L, and Spudich JL (2019) Crystal structure of a natural light-gated anion channelrhodopsin. *Elife* 8.

Li SJ, Vaughan A, Sturgill JF, and Kepecs A (2018) A viral receptor complementation strategy to overcome CAV-2 tropism for efficient retrograde targeting of neurons. *Neuron* 98: 905-917 e905.

Liang H, Paxinos G, and Watson C (2011) Projections from the brain to the spinal cord in the mouse. *Brain Struct Funct* 215: 159-186.

Lim ST, Antonucci DE, Scannevin RH, and Trimmer JS (2000) A novel targeting signal for proximal clustering of the Kv2.1 K+ channel in hippocampal neurons. *Neuron* 25: 385-397.

Lin D, Boyle MP, Dollar P, Lee H, Lein ES, Perona P, and Anderson DJ (2011) Functional identification of an aggression locus in the mouse hypothalamus. *Nature* 470: 221-226.

Lin MZ, and Schnitzer MJ (2016) Genetically encoded indicators of neuronal activity. *Nat Neurosci* 19: 1142-1153.

Liu B, Paton JF, and Kasparov S (2008) Viral vectors based on bidirectional cell-specific mammalian promoters and transcriptional amplification strategy for use in vitro and in vivo. *BMC Biotechnol* 8: 49.

Liu CL, Eriste E, Sutton S, Chen JC, Roland B, Kuei C, Farmer N, Jornvall H, et al. (2003) Identification of relaxin-3/INSL7 as an endogenous ligand for the orphan G-protein-coupled receptor GPCR135. *J Biol Chem* 278: 50754-50764.

Liubashina O, Bagaev V, and Khotiantsev S (2002) Amygdalofugal modulation of the vago-vagal gastric motor reflex in rat. *Neurosci Lett* 325: 183-186.

Livet J, Weissman TA, Kang H, Draft RW, Lu J, Bennis RA, Sanes JR, and Lichtman JW (2007) Transgenic strategies for combinatorial expression of fluorescent proteins in the nervous system. *Nature* 450: 56-62.

Llinas RR (2003) The contribution of Santiago Ramon y Cajal to functional neuroscience. *Nat Rev Neurosci* 4: 77-80.

Loewi O (1945) Chemical transmission of nerve impulses. *Am Sci* 33: 159-174.

Lopez-Munoz F, Boya J, and Alamo C (2006) Neuron theory, the cornerstone of neuroscience, on the centenary of the Nobel Prize award to Santiago Ramon y Cajal. *Brain Res Bull* 70: 391-405.

Luo L, Ambrozkiewicz MC, Benseler F, Chen C, Dumontier E, Falkner S, Furlanis E, Gomez AM, et al. (2020) Optimizing nervous system-specific gene targeting with Cre driver lines: prevalence of germline recombination and influencing factors. *Neuron* 106: 37-65 e35.

Luria SE, Adams JN, and Ting RC (1960) Transduction of lactose-utilizing ability among strains of E. coli and S. dysenteriae and the properties of the transducing phage particles. *Virology* 12: 348-390.

Lyubashina OA (2004) Possible mechanisms of involvement of the amygdaloid complex in the control of gastric motor function. *Neurosci Behav Physiol* 34: 379-388.

Ma L, Merenmies J, and Parada LF (2000) Molecular characterization of the TrkA/NGF receptor minimal enhancer reveals regulation by multiple cis elements to drive embryonic neuron expression. *Development* 127: 3777-3788.

Ma S, Bonaventure P, Ferraro T, Shen PJ, Burazin TC, Bathgate RA, Liu C, Tregear GW, et al. (2007) Relaxin-3 in GABA projection neurons of nucleus incertus suggests widespread influence on forebrain circuits via G-protein-coupled receptor-135 in the rat. *Neuroscience* 144: 165-190.

Ma S, Olucha-Bordonau FE, Hossain MA, Lin F, Kuei C, Liu CL, Wade JD, Sutton SW, et al. (2009a) Modulation of hippocampal theta oscillations and spatial memory by relaxin-3 neurons of the nucleus incertus. *Learn Memory* 16: 730-742.

Ma S, Sang Q, Lanciego JL, and Gundlach AL (2009b) Localization of relaxin-3 in brain of Macaca fascicularis: Identification of a nucleus incertus in primate. *J Comp Neurol* 517: 856-872.

Ma S, Blasiak A, Olucha-Bordonau FE, Verberne AJM, and Gundlach AL (2013) Heterogeneous responses of nucleus incertus neurons to corticotrophin-releasing factor and coherent activity with hippocampal theta rhythm in the rat. *J Physiol (London)* 591: 3981-4001.

Ma S, and Gundlach AL (2015) Ascending control of arousal and motivation: role of nucleus incertus and its peptide neuromodulators in behavioural responses to stress. *J Neuroendocrinol* 27: 457-467.

Ma S, Allocca G, Ong-Palsson EKE, Singleton CE, Hawkes D, McDougall SJ, Williams SJ, Bathgate RAD, et al. (2017a) Nucleus incertus promotes cortical desynchronization and behavioral arousal. *Brain Struct Funct* 222: 515-537.

Ma S, Smith CM, Blasiak A, and Gundlach AL (2017b) Distribution, physiology and pharmacology of relaxin-3/RXFP3 systems in brain. *Br J Pharmacol* 174: 1034-1048.

Ma S, Hangya B, Leonard CS, Wisden W, and Gundlach AL (2018) Dual-transmitter systems regulating arousal, attention, learning and memory. *Neurosci Biobehav Rev* 85: 21-33.

MacGillavry HD, Kerr JM, and Blanpied TA (2011) Lateral organization of the postsynaptic density. *Mol Cell Neurosci* 48: 321-331.

Machado BH, Mauad H, Chianca Junior DA, Haibara AS, and Colombari E (1997) Autonomic processing of the cardiovascular reflexes in the nucleus tractus solitarii. *Braz J Med Biol Res* 30: 533-543.

Macmillan M (1992) Inhibition and the control of behavior: from Gall to Freud via Phineas Gauge and the frontal lobes. *Brain Cognition* 19: 72-104.

Madisen L, Garner AR, Shimaoka D, Chuong AS, Klapoetke NC, Li L, van der Bourg A, Niino Y, et al. (2015) Transgenic mice for intersectional targeting of neural sensors and effectors with high specificity and performance. *Neuron* 85: 942-958.

Maehle AH (2004) "Receptive substances": John Newport Langley (1852-1925) and his path to a receptor theory of drug action. *Med Hist* 48: 153-174.

Magnus CJ, Lee PH, Atasoy D, Su HH, Looger LL, and Sternson SM (2011) Chemical and genetic engineering of selective ion channel-ligand interactions. *Science* 333: 1292-1296.

Magnus CJ, Lee PH, Bonaventura J, Zemla R, Gomez JL, Ramirez MH, Hu X, Galvan A, et al. (2019) Ultrapotent chemogenetics for research and potential clinical applications. *Science* 364.

Mahn M, Prigge M, Ron S, Levy R, and Yizhar O (2016) Biophysical constraints of optogenetic inhibition at presynaptic terminals. *Nat Neurosci* 19: 554-556.

Mahn M, Gibor L, Patil P, Cohen-Kashi Malina K, Oring S, Printz Y, Levy R, Lampl I, et al. (2018) High-efficiency optogenetic silencing with soma-targeted anion-conducting channelrhodopsins. *Nat Commun* 9: 4125.

Mahn M, Klavir O, and Yizhar O. 2020. 'Optogenetic modulation of neural circuits.' in F. S. Pavone and S. Shoham (eds.), *Handbook of Neurophotonics* (CRC Press: Boca Raton, FL).

Malyshev AY, Roshchin MV, Smirnova GR, Dolgikh DA, Balaban PM, and Ostrovsky MA (2017) Chloride conducting light activated channel GtACR2 can produce both cessation of firing and generation of action potentials in cortical neurons in response to light. *Neurosci Lett* 640: 76-80.

Mansour SL, Thomas KR, and Capecchi MR (1988) Disruption of the proto-oncogene int-2 in mouse embryo-derived stem cells: a general strategy for targeting mutations to non-selectable genes. *Nature* 336: 348-352.

Mao T, O'Connor DH, Scheuss V, Nakai J, and Svoboda K (2008) Characterization and subcellular targeting of GCaMP-type genetically-encoded calcium indicators. *PLoS One* 3.

Masaoka Y, Hirasawa K, Yamane F, Hori T, and Homma I (2003) Effects of left amygdala lesions on respiration, skin conductance, heart rate, anxiety, and activity of the right amygdala during anticipation of negative stimulus. *Behav Mod* 27: 607-619.

Mattis J, Tye KM, Ferenczi EA, Ramakrishnan C, O'Shea DJ, Prakash R, Gunaydin LA, Hyun M, et al. (2011) Principles for applying optogenetic tools derived from direct comparative analysis of microbial opsins. *Nat Methods* 9: 159-172.

Matz MV, Fradkov AF, Labas YA, Savitsky AP, Zaraisky AG, Markelov ML, and Lukyanov SA (1999) Fluorescent proteins from nonbioluminescent Anthozoa species. *Nat Biotechnol* 17: 969-973.

May OL, and Hill DL (2006) Gustatory terminal field organization and developmental plasticity in the nucleus of the solitary tract revealed through triple-fluorescence labeling. *J Comp Neurol* 497: 658-669.

Mazzarello P (1999) A unifying concept: the history of cell theory. *Nat Cell Biol* 1: E13-15.

McGowan BM, Stanley SA, Smith KL, Minnion JS, Donovan J, Thompson EL, Patterson M, Connolly MM, et al. (2006) Effects of acute and chronic relaxin-3 on food intake and energy expenditure in rats. *Regul Pept* 136: 72-77.

Meister M (2016) Physical limits to magnetogenetics. *Elife* 5: e17210.

Meng Y, Hynynen K, and Lipsman N (2020) Applications of focused ultrasound in the brain: from thermoablation to drug delivery. *Nat Rev Neurol* 17: 7–22.

Menuet C, Sevigny CP, Connelly AA, Bassi JK, Jancovski N, Williams DA, Anderson CR, Llewellyn-Smith IJ, et al. (2014) Catecholaminergic C3 neurons are sympathoexcitatory and involved in glucose homeostasis. *J Neurosci* 34: 15110-15122.

Menuet C, Le S, Dempsey B, Connelly AA, Kamar JL, Jancovski N, Bassi JK, Walters K, et al. (2017) Excessive respiratory modulation of blood pressure triggers hypertension. *Cell Metab* 25: 739-748.

Mertz JE, and Davis RW (1972) Cleavage of DNA by RI restriction endonuclease generates cohesive ends. *Proc Natl Acad Sci U S A* 69: 3370-3374.

Messier JE, Chen H, Cai ZL, and Xue M (2018) Targeting light-gated chloride channels to neuronal somatodendritic domain reduces their excitatory effect in the axon. *Elife* 7: e38506.

Miesenbock G, De Angelis DA, and Rothman JE (1998) Visualizing secretion and synaptic transmission with pH-sensitive green fluorescent proteins. *Nature* 394: 192-195.

Miyamoto Y, Watanabe Y, and Tanaka M (2008) Developmental expression and serotonergic regulation of relaxin 3/INSL7 in the nucleus incertus of rat brain. *Regul Pept* 145: 54-59.

Miyawaki A, Llopis J, Heim R, McCaffery JM, Adams JA, Ikura M, and Tsien RY (1997) Fluorescent indicators for Ca2+ based on green fluorescent proteins and calmodulin. *Nature* 388: 882-887.

Miyawaki A (2005) Innovations in the imaging of brain functions using fluorescent proteins. *Neuron* 48: 189-199.

Mizuno N, Takahashi O, Satoda T, and Matsushima R (1985) Amygdalospinal projections in the macaque monkey. *Neurosci Lett* 53: 327-330.

Mogenson GJ, and Calaresu FR (1973) Cardiovascular responses to electrical stimulation of the amygdala in the rat. *Exp Neurol* 39: 166-180.

Molnar Z, and Brown RE (2010) Insights into the life and work of Sir Charles Sherrington. *Nat Rev Neurosci* 11: 429-436.

Morrow JF, Cohen SN, Chang AC, Boyer HW, Goodman HM, and Helling RB (1974) Replication and transcription of eukaryotic DNA in Escherichia coli. *Proc Natl Acad Sci U S A* 71: 1743-1747.

Moruzzi G (1996) The electrophysiological work of Carlo Matteucci. *Brain Res Bull* 40: 69-91.

Mouse Genome Sequencing Consortium, Waterston RH, Lindblad-Toh K, Birney E, Rogers J, Abril JF, Agarwal P, Agarwala R, et al. (2002) Initial sequencing and comparative analysis of the mouse genome. *Nature* 420: 520-562.

Mulckhuyse M, and Theeuwes J (2010) Unconscious attentional orienting to exogenous cues: A review of the literature. *Acta Psychol (Amst)* 134: 299-309.

Mulligan RC, and Berg P (1980) Expression of a bacterial gene in mammalian-cells. *Science* 209: 1422-1427.

Munshi R, Qadri SM, Zhang Q, Castellanos Rubio I, Del Pino P, and Pralle A (2017) Magnetothermal genetic deep brain stimulation of motor behaviors in awake, freely moving mice. *Elife* 6: e27069.

Myelnikov D (2019) Tinkering with genes and embryos: the multiple invention of transgenic mice c. 1980. *Hist Technol* 35: 425-452.

Nagel G, Szellas T, Huhn W, Kateriya S, Adeishvili N, Berthold P, Ollig D, Hegemann P, et al. (2003) Channelrhodopsin-2, a directly light-gated cation-selective membrane channel. *Proc Natl Acad Sci U S A* 100: 13940-13945.

Nagy FZ, and Pare D (2008) Timing of impulses from the central amygdala and bed nucleus of the stria terminalis to the brain stem. *J Neurophysiol* 100: 3429-3436.

Nakada C, Ritchie K, Oba Y, Nakamura M, Hotta Y, Iino R, Kasai RS, Yamaguchi K, et al. (2003) Accumulation of anchored proteins forms membrane diffusion barriers during neuronal polarization. *Nat Cell Biol* 5: 626-632.

Nakagawa T, Katsuya A, Tanimoto S, Yamamoto J, Yamauchi Y, Minami M, and Satoh M (2003) Differential patterns of c-fos mRNA expression in the amygdaloid nuclei induced by chemical somatic and visceral noxious stimuli in rats. *Neurosci Lett* 344: 197-200.

Naldini L, Blomer U, Gallay P, Ory D, Mulligan R, Gage FH, Verma IM, and Trono D (1996) In vivo gene delivery and stable transduction of nondividing cells by a lentiviral vector. *Science* 272: 263-267.

Namburi P, Al-Hasani R, Calhoon GG, Bruchas MR, and Tye KM (2016) Architectural representation of valence in the limbic system. *Neuropsychopharmacology* 41: 1697-1715.

Nasirova N, Quina LA, Morton G, Walker A, and Turner EE (2020) Mapping cell types and efferent pathways in the ascending relaxin-3 system of the nucleus incertus. *eNeuro* 7: 1-23.

Nectow AR, and Nestler EJ (2020) Viral tools for neuroscience. *Nat Rev Neurosci* 21: 669-681.

Neher E, and Sakmann B (1992) The patch clamp technique. *Sci Am* 266: 44-51.

Neupert C, Schneider R, Klatt O, Reissner C, Repetto D, Biermann B, Niesmann K, Missler M, et al. (2015) Regulated dynamic trafficking of neurexins inside and outside of synaptic terminals. *J Neurosci* 35: 13629-13647.

Ngo HB, Melo MR, Layfield S, Connelly AA, Bassi JK, Xie L, Menuet C, McDougall SJ, et al. (2020) A chemogenetic tool that enables functional neural circuit analysis. *Cell Rep* 32.

Nirschl JJ, Ghiretti AE, and Holzbaur ELF (2017) The impact of cytoskeletal organization on the local regulation of neuronal transport. *Nat Rev Neurosci* 18: 585-597.

Nosaka S, Yamamoto T, and Yasunaga K (1979) Localization of vagal cardioinhibitory preganglionic neurons with rat brain stem. *J Comp Neurol* 186: 79-92.

Nudo RJ, and Masterton RB (1988) Descending pathways to the spinal cord: a comparative study of 22 mammals. *J Comp Neurol* 277: 53-79.

O'Gorman S, Fox DT, and Wahl GM (1991) Recombinase-mediated gene activation and site-specific integration in mammalian-cells. *Science* 251: 1351-1355.

Obata K, Oide M, and Tanaka H (1978) Excitatory and inhibitory actions of GABA and glycine on embryonic chick spinal neurons in culture. *Brain Res* 144: 179-184.

Ogawa Y, and Rasband MN (2008) The functional organization and assembly of the axon initial segment. *Curr Opin Neurobiol* 18: 307-313.

Okada A, Lansford R, Weimann JM, Fraser SE, and McConnell SK (1999) Imaging cells in the developing nervous system with retrovirus expressing modified green fluorescent protein. *Exp Neurol* 156: 394-406.

Okada Y, Yamazaki H, Sekine-Aizawa Y, and Hirokawa N (1995) The neuron-specific kinesin superfamily protein KIF1A is a unique monomeric motor for anterograde axonal transport of synaptic vesicle precursors. *Cell* 81: 769-780.

Olucha-Bordonau FE, Teruel V, Barcia-Gonzalez J, Ruiz-Torner A, Valverde-Navarro AA, and Martinez-Soriano F (2003) Cytoarchitecture and efferent projections of the nucleus incertus of the rat. *J Comp Neurol* 464: 62-97.

Onai T, Takayama K, and Miura M (1987) Projections to areas of the nucleus tractus solitarii related to circulatory and respiratory responses in cats. *J Auton Nerv Syst* 18: 163-175.

Ormo M, Cubitt AB, Kallio K, Gross LA, Tsien RY, and Remington SJ (1996) Crystal structure of the Aequorea victoria green fluorescent protein. *Science* 273: 1392-1395.

Owen SF, Liu MH, and Kreitzer AC (2019) Thermal constraints on in vivo optogenetic manipulations. *Nat Neurosci* 22: 1061-1065.

Pace-Schott EF, Amole MC, Aue T, Balconi M, Bylsma LM, Critchley H, Demaree HA, Friedman BH, et al. (2019) Physiological feelings. *Neurosci Biobehav Rev* 103: 267-304.

Packer AM, Roska B, and Hausser M (2013) Targeting neurons and photons for optogenetics. *Nat Neurosci* 16: 805-815.

Parent A (2003) Auguste Forel on ants and neurology. *Can J Neurol Sci* 30: 284-291.

Parent A (2004) Giovanni Aldini: from animal electricity to human brain stimulation. *Can J Neurol Sci* 31: 576-584.

Parent A (2012) The history of the basal ganglia: the contribution of Karl Friedrich Burdach *Neurosci Med* 3: 374-379.

Patriarchi T, Cho JR, Merten K, Howe MW, Marley A, Xiong WH, Folk RW, Broussard GJ, et al. (2018) Ultrafast neuronal imaging of dopamine dynamics with designed genetically encoded sensors. *Science* 360.

Paxinos GC, P.; Wang, H.; Wang, P.Y. (1999) *Chemoarchitectonic Atlas of the Rat Brainstem,* Academic Press: San Diego, CA.

Paxinos GG, and Watson C. (2014) *The rat brain in stereotaxic coordinates,* Academic Press: San Diego.

Pearce JM (2009) Marie-Jean-Pierre Flourens (1794-1867) and cortical localization. *Eur Neurol* 61: 311-314.

Penfield W, and Boldrey E (1937) Somatic motor and sensory representation in the cerebral cortex of man as studied by electrical stimulation. *Brain* 60: 389-443.

Penzo MA, Robert V, and Li B (2014) Fear conditioning potentiates synaptic transmission onto long-range projection neurons in the lateral subdivision of central amygdala. *J Neurosci* 34: 2432-2437.

Peterka DS, Takahashi H, and Yuste R (2011) Imaging voltage in neurons. *Neuron* 69: 9-21.

Pevsner J (2002) Leonardo da Vinci's contributions to neuroscience. *Trends Neurosci* 25: 217-220.

Piccolino M (1998) Animal electricity and the birth of electrophysiology: the legacy of Luigi Galvani. *Brain Res Bull* 46: 381-407.

Piccolino M (2002) Fifty years of the Hodgkin-Huxley era. *Trends Neurosci* 25: 552-553.

Pickering AE, and Paton JF (2006) A decerebrate, artificially-perfused in situ preparation of rat: utility for the study of autonomic and nociceptive processing. *J Neurosci Methods* 155: 260-271.

Pillay S, Meyer NL, Puschnik AS, Davulcu O, Diep J, Ishikawa Y, Jae LT, Wosen JE, et al. (2016) An essential receptor for adeno-associated virus infection. *Nature* 530: 108-112.

Pitts RF (1946) Organization of the respiratory center. *Physiol Rev* 26: 609-630.

Poo MM, Pignatelli M, Ryan TJ, Tonegawa S, Bonhoeffer T, Martin KC, Rudenko A, Tsai LH, et al. (2016) What is memory? The present state of the engram. *Bmc Biology* 14.

Possenti L, and Selleri S (2017) Leopoldo Nobili: his galvanometer and his connections to the Faraday-Neuman-Lenz law of induction. *Radio Sci Bull*: 77-79.

Prasher DC, Eckenrode VK, Ward WW, Prendergast FG, and Cormier MJ (1992) Primary structure of the Aequorea victoria green-fluorescent protein. *Gene* 111: 229-233.

Preston AR, and Eichenbaum H (2013) Interplay of hippocampus and prefrontal cortex in memory. *Curr Biol* 23: R764-773.

Price GD, and Trussell LO (2006) Estimate of the chloride concentration in a central glutamatergic terminal: a gramicidin perforated-patch study on the calyx of Held. *J Neurosci* 26: 11432-11436.

Price JL, and Amaral DG (1981) An autoradiographic study of the projections of the central nucleus of the monkey amygdala. *J Neurosci* 1: 1242-1259.

Pushpalatha KV, and Besse F (2019) Local translation in axons: when membraneless RNP granules meet membrane-bound organelles. *Front Mol Biosci* 6: 129.

Rabut C, Yoo S, Hurt RC, Jin Z, Li H, Guo H, Ling B, and Shapiro MG (2020) Ultrasound technologies for imaging and modulating neural activity. *Neuron* 108: 93-110.

Rader KA. (2004) *Making mice: standardizing animals for American biomedical research, 1900-1955,* Princeton University Press.

Rajasethupathy P, Ferenczi E, and Deisseroth K (2016) Targeting neural circuits. *Cell* 165: 524-534.

Rao S, Chen R, LaRocca AA, Christiansen MG, Senko AW, Shi CH, Chiang PH, Varnavides G, et al. (2019) Remotely controlled chemomagnetic modulation of targeted neural circuits. *Nat Nanotechnol* 14: 967–973.

Rasband MN (2010) The axon initial segment and the maintenance of neuronal polarity. *Nat Rev Neurosci* 11: 552-562.

Ratiu P, Talos IF, Haker S, Lieberman D, and Everett P (2004) The tale of Phineas Gage, digitally remastered. *J Neurotrauma* 21: 637-643.

Reilly S, and Bornovalova MA (2005) Conditioned taste aversion and amygdala lesions in the rat: a critical review. *Neurosci Biobehav Rev* 29: 1067-1088.

Rengachary SS, Xavier A, Manjila S, Smerdon U, Parker B, Hadwan S, and Guthikonda M (2008) The legendary contributions of Thomas Willis (1621-1675): the arterial circle and beyond. *J Neurosurg* 109: 765-775.

Rinaman L, Levitt P, and Card JP (2000) Progressive postnatal assembly of limbic-autonomic circuits revealed by central transneuronal transport of pseudorabies virus. *J Neurosci* 20: 2731-2741.

Rinaman L, and Schwartz G (2004) Anterograde transneuronal viral tracing of central viscerosensory pathways in rats. *J Neurosci* 24: 2782-2786.

Rivera C, Voipio J, Payne JA, Ruusuvuori E, Lahtinen H, Lamsa K, Pirvola U, Saarma M, et al. (1999) The K+/Cl- co-transporter KCC2 renders GABA hyperpolarizing during neuronal maturation. *Nature* 397: 251-255.

Rivnay J, Wang H, Fenno L, Deisseroth K, and Malliaras GG (2017) Next-generation probes, particles, and proteins for neural interfacing. *Sci Adv* 3: e1601649.

Rocamora N, Pascual M, Acsady L, de Lecea L, Freund TF, and Soriano E (1996) Expression of NGF and NT3 mRNAs in hippocampal interneurons innervated by the GABAergic septohippocampal pathway. *J Neurosci* 16: 3991-4004.

Rodriguez EA, Tran GN, Gross LA, Crisp JL, Shu X, Lin JY, and Tsien RY (2016) A far-red fluorescent protein evolved from a cyanobacterial phycobiliprotein. *Nat Methods* 13: 763-769.

Rodriguez EA, Campbell RE, Lin JY, Lin MZ, Miyawaki A, Palmer AE, Shu X, Zhang J, et al. (2017) The growing and glowing toolbox of fluorescent and photoactive proteins. *Trends Biochem Sci* 42: 111-129.

Roozendaal B, Koolhaas JM, and Bohus B (1990) Differential effect of lesioning of the central amygdala on the bradycardiac and behavioral response of the rat in relation to conditioned social and solitary stress. *Behav Brain Res* 41: 39-48.

Rosen JB, Hitchcock JM, Sananes CB, Miserendino MJD, and Davis M (1991) A direct projection from the central nucleus of the amygdala to the acoustic startle pathway - Anterograde and retrograde tracing studies. *Behav Neurosci* 105: 817-825.

Rost BR, Schneider-Warme F, Schmitz D, and Hegemann P (2017) Optogenetic tools for subcellular applications in neuroscience. *Neuron* 96: 572-603.

Rothermel M, Brunert D, Zabawa C, Diaz-Quesada M, and Wachowiak M (2013) Transgene expression in target-defined neuron populations mediated by retrograde infection with adeno-associated viral vectors. *J Neurosci* 33: 15195-15206.

Ryan PJ, Buchler E, Shabanpoor F, Hossain MA, Wade JD, Lawrence AJ, and Gundlach AL (2013) Central relaxin-3 receptor (RXFP3) activation decreases anxiety- and depressive-like behaviours in the rat. *Behav Brain Res* 244: 142-151.

Rytova V, Ganella DE, Hawkes D, Bathgate RAD, Ma S, and Gundlach AL (2019) Chronic activation of the relaxin-3 receptor on GABA neurons in rat ventral hippocampus promotes anxiety and social avoidance. *Hippocampus*: doi: 10.1002/HIPO.23089.

Sacristan MP, de Diego JG, Bonilla M, and Martin-Zanca D (1999) Molecular cloning and characterization of the 5 ' region of the mouse trkA proto-oncogene. *Oncogene* 18: 5836-5842.

Saha S, Batten TF, and Henderson Z (2000) A GABAergic projection from the central nucleus of the amygdala to the nucleus of the solitary tract: a combined anterograde tracing and electron microscopic immunohistochemical study. *Neuroscience* 99: 613-626.

Saha S, Henderson Z, and Batten TFC (2002) Somatostatin immunoreactivity in axon terminals in rat nucleus tractus solitarii arising from central nucleus of amygdala: coexistence with GABA and postsynaptic expression of sst(2A) receptor. *J Chem Neuroanat* 24: 1-13.

Saha S, Gamboa-Esteves FO, and Batten TFC (2010) Differential distribution of 5-HT1A and 5-HT1B-like immunoreactivities in rat central nucleus of the amygdala neurones projecting to the caudal dorsomedial medulla oblongata. *Brain Res* 1330: 20-30.

Saleeba C, Dempsey B, Le S, Goodchild A, and McMullan S (2019) A student's guide to neural circuit tracing. *Front Neurosci* 13: 897.

Salinas S, Bilsland LG, Henaff D, Weston AE, Keriel A, Schiavo G, and Kremer EJ (2009) CAR-associated vesicular transport of an adenovirus in motor neuron axons. *PLoS Pathog* 5: e1000442.

Salmond GP, and Fineran PC (2015) A century of the phage: past, present and future. *Nat Rev Microbiol* 13: 777-786.

Sampo B, Kaech S, Kunz S, and Banker G (2003) Two distinct mechanisms target membrane proteins to the axonal surface. *Neuron* 37: 611-624.

Sandrew BB, Edwards DL, Poletti CE, and Foote WE (1986) Amygdalospinal projections in the cat. *Brain Res* 373: 235-239.

Sasse P (2018) Sympathetic control of cardiac output by noradrenaline: quasi-synaptic quantal release or interstitial diffusion and spillover? *J Physiol* 596: 2031-2032.

Sauer B, and Henderson N (1988) Site-specific DNA recombination in mammalian cells by the Cre recombinase of bacteriophage P1. *Proc Natl Acad Sci U S A* 85: 5166-5170.

Sawchenko PE, and Swanson LW (1981) A method for tracing biochemically defined pathways in the central nervous-system using combined fluorescence retrograde transport and immunohistochemical techniques. *Brain Res* 210: 31-51.

Sawin CT (1999) Ulf Svante von Euler (1905-1983) and the neurosecretion of norepinephrine. *Endocrinologist* 9: 327-330.

Schindelin J, Arganda-Carreras I, Frise E, Kaynig V, Longair M, Pietzsch T, Preibisch S, Rueden C, et al. (2012) Fiji: an open-source platform for biological-image analysis. *Nat Methods* 9: 676-682.

Schmidt EF, Kus L, Gong S, and Heintz N (2013) BAC transgenic mice and the GENSAT database of engineered mouse strains. *Cold Spring Harb Protoc* 2013.

Schnutgen F, Doerflinger N, Calleja C, Wendling O, Chambon P, and Ghyselinck NB (2003) A directional strategy for monitoring Cre-mediated recombination at the cellular level in the mouse. *Nat Biotechnol* 21: 562-565.

Schwaber JS, Kapp BS, and Higgins G (1980) The origin and extent of direct amygdala projections to the region of the dorsal motor nucleus of the vagus and the nucleus of the solitary tract. *Neurosci Lett* 20: 15-20.

Schwaber JS, Kapp BS, Higgins GA, and Rapp PR (1982) Amygdaloid and basal forebrain direct connections with the nucleus of the solitary tract and the dorsal motor nucleus. *J Neurosci* 2: 1424-1438.

Schwanzel-Fukuda M, Morrell JI, and Pfaff DW (1984) Localization of forebrain neurons which project directly to the medulla and spinal-cord of the rat by retrograde tracing with wheat-germ-agglutinin. *J Comp Neurol* 226: 1-20.

Schwarz J, Burguet J, Rampin O, Fromentin G, Andrey P, Tome D, Maurin Y, and Darcel N (2010) Three-dimensional macronutrient-associated Fos expression patterns in the mouse brainstem. *PLoS One* 5: e8974.

Scott DJ, Gunn NJ, Yong KJ, Wimmer VC, Veldhuis NA, Challis LM, Haidar M, Petrou S, et al. (2018) A novel ultra-stable, monomeric green fluorescent protein for direct volumetric imaging of whole organs using CLARITY. *Sci Rep* 8: 667.

Sevigny CP, Bassi J, Williams DA, Anderson CR, Thomas WG, and Allen AM (2012) Efferent projections of C3 adrenergic neurons in the rat central nervous system. *J Comp Neurol* 520: 2352-2368.

Shabanpoor F, Hossain MA, Ryan PJ, Belgi A, Layfield S, Kocan M, Zhang SD, Samuel CS, et al. (2012) Minimization of human relaxin-3 leading to high-affinity analogues with increased selectivity for relaxin-family peptide 3 receptor (RXFP3) over RXFP1. *J Med Chem* 55: 1671-1681.

Shaner NC, Campbell RE, Steinbach PA, Giepmans BN, Palmer AE, and Tsien RY (2004) Improved monomeric red, orange and yellow fluorescent proteins derived from Discosoma sp. red fluorescent protein. *Nat Biotechnol* 22: 1567-1572.

Shealy CN, and Peele TL (1957) Studies on amygdaloid nucleus of cat. *J Neurophysiol* 20: 125-139.

Shemesh OA, Tanese D, Zampini V, Linghu CY, Piatkevich K, Ronzitti E, Papagiakoumou E, Boyden ES, et al. (2017) Temporally precise single-cell-resolution optogenetics. *Nat Neurosci* 20: 1796-1806.

Shepherd GM. (2015) *Foundations of the neuron doctrine,* Oxford University Press: New York, NY.

Sherman D, Worrell JW, Cui Y, and Feldman JL (2015) Optogenetic perturbation of preBotzinger complex inhibitory neurons modulates respiratory pattern. *Nat Neurosci* 18: 408-414.

Shi SH, Jan LY, and Jan YN (2003) Hippocampal neuronal polarity specified by spatially localized mPar3/mPar6 and PI 3-kinase activity. *Cell* 112: 63-75.

Shykoff BE, Naqvi SS, Menon AS, and Slutsky AS (1991) Respiratory sinus arrhythmia in dogs. Effects of phasic afferents and chemostimulation. *J Clin Invest* 87: 1621-1627.

Sierra YA, Rost BR, Pofahl M, Fernandes AM, Kopton RA, Moser S, Holtkamp D, Masala N, et al. (2018) Potassium channel-based optogenetic silencing. *Nat Commun* 9: 4611.

Simms AE, Paton JFR, Pickering AE, and Allen AM (2009) Amplified respiratory-sympathetic coupling in the spontaneously hypertensive rat: does it contribute to hypertension? *J Physiol (London)* 587: 597-610.

Singh P, Schimenti JC, and Bolcun-Filas E (2015) A mouse geneticist's practical guide to CRISPR applications. *Genetics* 199: 1-15.

Slimko EM, McKinney S, Anderson DJ, Davidson N, and Lester HA (2002) Selective electrical silencing of mammalian neurons in vitro by the use of invertebrate ligand-gated chloride channels. *J Neurosci* 22: 7373-7379.

Smith CM, Shen PJ, Banerjee A, Bonaventure P, Ma S, Bathgate RAD, Sutton SW, and Gundlach AL (2010) Distribution of relaxin-3 and RXFP3 within arousal, stress, affective, and cognitive circuits of mouse brain. *J Comp Neurol* 518: 4016-4045.

Smith CM, Chua BE, Zhang C, Walker AW, Haidar M, Hawkes D, Shabanpoor F, Hossain MA, et al. (2014a) Central injection of relaxin-3 receptor (RXFP3) antagonist peptides reduces motivated food seeking and consumption in C57BL/6J mice. *Behav Brain Res* 268: 117-126.

Smith CM, Walker AW, Hosken IT, Chua BE, Zhang C, Haidar M, and Gundlach AL (2014b) Relaxin-3/RXFP3 networks: an emerging target for the treatment of depression and other neuropsychiatric diseases? *Front Pharmacol* 5: 46.

Smith R, Thayer JF, Khalsa SS, and Lane RD (2017) The hierarchical basis of neurovisceral integration. *Neurosci Biobehav Rev* 75: 274-296.

Smith SM, and Vale WW (2006) The role of the hypothalamic-pituitary-adrenal axis in neuroendocrine responses to stress. *Dialogues Clin Neurosci* 8: 383-395.

Smotherman M, Kobayasi K, Ma J, Zhang S, and Metzner W (2006) A mechanism for vocal-respiratory coupling in the mammalian parabrachial nucleus. *J Neurosci* 26: 4860-4869.

Sobotzik JM, Sie JM, Politi C, Del Turco D, Bennett V, Deller T, and Schultz C (2009) AnkyrinG is required to maintain axo-dendritic polarity in vivo. *Proc Natl Acad Sci U S A* 106: 17564-17569.

Sobreviela T, Clary DO, Reichardt LF, Brandabur MM, Kordower JH, and Mufson EJ (1994) TrkA-immunoreactive profiles in the central nervous system: colocalization with neurons containing p75 nerve growth factor receptor, choline acetyltransferase, and serotonin. *J Comp Neurol* 350: 587-611.

Song AH, Wang D, Chen G, Li Y, Luo J, Duan SM, and Poo MM (2009) A selective filter for cytoplasmic transport at the axon initial segment. *Cell* 136: 1148-1160.

Sotelo C (2003) Viewing the brain through the master hand of Ramon y Cajal. *Nat Rev Neurosci* 4: 71-77.

Soudais C, Boutin S, Hong SS, Chillon M, Danos O, Bergelson JM, Boulanger P, and Kremer EJ (2000) Canine adenovirus type 2 attachment and internalization: coxsackievirus-adenovirus receptor, alternative receptors, and an RGD-independent pathway. *J Virol* 74: 10639-10649.

Stachniak TJ, Ghosh A, and Sternson SM (2014) Chemogenetic synaptic silencing of neural circuits localizes a hypothalamus -> midbrain pathway for feeding behavior. *Neuron* 82: 797-808.

Stanley SA, Kelly L, Latcha KN, Schmidt SF, Yu X, Nectow AR, Sauer J, Dyke JP, et al. (2016) Bidirectional electromagnetic control of the hypothalamus regulates feeding and metabolism. *Nature* 531: 647-650.

Stec DE, Keen HL, and Sigmund CD (2002) Lower blood pressure in floxed angiotensinogen mice after adenoviral delivery of Cre-recombinase. *Hypertension* 39: 629-633.

Stein V, Hermans-Borgmeyer I, Jentsch TJ, and Hubner CA (2004) Expression of the KCl cotransporter KCC2 parallels neuronal maturation and the emergence of low intracellular chloride. *J Comp Neurol* 468: 57-64.

Steinberg EE, Gore F, Heifets BD, Taylor MD, Norville ZC, Beier KT, Foldy C, Lerner TN, et al. (2020) Amygdala-midbrain connections modulate appetitive and aversive learning. *Neuron*.

Sternson SM, and Roth BL (2014) Chemogenetic tools to interrogate brain functions. *Annu Rev Neurosci* 37: 387-407.

Stone MC, Roegiers F, and Rolls MM (2008) Microtubules have opposite orientation in axons and dendrites of Drosophila neurons. *Mol Biol Cell* 19: 4122-4129.

Stratford JM, and Finger TE (2011) Central representation of postingestive chemosensory cues in mice that lack the ability to taste. *J Neurosci* 31: 9101-9110.

Sun F, Zeng J, Jing M, Zhou J, Feng J, Owen SF, Luo Y, Li F, et al. (2018) A genetically encoded fluorescent sensor enables rapid and specific detection of dopamine in flies, fish, and mice. *Cell* 174: 481-496 e419.

Sun L, Tang Y, Yan K, Yu J, Zou Y, Xu W, Xiao K, Zhang Z, et al. (2019) Differences in neurotropism and neurotoxicity among retrograde viral tracers. *Mol Neurodegener* 14: 8.

Sun N, Roberts L, and Cassell MD (1991) Rat central amygdaloid nucleus projections to the bed nucleus of the stria terminalis. *Brain Res Bull* 27: 651-662.

Szablowski JO, Lee-Gosselin A, Lue B, Malounda D, and Shapiro MG (2018) Acoustically targeted chemogenetics for the non-invasive control of neural circuits. *Nat Biomed Eng* 2: 475-484.

Szonyi A, Sos KE, Nyilas R, Schlingloff D, Domonkos A, Takacs VT, Posfai B, Hegedus P, et al. (2019) Brainstem nucleus incertus controls contextual memory formation. *Science* 364: eaaw0445.

Takayama K, Okada J, and Miura M (1990) Evidence that neurons of the central amygdaloid nucleus directly project to the site concerned with circulatory and respiratory regulation in the ventrolateral nucleus of the cat - a WGA-HRP Study. *Neurosci Lett* 109: 241-246.

Tan W, Janczewski WA, Yang P, Shao XM, Callaway EM, and Feldman JL (2008) Silencing preBotzinger complex somatostatin-expressing neurons induces persistent apnea in awake rat. *Nat Neurosci* 11: 538-540.

Tanaka M, Iijima N, Miyamoto Y, Fukusumi S, Itoh Y, Ozawa H, and Ibata Y (2005) Neurons expressing relaxin 3/INSL 7 in the nucleus incertus respond to stress. *Eur J Neurosci* 21: 1659-1670.

Tanaka M, Watanabe Y, and Yoshimoto K (2009) Regulation of relaxin 3 gene expression via cAMP-PKA in a neuroblastoma cell line. *J Neurosci Res* 87: 820-829.

Tanimoto S, Nakagawa T, Yamauchi Y, Minami M, and Satoh M (2003) Differential contributions of the basolateral and central nuclei of the amygdala in the negative affective component of chemical somatic and visceral pains in rats. *Eur J Neurosci* 18: 2343-2350.

Tascioglu AO, and Tascioglu AB (2005) Ventricular anatomy: illustrations and concepts from antiquity to Renaissance. *Neuroanatomy* 4: 57-63.

Taylor EW, Jordan D, and Coote JH (1999) Central control of the cardiovascular and respiratory systems and their interactions in vertebrates. *Physiological Reviews* 79: 855-916.

Tehovnik EJ (1996) Electrical stimulation of neural tissue to evoke behavioral responses. *J Neurosci Methods* 65: 1-17.

Temkin O (1947) Gall and the phrenological movement. *Bull Hist Med* 21: 275-321.

Ter Horst GJ, and Postema F (1997) Forebrain parasympathetic control of heart activity: retrograde transneuronal viral labeling in rats. *Am J Physiol* 273: H2926-2930.

Tervo DG, Hwang BY, Viswanathan S, Gaj T, Lavzin M, Ritola KD, Lindo S, Michael S, et al. (2016) A designer AAV variant permits efficient retrograde access to projection neurons. *Neuron* 92: 372-382.

Thayer JF, and Lane RD (2000) A model of neurovisceral integration in emotion regulation and dysregulation. *J Affect Disord* 61: 201-216.

Thayer JF, Hansen AL, Saus-Rose E, and Johnsen BH (2009a) Heart rate variability, prefrontal neural function, and cognitive performance: the neurovisceral integration perspective on self-regulation, adaptation, and health. *Ann Behav Med* 37: 141-153.

Thayer JF, and Lane RD (2009b) Claude Bernard and the heart-brain connection: further elaboration of a model of neurovisceral integration. *Neurosci Biobehav Rev* 33: 81-88.

Thompson RL, and Cassell MD (1989) Differential distribution and non-collateralization of central amygdaloid neurons projecting to different medullary regions. *Neurosci Lett* 97: 245-251.

Tian L, Hires SA, Mao T, Huber D, Chiappe ME, Chalasani SH, Petreanu L, Akerboom J, et al. (2009) Imaging neural activity in worms, flies and mice with improved GCaMP calcium indicators. *Nat Methods* 6: 875-881.

Titford M (2005) The long history of hematoxylin. *Biotech Histochem* 80: 73-78.

Tixier-Vidal A, Faivre-Bauman A, Picart R, and Wiedenmann B (1988) Immunoelectron microscopic localization of synaptophysin in a Golgi subcompartment of developing hypothalamic neurons. *Neuroscience* 26: 847-861.

Todman D (2008) Henry Dale and the discovery of chemical synaptic transmission. *Eur Neurol* 60: 162-164.

Toor R, Sun QJ, Kumar NN, Le S, Hildreth CM, Phillips JK, and McMullan S (2019) Neurons in the intermediate reticular nucleus coordinate postinspiratory activity, swallowing, and respiratory-sympathetic coupling in the rat. *J Neurosci* 39: 9757-9766.

Torvik A (1956) Afferent connections to the sensory trigeminal nuclei, the nucleus of the solitary tract and adjacent structures; an experimental study in the rat. *J Comp Neurol* 106: 51-141.

Travagli RA, Hermann GE, Browning KN, and Rogers RC (2006) Brainstem circuits regulating gastric function. *Annu Rev Physiol* 68: 279-305.

Turner-Bridger B, Caterino C, and Cioni JM (2020) Molecular mechanisms behind mRNA localization in axons. *Open Biol* 10: 200177.

Uematsu A, Tan BZ, Ycu EA, Cuevas JS, Koivumaa J, Junyent F, Kremer EJ, Witten IB, et al. (2017) Modular organization of the brainstem noradrenaline system coordinates opposing learning states. *Nat Neurosci* 20: 1602-1611.

Vaidya AR, Pujara MS, Petrides M, Murray EA, and Fellows LK (2019) Lesion studies in contemporary neuroscience. *Trends Cogn Sci* 23: 653-671.

Vale RD (2003) The molecular motor toolbox for intracellular transport. *Cell* 112: 467-480.

Valenstein ES. (2007) *The war of the soups and the sparks: the discovery of neurotransmitters and the dispute over how nerves communicate,* Columbia University Press.

van der Kooy D, Koda LY, McGinty JF, Gerfen CR, and Bloom FE (1984) The organization of projections from the cortex, amygdala, and hypothalamus to the nucleus of the solitary tract in rat. *J Comp Neurol* 224: 1-24.

Van der Westhuizen ET, Sexton PM, Bathgate RA, and Summers RJ (2005) Responses of GPCR135 to human gene 3 (H3) relaxin in CHO-K1 cells determined by microphysiometry. *Ann N Y Acad Sci* 1041: 332-337.

Vardy E, Robinson JE, Li C, Olsen RHJ, DiBerto JF, Giguere PM, Sassano FM, Huang XP, et al. (2015) A new DREADD facilitates the multiplexed chemogenetic interrogation of behavior. *Neuron* 86: 936-946.

Veening JG, Swanson LW, and Sawchenko PE (1984) The organization of projections from the central nucleus of the amygdala to brainstem sites involved in central autonomic regulation: a combined retrograde transport-immunohistochemical study. *Brain Res* 303: 337-357.

Veinante P, and Freund-Mercier MJ (2003) Branching patterns of central amygdaloid nucleus efferents in the rat: single-axon reconstructions. *Ann N Y Acad Sci* 985: 552-553.

Viviani D, Charlet A, van den Burg E, Robinet C, Hurni N, Abatis M, Magara F, and Stoop R (2011) Oxytocin selectively gates fear responses through distinct outputs from the central amygdala. *Science* 333: 104-107.

Vrang N, Phifer CB, Corkern MM, and Berthoud HR (2003) Gastric distension induces c-Fos in medullary GLP-1/2-containing neurons. *Am J Physiol Regul Integr Comp Physiol* 285: R470-478.

Wagner EF, Stewart TA, and Mintz B (1981a) The human beta-globin gene and a functional viral thymidine kinase gene in developing mice. *Proc Natl Acad Sci U S A* 78: 5016-5020.

Wagner TE, Hoppe PC, Jollick JD, Scholl DR, Hodinka RL, and Gault JB (1981b) Microinjection of a rabbit beta-globin gene into zygotes and its subsequent expression in adult mice and their offspring. *Proc Natl Acad Sci U S A* 78: 6376-6380.

Walker LC, Kastman HE, Koeleman JA, Smith CM, Perry CJ, Krstew EV, Gundlach AL, and Lawrence AJ (2017) Nucleus incertus corticotrophin-releasing factor 1 receptor signalling regulates alcohol seeking in rats. *Addict Biol* 22: 1641-1654.

Walther W, and Stein U (1996) Cell type specific and inducible promoters for vectors in gene therapy as an approach for cell targeting. *J Mol Med* 74: 379-392.

Wang D, Tai PWL, and Gao GP (2019a) Adeno-associated virus vector as a platform for gene therapy delivery. *Nat Rev Drug Discov* 18: 358-378.

Wang L, Jackson WC, Steinbach PA, and Tsien RY (2004) Evolution of new nonantibody proteins via iterative somatic hypermutation. *Proc Natl Acad Sci U S A* 101: 16745-16749.

Wang L, Chen IZ, and Lin DY (2015) Collateral pathways from the ventromedial hypothalamus mediate defensive behaviors. *Neuron* 85: 1344-1358.

Wang W, Kim CK, and Ting AY (2019b) Molecular tools for imaging and recording neuronal activity. *Nat Chem Biol* 15: 101-110.

Watanabe Y, Tsujimura A, Takao K, Nishi K, Ito Y, Yasuhara Y, Nakatomi Y, Yokoyama C, et al. (2011) Relaxin-3-deficient mice showed slight alteration in anxiety-related behavior. *Front Behav Neurosci* 5: 50.

Watson JD, and Crick FH (1953) Molecular structure of nucleic acids; a structure for deoxyribose nucleic acid. *Nature* 171: 737-738.

Westerhaus MJ, and Loewy AD (2001) Central representation of the sympathetic nervous system in the cerebral cortex. *Brain Res* 903: 117-127.

Wheeler MA, Smith CJ, Ottolini M, Barker BS, Purohit AM, Grippo RM, Gaykema RP, Spano AJ, et al. (2016) Genetically targeted magnetic control of the nervous system. *Nat Neurosci* 19: 756-761.

Wheeler MA, Deppmann CD, Patel MK, and Güler AD (2020) Reply to: Magneto is ineffective in controlling electrical properties of cerebellar Purkinje cells, Assessing the utility of Magneto to control neuronal excitability in the somatosensory cortex and Revaluation of magnetic properties of Magneto. *Nat Neurosci* 23: 1051-1054.

White MD, Milne RVJ, and Nolan MF (2011) A molecular toolbox for rapid generation of viral vectors to up- or down-regulate neuronal gene expression in vivo. *Front Mol Neurosci* 4.

Wickens AP. (2014) *A history of the brain: from stone age surgery to modern neuroscience,* Psychology Press.

Wickersham IR, Finke S, Conzelmann KK, and Callaway EM (2007a) Retrograde neuronal tracing with a deletion-mutant rabies virus. *Nat Methods* 4: 47-49.

Wickersham IR, Lyon DC, Barnard RJ, Mori T, Finke S, Conzelmann KK, Young JA, and Callaway EM (2007b) Monosynaptic restriction of transsynaptic tracing from single, genetically targeted neurons. *Neuron* 53: 639-647.

Wiegert JS, and Oertner TG (2016) How (not) to silence long-range projections with light. *Nat Neurosci* 19: 527-528.

Wietek J, Wiegert JS, Adeishvili N, Schneider F, Watanabe H, Tsunoda SP, Vogt A, Elstner M, et al. (2014) Conversion of channelrhodopsin into a light-gated chloride channel. *Science* 344: 409-412.

Wijdicks EFM (2019) Noeud vital and the respiratory centers. *Neurocrit Care* 31: 211-215.

Wills A (1999) Herophilus, Erasistratus, and the birth of neuroscience. *Lancet* 354: 1719-1720.

Wold WS, and Toth K (2013) Adenovirus vectors for gene therapy, vaccination and cancer gene therapy. *Curr Gene Ther* 13: 421-433.

Won SM, Song E, Reeder JT, and Rogers JA (2020) Emerging modalities and implantable technologies for neuromodulation. *Cell* 181: 115-135.

Wu CW, Ivanova E, Zhang Y, and Pan ZH (2013) rAAV-mediated subcellular targeting of optogenetic tools in retinal ganglion cells in vivo. *PLoS One* 8.

Wu X, Zhu X, Chong P, Liu J, Andre LN, Ong KS, Brinson K, Jr., Mahdi AI, et al. (2019) Sono-optogenetics facilitated by a circulation-delivered rechargeable light source for minimally invasive optogenetics. *Proc Natl Acad Sci U S A* 52: 26332–26342.

Wu Z, Yang H, and Colosi P (2010) Effect of genome size on AAV vector packaging. *Mol Ther* 18: 80-86.

Wykes AD, Ma S, Bathgate RAD, and Gundlach AL (2020) Targeted viral vector transduction of relaxin-3 neurons in the rat nucleus incertus using a novel cell-type specific promoter. *IBRO Rep* 8: 1-10.

Xie J, Xie Q, Zhang H, Ameres SL, Hung JH, Su Q, He R, Mu X, et al. (2011) MicroRNA-regulated, systemically delivered rAAV9: a step closer to CNS-restricted transgene expression. *Mol Ther* 19: 526-535.

Xu C, Krabbe S, Grundemann J, Botta P, Fadok JP, Osakada F, Saur D, Grewe BF, et al. (2016) Distinct hippocampal pathways mediate dissociable roles of context in memory retrieval. *Cell* 167: 961-972.

Xu L, Yee JK, Wolff JA, and Friedmann T (1989) Factors affecting long-term stability of Moloney murine leukemia virus-based vectors. *Virology* 171: 331-341.

Yahiro T, Kataoka N, Nakamura Y, and Nakamura K (2017) The lateral parabrachial nucleus, but not the thalamus, mediates thermosensory pathways for behavioural thermoregulation. *Sci Rep* 7: 1-10.

Yamada H, Ezure K, and Manabe M (1988) Efferent projections of inspiratory neurons of the ventral respiratory group. A dual labeling study in the rat. *Brain Res* 455: 283-294.

Yamada J, Okabe A, Toyoda H, Kilb W, Luhmann HJ, and Fukuda A (2004) Cl- uptake promoting depolarizing GABA actions in immature rat neocortical neurones is mediated by NKCC1. *J Physiol (London)* 557: 829-841.

Yamamoto T, and Sawa K (2000) Comparison of c-fos-like immunoreactivity in the brainstem following intraoral and intragastric infusions of chemical solutions in rats. *Brain Res* 866: 144-151.

Yamanaka K, Takagishi M, Kim J, Gouraud SS, and Waki H (2018) Bidirectional cardiovascular responses evoked by microstimulation of the amygdala in rats. *J Physiol Sci* 68: 233-242.

Yang CF, and Feldman JL (2018) Efferent projections of excitatory and inhibitory preBotzinger Complex neurons. *J Comp Neurol* 526: 1389-1402.

Yang M, Card JP, Tirabassi RS, Miselis RR, and Enquist LW (1999) Retrograde, transneuronal spread of pseudorabies virus in defined neuronal circuitry of the rat brain is facilitated by gE mutations that reduce virulence. *J Virol* 73: 4350-4359.

Yang W, and Yuste R (2017) In vivo imaging of neural activity. *Nat Methods* 14: 349-359.

Yetman MJ, Washburn E, Hyun JH, Osakada F, Hayano Y, Zeng H, Callaway EM, Kwon HB, et al. (2019) Intersectional monosynaptic tracing for dissecting subtype-specific organization of GABAergic interneuron inputs. *Nat Neurosci* 22: 492-502.

Yizhar O, Fenno LE, Davidson TJ, Mogri M, and Deisseroth K (2011) Optogenetics in neural systems. *Neuron* 71: 9-34.

Yogev S, and Shen K (2017) Establishing Neuronal Polarity with Environmental and Intrinsic Mechanisms. *Neuron* 96: 638-650.

Yoshimura T, Kawano Y, Arimura N, Kawabata S, Kikuchi A, and Kaibuchi K (2005) GSK-3beta regulates phosphorylation of CRMP-2 and neuronal polarity. *Cell* 120: 137-149.

Young JZ (1936) The structure of nerve fibres in Cephalopods and Crustacea. *Proceedings of the Royal Society Series B-Biological Sciences* 121: 319-337.

Zahm DS, Jensen SL, Williams ES, and Martin JR, 3rd (1999) Direct comparison of projections from the central amygdaloid region and nucleus accumbens shell. *Eur J Neurosci* 11: 1119-1126.

Zallen DT (2003) Despite Franklin's work, Wilkins earned his Nobel. *Nature* 425: 15.

Zeng WB, Jiang HF, Gang YD, Song YG, Shen ZZ, Yang H, Dong X, Tian YL, et al. (2017) Anterograde monosynaptic transneuronal tracers derived from herpes simplex virus 1 strain H129. *Mol Neurodegener* 12: 38.

Zhang C, Chua BE, Yang AN, Shabanpoor F, Hossain MA, Wade JD, Rosengren KJ, Smith CM, et al. (2015a) Central relaxin-3 receptor (RXFP3) activation reduces elevated, but not basal, anxiety-like behaviour in C57BL/6J mice. *Behav Brain Res* 292: 125-132.

Zhang F, Wang LP, Brauner M, Liewald JF, Kay K, Watzke N, Wood PG, Bamberg E, et al. (2007) Multimodal fast optical interrogation of neural circuitry. *Nature* 446: 633-639.

Zhang X, Cui J, Tan Z, Jiang C, and Fogel R (2003) The central nucleus of the amygdala modulates gut-related neurons in the dorsal vagal complex in rats. *J Physiol* 553: 1005-1018.

Zhang XH, Tee LY, Wang XG, Huang QS, and Yang SH (2015b) Off-target effects in CRISPR/Cas9-mediated genome engineering. *Mol Ther Nucleic Acids* 4: e264.

Zhou DX, Lambert S, Malen PL, Carpenter S, Boland LM, and Bennett V (1998) AnkyrinG is required for clustering of voltage-gated Na channels at axon initial segments and for normal action potential firing. *Mol Biol Cell* 9: 37a-37a.

Zimmer HG (2006) Otto Loewi and the chemical transmission of vagus stimulation in the heart. *Clinical Cardiology* 29: 135-136.

Zinder ND (1992) Forty years ago: the discovery of bacterial transduction. *Genetics* 132: 291-294.

Zingg B, Chou XL, Zhang ZG, Mesik L, Liang F, Tao HW, and Zhang LI (2017) AAV-mediated anterograde transsynaptic tagging: mapping corticocollicular input-defined neural pathways for defense behaviors. *Neuron* 93: 33-47.

Zoccal DB, Furuya WI, Bassi M, Colombari DS, and Colombari E (2014) The nucleus of the solitary tract and the coordination of respiratory and sympathetic activities. *Front Physiol* 5: 238.

Zola-Morgan S (1995) Localization of brain function: the legacy of Franz Joseph Gall (1758-1828). *Annu Rev Neurosci* 18: 359-383.

Zolotukhin S, Potter M, Hauswirth WW, Guy J, and Muzyczka N (1996) A "humanized" green fluorescent protein cDNA adapted for high-level expression in mammalian cells. *J Virol* 70: 4646-4654.

Zolotukhin S, Byrne BJ, Mason E, Zolotukhin I, Potter M, Chesnut K, Summerford C, Samulski RJ, et al. (1999) Recombinant adeno-associated virus purification using novel methods improves infectious titer and yield. *Gene Ther* 6: 973-985.

Zseli G, Vida B, Szilvasy-Szabo A, Toth M, Lechan RM, and Fekete C (2018) Neuronal connections of the central amygdalar nucleus with refeeding-activated brain areas in rats. *Brain Struct Funct* 223: 391-414.

Zussy C, Loustalot F, Junyent F, Gardoni F, Bories C, Valero J, Desarmenien MG, Bernex F, et al. (2016) Coxsackievirus adenovirus receptor loss impairs adult neurogenesis, synapse content, and hippocampus plasticity. *J Neurosci* 36: 9558-9571.

Appendix I

Promoter sequences

Details of promoter sequences used in constructs developed in Chapter 2 are provided below.

Rat relaxin-3 (Rln3) promoter sequence (5'→3'; 1,736 bp)

CCTGCAAACTTGTCTGTGTACCATTTGCATGTCTGGAACCTGTAGAGGCCAGAAGAAGGCATCAGATTC
CATGAACATGGAGTCACTGACAGTTGTGAGTTGCCATGTGGGTGCTGGGAGCTGAACCTGGGTCCTCT
GGAAGAACAGCCAGTATACATAAACTCTGAGCTATCTCTGTCTCTCCAGCCCTAAGGTTGTTCCAGGCC
ACCCCAGAGAGTCCCCTCTGCAGAGGGGCAAGCGGCAGCACAGTGGTTAGAGCATTTTCTCCTTGTAT
GGGGACCCAGGTTCTGTTCCCAGCAGCCATGTCAGCAGCACAACCTGTAACTTGAGCTCCAGGAGTTT
GATGCCCACTTTTGACCTCTACAAGAACCCACATAAATGTGGTACACACACAGTCACACACACAGTCAC
ACACACAGTCACAAACACACACACATAGTCACAGACACAGACACACACATACAGTCACATACATAGACA
CAGACACAGACACACACACACAATCACACACAATCACACACACACAGTCACACACACAGACACAGTCAC
ACACACACATAAATGAAAAATACATAACTCTAAAACAGCAGACAAAATTGGGCTTTTTTTTTTGACCCAA
TTTATCAGATATAATTGCCCACCCAAACATACAAAGCCCAATACACATCCATCCCTTAAAAACATTCATA
ACGGGGGTTGGGGATTTAGCTCAGTGGTAGAGCGCTTACCTAGGAAGCGCAGGGCCCTGGGTTCGGT
CCCCAGCTCCGGAAAAAAAAAAAAGAAGATGTAACACACACACACACACACACACACACACACACACA
TACACACATTCACTCACACAGAGACTGAACCACCAAAGAGCAAACATGGGACTGACTTAGGCCCTCTGC
ACGTGTTACAGTTGTATATGCGGGACTCCTACAGTGGGAGCAGGGGTGTCTCTGACTATTTTGCCTGCT
TTTGAGACCCTTTCTTCCTACTGGGCTGCCTCTTCCAGCCTCAGCAGGAGAAGGTGTGCCTGGTCTCACT
GCAACTTCATACACCTGGGCTAGTTGATCTACAGCGGAGATCTCTTTTCTGAAGAGAAGTGGGGGCAG
AGTGGATAAGGGGAAAGGTGGGGGGAAAGACTGGGAGGAGAGGAGGGAGGGGGAACTGTGGTCA
GGATGTAAAATAAATACATTTATTCATTGTAAAGAGAGATGCGGGTGTTTATTGTTATTTATGTTGGTAC
ATGCGCACATATGTATGTGCATGTGTGCGCAGGCTCCATGGGGGCGTCGAATCCCCTGGAGCTGGAGT
TACAGGAAACTGTGAGTTGCCTGCTTTGGGTAGTGGGCACCGAACTCAGGCCATCCGGAAGAGCAGG
AAGCGTCTTATCTACTGTGCCACCTCCCCAGCTCCAGCGGAGAGTTTGAGGCTAGCCAGGCTAGGGGA
TTCTGCCTAACAAGAAGAGCGTTGGTTGATGGCTTACTCCTATAATCCCAGCACTTAGCAGTAGACTGA
AGCAGGAGAATTGCTCGGGTGCGGAAGATGACAGGGAGCTGAGCCATGCCACCCTGTCTGCGTGAAA
GGTTATCTCTTGGCAAGGAGATGGTAAAGGTCAGGTTGCCAACTGCCTCTCCTCTGCTCAGAAGATAAC
CCAGGTCAGCGGGCGGGGCTGGAAGCCAGGCTGTATAAATAGGGGATTGGAGGTGGTGCCGACAGA
GCCACCTGGGTCGCAGGCATCTCAGCTG

Rat tropomyosin receptor kinase A (TrkA) promoter sequence (5'→3'; 880 bp)

GAACGGTTCCCAGCTCACACGTCCGAAGAACTAAGAGATCTATTAATTTCTCCGCACAGAAATCGATGC
TCTTGTCAGGACGGCGATCGATGCCAGGCTTGGTCTGCCTGGCCAAACCCCGGCTCTGGGGCCGCAGC
TGGCTGGCTAGGATTGGGAACTGACCCCAAGACCAGAGAGGCACAGTCAAGCAAGGCTCCGAACAGC
TTTCCCCGGCCCTCGCCCTCGGAGCCCCAGGCCAATCGCAACGCCCCGGCGCGAGGGCTTCTAGCGCC
ACCCTGTGGGCTCTTGAGGACCGAGAGGTCTCCACTTTCCAATCTCCCTCCAGCTGTGTTCAAAGGACT
CTTCTTTACCCCTGTTTTCCTCCCCAGATTCTGCGTCCAGCCTCAGCGAGGCCTCTCCCTTTCCTTACTAG
GGTCTGGAGAGCGTACATCTAACTTATTCCAAGTGACGTGAACACTCTCTTAGGTAAAGTGCACGGTGA
GGCTGGCTGGGCTGACCCGGACTTCAACCTTTTTCTTGCTCAATCTCTCCTGGTCCCCGCAAATCTGAAA
ATGCAGCTGTTTTACTGTGAGAAATAGGGTATCGGCTTCCTAGCTCCCCCAGCCTCAGAAGACACATGT
GAAGCAATCTGTGGCAGTCCCCCGCCCCAGGTCTCCTGCAGCCGTGAGGGACATGAGGAAGGCGAGC
TGGCAATAGGGCCCCGAAAGGGGAGGGGGCACTGGGGGCATCGGCAGGCGGGGCGGGGCGGGGCC
GTGGGTGCCGCCCTCTCCTGGTGGCTAGTCTTTAACACCGCCCCGCGCACGTGTCGCGCGAGGCCGGG
CGGCGGCAGCCAGGAGCGCACGGACGGCCGCGCGGCCCGAGCTAGGCGGGCGCCGCCGCG

Appendix II

Additional viral vector constructs

The following AAV vectors were developed during my candidature and undergoing functional validation at the time this thesis was submitted. Details of their construction are recorded here for future reference and interest in relation to studies described in the main text.

Name: AAV1/2-Rln3-Cre

Purpose: This vector was developed for cell-type specific expression of Cre-recombinase in relaxin-3 neurons, mediated by the relaxin-3 promoter sequence identified in Chapter 2.

Plasmid construction: To facilitate construction of AAV-Rln3-Cre using the Gateway® cloning system, the Cre-recombinase protein coding sequence was cloned from pTYF-BS-TPH2-Cre-IRES-GAL4p65 plasmid (kindly provided by Prof. Sergey Kasparov, University of Bristol, UK) using forward (5'-attB5-ATGTCCAATTTACTGACCGTACACC) and reverse (5'-attB2-CTAATCGCCATCTTCCAGCAGG) primers (synthesised by Sigma-Aldrich (NSW, Australia)). Fifty fmol of the resultant PCR product was used to create pENTR-L5-Cre-L2 plasmid, via recombination with pDONR-P5-P2 plasmid (a gift from Dr. Melanie White (A*STAR, Singapore)). Subsequent recombination of pENTR-L5-Cre-L2 with pENTR-L1-Rln3-R2 (10 fmol each) and pAM-Gateway (see Section 2.2.3; Wykes et al. (2020)) (20 fmol) generated pAM-Rln3-Cre. All recombination reactions were carried out using Clonase™II reagents (Life Technologies, VIC, Australia), and incubated for 16 h at 25 ˚C. The PCR-amplified Cre-recombinase coding sequence incorporated into pENTR-L5-Cre-L2 was verified by Sanger sequencing (Australian Genome Research Facility, VIC, Australia).

AAV vector production: Vector production and titration were performed as described in Section 2.2.4. In brief, AAV1/2-Rln3-Cre vector was produced in, and harvested from, HEK293FT cells following PEI co-transfection with pAM-Rln3-Cre and pDPI/pDPII helper plasmids (Grimm et al. 2003). Harvested vectors were purified by iodixanol gradient ultracentrifugation, and titre determined using qPCR against the WPRE sequence.

Name: AAV1/2-CAG-DIO-(hCAR)$_{off}$-(*Gt*ACR2$^{Kv2.1}$)$_{on}$-W3SL

Purpose: AAV1/2-CAG-DIO-(hCAR)$_{off}$-(*Gt*ACR2$^{Kv2.1}$)$_{on}$-W3SL is analogous to the AAV1/2-hSyn-DIO-(hCAR)$_{off}$-(*Gt*ACR2$^{Kv2.1}$)$_{on}$-W3SL vector described in Chapter 4, with modification to provide expression under a CAG promoter sequence, rather than hSyn promoter. As such, this vector provides CAG promoter-driven hCAR or *Gt*ACR2$^{Kv2.1}$ expression in transduced cells, prior to or following Cre recombination, respectively.

Plasmid construction: pAAV-hSyn-DIO-(hCAR)$_{off}$-(*Gt*ACR2$^{Kv2.1}$)$_{on}$-W3SL (as described in Section 4.2.2) and pUC57-CAG (synthesised by GenScript (NJ, USA)) plasmids were digested with XbaI enzyme (Promega, NSW, Australia), excising the respective promoter sequences. Subsequent ligation of the CAG promoter into the open pAAV-DIO-(hCAR)$_{off}$-(*Gt*ACR2$^{Kv2.1}$)$_{on}$-W3SL backbone, using T4 Ligase (Promega), created the pAAV-CAG-DIO-(hCAR)$_{off}$-(*Gt*ACR2$^{Kv2.1}$)$_{on}$-W3SL plasmid.

AAV vector production: Vector production and titration were performed as described in Section 4.2.2. In brief, AAV1/2-CAG-DIO-(hCAR)$_{off}$-(*Gt*ACR2$^{Kv2.1}$)$_{on}$-W3SL vector was produced in, and harvested from, HEK293FT cells following PEI co-transfection with pAAV-CAG-DIO-(hCAR)$_{off}$-(*Gt*ACR2$^{Kv2.1}$)$_{on}$-W3SL and pDPI/pDPII helper plasmids (Grimm et al. 2003). Harvested vectors were purified by iodixanol gradient ultracentrifugation, and titre determined using qPCR against the muGFP sequence.